UNITED STATES DEPARTMENT OF ENERGY

ORNL/CDIAC-114
NDP-067

The International Intercomparison Exercise of Underway fCO_2 Systems During the R/V Meteor Cruise 36/1 in the North Atlantic Ocean

Arne Körtzinger
Ludger Mintrop
Jan Duinker

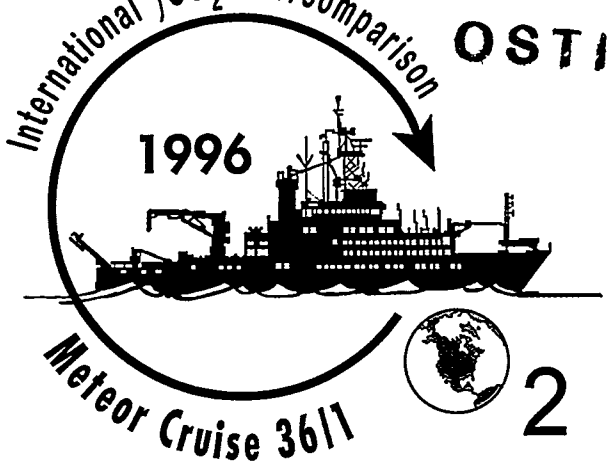

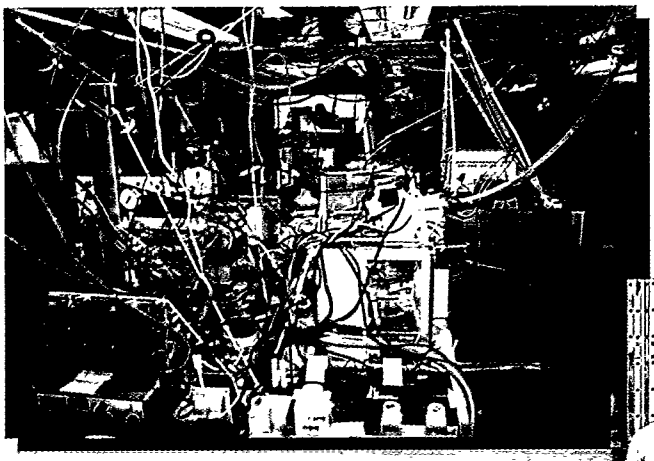

Carbon Dioxide Information Analysis Center
Oak Ridge National Laboratory

Institute of Marine Research
at the University of Kiel, Germany

DISCLAIMER

Portions of this document may be illegible in electronic image products. Images are produced from the best available original document.

ORNL/CDIAC-114
NDP-067

THE INTERNATIONAL INTERCOMPARISON EXERCISE OF UNDERWAY fCO_2 SYSTEMS DURING THE R/V *METEOR* CRUISE 36/1 IN THE NORTH ATLANTIC OCEAN

By
Arne Körtzinger,[1] Lutger Mintrop,[1] and Jan C. Duinker[1]

Other Data Contributors
Kenneth M. Johnson,[2] Craig Neill,[2] Douglas W. R. Wallace,[1] Bronte Tilbrook,[3] Philip Towler,[3] Hisayuki Inoue,[4] Masao Ishii,[4] Gary Shaffer,[5] Rodrigo Torres,[6] Eiji Ohtaki,[7] Eiji Yamashita,[7] Alain Poisson,[8] Christian Brunet,[8] Bernard Schauer,[8] Catherine Goyet,[9] and Greg Eischeid[9]

[1]Department of Marine Chemistry, Institute of Marine Research, University of Kiel, Kiel, Germany

[2]DOE, Brookhaven National Laboratory, Upton, New York

[3]Commonwealth Scientific and Industrial Research Organisation, Hobart, Tasmania, Australia

[4]Meteorological Research Institute, Tsukuba, Japan

[5]Niels Bohr Institute for Astronomy, University of Copenhagen, Copenhagen, Denmark

[6]Göteborg University and Chalmers University of Technology, Department of Analytical and Marine Chemistry, Göteborg, Sweden

[7]Okayama University, Okayama, Japan

[8]Université Pierre et Marie Curie, Laboratoire de Physique et Chimie Marines, Paris, France

[9]Woods Hole Oceanographic Institution, Department of Marine Chemistry and Geochemistry, Woods Hole, Massachusetts

Prepared by
Alexander Kozyr
Carbon Dioxide Information Analysis Center
Oak Ridge National Laboratory
Oak Ridge, Tennessee, U.S.A.

Environmental Sciences Division
Publication No. 4844

Date Published: March 1999

Prepared for the Environmental Sciences Division
Office of Biological and Environmental Research
U.S. Department of Energy
Budget Activity Numbers KP 12 02 03 0 and KP 12 04 01 0

Published by the
Carbon Dioxide Information Analysis Center
OAK RIDGE NATIONAL LABORATORY
Oak Ridge, Tennessee 37831-6335
managed by
LOCKHEED MARTIN ENERGY RESEARCH CORP.
for the
U.S. DEPARTMENT OF ENERGY
under contract DE-AC05-96OR22464

CONTENTS

LIST OF FIGURES

LIST OF TABLES

ABBREVIATIONS

A_T	total alkalinity
BMBF	Bundesministerium für Bildung, Wissenschaft, Forschung und Technologie (German Ministry for Education, Science, Research and Technology)
BNL	Brookhaven National Laboratory
CMDL	Climate Monitoring and Diagnostics Laboratory
CSIRO	Commonwealth Scientific and Industrial Research Organisation
C_T	total dissolved inorganic carbon (synonyms: DIC, TCO_2, ΣCO_2)
CTD	conductivity-temperature-depth probe
DFG	Deutsche Forschungsgemeinschaft (German Research Foundation)
DOE	U.S. Department of Energy
fCO_2	fugacity of CO_2
GMT	Greenwich mean time
GPS	global positioning system
IfMK	Institut für Meereskunde Kiel (Institute of Marine Research at the University of Kiel)
IOC	Intergovernmental Oceanographic Council
JGOFS	Joint Global Ocean Flux Study
MRI	Meteorological Research Institute
NBI	Niels Bohr Institute for Astronomy, Physics and Geophysics
NDIR	nondispersive infrared
NDP	numeric data package
NOAA	National Oceanic and Atmospheric Administration
OU	Okayama University
pCO_2	partial pressure of CO_2
pH	pH value
PSS	Practical Salinity Scale
RF	Reedereigemeinschaft Forschungsschiffahrt GmbH
R/V	Research Vessel
SCOR	Scientific Committee on Oceanic Research
SIO	Scripps Institution of Oceanography
SOMMA	single-operator multiparameter metabolic analyzer
UP&MC	Université Pierre et Marie Curie
UTC	universal time coordinated
WHOI	Woods Hole Oceanographic Institution
WMO	World Meteorological Organization
XBT	expendable bathythermograph
xCO_2	mole fraction of CO_2

ACKNOWLEDGMENTS

The authors would like to thank the following people for their cooperation and participation in this exercise. Their motivation and active involvement made this study possible. Our special thanks are addressed to those who joined the scientific party on board R/V *Meteor* for their willingness to cope with all the little problems such an exercise inevitably provides.

- Douglas Wallace, Kenneth Johnson, and Craig Neill, Brookhaven National Laboratory, Department of Applied Science, Upton, Long Island, New York, U.S.A.
- Bronte Tilbrook and Philip Towler, Commonwealth Scientific and Industrial Research Organisation, Division of Oceanography, Hobart, Tasmania, Australia
- Joanna Waniek, Susanne Schweinsberg, and Frank Malien, Institut für Meereskunde Kiel (Institute of Marine Research), Kiel, Germany
- Hisayuki Inoue and Masao Ishii, Meteorological Research Institute, Tsukuba, Japan
- Gary Shaffer, Niels Bohr Institute for Astronomy, Physics and Geophysics, University of Copenhagen, Copenhagen, Denmark, and Rodrigo Torres, Göteborg University and Chalmers University of Technology, Department of Analytical and Marine Chemistry, Göteborg, Sweden
- Eiji Ohtaki and Eiji Yamashita, Okayama University, Okayama, Japan
- Andrew Dickson and Justine Parks, Scripps Institution of Oceanography, Marine Physical Laboratory, La Jolla, California, U.S.A.
- Alain Poisson, Christian Brunet, and Bernard Schauer, Université Pierre et Marie Curie, Laboratoire de Physique et Chimie Marines, Paris, France
- Catherine Goyet and Greg Eischeid, Woods Hole Oceanographic Institution, Department of Marine Chemistry and Geochemistry, Woods Hole, Massachusetts, U.S.A.

In addition, we wish to thank the chief scientist of *Meteor* Cruise 36/1, Detlev Schulz-Bull, for perfect cooperation and for giving this exercise the high priority it needed. We appreciate the valuable comments and helpful advice from Andrew Dickson during the early stages of the exercise. Our thanks to Douglas Wallace and Andrew Watson for reviewing the manuscript and making helpful comments.

We also express our appreciation to the Reedereigemeinschaft Forschungsschiffahrt GmbH and the crew of R/V *Meteor* for their extremely helpful technical support before and throughout the cruise.

On behalf of the participants of this intercomparison exercise, we extend special thanks to all national funding agencies for providing the participants with the necessary funding.

Last but not least, the authors thank the Bundesministerium für Bildung, Wissenschaft, Forschung und Technologie (BMBF) for funding this exercise through German Joint Global Ocean Flux Study (JGOFS) funds as well as the Deutsche

Forschungsgemeinschaft (DFG) for making it possible to invite the international participants on this cruise.

ABSTRACT

Körtzinger, A., L. Mintrop, J. C. Duinker, K. M. Johnson, C. Neill, D. W. R. Wallace, B. Tilbrook, P. Towler, H. Inoue, M. Ishii, G. Shaffer, R. Torres, E. Ohtaki, E. Yamashita, A. Poisson, C. Brunet, B. Schauer, C. Goyet, G. Eischeid, and A. Kozyr (ed.). 1998. The International Intercomparison Exercise of Underway fCO_2 Systems During the R/V *Meteor* Cruise 36/1 in the North Atlantic Ocean. ORNL/CDIAC-114, NDP-067. Carbon Dioxide Information Analysis Center, Oak Ridge National Laboratory, U.S. Department of Energy, Oak Ridge, Tennessee, U.S.A. 150 pp.

Measurements of the fugacity of carbon dioxide (fCO_2) in surface seawater are an important part of studies of the global carbon cycle and its anthropogenic perturbation. An important step toward the thorough interpretation of the vast amount of available fCO_2 data is the establishment of a database system that would make such measurements more widely available for use in understanding the basin- and global-scale distribution of fCO_2 and its influence on the oceanic uptake of anthropogenic CO_2. Such an effort, however, is based on knowledge of the comparability of data sets from different laboratories. Currently, however, there is not much known about this subject.

In the light of the aforementioned situation, an International Intercomparison Exercise of Underway fCO_2 Systems was proposed and carried out by the Institut für Meereskunde Kiel (IfMK) (Institute of Marine Research at the University of Kiel), Kiel, Germany, during the R/V *Meteor* Cruise 36/1 from Hamilton, Bermuda, to Las Palmas, Gran Canaria, Spain. Nine groups from six countries (Australia, Denmark, Germany, France, Japan, and the United States) participated in this ambitious exercise, bringing together 15 participants with 7 underway fCO_2 systems, 1 discrete fCO_2 system, and 2 underway pH systems, as well as discrete systems for alkalinity and total dissolved inorganic carbon. This report presents only the results of the fCO_2 measurements.

The main idea of the exercise was to compare surface seawater fCO_2 synchronously measured by all participating instruments under identical conditions. This synchronicity was accomplished by providing the infrastructure during the exercise, such as a common seawater and calibration gas supply. Another important issue was checks of the performance of the calibration procedures for CO_2 and of all equilibrator temperature sensors. Furthermore a common procedure for the calculation of final fCO_2 was applied to all data sets. All these measures were taken in order to reduce the largest possible amount of controllable sources of error.

In this report we will demonstrate that the results of three of the seven underway systems agreed to within ±2 µatm throughout the cruise. This was not only the case for seawater fCO_2 measurements but also for measurements of the atmospheric mole fraction of CO_2 (xCO_2). One system was in good agreement (±2 µatm) for most of the time but showed a considerable positive offset of up to 9 µatm for about 40 h. However, it was found that significant offsets of up to 10 µatm occurred in underway fCO_2 measurements for three systems under typical and identical field work conditions. Although at least in one case this may be a consequence of a technical failure, it is an indication of significant

systematic differences in other cases. Finally, the discrete fCO_2 system measurements agreed within its nominal accuracy of 1% with the three most consistent underway fCO_2 systems data sets.

On the basis of a detailed comparison and evaluation of this large intercomparison data set, we offer general conclusions and recommendations for underway fCO_2 work. These may serve as background information for a successful preparation of a coherent database of surface ocean fCO_2 values. The results of this exercise certainly underline the need to carefully address the important issue of the interlaboratory comparability of fCO_2 data.

PART 1

OVERVIEW

1. INTRODUCTION

1.1 SCIENTIFIC BACKGROUND OF THE EXERCISE

Currently marine scientists are applying different concepts to quantify the oceanic uptake of CO_2. These efforts are being undertaken in the light of the atmospheric CO_2 perturbation and its possible impact on the earth's climate. One important concept is based on the determination of the partial pressure difference of CO_2 (ΔpCO_2) between the surface seawater and the overlying air, which is the thermodynamic driving force for any net exchange of CO_2. By means of a transfer coefficient, a measured ΔpCO_2 can be converted into a momentary net flux of CO_2 across the air–sea interface. Given the strong spatial and temporal variability of pCO_2 in the ocean, this concept faces the challenge of coming up with representative mean ΔpCO_2 values on a global grid. If this concept is to be successful in pinning down the present oceanic uptake of CO_2 reliably, the combined efforts of research groups all over the world are necessary. The Intergovernmental Oceanographic Council (IOC)/Scientific Committee on Oceanic Research (SCOR) Carbon Dioxide Advisory Panel recently established an international inventory of pCO_2 measurements that have been identified so far (http://cdiac.esd.ornl. gov/oceans/ pco2inv.html). One important requirement in this context is a good inter-laboratory comparability of the data sets, which were generated by quite different types of analytical systems. While the analytical precision of the various systems in use is mostly of the order of 1 µatm or better, not much is known presently about the comparability between different laboratories.

As a first important step to assess the current state of this parameter, an international shore-based intercomparison exercise of underway fugacity of CO_2 (fCO_2) systems was carried out by Andrew Dickson in June 1994 at the Scripps Institution of Oceanography, Marine Physical Laboratory, La Jolla, California, U.S.A. (http://www-mpl.ucsd.edu/people/adickson/CO2_QC) on behalf of the Joint IOC/SCOR CO_2 Advisory Panel. However, the general consensus in the scientific community was that a necessary second step would be an at-sea intercomparison under more typical and identical operation conditions. Such an exercise, to be carried out during the R/V *Meteor* cruise 36/1, was proposed by the Kiel CO_2 group in June 1995 and received very positive feedback within the scientific community. For a number of reasons the proposed cruise leg was perfectly suited for such an exercise. Funding of the exercise came through the German Joint Global Ocean Flux Study (JGOFS) program. More than fifteen research groups, representing a fairly good geographical distribution, were contacted and invited to participate in the exercise, nine of which were finally able to do so (Körtzinger et al. 1996a).

1.2 THE PRINCIPAL DESIGN OF THE EXERCISE

The basic idea of the exercise was to operate as many underway fCO_2 systems simultaneously for as much time as possible. Combined with in situ salinity and temperature as well as navigational and meteorological data, this combined underway fCO_2 data set is the mainstay of the exercise. Whereas shore-based intercomparison exercises allow researchers to devise special experiments that reflect extreme situations, ship-based exercises have to rely fully on the conditions that are provided by the ocean. The chosen cruise track reflects the attempt to include—within the limits of a single and comparatively short cruise—extreme oceanic regimes. Whereas the situation was very stable in the Eastern North Atlantic with not much variability in surface seawater temperatures and salinities and likewise fCO_2, the North Atlantic Drift region off Newfoundland provided extreme variability with steep gradients. The overall temperature range during the exercise was from 6.0°C to 25.1°C, while the salinity varied between 32.3 and 37.0. In the western part our cruise track hit warm and cold ring features. Associated with these rings were steep frontal gradients with changes of up to 15°C and more than 3 in salinity over a few nautical miles.

These different regimes provide different information about the performance and comparability of the participating systems. The stable situation during the second half of the exercise allows the detection of systematic offsets between the data sets, thus providing the basic information about the inter-laboratory comparability. In contrast to this, the strong gradient regime mimics to some extent the step experiments of shore-based intercomparison exercises. The fast change between two "batches" of seawater, which are characterized by different fCO_2 values, reveals the different time constants of the analytical systems. Fast responding systems are able to follow the signal much more closely than the more slowly responding ones. So, even if there are no systematic differences between two systems, the systems may have quite different response times, which translates into different spatial resolution in underway work.

Right from the beginning, it was regarded as high priority to measure as many parameters [i.e., pH, fCO_2, total dissolved organic carbon (C_T), and total alkalinity (A_T)] of the marine CO_2 system as possible rather than restricting the exercise to mere fCO_2 measurements. For this purpose, we followed two different sampling strategies (i.e., underway sampling and discrete sampling). As all participating fCO_2 systems (CSIRO, IfMK, MRI, NBI, OU, UP&MC, WHOI; see Sect. 2.1.2 for a list of participating institutions) were operated in an underway mode on the same seawater source, it was highly desirable to back up these fCO_2 measurements with additional underway measurements of other CO_2 parameters. This was accomplished by underway pH measurements with two different spectrophotometric systems (SIO, WHOI) as well as underway C_T measurements (BNL/IfMK) with a newly modified single-operator multiparameter metabolic analyzer (SOMMA) coulometric titration system (Johnson et al. 1998), all of which were hooked up to the seawater pumping system. Discrete sampling was carried out for discrete measurements of fCO_2 (BNL), C_T (BNL/IfMK), A_T (IfMK), and salinity (IfMK) as well as nutrients (IfMK) in samples taken regularly from the same seawater pumping system.

By measuring more than two parameters of the CO_2 system in seawater, the system is overdetermined, as all parameters can be calculated from any combination of two measured parameters and knowledge of the thermodynamic relationships involved. This was the case for both sampling strategies. Overdetermination will therefore allow for consistency checks on the data sets. It may also provide additional information in the question of the best set of thermodynamic constants for the CO_2 system. The broad CO_2 database furthermore serves as valuable background information and will strongly enhance further interpretation of the results.

The exercise also included checks on ancillary measurements, such as temperature and barometric pressure, as performed by most of the analytical systems. All temperature sensors were compared against a calibrated Pt-100 reference thermometer. The barometric pressure readings were also referenced against a high-quality digital barometer. In many cases, these checks revealed offsets and miscalibrations, which, if not corrected for, would have led to significant biases of the final fCO_2 values. These checks helped to identify the error contribution from these sources. They also allowed us to correct all fCO_2 measurements for these effects to reveal any systematic differences that cannot be attributed to the quality of temperature and pressure measurements.

Further checks were carried out with the calibration gases. The suite of calibration gases supplied by the organizer covered a range of CO_2 concentrations between 250 and 500 ppmv with nominal values of 250, 300, 350, 400, 450, and 500 ppmv. While every group required one or more of these calibration gases for their calibration procedure, they measured all other concentrations as unknown samples on their systems. The results provide information on the quality and reliability of the calibration procedures over the whole range from 250 to 500 ppmv. As the infrared detectors used by all groups generally show nonlinear response functions, the calibration procedure is a crucial point.

2. DESCRIPTION OF THE EXERCISE

2.1 THE CRUISE

2.1.1 R/V *Meteor*, Technical Details and Brief History

The R/V *Meteor* is owned by the Federal Republic of Germany, represented by the Ministry for Education, Science, Research and Technology (BMBF), which financed its construction. It is operated by the German Research Foundation (DFG), which provides about 70% of its operating funds (the remainder is supplied by the BMBF). The Senate Commission for Oceanography of the DFG plans expeditions from the scientific viewpoint and appoints cruise coordinators and chief scientists. The Operations Control Office of the University of Hamburg is responsible for management, logistics, execution, and supervision of ship operations. These functions are exercised by direct cooperation with expedition coordinators and the managing owner, the Reedereigemeinschaft Forschungsschiffahrt GmbH (RF). The latter is responsible for hiring, provisioning, and coordinating ship maintenance. Designed as a multipurpose vessel for living and

nonliving resources and worldwide operation, the R/V *Meteor* routinely carries scientists from many different countries. The basic technical details are

Port of registration	Hamburg
Call sign	DBBH
Classification	GL + 100 A4 E2 + MC Auto
Operator	University of Hamburg, Institute for Marine Research
Managing owner	RF Reedereigemeinschaft Forschungsschiffahrt GmbH, Bremen
Built	1985/86 at Schlichting Werft, Travemünde, Germany
Basic dimensions:	
Gross registered tonnage	4280 t
Net registered tonnage	1284 t
Displacement	4780 t
Length overall	97.50 m
Beam	16.50 m
Draught max.	5.60 m
Service speed	12 kn
Personnel	Crew: 32, Scientists: 28, German Weather Service: 2
Main engine	4 × Mak 6 M 332 = 4 × 1000 kW at 750 rpm
Propulsion	Diesel-electrical, tandem motor = 2 × 1150 kW
Maneuvring propulsion devices:	Special rudder with flap, type Becker FKSR Omnithruster-bowthruster 919 kW, 10 t thrust thwartships,
Fuel consumption	About 12 t IFO 80 per day at service speed
Maximum cruise duration	60 days
Nautical equipment	Integrated navigation system with data transfer to position computer, echo sounder synchronization and supervision, data processing facility
Science quarters	20 laboratories on the main deck with approximately 400 m^2 working space for multidisciplinary research. Air chemistry lab above the wheelhouse. About 400m^2 of free deck working area, mainly with timber planking. Very little vibration and noise achieved by special construction.

Meteor (I) was built in 1915 in Danzig as a gunboat for the German navy. However, it never reached completion as such and remained in an unfinished state until 1925, when it was converted in Wilhelmshaven to the first German research and survey vessel of that name. The steel-hull ship *Meteor* (I) had a length overall of 71.15 m, a displacement of 1179 t, and carried a crew of 122 plus 11 scientists. One of its first expeditions was the German Atlantic Ocean Expedition of 1925-27, which was organized by the Institute for Marine Research in Berlin. Thereafter, the vessel was used until 1934 for German physical, chemical, and microbiological marine investigations and for navy surveying as well as fishery protection duties.

Meteor (II) was carefully planned after the 1950s; it was jointly operated by the German Research Foundation (DFG) in Bonn and the German Hydrographic Institute

(DHI) in Hamburg. With a length overall of 82.10 m and a displacement of 3054 t, the second *Meteor* carried 52 in crew and 24 scientists. Commissioned in 1964, *Meteor* (II) participated in the International Indian Ocean Expedition. During 73 voyages between 1964 and 1985, the *Meteor* (II) sailed a total distance of about 650,000 nm to all parts of the world's oceans.

Meteor (III), used during the intercomparison exercise described here, was completed in 1986, replacing *Meteor* (II). Based in Hamburg, it is used for German marine research worldwide and for cooperative efforts with other nations in this field. The vessel serves scientists of all marine disciplines in all of the world's oceans.

2.1.2 R/V *Meteor*, Cruise 36/1 Information

Ship name	*Meteor*
Cruise/leg	36/1
Location	Hamilton, Bermuda, to Las Palmas, Gran Canaria, Spain
Dates	June 6–19, 1996
Chief scientist	D. Schulz-Bull, Institute of Marine Research, Kiel
Master	M. Kull

Institutions Participating in the Exercise

BNL	Brookhaven National Laboratory, Department of Applied Science, Upton, Long Island, New York, U.S.A.
CSIRO	Commonwealth Scientific and Industrial Research Organisation, Division of Oceanography, Hobart, Tasmania, Australia
IfMK	Institut für Meereskunde Kiel (Institute of Marine Research at the University of Kiel), Kiel, Germany
MRI	Meteorological Research Institute, Tsukuba, Japan
NBI	Niels Bohr Institute for Astronomy, Physics and Geophysics, University of Copenhagen, Copenhagen, Denmark
OU	Okayama University, Okayama, Japan
SIO	Scripps Institution of Oceanography, Marine Physical Laboratory, La Jolla, California, U.S.A.
UP&MC	Université Pierre et Marie Curie, Laboratoire de Physique et Chimie Marines, Paris, France
WHOI	Woods Hole Oceanographic Institution, Department of Marine Chemistry and Geochemistry, Woods Hole, Massachusetts, U.S.A.

Parameters measured	Institution	Principal investigators
Conductivity-temperature-depth (CTD), salinity, expendable bathythermograph (XBT)	IfMK	J. Waniek
Nutrients	IfMK	D. Schulz-Bull, A. Körtzinger
Oxygen	IfMK	D. Schulz-Bull, A. Körtzinger
Total dissolved inorganic carbon (C_T)	BNL, IfMK	K. Johnson, A. Körtzinger
Alkalinity (A_T)	IfMK	L. Mintrop
pH	WHOI	C. Goyet
	SIO	A. Dickson
	BNL	D. Wallace
Fugacity of CO_2 (fCO_2)	CSIRO	B. Tilbrook
	IfMK	A. Körtzinger
	MRI	H. Inoue
	NBI	R. Torres
	OU	E. Ohtaki
	UP & MC	A. Poisson
	WHOI	C. Goyet

2.1.3 Brief Cruise Summary

After completion of the previous cruise 35/4, the R/V *Meteor* reached Hamilton, Bermuda, on June 4, and Detlev Schulz-Bull (IfMK) relieved Dieter Meischner (University of Göttingen, Germany) as chief scientist. A reception for invited officials of governmental and scientific institutions as well as private companies was held on board the *Meteor* on June 4. The scientific party of cruise 36/1 embarked on June 5. Equipment setup began on the same day. The R/V *Meteor* departed Hamilton at 9:00 a.m. local time on June 6, 1996.

The cruise track of cruise 36/1 (Fig. 1) ran on straight lines from Bermuda to the Flemish Cap off Newfoundland, Canada, and then to Gran Canaria, Spain. The turning point was located at 46° 40′ N, 41° 54′ W. All seven underway pCO_2 systems were operated simultaneously for most of the time between June 7 and June 17. Small technical problems that occurred to some of the systems only caused short interruptions. Only one system suffered major problems: heavy damage to the infrared gas analyzer caused this system to cease operating on June 13. The two underway spectrophotometric pH systems were operated throughout the cruise. The newly modified coulometric SOMMA system for underway determination of C_T was tested successfully at sea and contributed about 450 high-quality underway C_T measurements along the cruise track (Johnson et al. 1998). Synchronized with the XBT survey, a total of 57 discrete samples were taken from the seawater supply and were analyzed for pH, C_T, and A_T. The discrete fCO_2 measurements could not be carried out on the same schedule; samples were taken for this parameter only at about 17 stations.

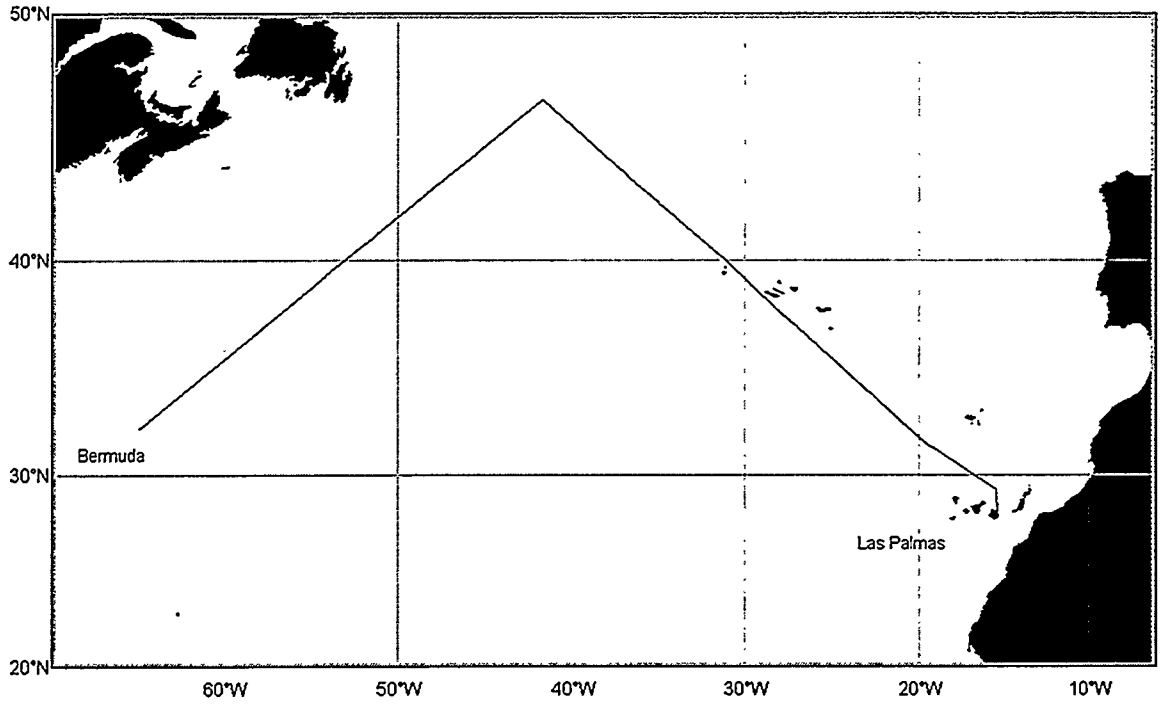

Fig. 1. Cruise track of R/V *Meteor* Cruise 36/1 from Hamilton, Bermuda to Las Palmas, Gran Canaria, Spain.

In addition to the various surface measurements (whether continuous or discrete), five hydrographic stations were occupied during the cruise. Samples were drawn for measurements of all four CO_2 system parameters (pH, fCO_2, C_T, A_T) thus yielding the highest possible overdetermination of the marine CO_2 system. The R/V *Meteor* arrived at Las Palmas, Gran Canaria, Spain, on June 19, 1996. Weather and sea conditions had been excellent throughout the cruise allowing for uninterrupted scientific work.

2.2 TECHNICAL ASPECTS OF THE EXERCISE

2.2.1 The Underway Pumping System

The intercomparison exercise was almost entirely based on continuous underway sampling of surface seawater. All participating groups operated their underway fCO_2 systems simultaneously on the same seawater pumping system. Like most up-to-date research vessels, the R/V *Meteor* provides a special seawater pumping system for scientific purposes. However, from experience, it is known that the use of this kind of pumping system for measurements of dissolved gases may be hampered by a number of problems. Pump action may cause cavitation when underpressure is applied to the water flow, thus making undisturbed gas measurements nearly impossible. Because of the location of the seawater intake close to the bow on R/V *Meteor*, air bubbles are introduced into the water lines in a rough sea. This again possibly biases the

concentration of dissolved gases or even makes seawater sampling technically impossible in such cases. Furthermore the unavoidable warming of seawater during its travel from the bow intake to the user may be quite significant. In the case of the fCO_2 intercomparison exercise, it was desirable to keep the temperature change as small as possible.

As a result of the sluggish exchange of CO_2 between the gas phase and the water phase, sampling for CO_2 measurements (e.g., fCO_2, pH, C_T) is less susceptible to biases caused by inadequate pumping techniques than is sampling of reactive gases like oxygen. Nevertheless a careful sampling technique was an important aspect of the exercise. For this reason, a simple and reliable underway pumping system (see also Körtzinger et al. 1996b) was designed for use in the "moon pool" of R/V *Meteor*. The system consisted of a small CTD probe (ECO type, ME Meerestechnik-Elektronik GmbH, Trappenkamp, Germany) for measuring in situ seawater temperature and salinity at the intake as well as a submersible pump, both of which were installed in the shell plating at the bottom of the "moon pool." Figure 2 shows a schematic drawing of this underway pumping system. The system also includes a separate Global Positioning System (GPS) receiver (GPS 120, Garmin/Europe Ltd., Romsey, Hampshire, U.K.). Navigational data from the GPS system as well as CTD data were continuously logged on a computer.

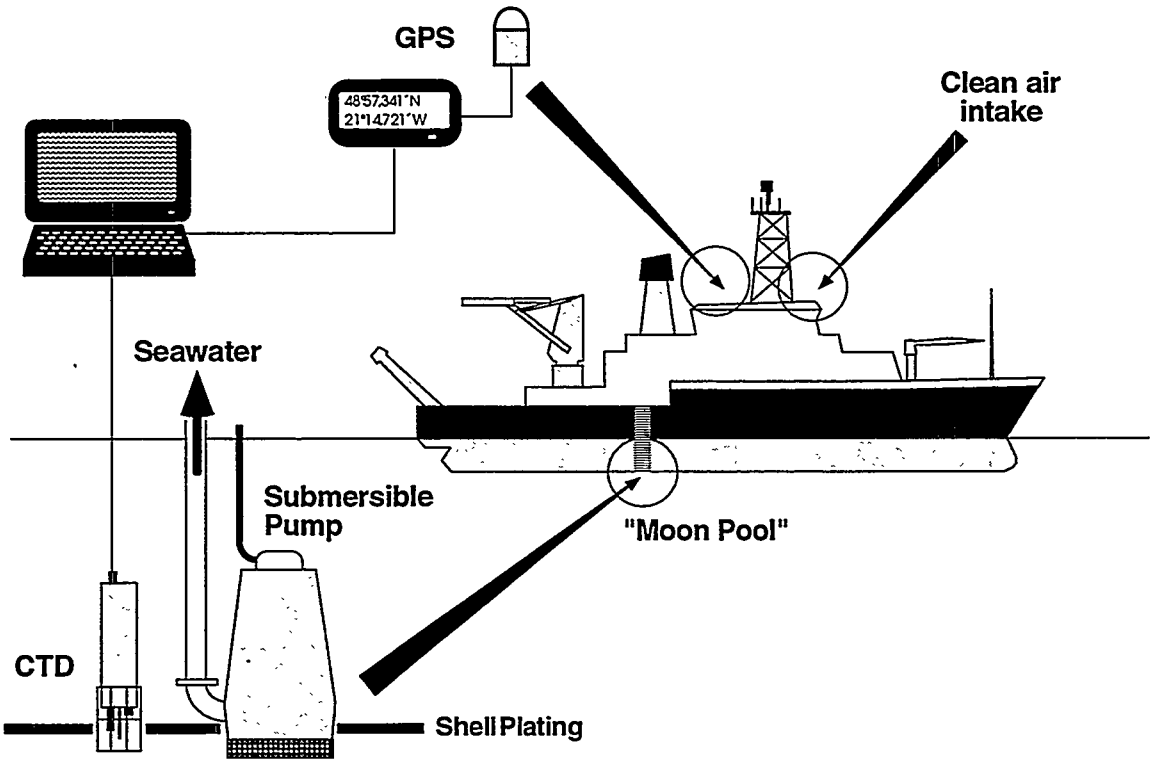

Fig. 2. Schematic diagram of the underway pumping system for use in the moon pool of research vessels as used during the intercomparison exercise. All underway systems were connected to this system.

The moon pool of R/V *Meteor* is specially designed for sampling purposes so that no cooling or wastewaters are emitted ahead of it and even at full speed or in a very rough sea no air bubbles reach it. Seawater was pumped through the moon pool from below the ship by means of a large submersible pump (multivane impeller pump, type CS 3060, ITT Flygt Pumpen GmbH, Langenhagen, Germany) at a pumping rate of about 350 L/min (pump head approx. 12 m). The CTD probe was installed next to the submersible pump. All underway fCO_2 systems were assembled in the geology lab of R/V *Meteor* (see Sect. 2.2.2). Two seawater supply lines (port and starboard) were teed-off from the main bypass and laid through the lab. All underway systems were hooked-up to these supply lines which delivered the necessary flow rates of seawater to each system (approx. 1–15 L/min).

The wastewater from the systems was collected in three 100-L carboys and from there was disposed of continuously through the floor drains of the geology lab. In case of (occasionally observed) clogging of the lab's floor drains as a result of rough sea conditions, small submersible pumps (multivane impeller pump, type GS 9565, ITT Flygt Pumpen GmbH, Langenhagen, Germany) were at hand to pump the wastewater actively out of the lab. These pumps did not have to be used during this cruise, however.

2.2.2 The Laboratory Setup

During cruise 36/1 four labs were reserved for the intercomparison exercise (Fig. 3). All underway systems were assembled side by side in the geology lab (no. 16), the largest lab on the R/V *Meteor*. It is located on the main deck, starboard side, with direct access to the working deck. Adjacent to the geology lab is the universal lab (no. 15, not shown in Fig. 3), where the dynamic transformer was installed. The SOMMA coulometric analyzer for C_T and the alkalinity titration system were installed in the clean lab (no. 4, not shown in Fig. 3) on the port side of the ship. The moon pool is located in the hold (Lab 17) for the CTD rosette. This lab is very close to the main lab of the exercise (Lab 16) thus allowing for short water lines of the seawater pumping system.

2.2.3 Other Infrastructure of the Exercise

In addition to the common seawater line (Sect. 2.2.1), a common supply of calibration gases was regarded a key requirement for the exercise, as otherwise systematic errors most likely would have been introduced. We therefore provided a whole suite of calibration gases. Fifteen cylinders with precisely known amounts of CO_2 in natural dry air covering a nominal concentration range from 250 ppmv to 500 ppmv were purchased from the National Oceanic and Atmospheric Administration (NOAA) Climate Monitoring Diagnostics Laboratory (CMDL) in Boulder, Colorado, U.S.A. Before final filling, all aluminum standard cylinders (Scott Specialty Gases Inc., Plumsteadville, Pennsylvania, U.S.A.) undergo a conditioning period of at least one week with clean ambient air. To prepare the standards, the cylinders are filled with ambient air at Niwot Ridge, Colorado. The air is dried using magnesium perchlorate and either scrubbed with Ascarite or spiked with a 10% CO_2-in-air mixture to obtain mixing ratios below or above

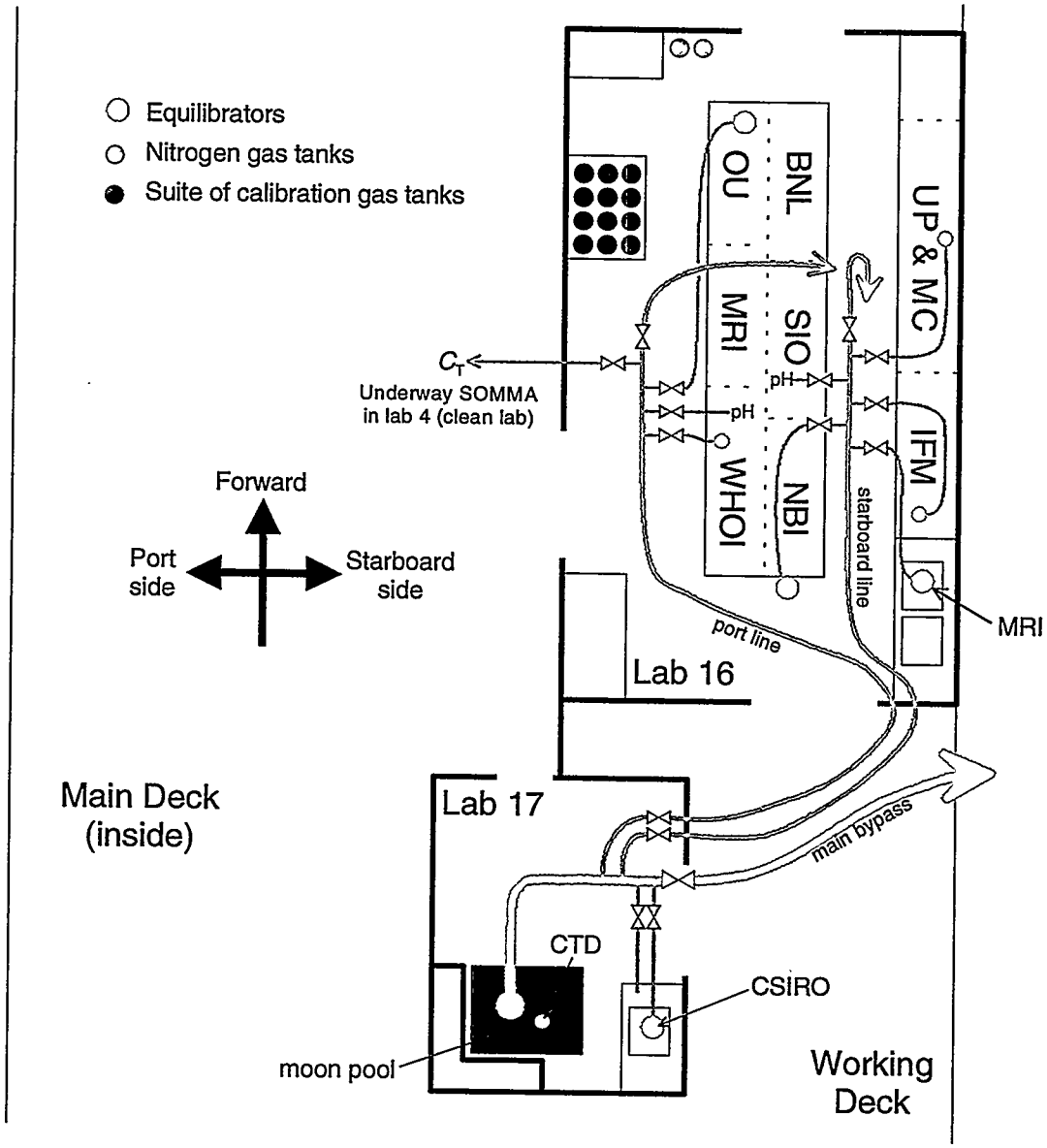

Fig. 3. Schematic diagram of the lab situation on R/V *Meteor* during the intercomparison exercise. The diagram is drawn to scale. All underway systems were assembled in Lab 16. The moon pool of R/V *Meteor* is located in Lab 17.

ambient levels, respectively (Zhao et al. 1997). Six cylinders of this consistent suite of gases were used during the exercise by all groups for calibrating their instruments. Additionally nitrogen (purity 99.999%) was used by some groups for zeroing their gas analyzers.

The mixing ratios of CO_2 in the cylinders were calibrated in the NOAA/CMDL Carbon Cycle Group laboratories on three separate days over a period of 2–3 weeks. The results of these calibrations are summarized in Table 1. The CO_2 mixing ratios are

reported as micromoles per mole (μmol/mol = ppmv) of dry air in the World Meteorological Organization (WMO) X85 mole fraction scale, traceable to primary standards at the Scripps Institution of Oceanography (SIO). The NOAA/CMDL calibrations are done by comparison on a nondispersive infrared CO_2 analyzer against four tertiary standards with assigned mixing ratios traceable to SIO (Thoning et al. 1987; Zhao et al. 1997). The uncertainty of the assigned values for the tertiary standards is approximately 0.06 ppmv. The tertiary set of standards used ranges between 250 and 450 ppmv CO_2. The repeatability of the NOAA/CMDL calibrations depends on the stability of the CO_2 mixing ratio in the cylinder and the fit of the analyzer response to the known tertiary standards. For cylinders that are stable and within the range of standards, the repeatability is on the order of 0.01 ppmv. The overall uncertainty associated with precision is therefore about 0.06 ppmv. When calibrating cylinders at the extremes of the tertiary standards or extrapolated outside the range, the reproducibility decreases. For mixing ratios above 450 ppmv, the reproducibility is on the order of ±0.3 ppmv and further decreases with the interpolation away from the tertiary standards. The absolute accuracy of the assigned mixing ratios is determined by the accuracy of the SIO standards (Keeling et al. 1986, and references therein).

Table 1. Summary of calibration results for six cylinders with CO_2 in natural dry air. The measurements were carried out at the NOAA/CMDL Carbon Cycle Group Laboratory in Boulder, Colorado, U.S.A. These six cylinders constitute the suite of calibration gases used by all participating groups during the exercise.

Cylinder #	Date of measurement (MM/DD/YY)	Measured CO_2 concentration (ppmv)	Average CO_2 concentration (ppmv)	Standard deviation (ppmv)
2178	03/06/96	252.42		
2178	03/11/96	252.46		
2178	03/14/96	252.45	252.44	0.02
1996	02/22/96	298.43		
1996	03/07/96	298.47		
1996	03/18/96	298.42	298.44	0.03
2172	02/05/96	349.53		
2172	03/14/96	349.52		
2172	03/18/96	349.51	349.52	0.01
1980	03/05/96	403.85		
1980	03/11/96	403.84		
1980	03/13/96	403.87	403.85	0.02
2186	02/27/96	450.69		
2186	02/29/96	450.68		
2186	03/13/96	450.73	450.70	0.03
2112	04/10/96	511.28		
2112	04/15/96	511.61		
2112	04/19/96	511.60	511.50	0.19

According to the different power requirements of the analytical systems, the ship provided three different power sources, the standard 220V/50Hz system as well as two additional systems for 110V/50Hz (static transformer) and 110V/60Hz (dynamic transformer).

3. METHODS AND PROCEDURES

3.1 PRINCIPLE OF MEASUREMENT OF THE FUGACITY OF CO_2

The principle of the measurement of the fugacity of CO_2 (fCO_2) in seawater is based on the determination of the CO_2 mixing ratio in a gas phase that is in equilibrium with a seawater sample at known temperature and pressure. The CO_2 mixing ratio can either be measured with a nondispersive infrared analyzer (NDIR) or with a gas chromatograph (GC) with flame ionization detector after catalytic conversion of the CO_2 into methane. Whereas the GC approach has a few advantages (e.g., small sample volume and the ability to measure additional trace gases), the more rugged infrared technique has shown better suitability for use at sea and allows measurements in a truly continuous fashion.

Depending on the sampling strategy (*discrete* or *continuous*), two different families of analytical systems have been developed. For the determination of the fCO_2 in air that is in equilibrium with a *discrete sample*, a known amount of seawater is isolated in a closed system containing a small known volume of air with a known initial CO_2 mixing ratio. For the determination of the fCO_2 in air that is in equilibrium with a *continuous flow* of seawater, a fixed volume of air is equilibrated with seawater that flows continuously through an equilibrator.

Continuous (or underway) fCO_2 systems are more widely used in marine CO_2 research. They provide important information about the saturation state of seawater at the air–sea interface when operated on board research vessels with a continuous flow of seawater usually obtained by means of a shipborne pumping system.

3.2 PARTICIPATING UNDERWAY fCO_2 SYSTEMS

Throughout this report we present technical details as well as the results of the participating systems in a semi-anonymous fashion. The main reason for this is the fact that the results of the exercise cannot easily be extrapolated to the performance of any participating system in general. Strictly they are only representative for this single cruise. To avoid the erroneous association in the scientific community of the performance of a particular system during this exercise with the general performance of this system, we choose to report in this semi-anonymous fashion.

Seven underway fCO_2 systems, all of which are based on NDIR detection of CO_2, participated in this exercise. Most of these systems have received detailed descriptions in the literature, which can therefore be omitted here. Where such publications are available, they are reprinted at the end of this report (Appendix B). For two systems, however, this is not the case. One is the fCO_2 system of CSIRO which features a slightly smaller Weiss-type equilibrator and is otherwise quite similar to the other systems. The second one is a system that is manufactured commercially by a U.K. company (Challenger Oceanic, Haslemere, Surrey, U.K.). For details about the latter system, further information is available through the company's internet site (http://www1.btwebworld.com/challengeroceanic/index.html).

Whereas most of the underway fCO_2 systems are similar in the general design and principle of measurement, they are considerably different in detail. For quick reference, the main features of all underway fCO_2 systems are summarized in Table 2. All different equilibrator design principles (i.e., showerhead, bubbler, and thin film type) were represented by at least one system, with the majority being of the showerhead type. In most systems (except "D" and "F") these equilibrators are vented to the atmosphere and thus operated at ambient pressure. The volumes of water and air in the equilibrators cover a wide range from a few milliliters to 15 liters. This is also true for the flow rates of water (0–15 L/min) and air (0.17–0.8 L/min) through the equilibrators.

Table 2. Summary of main features of the underway fCO_2 systems "A" through "G" that participated in the exercise

	"A"	"B"	"C"	"D"	"E"	"F"	"G"
Equilibrator							
Design	Showerhead	Bubbler	Showerhead	Thin film[a]	Showerhead	Bubbler	Showerhead
Total volume	1000 mL	1400 mL	13.1 L	119 mL	11.0 L	36 mL	1200 mL
Water volume	500 mL	1000 mL	2.3 L	21 mL	10.0 L	18 mL	~75 mL
Air volume	500 mL	400 mL	10.8 L	98 mL	1.0 L	18 mL	500 mL
Water flow rate	4–6 L/min	2.0 L/min	8.0 L/min	2.0 L/min	10–15 L/min	0 L/min[b]	1.2 L/min
Air flow rate	0.2 L/min	0.8 L/min	0.5 L/min	2.0 L/min	0.5 L/min	0.17 L/min	0.18 L/min
Vented?	Yes	Yes	Yes	No[c]	Yes	No	Yes
CO_2 measurement							
Method	NDIR	NDIR	NDIR	NDIR	NDIR	NDIR	NDIR
Wet/dry?	Wet	Wet	Dry	Dry	Dry	Dry	Wet
Analyzer calibration							
No. of stand. gases	2	2	2	2	4	2[d]	2
Zero gas?	No	Yes	No	No	No	Yes	No
Measurement cycle							
Calibration frequency	6–8 h	6 h	6 h	4–6 h	1.5 h	15 min	2 h
Air measurement frequency	6–8 h	1 h	6 h	4–6 h	0.5 h	n/a	7 min
Interrogation interval	6 sec	6 sec	1 sec	10 sec	0.1 sec	15 min	0.33 sec
Averaging interval	1; 3 min	1 min	4 min	5 min	1 min	n/a	1 sec
Data points/interval	10; 30	10	240	33	600	1	3

[a]Film thickness approximately 0.75 mm.
[b]Semicontinuous approach.
[c]Vented only every 20 min.
[d]Standard gas generator is initially calibrated using all six calibration gases; linearity checks are carried out for every sample with only two calibration gases.

A further distinction can be made in whether the sample gas is measured dry or wet. The traditional procedure is based on NDIR measurement of the dried sample gas ("D," "E," and "F"). However, in four systems ("A," "B," "C," and "G") the sample gas is not dried prior to NDIR measurement. This is feasible on the basis of the LI-6262 CO_2/H_2O gas analyzer (Li-Cor Inc., Lincoln, Nebraska, U.S.A.) which is a dual-channel instrument that simultaneously measures CO_2 and H_2O mole fractions of the sample gas and provides internal algorithms for correction of the diluting and pressure-broadening effects of water vapor on the CO_2 measurement (McDermitt et al. 1993).

All NDIR instruments were calibrated with the NOAA/CMDL CO_2 standards provided by the organizer (Table 1). Because of the individual calibration procedures, different numbers of gases (2 to 4) were required. Some systems also required a zero gas (nitrogen, purity 99.999%) for calibration purposes or as a reference gas.

Whereas underway fCO_2 systems "A" through "E" and "G" are similar in that fCO_2 is calculated from the CO_2 mixing ratio in a gas phase that is in equilibrium with a constantly renewed seawater phase, system "F" is of a principally different design. Here, for every fCO_2 measurement, five aliquots of a discrete seawater sample (semicontinuous mode) are equilibrated with five different standard gases bracketing the observed range of seawater fCO_2. For each equilibration run, changes with time in the standard gas CO_2 concentration as a result of CO_2 exchange with the sample aliquot are recorded in terms of positive or negative deviations from the standard's initial CO_2 concentration. If flow conditions during these five equilibration runs are kept identical, the heights of the resulting deviation peaks are proportional to the concentration difference between the carrier gas and a gas that is in equilibrium with the sample. If peak heights are plotted *versus* the initial xCO_2 of the standard gases, the equilibrium xCO_2 can be found where a linear regression to the five data points intersects the x-axis.

Participating groups were asked to operate their systems according to their typical operation profile (i.e., frequency of calibration and air measurements, interrogation, and averaging intervals, etc.). This strategy was chosen to ensure that all systems were operated in modes to which they have been optimized in the field and in which their operators have gained the highest confidence. The consequence, however, was quite different averaging and/or reporting intervals for the different groups. In particular, the averaging intervals between 1 and 5 minutes have certain implications that need to be taken into account when the data are being compared. This inherent discrepancy of the whole data set represents a certain limitation for the temporal resolution to which the interpretation can be extended. This is discussed in more detail in the results section.

3.3 PARTICIPATING DISCRETE fCO_2 SYSTEM

The only discrete fCO_2 system ("H") involved in this intercomparison exercise is based on a batch-equilibration, static-headspace technique that requires a small sample volume of 60 mL and has an average analysis time of only 2 min per sample. It includes closed-system equilibration of a headspace in a shaking water bath, followed by analysis

of the CO_2 mole fraction in the water-saturated equilibrated headspace by gas chromatography with flame-ionization detection (GC-FID). The method has been described in detail by Neill et al. (1997). This paper is also reprinted in Appendix B at the end of this report. It should be noted that this method is not specifically designed for work in surface seawater but for full-depth profiling. The equilibration temperature (i.e., the water bath temperature) was changed two times during the exercise, from 17°C (June 10) to 20°C (June 11–13, first sample) and, finally, to 25°C (from June 13, second sample). The magnitude of the correction of fCO_2 from the temperature of equilibration to the in situ temperature was 44–133 µatm (mean: 89 µatm) for the samples presented here.

3.4 CHECKS AND CALCULATION ROUTINES

The main idea of the exercise was to compare the surface seawater fCO_2 data as measured by all participating instruments under identical conditions. This was to some extent accomplished by providing the infrastructure during the exercise, such as a common seawater and calibration gas supply (Sect. 2.2). The same care, however, that had been taken on the side of the logistical infrastructure was also advisable with respect to ancillary measurements as well as the calculation procedures involved in the computation of final fCO_2 values. This issue was addressed in different ways. In the following sections we describe the results of two different experiments: (1) a check of the performance of the calibration procedures for CO_2 (Sect. 3.4.1), and (2) a check of all temperature sensors that were used to measure the seawater temperature in the equilibrators (Sect. 3.4.2). We also describe the common procedure of the calculation of final fCO_2 values (Sect. 3.4.3) and of the synchronization of the final fCO_2 profiles (Sect. 3.4.4).

3.4.1 Check of CO_2 Calibration Performance

In order to check the performance of the individual calibration procedures, every group measured between one and four NOAA/CMDL CO_2 standards in the nominal concentration range of 250–500 ppmv as "unknown samples." Depending on the individual calibration procedure, different CO_2 standards were measured. Figure 4 shows the results of this exercise. It should be pointed out that this check was carried out on the last day of the exercise (June 17). Therefore no data are available for system "A," which had to prematurely quit the exercise on June 13 because of major technical problems. For system "C" only one standard could be measured because the measurement range had been fixed to an upper limit of 400 ppmv, which was slightly exceeded by the relevant NOAA/CMDL standard (403.85 ppmv). System "F" required all six standards for initial calibration, which could therefore not be measured as "unknown samples."

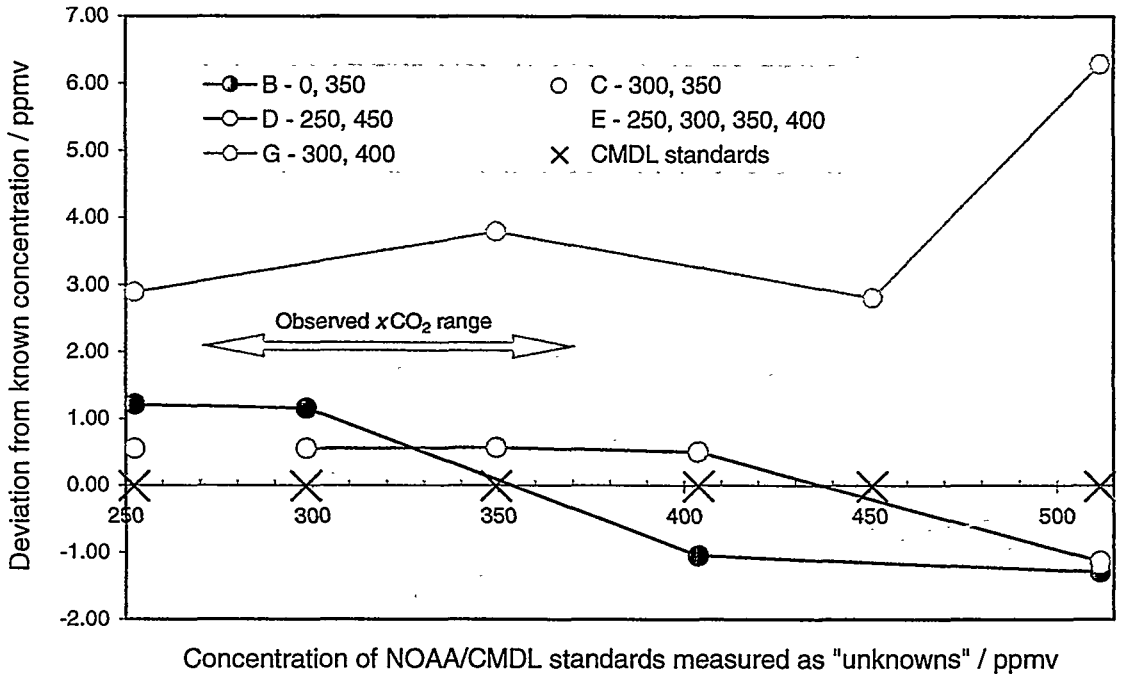

Fig. 4. Results from the check of the CO_2 calibration performance: Shown are the observed deviations from the concentrations of all measured NOAA/CMDL CO_2 standards. Pink crosses indicate the concentrations of the standards used in the exercise. The legend gives details of the nominal concentrations used for calibration. Also shown is the range of measured xCO_2 during the whole intercomparison.

The results show that essentially all checked NDIR instruments were calibrated to an accuracy on the order of 1 ppmv or better over the whole concentration range of 250 to 500 ppmv. Only system "G" shows deviations of 3 to 6 ppmv. This is indicative of a systematic problem associated with the calibration of the CO_2 analyzer or with the measurement itself. Such deviations are clearly not tolerable and need to be addressed thoroughly. System "B" makes use of the factory calibration of the LI-COR LI-6262 instrument, which only requires the adjustment of "zero" (with a CO_2-free gas) and "span" (with a single CO_2 standard). It appears that some accuracy is lost by this somewhat crude calibration technique,[1] and the "classical" approach using at least two CO_2 standards spanning the range of anticipated CO_2 mixing ratios is preferred.

[1]This problem has been shown to be very reproducible. The calibration routine of system "B" therefore includes a small correction for this error which routinely removes it from the final xCO_2 values of system "B." Figure 4 shows uncorrected xCO_2 values only to demonstrate the magnitude of this error if left unaccounted for.

3.4.2 Check of Equilibrator Temperature Sensors

In marine applications, fCO_2 results are generally reported at in situ seawater temperature ($T_{\text{in situ}}$). As the seawater temperature in the equilibrator during measurement (T_{eq}) usually deviates from $T_{\text{in situ}}$, a temperature correction needs to be applied. The size of this correction obviously depends on the choice of the parameterization (Sect. 3.4.3) and the size of the temperature deviation itself. As the fCO_2 strongly varies with temperature, measurements of $T_{\text{in situ}}$ and T_{eq} have to be made rather accurately. An error of 0.1°C in the resulting temperature deviation (T_{eq}–$T_{\text{in situ}}$) is equivalent to an error of about 0.4 % or 1.5 µatm in fCO_2 (at 350 µatm).

During the exercise, $T_{\text{in situ}}$ was measured with a CTD installed at the seawater intake in the bottom plate of the "moon pool" (see also Fig. 2). The CTD had been calibrated just before the exercise to an accuracy of ±0.05°C. These in situ temperature readings were used in the calculation of all fCO_2 data. In order to exclude possible errors contributed by inaccurate measurements of T_{eq}, all groups had their equilibrator temperature probes referenced against a recently calibrated platinum resistance thermometer (Pt-100) provided by WHOI. For every comparison, equilibrator probe and reference probe were kept together in a water bath until the readings had stabilized. In most cases this was done at three temperatures between 0°C and up to 30°C. Based on the deviation from the reference, an individual linear correction was calculated for every system and applied to its measurements of T_{eq}. In one case (lab "F"), the temperature probe could not be removed easily from the water bath surrounding the equilibrator and the reference probe had to be installed next to it in the bath thus yielding only a single measurement which was then treated as a uniform offset.

Figure 5 shows measured deviations and the resulting correction lines of only those temperature sensors which were used in the calculation of final fCO_2 values (some systems feature up to three equilibrator temperature sensors). The observed deviations are roughly between –0.5°C and +0.1°C with a clear tendency towards negative values and a negative slope of the linear correction line. If this inconsistency of the temperature measurements is not accounted for, differences of up to 2% or about 7 µatm (at 350 µatm) in the final fCO_2 values are caused as an artifact entirely the result of inaccurate temperature measurements.

Even though the CTD as well as the WHOI reference thermometer may themselves have been affected by some degree of miscalibration, the present procedure of referencing all measurements to these two temperature sources removes the incompatibility of all temperature readings to better than 0.1°C or 1.5 µatm. It should be pointed out that the observed deviations of up to 0.5°C are clearly above a tolerable level. Temperature readings have to be carried out with an accuracy of at least 0.1°C. Ideally they should be checked for consistency with the temperature probe used to measure in situ temperature.

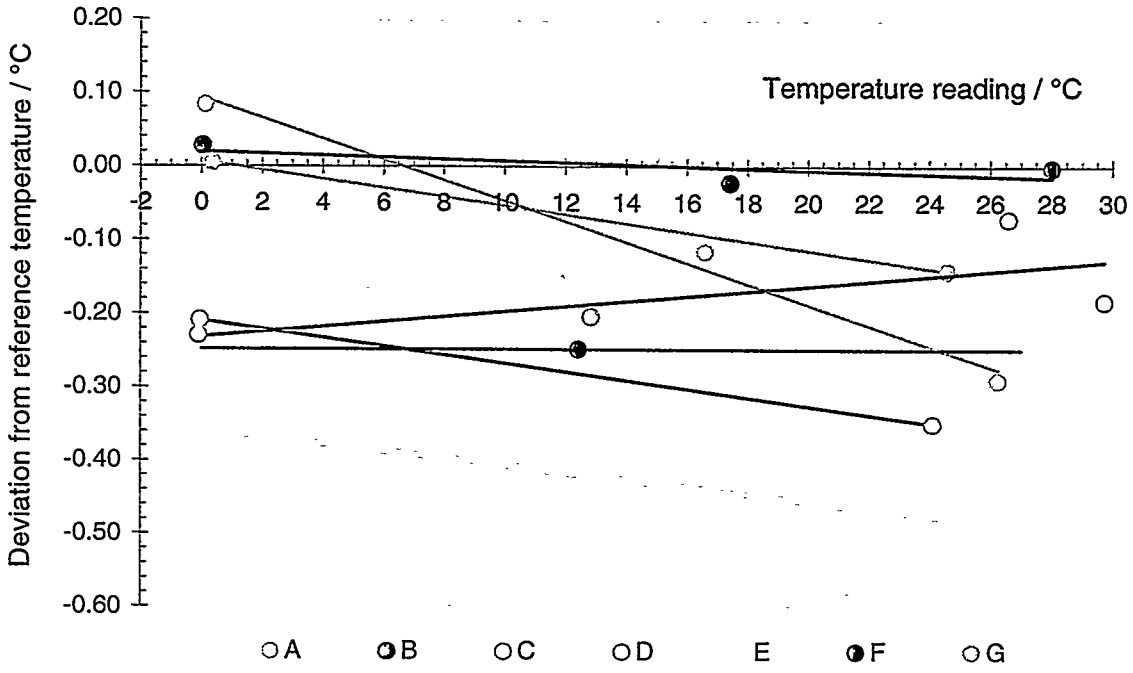

Fig. 5. Results of the check of the equilibrator temperature probes from systems "A" through "G": Shown are the deviations of the measured temperatures from the reference temperature. Equilibrator probe and reference probe were kept together in the same water bath until readings became stable. Also shown are the linear correction lines that were applied to temperature readings of that particular system.

3.4.3 Calculation of fCO_2 Results

The calculation of final fCO_2 values from the raw voltage readings of an NDIR analyzer involves a number of steps that are only briefly described here. More detail of the calculation procedure can be found in Appendix A and in the reprints of the pertinent literature section (Appendix B).

The NDIR detector signal depends on the number of CO_2 molecules in the optical path which, in turn, is mainly a function of pressure and temperature for a given CO_2 mixing ratio. The calculation procedure, therefore, requires temperature and pressure corrections to account for any fluctuations in these parameters as well as a calibration function. First the raw voltage readings are corrected to a standard pressure of one atmosphere (p^0) to account for fluctuations of the NDIR cell pressure. This requires continuous monitoring of the pressure in the cell. It has been found empirically (Welles and Eckles 1991) that pressure p affects the voltage signal v of NDIR analyzers in a linear fashion:

$$v' = v \cdot \frac{p^0}{p}$$

NDIR instruments are calibrated using standard gases with known CO_2 mixing ratios in dry air. The mixing ratio of a component gas (like CO_2) in a mixture of gases (like air) is equivalent to its mole fraction (xCO_2), assuming ideal behavior. The CO_2 mixing ratio of the standard gases should closely bracket the expected range of the sample xCO_2. Although the response of NDIR analyzers is considerably nonlinear, the use of a simple linear calibration function is generally justified over a small concentration range of 100–200 ppmv. The error incurred by this approximation is typically on the order of a few tenths of a ppmv. Furthermore any deviation of the NDIR cell temperature T from the calibration temperature T^0 has to be accounted for. Welles and Eckles (1991) have shown that the mole fraction xCO_2^* is scaled linearly with the inverse of the absolute temperature:

$$xCO_2 = xCO_2^* \cdot \frac{T}{T^0}$$

The resulting CO_2 mole fraction xCO_2 in dry air is temperature and pressure corrected. The latter because the sample gas is either measured dry (i.e., after full removal of water vapor) or has been arithmetically corrected for the diluting and pressure-broadening effects of water vapor based on simultaneous wet xCO_2 and xH_2O measurements. As the air at the air–sea interface can be assumed to be at 100% humidity, a correction has to be applied to account for the increase of the CO_2 mole fraction that is the result of the (actual or arithmetical) removal of water vapor prior to the infrared measurement. Here the saturation water vapor pressure of seawater at equilibrator temperature was calculated using an equation by Weiss and Price (1980), which is valid over the temperature range 273–313 K and the salinity range 0–40 (see Appendix A, Part 1).

For very accurate interpretations the non-ideal behavior of CO_2 should be taken into account (i.e., fugacity has to be used instead of partial pressure). As the results are to be used later for consistency checks, together with other parameters of the CO_2 system in seawater, we decided to use fCO_2. The calculation of the fCO_2 at equilibrator temperature from the measured mole fraction (xCO_2) in dry air is described in detail in Appendix A (Part 2). The fugacity coefficient (i.e., the ratio between fugacity and partial pressure of CO_2), is on the order 0.996 to 0.997 under typical conditions (p = 1 atm, T = 270–300 K, pCO_2 = 350 µatm). Barometric pressure readings from the shipborne meteorological sensor were used for all calculations of final fCO_2 data.

Because the fCO_2 in seawater strongly varies with temperature, the final step in the calculation of fCO_2 (in situ) requires a correction to compensate for any difference between the equilibration temperature and the in situ seawater temperature. Different equations have been proposed for the temperature dependence of CO_2 partial pressure/fugacity in seawater (e.g., Gordon and Jones 1973; Weiss et al. 1982; Copin-Montegut 1988, 1989; Goyet et al. 1993; Takahashi et al. 1993). Because temperature deviations were typically on the order of a few tenths of a degree for all systems during the exercise, the correction is rather small and the choice from the above suite of equations is not critical. We have chosen the equation based on temperature and salinity given by Weiss et al. (1982), which is valid for ranges of 0 to 36°C in temperature, 30 to

38 in salinity, and 80 to 2000 µatm in fCO_2 (see Appendix A, Part 3.). All temperature corrections of the fCO_2 measurements during this exercise are based on this equation.

3.4.4 Synchronization of Surface Measurements

Profiles of in situ temperature and salinity in surface seawater, as measured by the CTD probe at the seawater intake, and the different seawater fCO_2 profiles had to be matched and synchronized. Given the strong gradients in surface seawater temperature encountered during some periods of the cruise, this was very important for a reliable estimation of the differences between equilibrator and in situ temperatures. At the beginning of the exercise, all systems were switched to Universal Time Coordinated (UTC) time. The UTC time readings of all measurements are therefore the primary criterion for matching the data sets. However, UTC time alone would not produce a proper synchronization of the profiles for two reasons. The first is the different time the water travels from the seawater intake (where its temperature and salinity are being measured) to a given equilibrator (where the equilibration temperature is determined). This depends mainly on the individual flow rate of water and to some extent also on the location of the equilibrator in the supply line. By running two separate supply lines (port and starboard side line), which were kept at roughly the same total flow rate, we tried to make the supply flow characteristics comparable for all systems. With a single supply line, the ratio of water consumed for analyses to the water bypassing through this supply line would have changed more strongly en route with unknown implications for the water characteristics (such as the temperature deviation). With the chosen setup (see also Fig. 3), we tried to make the supply similar for all systems. The second, rather trivial, reason for an insufficient synchronization of the profiles based on UTC readings alone is that there are errors in the UTC readings themselves, which in some cases appear to account for 1 to 2 min during the course of the exercise.

The final matching of the profiles is based on the assumption that the profiles of in situ and equilibrator temperature should be connected by a fixed daily temperature offset. This is a first-order approximation, because the offset certainly depends on the stability of the water flow rate and the difference between seawater and ambient temperature. Flow rates were usually kept constant during the course of the exercise. The change in seawater temperature was significant, but its effect was minimized by matching the profiles on a daily basis. The matching procedure involved correcting every fCO_2 profile with daily time lags in 1-min steps until the standard deviation of the difference between in situ and equilibrator temperature reached a minimum. This could always be achieved by time lags of $\leq$3 min. In other words the fCO_2 profiles were shifted minute-wise backwards in time against the CTD readings until the two temperature profiles showed the best match with the smallest standard deviation of the resulting offset.

This procedure proved very necessary. Even a mismatch of 2 min could cause a bias in the calculated temperature difference of up to 1°C and more (i.e., $\geq$10 µatm) in the strong gradient regime. In the more stable regime, toward the end of the exercise the effect of this synchronization procedure is less pronounced or even negligible. On the other hand, the profiles could not be synchronized to better than 1 min, which still allows

errors of the order of several µatm in some cases only because of temporal mismatch. This is an important aspect which restricts the interpretability of the results during passage of the very strong gradients.

Even after correction of all equilibrator temperature readings and after this synchronization procedure, the remaining uncertainty is on the order of 2 µatm for the largest portion of the cruise. To put it the other way round, any differences of ≤2 µatm between the final fCO_2 profiles are not significant under the circumstances of this exercise. During passage of the strongest gradients, the overall uncertainty is definitely higher than 2 µatm, at least for short periods, and may account for a mismatch of up to 5 µatm.

4. RESULTS

4.1 SURFACE TEMPERATURE AND SALINITY

As said before, the cruise track of the R/V *Meteor* during the exercise (Fig. 1) was chosen in order to provide the largest possible range of surface temperatures and salinities in the whole area of the North Atlantic Ocean accessible during this rather short cruise. It was assumed that this track should likely provide more stable conditions in the eastern part as well as a highly variably situation at the northern turning point near the Flemish Cap off Newfoundland. This assumption was later verified to a full extent by the encountered ranges of surface temperature and salinity.

Figure 6 shows the large observed ranges in surface temperature and salinity as measured during the course of the exercise: Surface seawater temperatures ranged from 6.2°C to 25.1°C while surface salinities covered a range from 32.6 to 37.0. This is equivalent to a span of 19°C in temperature as well as 4.4 in salinity. It should be pointed out that the observed temperature and salinity drop around 51° W was as large as 2.9°C/min and 0.4/min for salinity, which is equivalent to 4.2°C/km and 0.9/km, respectively. Such gradients can be regarded as extreme situations that represent a "worst case scenario" for any kind of intercomparison rather than a typical open ocean situation. Toward the eastern part of the cruise track, a more typical regime was found that represents the standard case for at-sea operation. In order to provide the hydrographic background for the fCO_2 data, measurements of surface temperature and salinity are given as 1-min averages in daily figures (Figs. 7–9) for the period June 8–16.

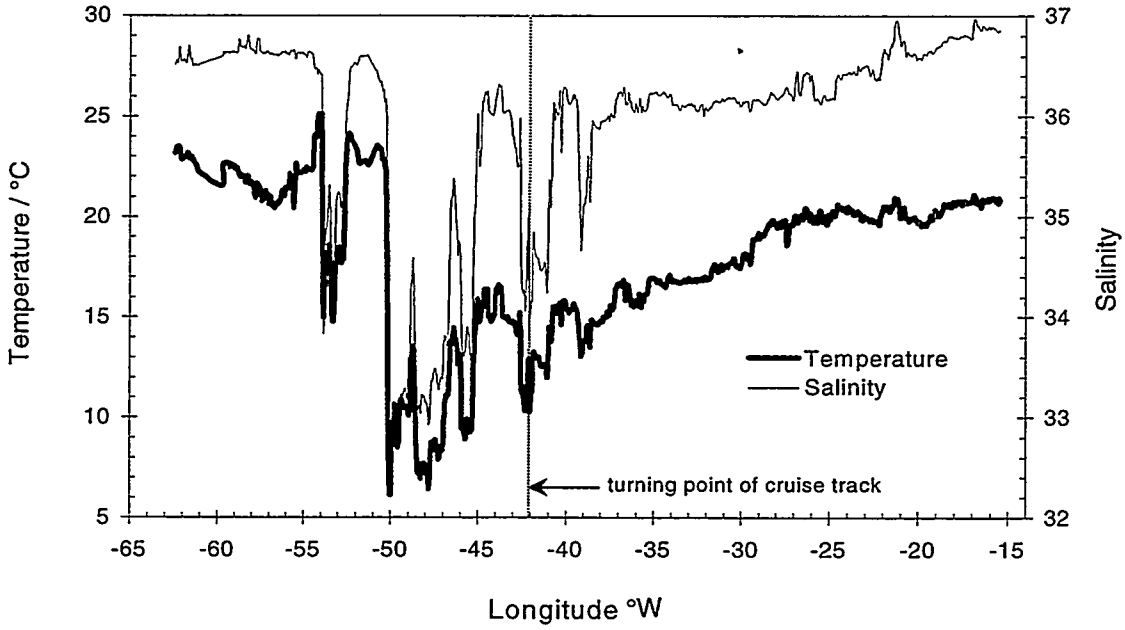

Fig. 6. Plot of surface temperature and salinity along the R/V *Meteor* Cruise 36/1 track from Hamilton, Bermuda, to Las Palmas, Gran Canaria, Spain. The dotted line around 42° W represents the northern turning point of the cruise track (see also Fig. 1).

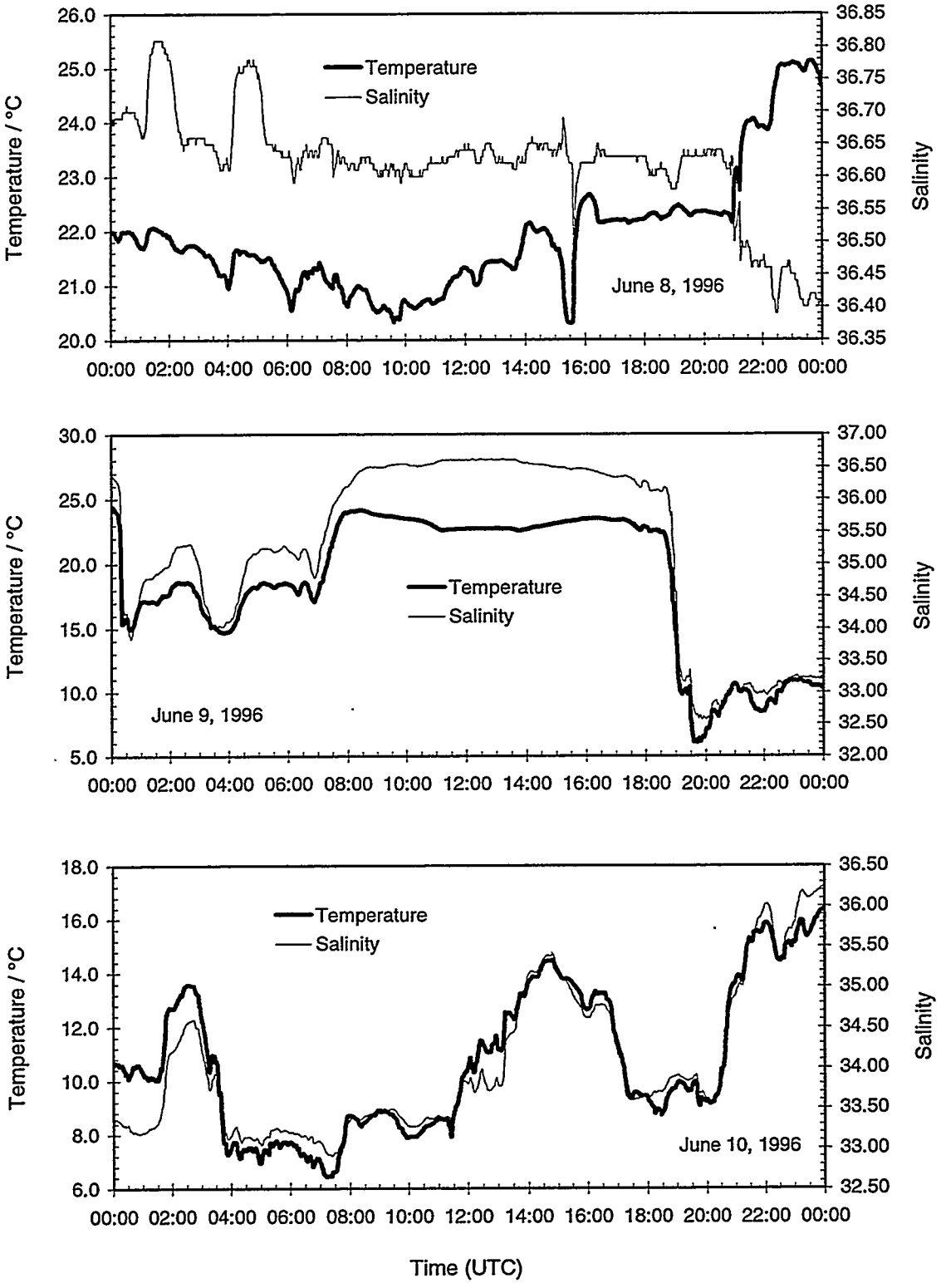

Fig. 7. One-minute averages of temperature and salinity of surface seawater from 5-m depth (at the seawater intake) along the R/V *Meteor* Cruise 36/1 track on June 8, 9, and 10, 1996. Please note the variable scales.

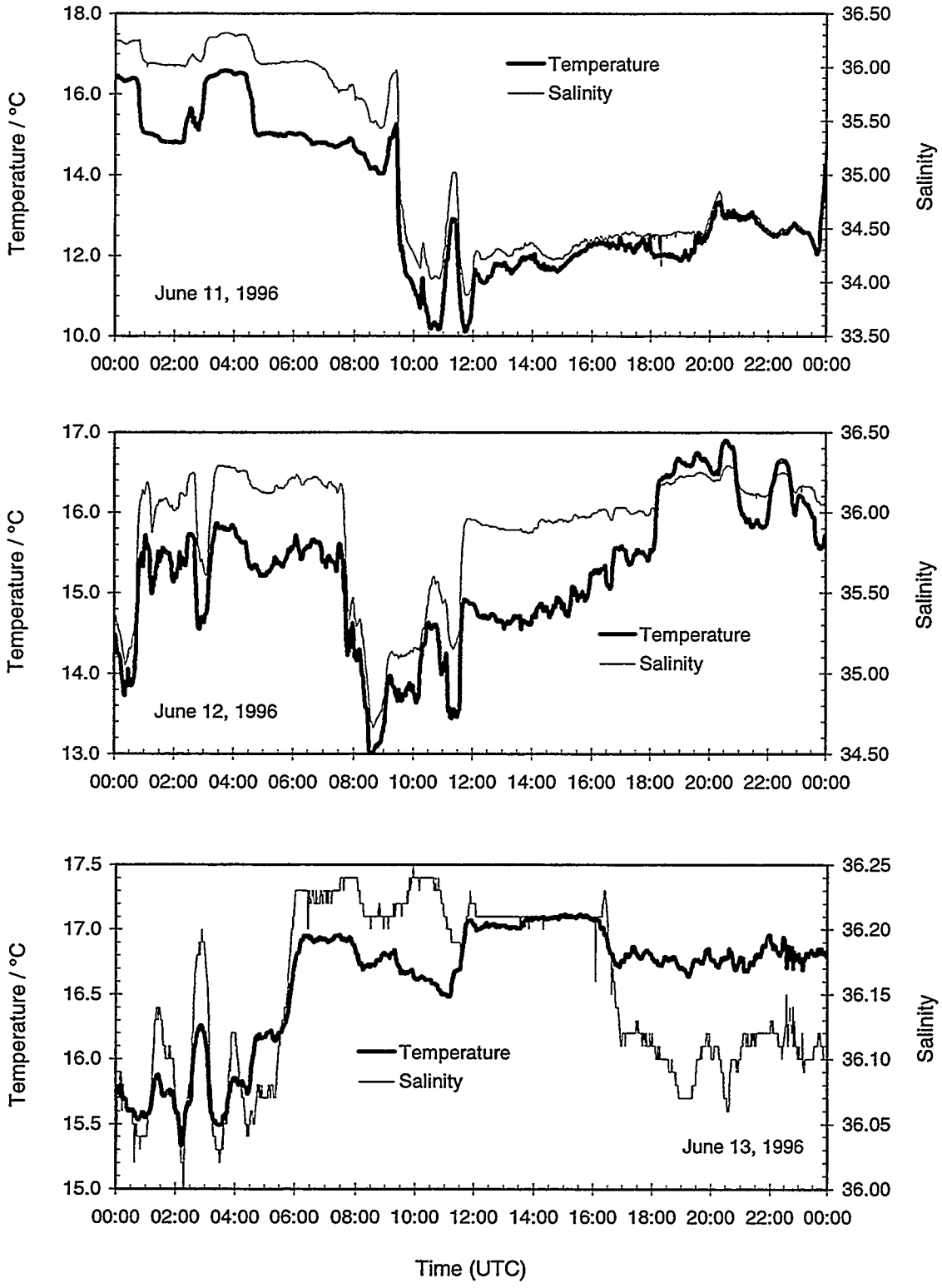

Fig. 8. One-minute averages of temperature and salinity of surface seawater from 5-m depth (at the seawater intake) along the R/V *Meteor* Cruise 36/1 track on June 11, 12, and 13, 1996. Please note the variable scales.

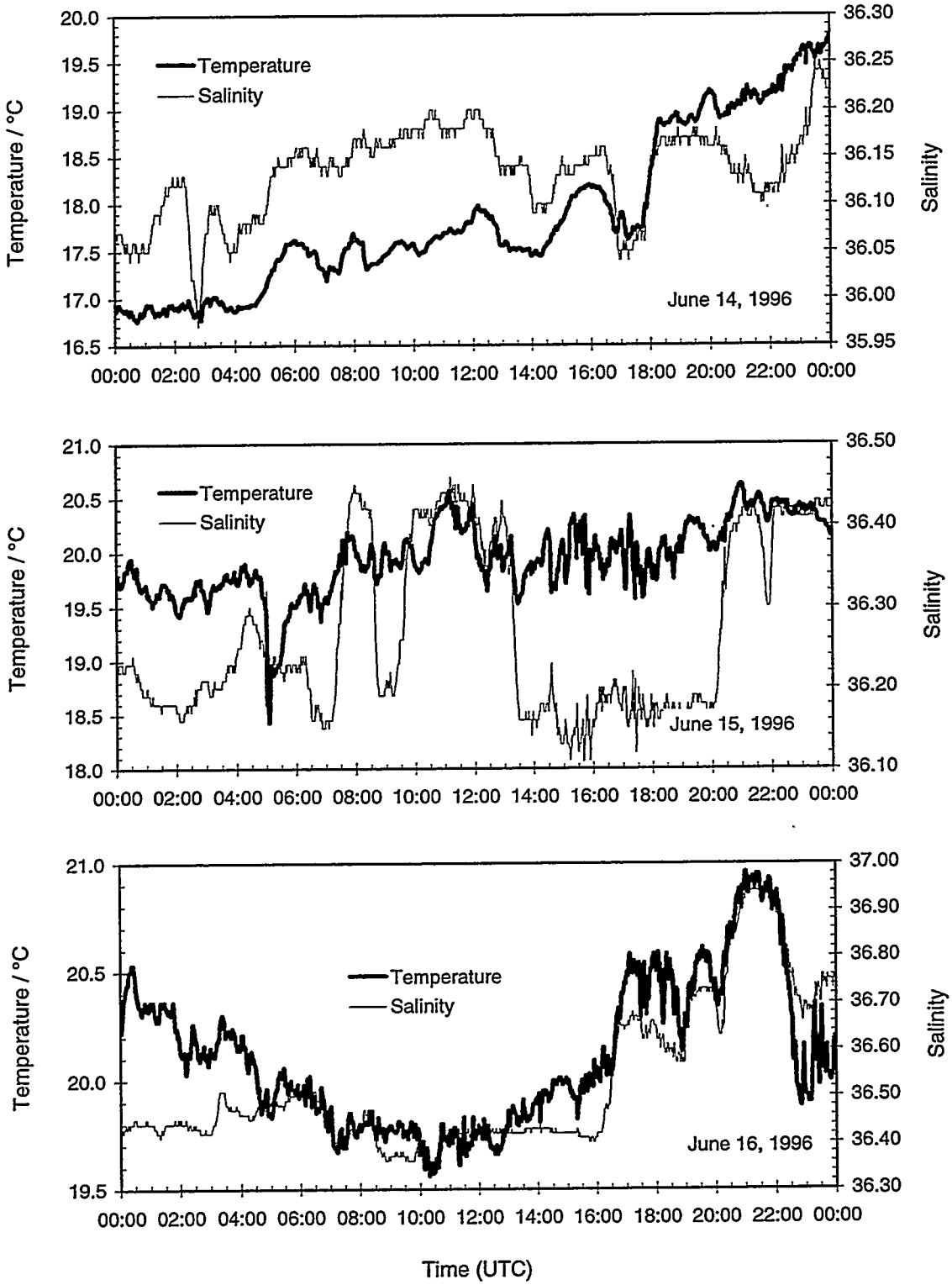

Fig. 9. One-minute averages of temperature and salinity of surface seawater from 5-m depth (at the seawater intake) along the R/V *Meteor* Cruise 36/1 track on June 14, 15, and 16, 1996. Please note the variable scales.

4.2 COMPARISON OF ATMOSPHERIC xCO_2 DATA

Measurements of the atmospheric xCO_2 were carried out by all underway fCO_2 systems except system "F" (see Table 2 in Sect. 3.2). As will be shown, the atmospheric xCO_2 data—while not immediate focus of this exercise—may still provide additional information for identifying likely sources of error in the surface fCO_2 profiles. All xCO_2 data are given (in ppmv) for dry air and shown in Fig. 10.

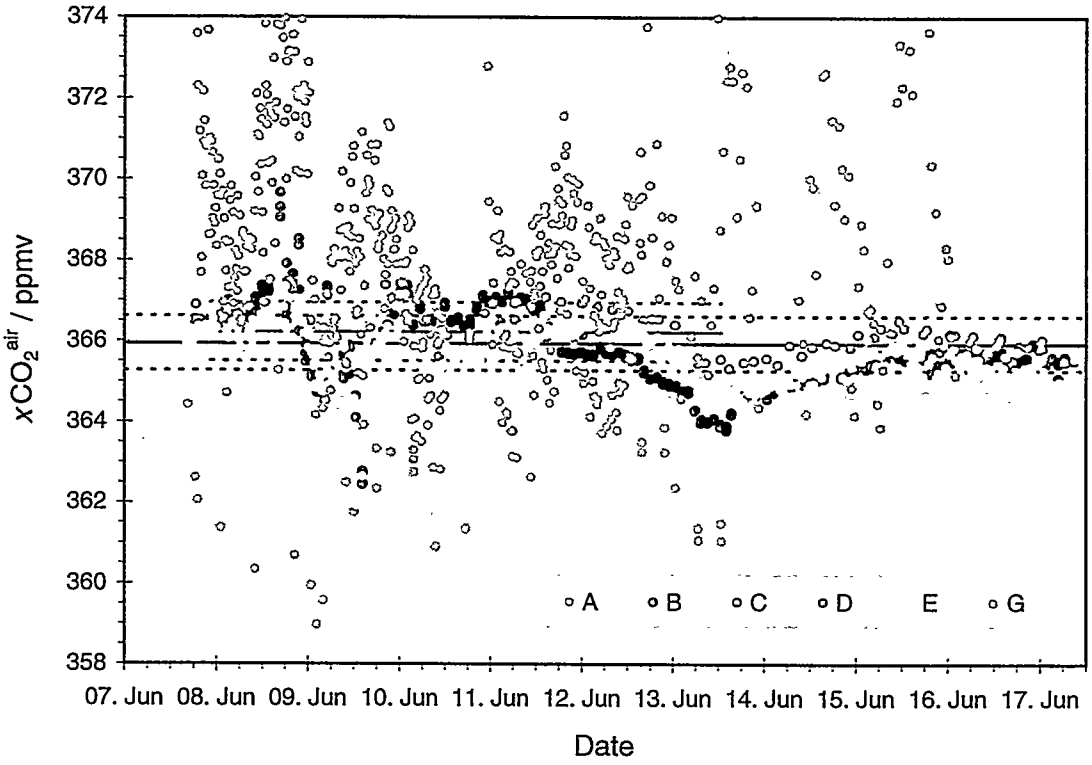

Fig. 10. Measurements of the CO_2 mole fraction in dry air [xCO_2 (air)] as carried out by laboratories "A" through "E" and "G" during the intercomparison exercise. The black horizontal lines represent the overall mean xCO_2 (air) value (±1 s.d.) calculated from profiles "B" through "E." The red horizontal lines represent the mean xCO_2 (air) value (±1 s.d.) calculated from profiles "B" through "E" only for the period where data from all six systems are available (June 7, 22:30 UTC, to June 13, 12:30 UTC).

Of the six data sets, four show good agreement to within ± 1 ppmv throughout the exercise: Profiles "C" and "D" show virtually identical values (except for a few data points), whereas profile "E" tends to values that are lower by –0.5 to –1 ppmv. Profile "B" is characterized by a somewhat variable behavior: For most of the time, "B" is in very good agreement with "E." However, from June 10, 08:30 UTC, to June 11, 14:30 UTC, "B" shows a positive offset of about 1 ppmv from "E," hereby agreeing perfectly with "C" and "D." In contrast, "B" deviates by –0.5 to –1.0 ppmv from "E" during the period from June 14, 14:30 UTC, until June 13, 18:00 UTC, which is

equivalent to an offset of –1.0 to –1.5 ppmv with respect to profiles "C" and "D." We have calculated a mean xCO_2 (air) of 366.21 ± 0.72 ppmv for the period of the exercise where data from all six systems are available from the means of profiles "B" through "E" which is shown in Fig. 10 (red line). Only results from this restricted period are used in the following comparison.

Two profiles ("A" and "G") are characterized by a much larger scatter which obscures the pattern of the atmospheric CO_2 contained in the other four profiles. This scatter is not a real property of the sampled air, as proved by profiles "B" through "E," and thus indicates an analytical problem associated with these systems. All air intakes were located on the same spot above the wheelhouse of R/V *Meteor* approximately 20 m above sea level, thus making differences in the properties of the sampled air very unlikely. The majority of measurements of "G" show a positive deviation of up to 8 ppmv which is consistent with the rather large positive offset of 3 to 6 ppmv determined during the checks of the CO_2 calibration performance (Sect. 3.4.1). The mean of "G" (368.27 ppmv) is 2.06 ppmv higher than the combined mean of "B" through "E" (366.21 ppmv). With a mean value of 362.89 ppmv, the xCO_2 measurements of "A" are clearly marked by a negative offset of 3.32 ppmv with respect to the mean of "B" through "E."

Figure 11 shows the individual mean and standard deviation of each data set as well as an overall mean calculated from the mean of profiles "B" through "E," all for the restricted period of time only. The individual standard deviations reflect the averaging

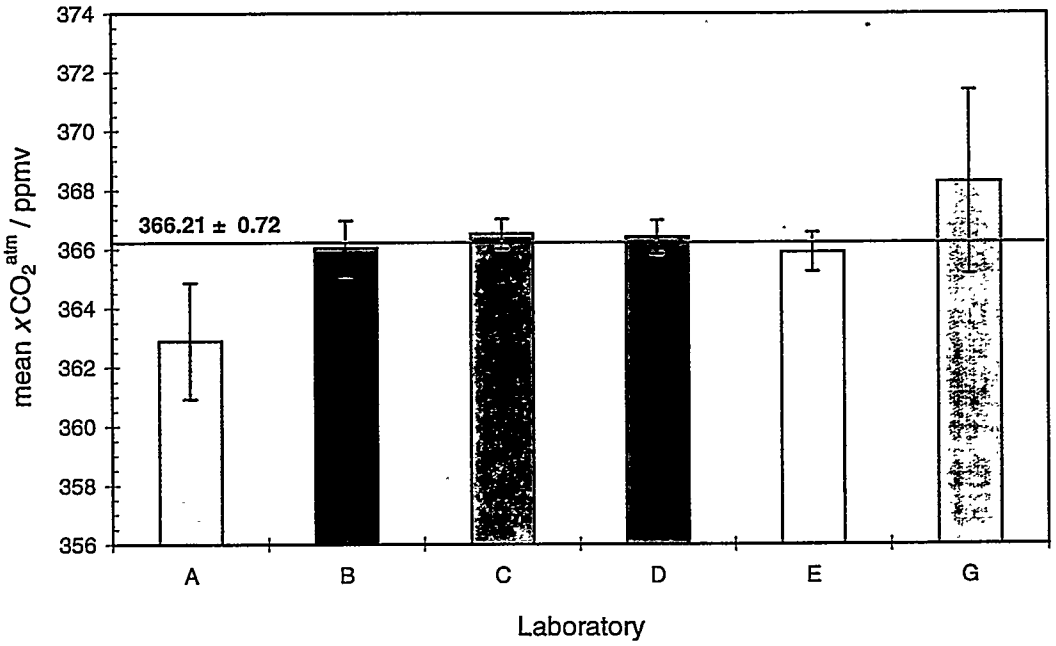

Fig. 11. Mean values of the CO_2 mole fraction in dry air [xCO_2 (air)] as measured by laboratories "A" through "E" and "G" during the period of the intercomparison exercise where data from all six systems are available (June 7, 22:30 UTC to June 13, 12:30 UTC). Also shown is the standard deviation of all xCO_2 (air) data sets from their mean. The horizontal line represents the mean xCO_2 (air) value calculated from the means of profiles "B" through "E" for this limited period of time.

interval in the case of laboratories "B" through "E," where the smaller scatter is associated with the longer averaging intervals of 4 to 5 min (laboratories "C" and "D") and the somewhat larger scatter reflects averaging intervals of 1 min (laboratories "B" and "E"). In the case of laboratories "A" and "G" the scatter is no obvious function of the averaging interval but an expression of an analytical problem.

In the comparison of surface fCO_2 data in Sect. 4.3, these results, sometimes referred to as the general trends of agreement or disagreement between the xCO_2 (air) data sets, will largely be retained in the fCO_2 data. The combination of both results provides much of the argument for the discussion of the overall results. We will demonstrate that the three laboratories "C," "D," and "E" show the same high degree of agreement in surface fCO_2 data as they do in xCO_2, and a strong case will be made that these systems represent the "best" values of xCO_2 (air) and fCO_2.

4.3 COMPARISON OF SURFACE fCO_2 DATA

As described in Sect. 3.4, the following main steps in the calculation of final fCO_2 values constitute the general procedure that was applied identically to all underway fCO_2 data sets:

- Calculation of xCO_2 in dry sample air (final data product received from every group)
- Synchronization of daily CTD and equilibrator profiles based on standard deviation of the temperature offset
- Calculation of fCO_2 in equilibrator (at T_{eq}, 100% humidity)
- Correction of fCO_2 to in situ seawater temperature based on corrected temperature readings

In order to gain better interpretability of any differences in the final fCO_2 data sets, we tried to exclude as many controllable sources of error as possible. This was accomplished by carefully addressing the following points:

- Temperature readings can be a significant source of error as shown in Sect. 3.4.2. However, on the basis of the checks of the temperature probes against a reference probe we were able to remove this error and assure consistent temperature measurements.
- The choice of the parameterizations for calculating the saturation water vapor pressure and for the temperature correction of fCO_2 also introduces some kind of uncertainty, which, however, in our case seems to be rather small compared with the errors of the temperature measurements. Again, the common calculation procedure (Sect. 3.4.3) excludes inconsistencies based on the use of different equations.
- Finally, the common infrastructure (i.e., the seawater and calibration gas supply) assured a physically identical background for all systems (Sect. 2.2).

It should be emphasized that none of these consistent conditions are usually present in typical fCO_2 measurements in the field (i.e., temperature probes are sometimes used uncalibrated or at least not calibrated to the same standard; calculation procedures vary; calibration gases are of different origin and likely quality, too; the seawater sources may be quite different or even inadequate for gas measurements etc.).

In the interpretation of the results, any differences of >2 µatm (up to >5 µatm in the highly variable regime) in the final fCO_2 data can be attributed either to differences in the equilibration process itself and/or to differences in the subsequent measurement of CO_2. A tool to separate these two possible sources of error is measurements of the atmospheric xCO_2, which were discussed in some detail in Sect. 4.2. Unlike the calibration gases, atmospheric air is comparable to the seawater equilibrated air in that it has a wet sample matrix. Thus atmospheric air undergoes the same procedure of (physical or arithmetical) drying. If, for example, differences between seawater fCO_2 data from two systems were also present in the atmospheric xCO_2 data, this is indicative of problems associated with the infrared CO_2 measurement and/or the drying procedure. If, in contrast, the atmospheric xCO_2 data turned out to be identical while seawater fCO_2 was different, the source of error must be attributed to the equilibration process and/or the way of handling of the seawater equilibrated air.

Whereas these reasons add to the interpretability of the results, it should be pointed out that any observed differences cannot per se be attributed to a particular data set or system. As a superior reference method was not available, the "true" fCO_2 values are simply not known. Given the still remaining uncertainty about the valid set of dissociation constants of carbonic acid in seawater, even consistency checks based on the other three parameters of the CO_2 system in seawater (i.e., C_T, A_T, pH)—although to be carried out later on—will not provide an unambiguous means of finding "true" fCO_2 values.

However, we found three data sets (systems "C," "D," and "E") to be very close in seawater fCO_2 and atmospheric xCO_2 values throughout the cruise, whereas the other data sets show variable offsets to these three profiles and some of them are also associated with significantly larger scatter. Because the general design of the three systems "C," "D," and "E" is significantly different (showerhead equilibrator—thin film equilibrator, small equilibrator volume—large equilibrator volume, small flow rates—large flow rates, equilibrator vented—equilibrator not vented, wet CO_2 measurement—dry CO_2 measurement, etc.), this agreement cannot simply be attributed to an essentially identical design. This is by no means a sufficient argument to regard the three consistent fCO_2 profiles as the "truth," although we feel that this marked agreement is at least a strong indication of this. However, with the lack of a superior method, this sort of discussion is to some extent futile and cannot be solved here.

When preparing the following figures, we wanted to discuss the fCO_2 results not only as absolute numbers but also as deviations from a reference. Because a superior method was not available and the choice of a single "true" fCO_2 profile was not feasible, we decided to calculate the deviation of every single fCO_2 data point from an 11-min running mean calculated from the three most consistent profiles (labs "C," "D," and "E"). In the light of the arguments given in the foregoing discussion, this choice remains arbitrary, but it nevertheless seems to be the most reasonable choice. However, it should

be kept in mind that these deviations are, of course, dependent on the choice of the reference and are therefore not independent results. We are fully aware that this is a somewhat critical step in the interpretation, which seems only justified by the better visualization of the differences and the enhanced interpretability of the data set.

A further problem associated with calculating deviations from an 11-min running mean stems from the fact that this reference represents a strongly smoothed profile, whereas the original fCO_2 data represent significantly smaller averaging intervals (minimum 1 min). Thus, all temporal variability on the minute-scale as contained in the fCO_2 data with higher temporal resolution (e.g., profiles "B" and "E") translates into a larger scatter than that of the deviations from the smoothed reference profile. This artifact has to be kept in mind, because it is of a different magnitude for the various fCO_2 data sets. This effect is more strongly obvious in the strong gradient regime (e.g., June 10). The main message of these deviation figures therefore has to be the general offset rather than the scatter of a profile.

Table 3 provides an overview of the minima, maxima, and differences of measured in situ temperature, salinity, and fCO_2 (11-min running mean from profiles "C," "D," and "E") on a daily basis. As intended with the choice of the cruise track and as already documented in the daily profiles of temperature and salinity (Sect. 4.1), the encountered conditions of the surface waters along the cruise track varied between a smooth regime with low variability during the second half of the cruise and a strong gradient regime with much higher variability in the area close to the northern turning point off Newfoundland (marked by shading) during the first half.

Table 3. Overview of minimum, maximum, and difference of measured values of temperature T (°C), salinity S, and the fugacity of CO_2 (fCO_2, 11-min running mean from profiles "C," "D," and "E"). The strong gradient regime is shaded.

	June 8	June 9	June 10	June 11	June 12	June 13	June 14	June 15	June 16
T_{min}	20.3	6.0	6.4	10.1	12.9	15.3	16.8	18.4	19.6
T_{max}	25.1	24.5	16.4	16.6	16.9	17.1	19.8	20.6	21.0
ΔT	4.8	18.5	10.0	6.5	4.0	1.8	3.0	2.2	1.4
S_{min}	36.38	32.57	32.90	33.88	34.66	35.98	35.97	36.11	36.35
S_{max}	36.81	36.61	36.24	36.32	36.29	36.25	36.25	36.46	36.96
ΔS	0.43	4.04	3.34	2.44	1.63	0.27	0.28	0.35	0.61
$fCO_{2,min}$	315.6	270.2	264.6	281.5	276.9	303.8	306.7	332.2	338.6
$fCO_{2,max}$	340.7	339.2	321.0	327.9	327.3	326.4	346.4	359.3	355.7
ΔfCO_2	25.1	69.0	56.4	46.4	50.4	22.6	39.7	27.1	17.1

4.3.1 Underway Profiles

Figures 12–20 show the final underway fCO_2 profiles "A" through "G" as well as the discrete fCO_2 data of laboratory "H" (top) and the deviations of all fCO_2 data from the 11-min running mean calculated from profiles "C," "D," and "E" (bottom). It should be noted that the top figures show variable scaling of the y-axis (see 5 µatm bar indicator), while the bottom figure is always at the same scale. The latter also includes two horizontal lines, one at +2 and one at –2 µatm deviation which is about the limit of interpretation.

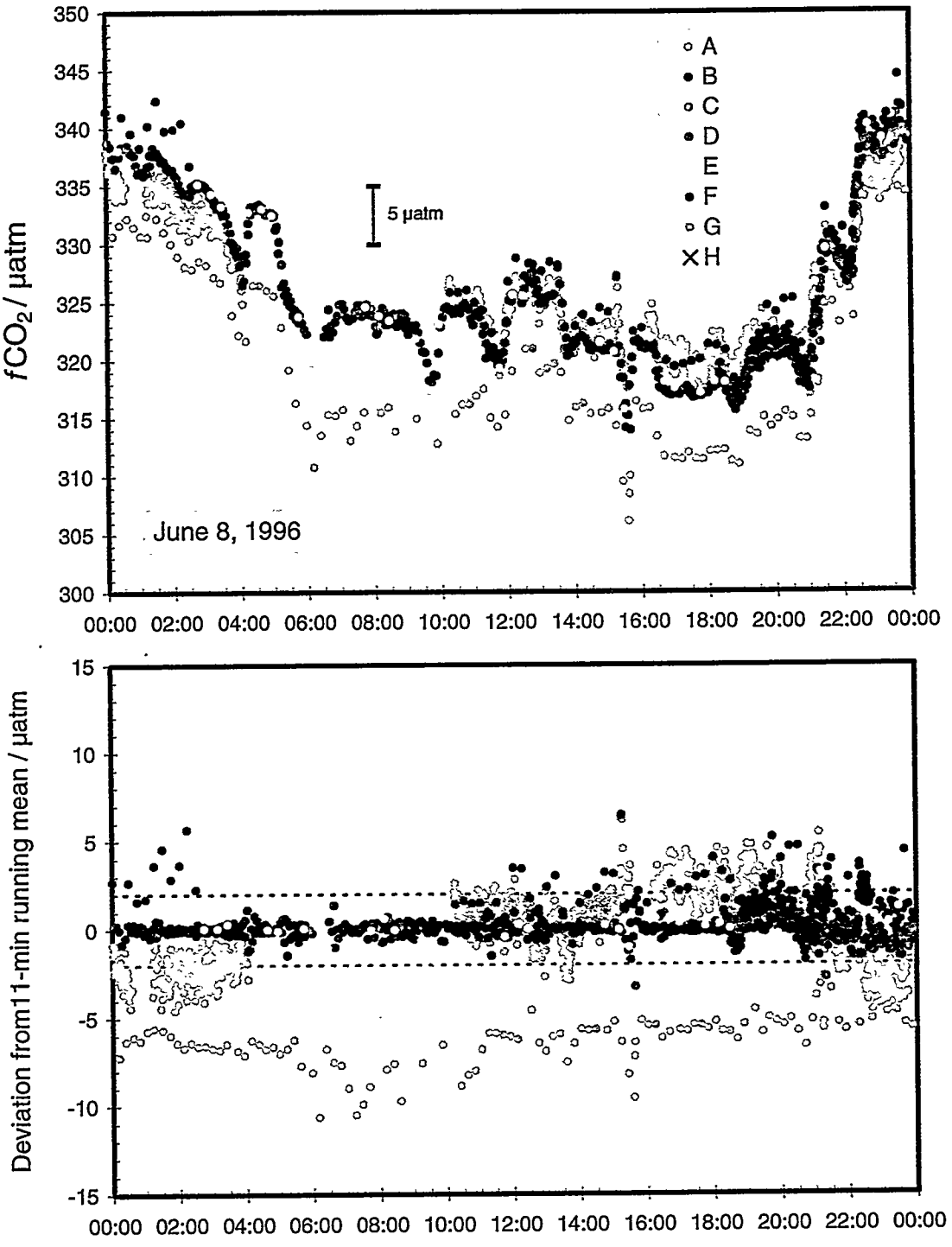

Fig. 12. June 8, 1996, fCO_2 data collected by R/V *Meteor* Cruise 36/1 in the North Atlantic: (top) underway ("A" through "G") and discrete ("H") data; (bottom) deviation of all fCO_2 measurements ("A" through "H") from an 11-minute running mean calculated from profiles "C," "D," and "E." The bottom graph also shows the ±2-µatm deviation range.

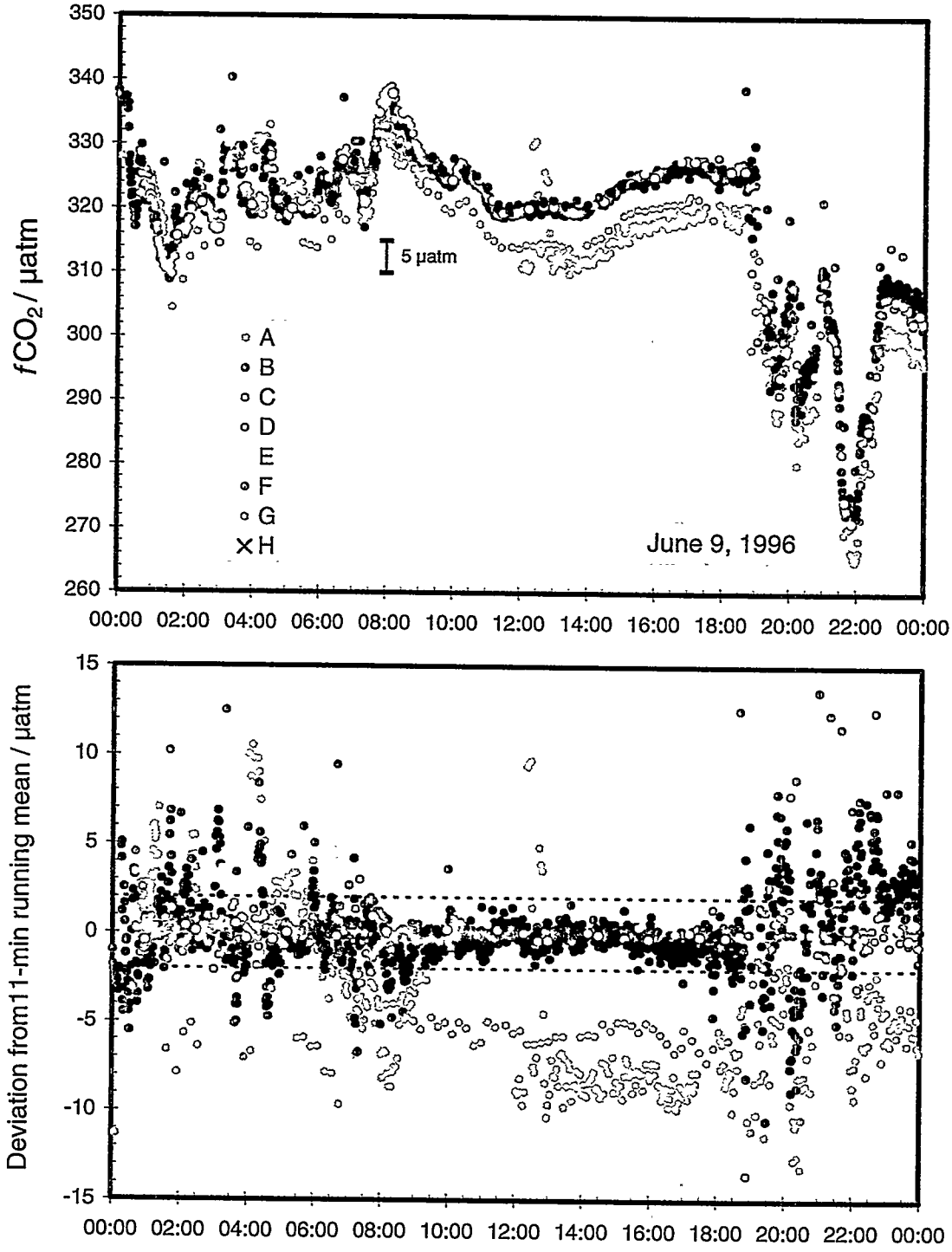

Fig. 13. June 9, 1996, fCO_2 data collected by R/V *Meteor* Cruise 36/1 in the North Atlantic: (top) underway ("A" through "G") and discrete ("H") data; (bottom) deviation of all fCO_2 measurements ("A" through "H") from an 11-minute running mean calculated from profiles "C," "D," and "E." The bottom graph also shows the ±2-µatm deviation range.

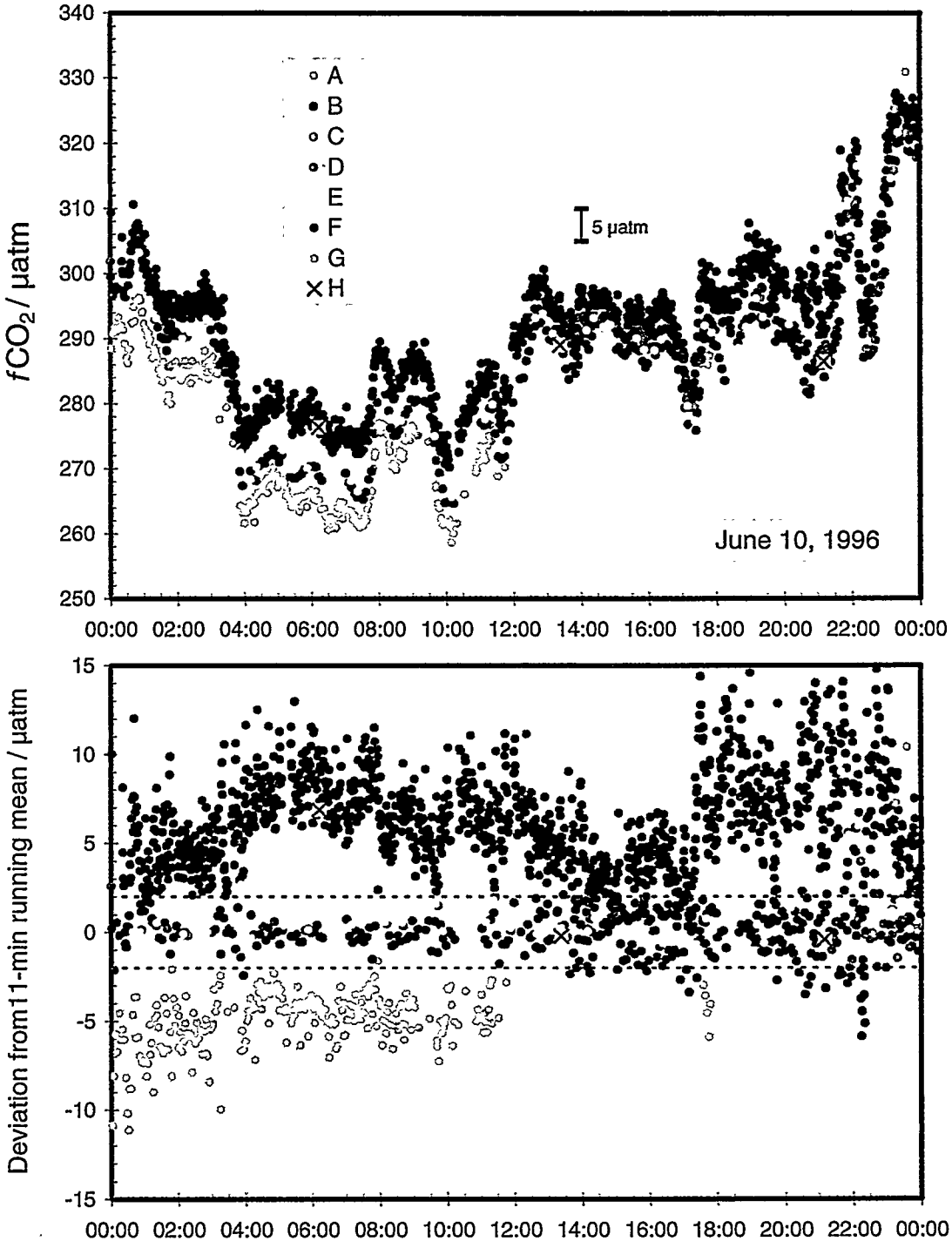

Fig. 14. June 10, 1996, fCO_2 data collected by R/V *Meteor* Cruise 36/1 in the North Atlantic: (top) underway ("A" through "G") and discrete ("H") data; (bottom) deviation of all fCO_2 measurements ("A" through "H") from an 11-minute running mean calculated from profiles "C," "D," and "E." The bottom graph also shows the ±2-µatm deviation range.

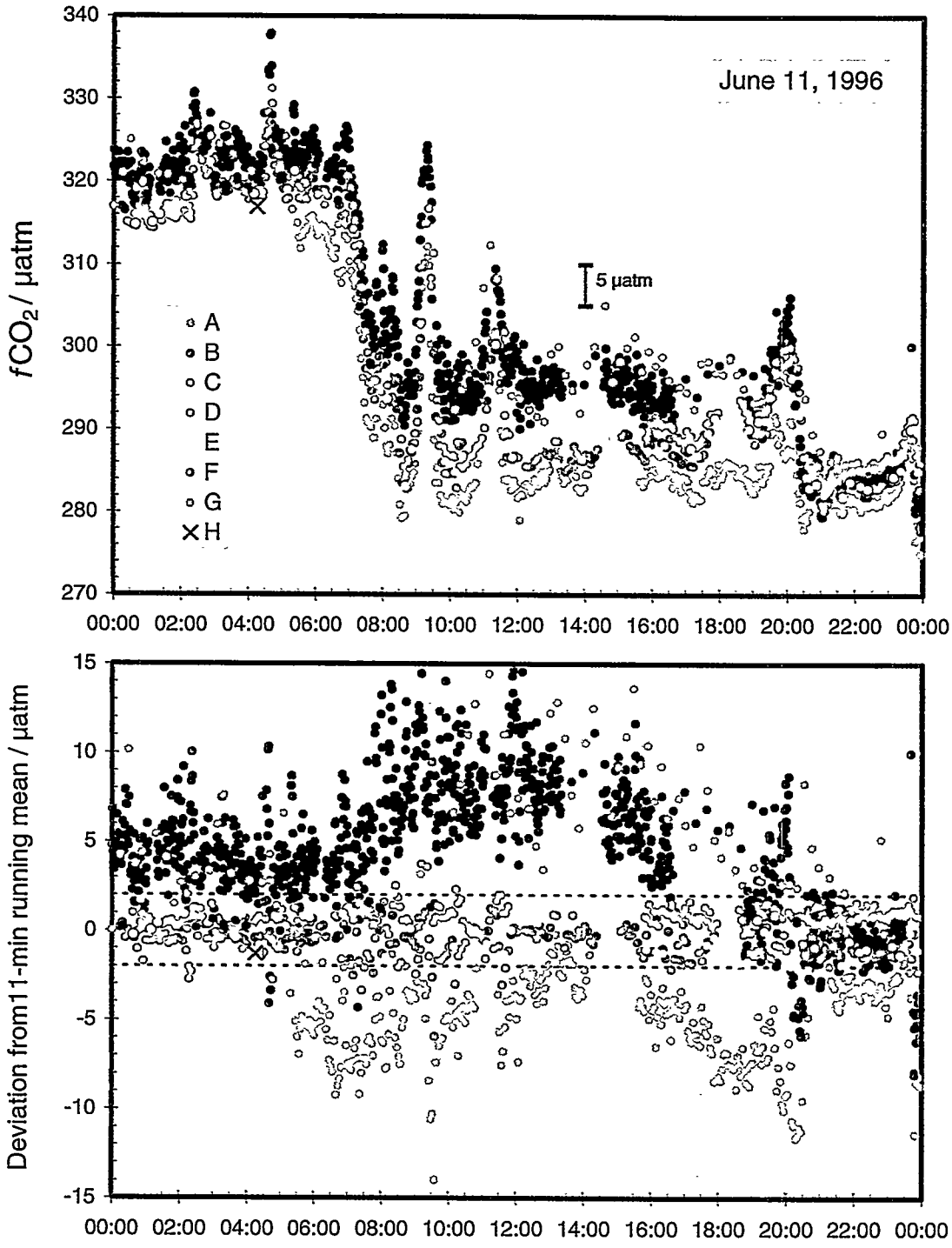

Fig. 15. June 11, 1996, fCO_2 data collected by R/V *Meteor* Cruise 36/1 in the North Atlantic: (top) underway ("A" through "G") and discrete ("H") data; (bottom) deviation of all fCO_2 measurements ("A" through "H") from an 11-minute running mean calculated from profiles "C," "D," and "E." The bottom graph also shows the ±2-µatm deviation range.

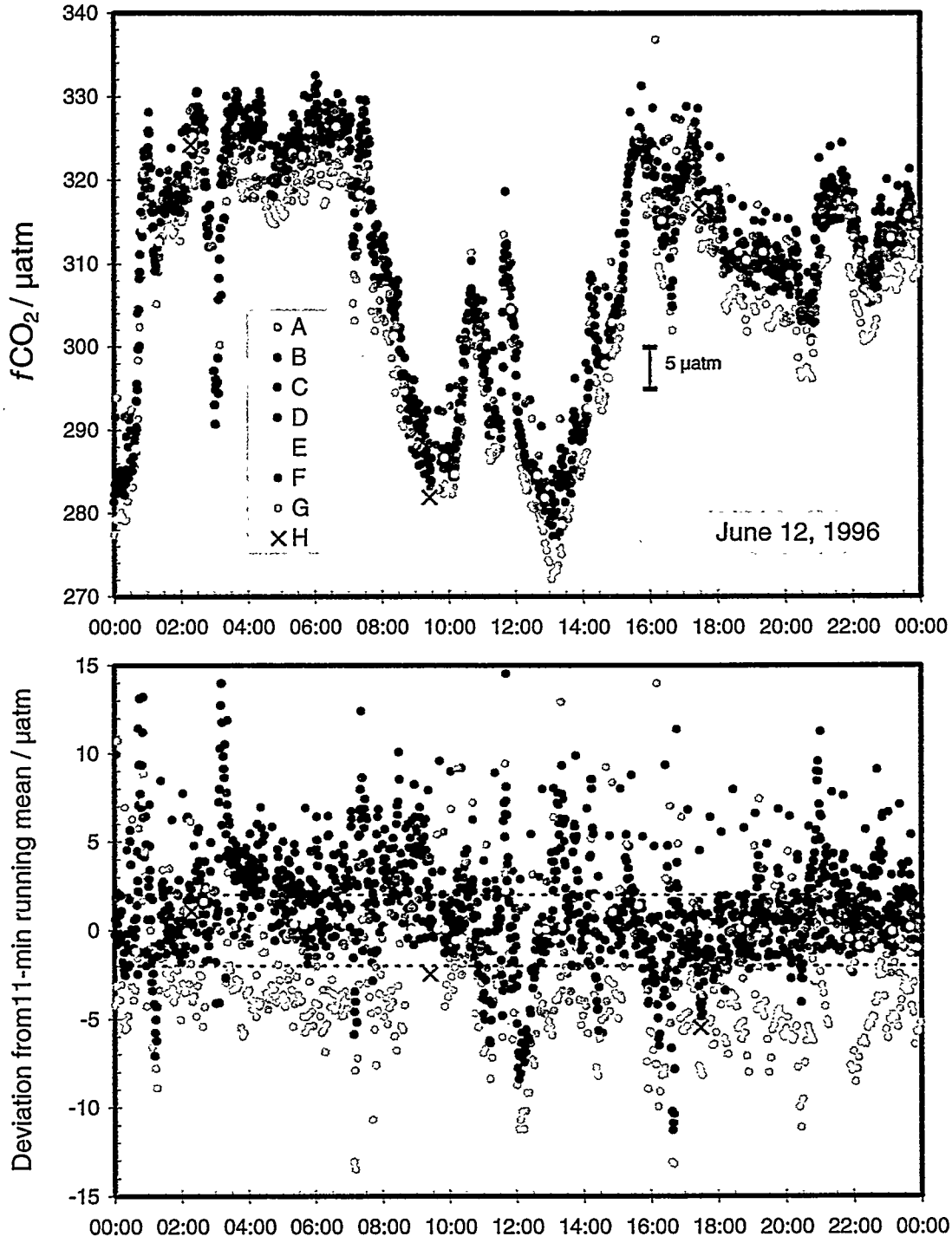

Fig. 16. June 12, 1996, fCO_2 data collected by R/V *Meteor* Cruise 36/1 in the North Atlantic: (top) underway ("A" through "G") and discrete ("H") data; (bottom) deviation of all fCO_2 measurements ("A" through "H") from an 11-minute running mean calculated from profiles "C," "D," and "E." The bottom graph also shows the ±2-µatm deviation range.

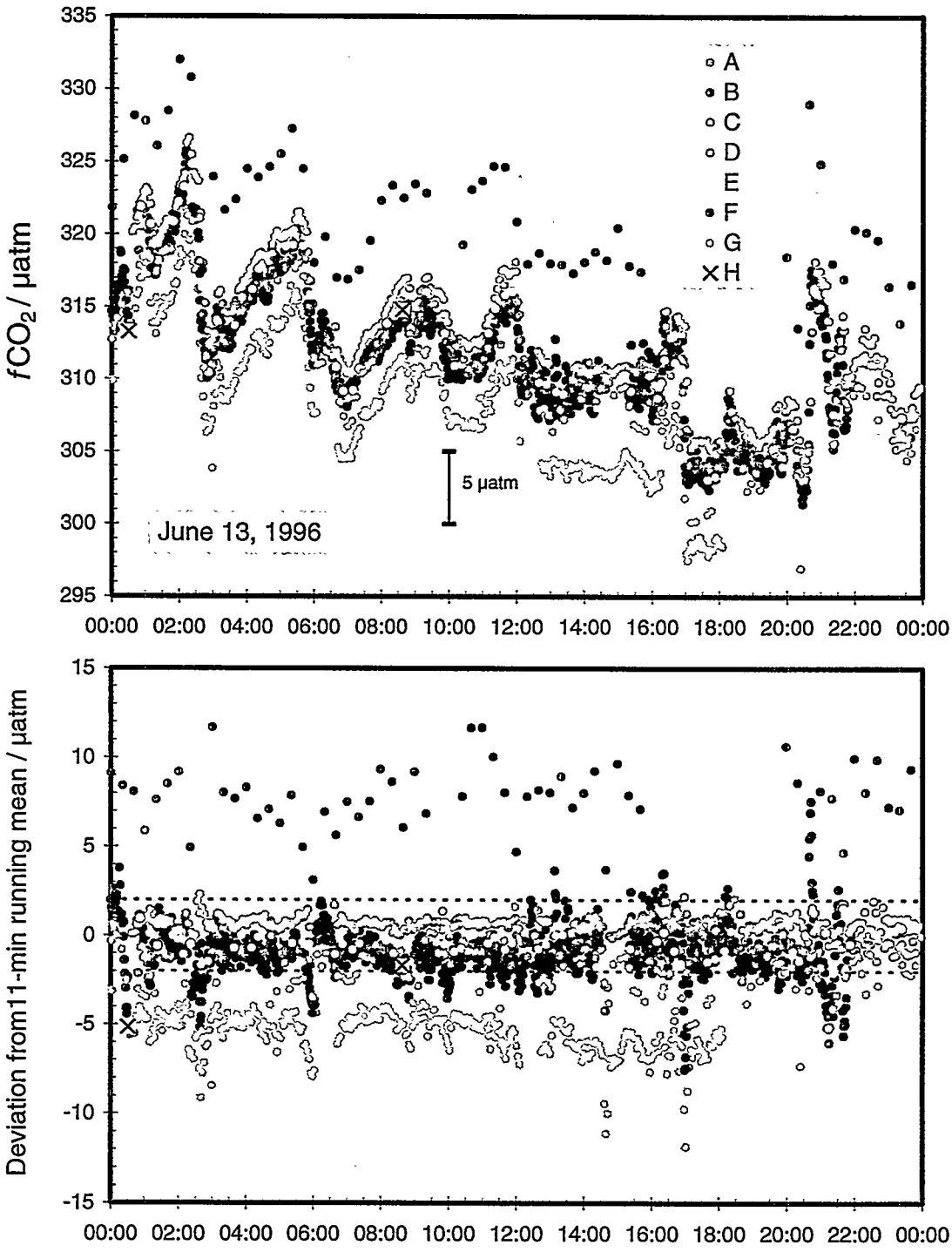

Fig. 17. June 13, 1996, fCO_2 data collected by R/V *Meteor* Cruise 36/1 in the North Atlantic: (top) underway ("A" through "G") and discrete ("H") data; (bottom) deviation of all fCO_2 measurements ("A" through "H") from an 11-minute running mean calculated from profiles "C," "D," and "E." The bottom graph also shows the ±2-µatm deviation range.

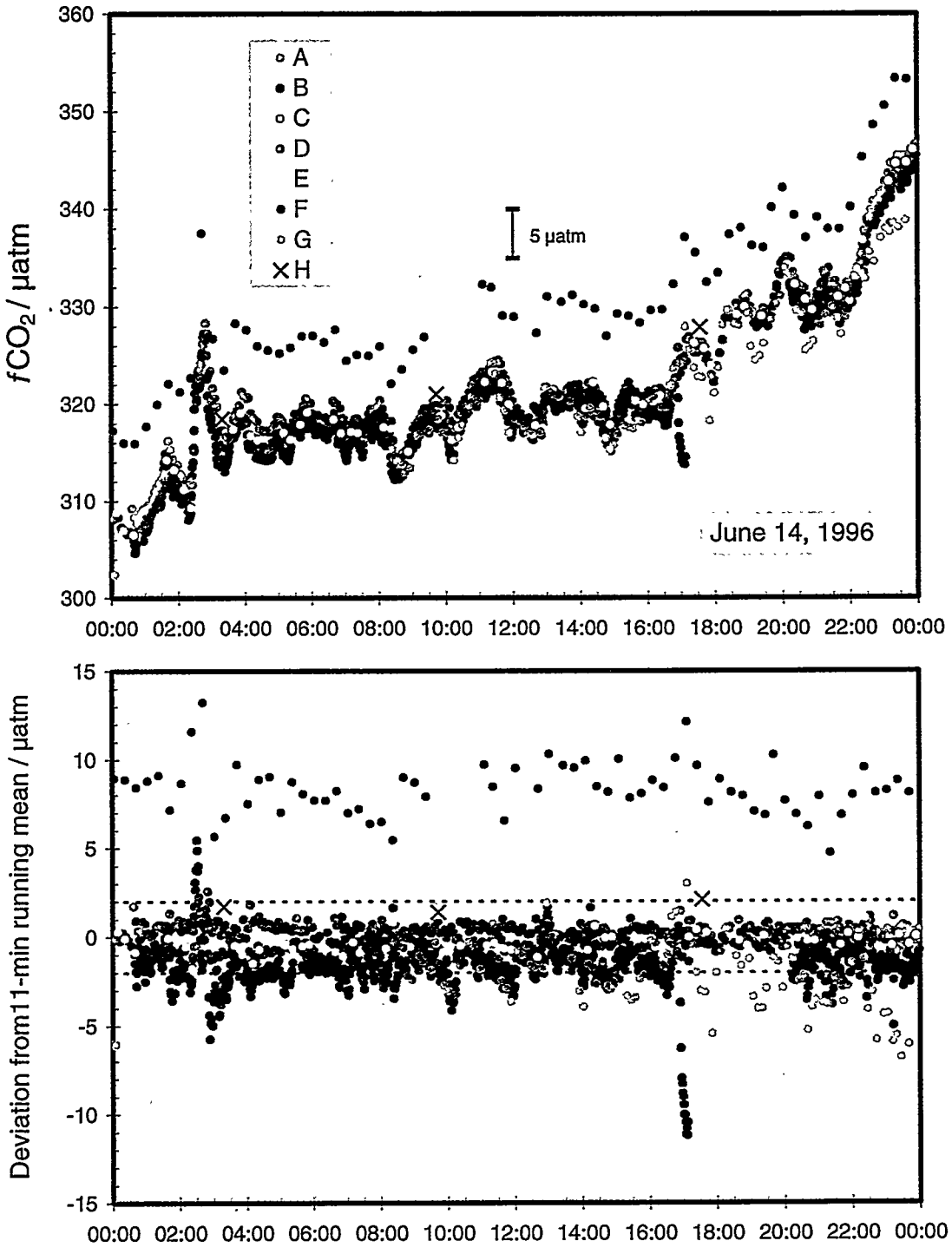

Fig. 18. June 14, 1996, fCO_2 data collected by R/V Meteor Cruise 36/1 in the North Atlantic: (top) underway ("A" through "G") and discrete ("H") data; (bottom) deviation of all from fCO_2 measurements ("A" through "H") from an 11-minute running mean calculated from profiles "C," "D," and "E." The bottom graph also shows the ±2-µatm deviation range.

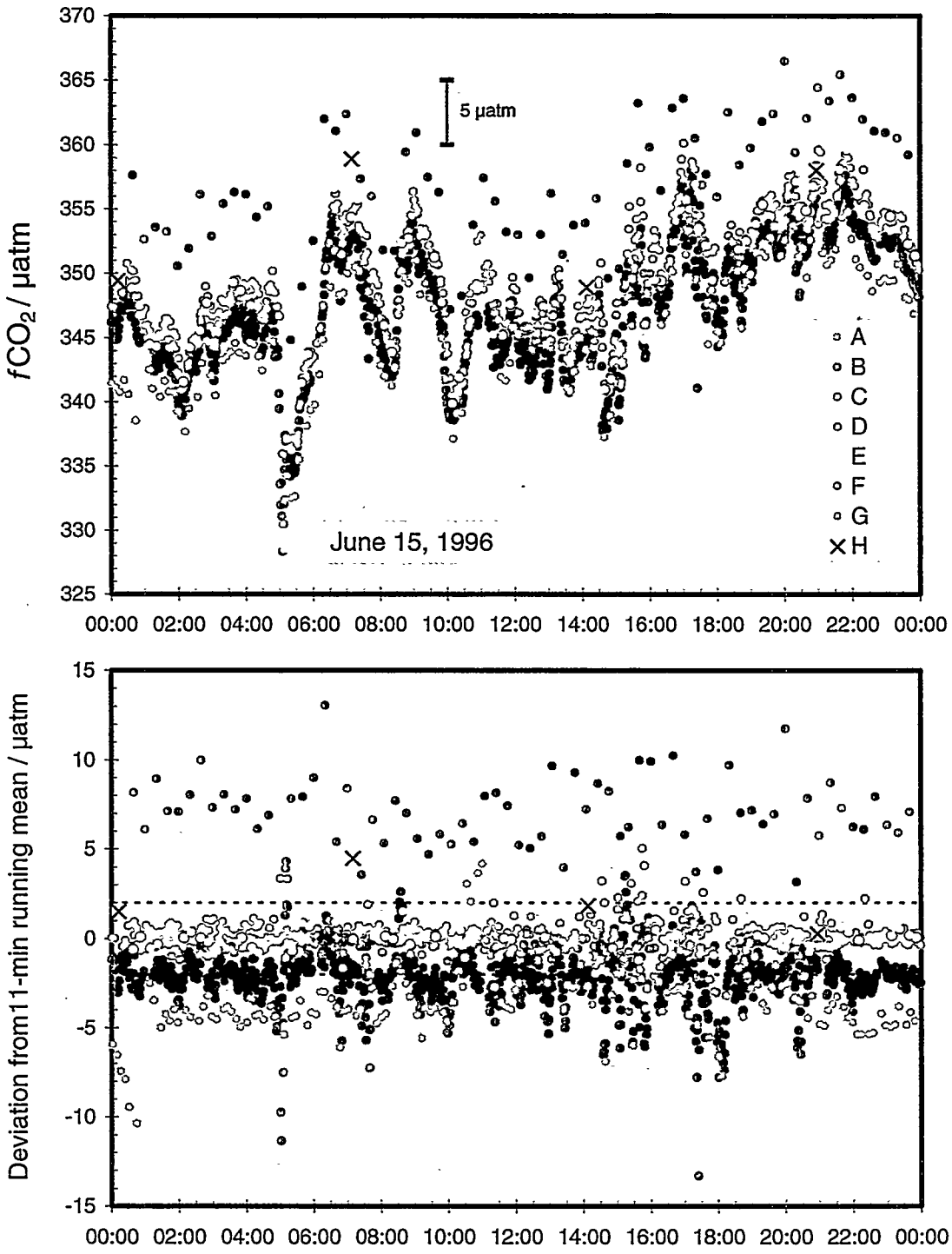

Fig. 19. June 15, 1996, fCO_2 data collected by R/V *Meteor* Cruise 36/1 in the North Atlantic: (top) underway ("A" through "G") and discrete ("H") data; (bottom) deviation of all fCO_2 measurements ("A" through "H") from an 11-minute running mean calculated from profiles "C," "D," and "E." The bottom graph also shows the ±2-µatm deviation range.

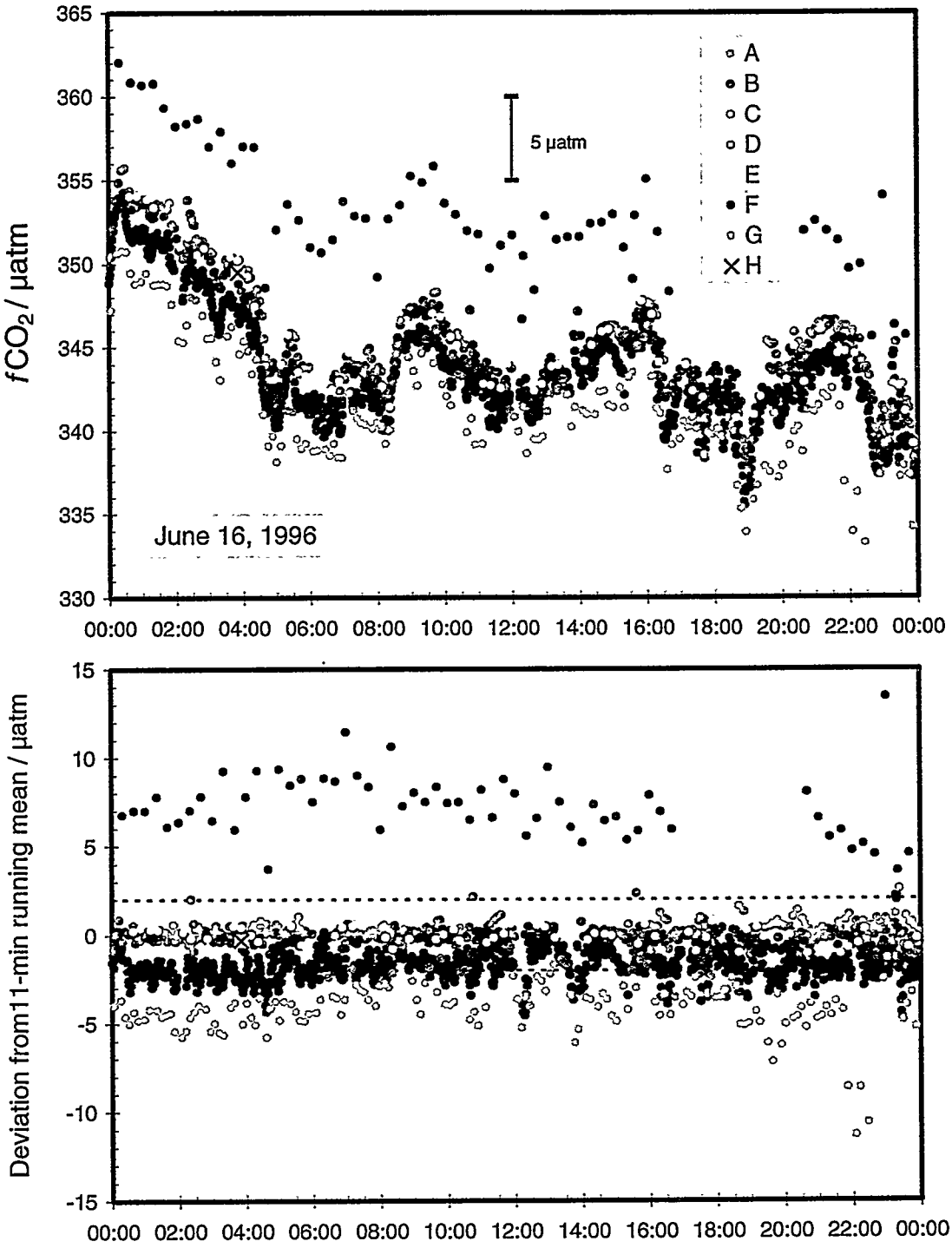

Fig. 20. June 16, 1996, fCO_2 data collected by R/V *Meteor* Cruise 36/1 in the North Atlantic: (top) underway ("A" through "G") and discrete ("H") data; (bottom) deviation of all fCO_2 measurements ("A" through "H") from an 11-minute running mean calculated from profiles "C," "D," and "E." The bottom graph also shows the ±2-µatm deviation range.

4.3.2 Discussion of Profiles

Following is a brief day-by-day description of the major features contained in Figs. 12–20. We tried to identify the most important results and to point to some major trends and changes. Again we would like to emphasize that the scatter of the bottom figures is mainly an artifact of the referencing procedure. This can be readily observed in Fig. 13 (June 9, 1996): Between 08:00 and 19:00 UTC the seawater exhibits low variability resulting in very little scatter in the bottom figure. Immediately before and after this period the seawater was much more variable which translates into the high scatter of the deviation figure. The observed offsets discussed here can therefore only be identified in the trends and have to be regarded as rough approximations.

June 8, 1996

Missing data – "A": 04:00 to 10:00 UTC, "B": before 18:30 UTC (start delayed because of sample gas leakage), "F": 03:00 to 10:30 UTC, "H": no samples measured. *Agreement to within ± 2 µatm* – "B," "C," "D," and "E." *Positive offset* – "F": 3 µatm. *Negative offset* – "G": 6 µatm. *Variable offset* – "A": –3 to +3 µatm. *Comment* – "G" starts with a marked negative offset, which turns slowly into a positive offset during the next days and then disappears toward the end of the exercise. However, the large scatter of "G" seen in the atmospheric xCO_2 readings is not visible here, which points toward problems with the handling of atmospheric air within this system (e.g., leakage in air pump, valves, or tubing).

June 9, 1996

Missing data – "A": 10:00 to 12:00 UTC, "C": 13:00 to 24:00 UTC, "H": no samples measured. *Agreement to within ±2 µatm* – "B," "C," "D," and "E." *Negative offset* – "G": 6 µatm. *Variable offset* – "A": within ±2 µatm (before 07:00 UTC), –5 to –8 µatm after 12:00 UTC; "F": within ±2 µatm (09:00 to 19:00 UTC), +5 to +10 µatm (before 09:00 UTC and after 19:00 UTC). *Comment* – "A" shows a sudden change around 12:00 UTC from good agreement to a negative offset of the order of 5 µatm. This offset remained until the end of the exercise. The scatter of profile "A" (3-min intervals) is significantly larger than in the 1-min averages of "B" as can be seen in the smooth period (13:00 to 17:00 UTC). This is contradictory to what one would expect and may be related to the rather large scatter observed in the atmospheric xCO_2 readings of "A." Interestingly, the offset of the latter showed up from the beginning of the exercise (i.e., before June 9, 12:00 UTC when it suddenly appeared in seawater fCO_2 readings). This is indicative of different reasons for the offsets observed in atmospheric xCO_2 and seawater fCO_2 readings of "A."

June 10, 1996

Missing data – "A": after 12:00 UTC, "C": before 13:00 UTC, "G": 12:00 to 23:00 UTC. *Agreement to within ±2 µatm* – "C," "D," and "E." *Positive offset* – "B": 3 to 9 µatm, "F": 4 to 10 µatm. *Negative offset* – "A": 5 µatm, "G": 5 µatm. *Variable offset* – "H": within ±2 µatm at 13:22 and 21:09 UTC, +7 µatm at 06:12 UTC. *Comments* – "B" immediately started to develop a positive offset which more or less remained until about 18:00 UTC of the following day. This offset is not seen in atmospheric xCO_2 measurements of "B." "F" also lost its good agreement and started to develop a positive offset which stabilized toward the end of the exercise. Interestingly these offsets of "B" and "F" show up at about the same time and with a very similar pattern over the 2-day period. Furthermore, the 06:12 UTC data point of "H" has the same positive offset as "B" and "F." Whether this is pure coincidence or an expression of something real is not known. These three systems, however, are very different in their principle of measurement and the location in the seawater supply line so that a common systematic error can be ruled out. Also their common offset seems to be inversely correlated with seawater temperature (see Fig. 7). On the basis of this observation it also has to be questioned whether a systematic offset may be present in the "reference" profiles "C," "D," and "E." This puzzle, however, cannot be solved here.

June 11, 1996

Missing data – "A": before 05:30 UTC, "B": 17:00 to 19:00 UTC, "C": 12:00 to 16:00 UTC, "F": 20:30 to 23:30 UTC. *Agreement to within ±2 µatm* – "C," "D," "E," and "H." *Positive offset* – "F": 2 to 8 µatm, "G": 2 to 9 µatm. *Negative offset* – "A" 3 to 8 µatm. *Variable offset* – "B": within ±2 µatm (after 18:00 UTC), +3 to +9 µatm (00:00 to 17:00 UTC). *Comment* – Positive offsets of "B," "F," and "G" are essentially parallel throughout the day (see also comment of the previous day). Between 12:00 and 19:00 UTC the positive offset of "B" slowly disappears while at the same time a negative offset in the atmospheric xCO_2 measurements of "B" develops.

June 12, 1996

Missing data – "C": before 16:00 UTC. *Agreement to within ±2 µatm* – "C," "D," and "E." *Positive offset* – "F": 3 to 9 µatm. *Negative offset* – "A": 3 to 6 µatm. *Variable offset* – "B": 0 to +3 µatm, "G" –2 to +8 µatm, "H": +1 to –6 µatm. *Comments* – The top figure shows nice parallel patterns of all fCO_2 profiles even in this strongly variable environment. The bottom figure heavily suffers from the artificial scatter but nevertheless reveals the general offsets and trends. The negative offset of "H" at 17:29 UTC is likely due to this artifact because "H" is in very good agreement with "B" which does not show a general offset here.

June 13, 1996

Missing data – "A": after 18:00 UTC, "B": after 22:00 UTC, "F": 16:00 to 20:00 UTC, "G": 03:00 to 05:00 UTC. *Agreement to within ±2 µatm* – "B," "C," "D," "E," and "G." *Positive offset* – "F": 6 to 9 µatm. *Negative offset* – "A": 5 to 6 µatm. *Variable offset* – "H": –2 and –5 µatm. *Comment* – This is about the beginning of the "smooth regime" with comparatively low variability in surface water which persisted for the rest of the exercise. The kind of agreement seen in this figure continues to exist in the following figures with very little alteration. In contrast to the highly variable situation encountered earlier this cruise, this situation is probably more representative of typical oceanic conditions in underway fCO_2 field work. Again, the negative offset of "H" at 00:31 UTC is likely an artifact as it follows the profile of "B" which itself is in good agreement with "C," "D," and "E." System "A" had to quit the exercise at about 18:00 UTC because of a technical problem associated with the NDIR instrument, and no more data from this system are available beyond this point.

June 14, 1996

Missing data – "A": no data available, "B": 17:00 to 22:00 UTC, "G": before 09:00 UTC. *Agreement to within ±2 µatm* – "B," "C," "D," "E," "G," and "H." *Positive offset* – "F": 7 to 10 µatm. *Comment* – Whereas the general agreement of all profiles except "F" is rather good, even among them slight trends toward positive ("H") or negative ("B" and "G") offsets can be identified that persist for the rest of the exercise.

June 15, 1996

Missing data – "A": no data available. *Agreement to within ±2 µatm* – "C," "D," and "E." *Positive offset* – "F": 5 to 10 µatm. *Negative offset* – "B": 3 µatm, "G": 4 µatm. *Variable offset* – "H": +1.5 to +4.5 µatm. *Comment* – See comment for previous day.

June 16, 1996

Missing data – "A": no data available, "F": 17:00 to 21:00 UTC. *Agreement to within ±2 µatm* – "C," "D," "E," and "H." *Positive offset* – "F": 5 to 8 µatm. *Negative offset* – "B": 2 to 3 µatm, "G": 2 to 4 µatm. *Comment* – As the hydrographic conditions have become much less variable, the overall picture of agreement among the various systems is very consistent for the last three days of the exercise.

Overview

The overall picture of agreement is characterized by a very good agreement of profiles "C," "D," and "E" essentially throughout the cruise. While also in good agreement for most of the time, profile "B" shows a 2-day period with a marked positive offset. Two profiles show a more or less constant sign of deviation, which is positive in the case of "F" and negative in the case of "A." The reason for this could not be identified easily. However, for system "A" we know of an instance of severe damage in the NDIR instrument toward the end of the exercise, which may well have started biasing the measurements in an early stage of the exercise. With respect to system "F," which is of a principally different design (see Sect. 3.2, Table 2), the question of whether the different principle of measurement could be the reason for the rather large observed offset should be addressed carefully. Finally, system "G" shows anything from large negative offsets over periods of good agreement to rather strong positive offsets. These problems were also apparent in atmospheric xCO_2 measurements and checks of the CO_2 calibration performance probably because of an improper calibration technique. The calibration of the system appears to lack—at least during this exercise—the necessary reproducibility (i.e., it may be good in one case and bad in another one). This obvious problem of system "G" also needs careful checks.

In addition to the daily figures (Figs. 12 to 20) representing the full data set, we present three figures (Figs. 21 to 23) with enlarged views of shorter periods. These were chosen because they reveal more detail than is available in the daily figures. Furthermore they also cover the whole range of situations, from smooth to highly variable.

Figure 21 shows a 3-hour period of measurements on June 9 that was characterized by very low variability in the surface seawater fCO_2 (Fig. 13) as well as temperature and salinity (Fig. 7). The total change in fCO_2 values during this period of time is about 6 µatm. This is uniformly seen in all profiles, which are almost perfectly parallel. Profiles "B," "D," "E," and "F" agree to within 1 µatm, while profiles "A" and "G" are characterized by a negative offset of about 8 µatm and 5 µatm, respectively. The scatter is smallest in profile "D" (averaging interval 5 min; large time constant, as shown) and highest in profile "A" (averaging interval 3 min; short time constant). The comparatively small scatter in profile "B" with 1-min averaging intervals shows that much of the scatter in profile "A" (also seen in the atmospheric xCO_2 data of "A") is not real and may thus indicate again the existence of a technical problem.

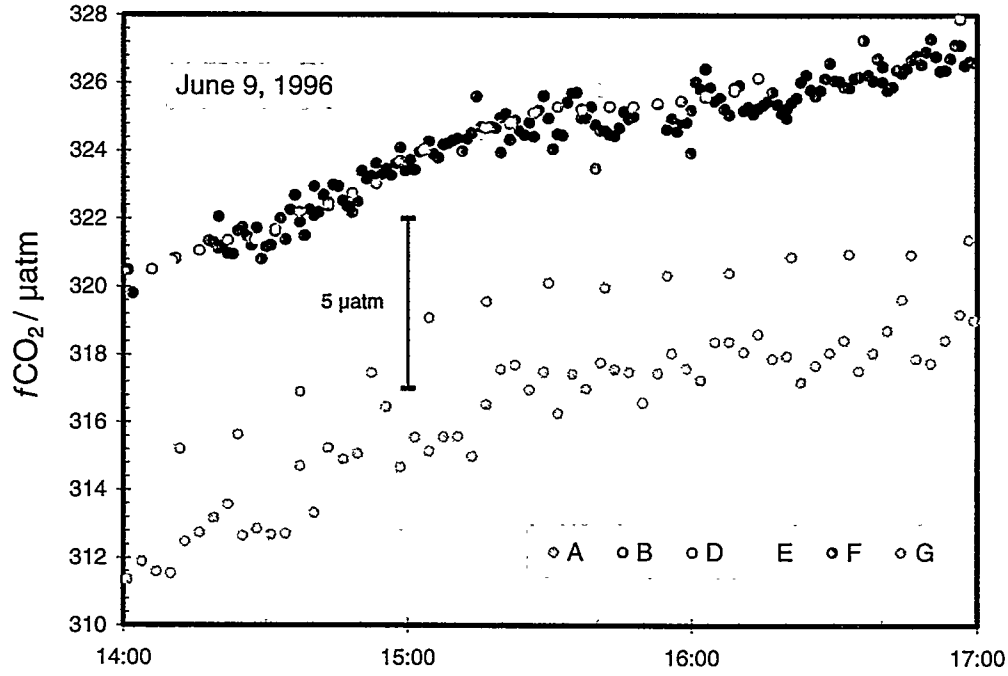

Fig. 21. Comparison of fCO_2 data measured during a 3-hour period on June 9 showing rather low variability in surface water fCO_2 (no data available for "C" and "H").

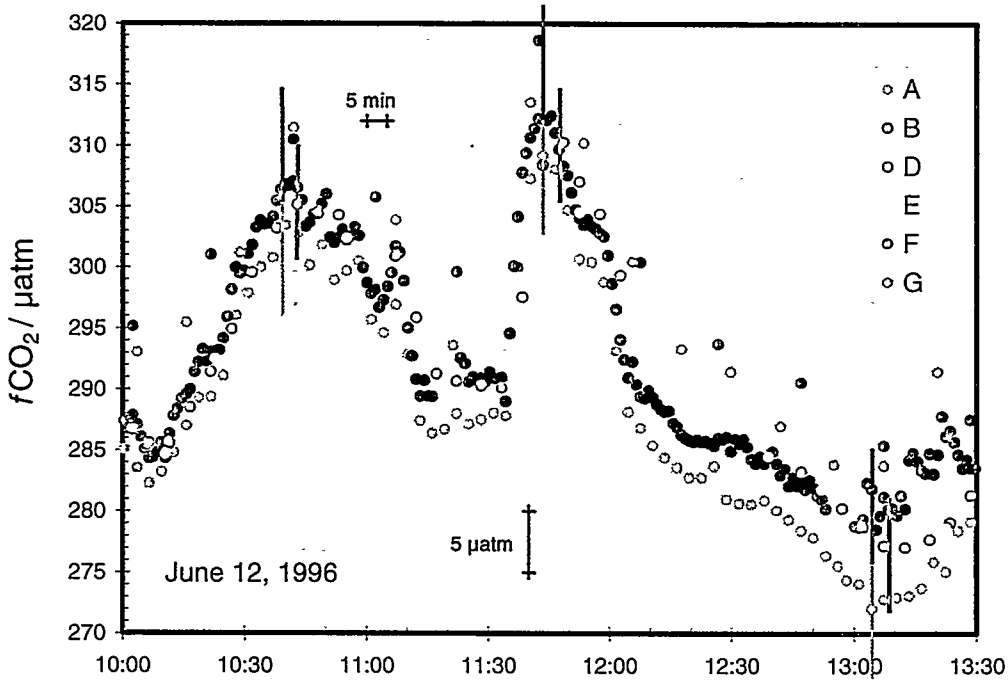

Fig. 22. Comparison of fCO_2 data measured during a 3.5-hour period on June 12 (no data available for "C" and "E"). Vertical lines indicate approximate relative maxima and minima observed in the fCO_2 profiles.

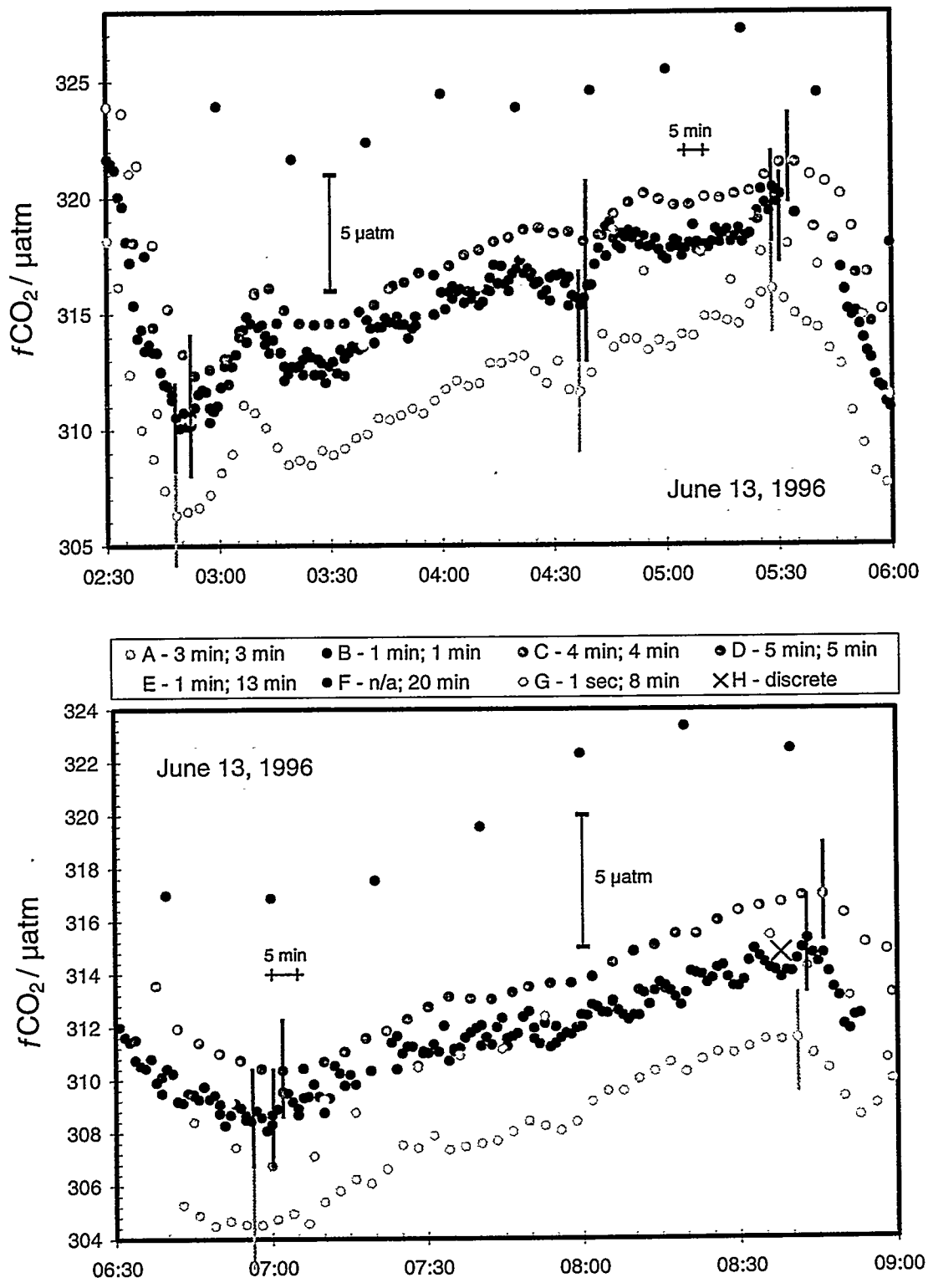

Fig. 23. Comparison of fCO_2 data measured during two periods on June 13, 1996: (top) 3.5 h and (bottom) 2.5 h. Vertical lines indicate approximate relative maxima and minima observed in the fCO_2 profiles. The legend includes the averaging and reporting intervals of all systems.

In contrast, Fig. 22 shows the much more variable situation of a 3.5-hour period of measurements during June 12. The total range of fCO_2 values covered during this period is about 35 µatm with gradients of up to 3 µatm/min. Again, the agreement is good in profiles "B," "D," and "E." Profiles "F" and "G" show positive offsets, while profile "A" has a negative offset of a few µatm.

Individual time constants involved in the equilibration process going on in every system can be estimated rather precisely with step experiments carried out under well-defined conditions in a shore-based laboratory (Copin-Montegut 1988; Körtzinger et al. 1996b). This is definitely not the case in the present intercomparison exercise. We therefore do not try make any estimates of individual time constants. Nevertheless, in addition to the examination of offsets we do try to gain insight into the apparent time constants (i.e., we want to see whether there is any indication of differences in kinetic aspects of the equilibration processes). Because most time constants are on the order of a few minutes, this analysis is only feasible where fCO_2 was measured at rather short intervals of ≤5 min (only profiles "A," "B," "C," and "D"), but even in these cases this is not a sound approach.

We have marked approximate relative minima and maxima observed in the enlarged periods shown in Figs. 22 and 23. The pattern of vertical lines observed in these groups is highly consistent: Extrema always occur first and simultaneously in profiles "A" and "B," while profiles "C" and "D" lag behind by 5 to 8 min and 2 to 5 min, respectively. The range is mainly a consequence of the different averaging intervals. These time lags cannot be attributed to a temporal mismatch of the profiles (see Sect. 3.4.4). They are, however, clearly related to differences in the general design of these systems. Systems "A" and "B" are similar with respect to volumes and flow rates of water and air. For example, the total air volume of the equilibrator is exchanged every 2.5 min and 0.5 min, respectively, hence the similar equilibration times. In system "C" the large volume of air in the equilibrator is only exchanged every 20 min, which explains the more sluggish response seen in Fig. 23. System "D" is of the thin film type (i.e., unlike in the other system no turbulent mixing occurs in the equilibrator). It is known that this equilibration concept is characterized by somewhat larger time constants.

We would like to point out that different time constants are no quality criterion per se but rather must be seen in the context of the application. A detailed process study would certainly require high spatial and temporal resolution and hence an fCO_2 system with rather small time constants to resolve small-scale features. This is not equally the case in a basin-wide assessment of the fCO_2 in surface seawater, where the large-scale averaging would eliminate the effect of different time constants. The main point here is simply to show that these different characteristics are clearly reflected in the fCO_2 data set.

5. CONCLUSIONS

We have provided a common infrastructure to all participating groups in this exercise. We also have carried out several checks to exclude possible sources of error. Furthermore all raw data were run through the same calculation procedure. All these measures were taken in order to reduce as much as possible controllable sources of error. In this respect the exercise was technically a full success, and as summarized in the following discussion we also think that the exercise was a success scientifically.

We have demonstrated that the results of three out of seven underway systems agree to within about ±2 µatm throughout the cruise. This is not only the case for underway seawater fCO_2 measurements but also for measurements of atmospheric xCO_2. Interestingly, these three systems represent differences in such aspects as the design principle of the equilibrator, the volumes and flow rates of water and air involved, and the choice of wet or dry NDIR measurements. Thus this perfect agreement shows that—at least for NDIR instruments—the variety of designs used in the scientific community does not necessarily give rise to comparability problems or, to put it the other way round, systems of different design can produce reliable and consistent results.

We have also demonstrated that significant offsets of up to 10 µatm can be found in underway fCO_2 measurements under typical and identical field work conditions. Although in at least one case this may be a consequence of a technical failure, it is an indication of significant systematic differences in other cases. We certainly cannot claim that the observed differences are representative for these fCO_2 systems in general. They may also be typical only for the specific conditions of this particular cruise. There is, however, no indication that this cruise provided in any way untypical circumstances that could be made responsible for some of the observed deviations.

Finally we were able to demonstrate that discrete fCO_2 measurements agree with the results of the three most consistent underway fCO_2 systems. Therefore, measurements with these quite different approaches can be made with sufficient consistency, and the horizontal and vertical fCO_2 profiles generated from these different techniques can be expected to match in surface waters.

In conclusion, therefore, three main messages can be derived from this exercise:

- Underway measurements of the CO_2 fugacity in surface seawater and overlying air can be done to a high degree of agreement (±1 µatm) with a variety of possible equilibrator and system designs.

- Even well-designed systems, which are operated without any obvious sign of malfunction, can show significant differences of up to 10 µatm.

- The discrete fCO_2 measurements are in good agreement with the three most consistent underway fCO_2 data sets, at least to within its nominal accuracy of 1%.

These results pose the important question of how fCO_2 data sets acquired from different groups can be combined into a common database in light of possible

incompatibilities of up to 10 µatm. Although the results of this exercise do not solve this problem, they underline the importance of this aspect which must be taken into account in the construction of a consistent global fCO_2 database. Contributing to this dilemma is the fact that, in contrast to this exercise, other sources of error (temperature and pressure measurements, calibration gases etc.) further contribute to this uncertainty in field data.

In addition to this more general outcome, some of the results in more concrete terms follow. These may also serve as recommendations for future fCO_2 work in the ocean.

- The exercise shows no "best choice" for the type of the equilibrator (i.e., "showerhead," "bubbler," or "thin film") nor specifics on its dimensions and flow rates of seawater and air in regard to the achievable accuracy of the fCO_2 system.

- In contrast, the equilibrator type and its flow rates of seawater and air are important aspects with respect to the time constant of the equilibration process.

- Wet measurements can be done on the basis of the LI-6262 CO_2/H_2O gas analyzer (LI-COR Inc., U.S.A.) without necessary loss of accuracy when compared with traditional dry measurements.

- The factory calibration of the LI-COR LI-6262 CO_2/H_2O gas analyzer, which only requires the user to adjust "zero" and "span" of the instrument, seems to result in a loss of accuracy, which can easily be avoided by establishing an individual calibration curve on the basis of measurements of standard gases.

- The importance of rather accurate measurements of in situ and equilibrator temperature does not seem to be addressed adequately in the community. The observed differences between temperature measurements are clearly above a tolerable level and contribute—if representative and usually left unaccounted for—inconsistencies of several µatm (up to about 7 µatm in the present exercise).

- Calibration gases are an important issue. Even with the provided suite of consistent calibration gases, the NDIR analyzers could only be calibrated to an accuracy of 0.5 to 1.0 ppmv. We feel that this is about the tolerable limit. So any further error contribution from the calibrated standard concentrations worsens the situation. Use of calibration gases that are traceable to the same primary standards, such as the WMO primary standards maintained at SIO, would be desirable.

6. DATA CHECKS AND PROCESSING PERFORMED BY CDIAC

An important part of the numeric data package (NDP) process at the Carbon Dioxide Information Analysis Center (CDIAC) involves the quality assurance (QA) of data before distribution. Data received at CDIAC are rarely in a condition that would permit immediate distribution, regardless of the source. To guarantee data of the highest possible quality, CDIAC conducts extensive QA reviews that involve examining the data for completeness, reasonableness, and accuracy. Although they have common objectives, these reviews are tailored to each data set and often require extensive programming efforts. In short, the QA process is a critical component in the value-added concept of supplying accurate, usable data for researchers.

The following information summarizes the data-processing and QA checks performed by CDIAC on the underway data obtained during the R/V *Meteor* Cruise 36/1 in the North Atlantic Ocean.

1. All data files were provided to CDIAC as 10 comma-separated files (9 for surface seawater underway measurements of fCO_2 and 1 for all marine air xCO_2 measurements) by Dr. Arne Körtzinger of IfMK. A FORTRAN 77 retrieval program was written and used to reformat the original files into uniform ASCII-formatted "water" and "air" data files.

2. All underway "water" data are presented as 9 daily data files. These files can be merged into a single data file by request.

3. All data were plotted to check for obvious outliers.

4. Dates and times were checked for bogus values (e.g., values of MONTH < or >6, DAY <8 or >16, YEAR < or >1996, TIME <0000 or >2400.

5. The cruise track was plotted using the coordinates presented in data files and compared with the maps and cruise information supplied by A. Körtzinger.

7. HOW TO OBTAIN THE DATA AND DOCUMENTATION

This NDP-067 database is available free of charge from CDIAC and may be obtained in a variety of ways. The data are available from CDIAC's anonymous file transfer protocol (FTP) area via the Internet. Please note: your computer needs to have FTP software loaded on it (this is built into most newer operating systems). Use the following commands to obtain the database.

>ftp cdiac.esd.ornl.gov or >ftp 128.219.24.36
Login: "anonymous" or "ftp"
Password: *your e-mail name@your internet address*
ftp> cd pub/ndp067/
ftp> dir
ftp> mget (files)
ftp> quit

The complete documentation and data may also be obtained from the CDIAC oceanographic Web page (http://cdiac.esd.ornl.gov/oceans/doc.html).

You may also order through CDIAC's online ordering system (http://cdiac.esd.ornl.gov/pns/ how_order.html) or by contacting CDIAC directly to request the data on your choice of media.

For additional information, contact CDIAC.

Address: Carbon Dioxide Information Analysis Center
Oak Ridge National Laboratory
P.O. Box 2008
Oak Ridge, Tennessee 37831-6335
U.S.A.

Telephone: (423) 574-3645 (voice)
(423) 574-2232 (fax)

Electronic mail: cdiac@ornl.gov

Internet: http://cdiac.esd.ornl.gov/

8. REFERENCES

Copin-Montegut, C. 1988. A method for the continuous determination of the partial pressure of carbon dioxide in the upper ocean. *Mar. Chem.* 17:13–21.

Copin-Montegut, C. 1989. A new formula for the effect of temperature on the partial pressure of CO_2 in seawater. Corrigendum. *Mar. Chem.* 27:143–44.

Gordon, L. I., and L. B. Jones. 1973. The effect of temperature on carbon dioxide partial pressure in seawater. *Mar. Chem.* 1:317–22.

Goyet, C., F. J. Millero, A. Poisson, and D. K. Shafer. 1993. Temperature dependence of CO_2 fugacity in seawater. *Mar. Chem.* 44:205–19.

Goyet, C., and E. Peltzer. 1994. Comparison of the August-September 1991 and 1979 surface partical pressure of CO_2 distribution in the Equatorial Pacific Ocean near 150° W. *Mar. Chem.* 45:257–66.

Guggenheim, E. A. 1967. pp. 175–77 In: *Thermodynamics*, North-Holland, Amsterdam.

Johnson, K. M., A. Körtzinger, L. Mintrop, J. C. Duinker, and D. W. R. Wallace. 1998. Coulometric total carbon dioxide analysis for marine studies: Measurement and internal consistency of underway surface TCO_2 concentrations. *Mar. Chem.* (in press).

Keeling, C. D., P. R. Guenther, and D. J. Moss. 1986. *Scripps Reference Gas Calibration System for Carbon Dioxide-in-Air Standards: Revision of 1985.* WMO Environmental Pollution Monitoring and Research Programme No. 42, Technical Document WMO/TD-125, World Meteorological Organization, Geneva, Switzerland.

Körtzinger, A., L. Mintrop, and J. C. Duinker. 1996a. The floating dripstone cave: CO_2 teams compare underway systems. *U.S. JGOFS News* 7(4):14–15.

Körtzinger, A., H. Thomas, B. Schneider, N. Gronau, L. Mintrop, and J. C. Duinker. 1996b. At-sea intercomparison of two newly designed underway pCO_2 systems: Encouraging results. *Mar. Chem.* 52:133–45.

McDermitt, D. K., J. M. Welles, and R. D. Eckles. 1993. *Effects of Temperature, Pressure, and Water Vapor on Gas Phase Infrared Absorption by CO_2.* Li-Cor Inc., Lincoln, Nebraska, U.S.A.

Neill, C., K. M. Johnson, E. Lewis, and D. W. R. Wallace. 1997. Accurate headspace analysis of fCO_2 in discrete water samples using batch equilibration. *Limnol. Oceanogr.* 42:1774–83.

Ohtaki, E., E. Yamashita, and F. Fujiwara. 1993. Carbon dioxide in surface seawaters of the Seto Inland Sea, *Japan. J. Oceanogr.* 49:295–304.

Poisson, A., N. Metzl, C. Brunet, B. Schauer, B. Bres, D. Ruiz-Pino, and F. Louanchi. 1995. Variability of sources and sinks of CO_2 in the Western Indian and Southern Oceans during the year 1991. *J. Geophys. Res.* 98(C12):22759–778.

Robertson, J. E., and A. J. Watson. 1992. Thermal skin effect of the surface ocean and its implications for CO_2 uptake. *Nature* 358:738–40.

Schluessel, P., W. J. Emery, H. Grassl, and T. Mammen. 1990. On the bulk-skin temperature difference and its impact on satellite remote sensing of sea surface temperature. *J. Geophys. Res.* 95:13341–356.

Takahashi, T., J. Olafsson, J. G. Goddard, D. W. Chipman, and S. C. Sutherland. 1993. Seasonal variations of CO_2 and nutrient salts in the high latitude oceans: A comparative study. *Global Biogeochem. Cycles* 7:843–848.

Thoning, K. W., P. Tans, T. J. Conway, and L. S. Waterman. 1987. *NOAA/GMCC calibrations of CO_2-in-air reference gases: 1979-1985*, NOAA Technical Memorandum ERL/ARL-150. Environmental Research Laboratory, Boulder, Colorado.

Welles, J. M., and R. D. Eckles. 1991. *Li-Cor 6262 CO_2/H_2O Analyzer Operating and Service Manual.* Publication No. 9003-59. Li-COR Inc., Lincoln, Nebraska, U.S.A.

Weiss, R. F. 1974. Carbon dioxide in water and seawater: The solubility of a non-ideal gas. *Mar. Chem.* 2:203–15.

Weiss, R. F., and B. A. Price. 1980. Nitrous oxide solubility in water and seawater. *Mar. Chem.* 8:347–59.

Weiss, R. F., R. A. Jahnke, and C. D. Keeling. 1982. Seasonal effects of temperature and salinity on the partial pressure of CO_2 in seawater. *Nature* 300:511–13.

Zhao, C. L., P. P. Tans, and K. W. Thoning. 1997. A high precision manometric system for absolute calibrations of CO_2 in dry air. *J. Geophys. Res.* 102:5885–94.

PART 2

CONTENT AND FORMAT OF DATA FILES

9. FILE DESCRIPTIONS

This section describes the content and format of each of the 13 files that make up this NDP (see Table 4). Because CDIAC distributes the data set in several ways (e.g., via anonymous FTP and on floppy diskette), each of the 13 files is referenced by both a file number and an ASCII file name, which is given in lowercase, bold-faced type (e.g., **ndp067.doc**). The remainder of this section describes (or lists, where appropriate) the contents of each file.

Table 4. Content, size, and format of data files

File number, name, and description	Logical records	File size in bytes
1. **ndp067.txt:** A detailed description of the cruise network, the two FORTRAN 77 data-retrieval routines, and the ten oceanographic data files	3,059	122,515
2. **fco2wat.for:** A FORTRAN 77 data-retrieval routine to read and print all ***w.txt** files (Files 4–12)	54	2,005
3. **xco2air.for:** A FORTRAN 77 data-retrieval routine to read and print **xco2air.txt** (File 13)	42	1,264
4. **080696w.txt:** Underway measurements of surface seawater fCO_2 and hydrographic parameters during 8 June 1996	1,444	218,336
5. **090696w.txt:** Underway measurements of surface seawater fCO_2 and hydrographic parameters during 9 June 1996	1,442	218,032
6. **100696w.txt:** Underway measurements of surface seawater fCO_2 and hydrographic parameters during 10 June 1996	1,442	218,032
7. **110696w.txt:** Underway measurements of surface seawater fCO_2 and hydrographic parameters during 11 June 1996	1,442	218,183
8. **120696w.txt:** Underway measurements of surface seawater fCO_2 and hydrographic parameters during 12 June 1996	1,442	218,032
9. **130696w.txt:** Underway measurements of surface seawater fCO_2 and hydrographic parameters during 13 June 1996	1,442	218,032
10. **140696w.txt:** Underway measurements of surface seawater fCO_2 and hydrographic parameters during 14 June 1996	1,443	218,184
11. **150696w.txt:** Underway measurements of surface seawater fCO_2 and hydrographic parameters during 15 June 1996	1,443	218,184
12. **160696w.txt:** Underway measurements of surface seawater fCO_2 and hydrographic parameters during 16 June 1996	1,444	218,336
13. **xco2air.txt:** Underway measurements of air xCO_2 during the entire expedition	1,744	104,604
Total	17,883	2,193,739

9.1 ndp067.txt (FILE 1)

This file contains a detailed description of the data set, the two FORTRAN 77 data-retrieval routines, and the ten oceanographic data files. It exists primarily for the benefit of individuals who acquire this database as machine-readable data files from CDIAC.

9.2 fco2wat.for (FILE 2)

This file contains a FORTRAN 77 data-retrieval routine to read and print all *w.txt files. The following is a listing of this program. For additional information regarding variable definitions, variable lengths, variable types, units, and codes, please see the description for *w.txt files in Sect. 9.4.

```
c*****************************************************************
c* FORTRAN 77 data retrieval routine to read and print the files
c* named "*w.txt" (Files 4-12)
c*****************************************************************

c*Defines variables*

        CHARACTER date*10, time*8
        INTEGER course
        REAL latdcm, londcm, speed, temp, salt, press, fco2a, fco2b
        REAL fco2c, fco2d, fco2e, fco2f, fco2g, fco2h
        OPEN (unit=1, file='input.txt')
        OPEN (unit=2, file='output.txt')
        write (2, 5)

c*Writes out column labels*

 5      format (5X,'DATE',9X,'TIME',5X,'LATITUDE',3X,'LONGITUDE',
     1  3X,'SPEED',1X,'COURSE',4X,'TEMP',2X,'SALNTY',4X,
     2  'PRESS',4X,8('fCO2',4X),/,5X,'GMT',10X,'GMT',8X,
     3  'DEG N',6X,'DEG E',7X,'KN',3X,'DEG',5X,'DEG C',
     4  2X,'PSS-78',5X,'hPA',5X,8('µatm',4X),/,
     5  2X,'DD.MM.YYYY',4X,'HH:MM:SS',66X,'LAB A',3X,
     6  'LAB B',3X,'LAB C',3X,'LAB D',3X,'LAB E',3X,
     7  'LAB F',3X,'LAB G',3X,'LAB H')

c*Sets up a loop to read and format all the data in the file*

        read (1, 6)
 6      format (////////////)
```

```
 7      CONTINUE
        read (1, 10, end=999) date, time, latdcm, londcm, speed,
     1  course, temp, salt, press, fco2a, fco2b, fco2c, fco2d,
     2  fco2e, fco2f, fco2g, fco2h

 10     format (2X, A10, 4X, A8, 4X, F7.4, 4X, F8.4, 4X, F4.1,
     1  2X, I3, 5X, F5.2, 3X, F5.2, 3X, F6.1, 1X, F7.2, 1X, F7.2,
     2  1X, F7.2, 1X, F7.2, 1X, F7.2, 1X, F7.2, 1X, F7.2, 1X, F7.2)

        write (2, 20) date, time, latdcm, londcm, speed,
     1  course, temp, salt, press, fco2a, fco2b, fco2c, fco2d,
     2  fco2e, fco2f, fco2g, fco2h

 20     format (2X, A10, 4X, A8, 4X, F7.4, 4X, F8.4, 4X, F4.1,
     1  2X, I3, 5X, F5.2, 3X, F5.2, 3X, F6.1, 1X, F7.2, 1X, F7.2,
     2  1X, F7.2, 1X, F7.2, 1X, F7.2, 1X, F7.2, 1X, F7.2, 1X, F7.2)

        GOTO 7
 999    close(unit=1)
        close(unit=2)
        stop
        end
```

9.3 xco2air.for (FILE 3)

This file contains a FORTRAN 77 data-retrieval routine to read and print xco2air.txt file. The following is a listing of this program. For additional information regarding variable definitions, variable lengths, variable types, units, and codes, please see the description for xco2air.txt file in Sect. 9.5.

```
c*****************************************************************
c* FORTRAN 77 data retrieval routine to read and print the files
c* named "xco2air.txt" (File 13)
c*****************************************************************

c*Defines variables*

        CHARACTER date*10, time*8, lab*1
        REAL latdcm, londcm, xco2
        OPEN (unit=1, file='xco2air.txt')
        OPEN (unit=2, file='xco2air.dat')
        write (2, 5)

c*Writes out column labels*

 5      format (5X,'DATE',9X,'TIME',4X,'LATITUDE',2X,'LONGITUDE',
     1  2X,'xCO2_AIR',1X,'LAB',/,5X,'GMT',10X,'GMT',7X,
     3  'DEG N',6X,'DEG E',5X,'PPMV',4X,'NO',/,
     5  2X,'DD.MM.YYYY',4X,'HH:MM:SS')
```

```
c*Sets up a loop to read and format all the data in the file*

      read (1, 6)
 6    format (////////////)

 7    CONTINUE
      read (1, 10, end=999) date, time, latdcm, londcm, xco2, lab

 10   format (2X, A10, 4X, A8, 4X, F6.3, 4X, F7.3, 4X, F6.2,
     1 3X, A1)

      write (2, 20) date, time, latdcm, londcm, xco2, lab

 20   format (2X, A10, 4X, A8, 4X, F6.3, 4X, F7.3, 4X, F6.2,
     1 3X, A1)

      GOTO 7
 999  close(unit=1)
      close(unit=2)
      stop
      end
```

9.4 *w.txt (FILES 4–12)

These 9 data files contain the underway measurements of surface seawater fCO_2 and hydrographic parameters made by participants in the systems intercomparison exercise during the R/V *Meteor* Cruise 36/1 in the North Atlantic Ocean. All files have the same ASCII format and can be read by using the following FORTRAN 77 code [contained in fco2wat.for (File 2)]:

```
      CHARACTER date*10, time*8
      INTEGER course
      REAL latdcm, londcm, speed, temp, salt, press, fco2a, fco2b
      REAL fco2c, fco2d, fco2e, fco2f, fco2g, fco2h

      read (1, 10, end=999) date, time, latdcm, londcm, speed,
     1 course, temp, salt, press, fco2a, fco2b, fco2c, fco2d,
     2 fco2e, fco2f, fco2g, fco2h

 10   format (2X, A10, 4X, A8, 4X, F7.4, 4X, F8.4, 4X, F4.1,
     1 2X, I3, 5X, F5.2, 3X, F5.2, 3X, F6.1, 1X, F7.2, 1X, F7.2,
     2 1X, F7.2, 1X, F7.2, 1X, F7.2, 1X, F7.2, 1X, F7.2, 1X, F7.2)
```

Stated in tabular form, the contents include the following:

Variable	Variable type	Variable width	Starting column	Ending column
date	Character	10	3	12
time	Character	8	17	24
latdcm	Numeric	7	29	35
londcm	Numeric	8	40	47
speed	Numeric	4	52	55
course	Numeric	3	58	60
temp	Numeric	5	66	70
salt	Numeric	5	74	78
press	Numeric	6	82	87
fco2a	Numeric	7	89	95
fco2b	Numeric	7	97	103
fco2c	Numeric	7	105	111
fco2d	Numeric	7	113	119
fco2e	Numeric	7	121	127
fco2f	Numeric	7	129	135
fco2g	Numeric	7	137	143
fco2h	Numeric	7	145	151

The variables are defined as follows:

date is the sampling date (day/month/year);

time is the sampling time [Greenwich mean time (GMT)];

latdcm is the latitude of the sampling location (decimal degrees; negative values indicate the Southern Hemisphere);

londcm is the longitude of the sampling location (decimal degrees; negative values indicate the Western Hemisphere);

speed is the speed of the ship during the measurements (kn);

course is the course of the ship during the measurements (degrees);

temp is the sea-surface temperature (°C);

salt is the sea-surface salinity [on the Practical Salinity Scale (PSS)];

press is the atmospheric pressure (hPA);

fco2a is the underway fugacity of CO_2 in surface seawater (µatm) measured by laboratory A;

fco2b is the underway fugacity of CO_2 in surface seawater (µatm) measured by laboratory B;

fco2c is the underway fugacity of CO_2 in surface seawater (µatm) measured by laboratory C;

fco2d is the underway fugacity of CO_2 in surface seawater (µatm) measured by laboratory D;

fco2e is the underway fugacity of CO_2 in surface seawater (µatm) measured by laboratory E;

fco2f is the underway fugacity of CO_2 in surface seawater (µatm) measured by laboratory F;

fco2g is the underway fugacity of CO_2 in surface seawater (µatm) measured by laboratory G;

fco2h is the discrete fugacity of CO_2 in surface seawater (µatm) measured by laboratory H.

9.5 xco2air.txt (FILE 13)

This data file contains the underway measurements of atmospheric xCO_2 made during R/V *Meteor* Cruise 36/1 in the North Atlantic Ocean. The data are presented in ASCII format and can be read by using the following FORTRAN 77 code [contained in **xco2air.for** (File 3)] in Sect. 9.3:

```
      CHARACTER date*10, time*8, lab*1
      REAL latdcm, longdcm, xco2

      read (1, 10, end=999) date, time, latdcm, londcm, xco2, lab

 10   format (2X, A10, 4X, A8, 4X, F6.3, 4X, F7.3, 4X, F6.2,
     1 3X, A1)
```

Stated in tabular form, the contents include the following:

Variable	Variable type	Variable width	Starting column	Ending column
date	Character	10	3	12
time	Character	8	17	24
latdcm	Numeric	6	29	34
londcm	Numeric	7	39	45
xco2	Numeric	6	50	55
lab	Character	1	59	59

The variables are defined as follows:

date is the sampling date (day/month/year);

time is the sampling time (GMT);

latdcm is the latitude of the sampling location (decimal degrees; negative values indicate the Southern Hemisphere);

londcm is the longitude of the sampling location (decimal degrees; negative values indicate the Western Hemisphere);

xco2 is the mole fraction of atmospheric CO_2 (ppmv) measured in dry air;

lab is the laboratory identifier.

APPENDIX A

CALCULATIONS

APPENDIX A: CALCULATIONS

A.1 CALCULATION OF THE WATER VAPOR PRESSURE

The water vapor pressure of seawater is generally calculated from seawater temperature and salinity. We used the method given by Weiss and Price (1980) in which the authors provide an equation to assess the saturation water vapor pressure of seawater over the temperature range 273 to 313 K and the salinity range 0 to 40:

$$\ln p_{sw} = 24.4543 - 67.4509 \cdot \left(\frac{100}{T}\right) - 4.8489 \cdot \ln\left(\frac{T}{100}\right) - 0.000544 \cdot S \ ,$$

where p_{sw} is the water vapor pressure (in atm), T is the temperature (in K), and S is the salinity on the Practical Salinity Scale.

A.2 CALCULATION OF fCO_2 FOR MOIST AIR CONDITIONS

The first step in the calculation procedure for final fCO_2 values, either for the atmosphere or for surface seawater, is the calculation of the fCO_2 for moist air from the measured mole fraction (xCO_2) in dry air. Weiss and Price (1980) give the theoretical basis for this calculation based on equations given by Guggenheim (1967) for calculating fugacities in binary mixtures:

$$f_1 = x_1 \cdot P \cdot \exp\left[\frac{\left(B_{11} + 2(x_2)^2 \cdot \delta_{12}\right) \cdot P}{R \cdot T}\right] ,$$

where x_1 is the mole fraction of pure gas 1, x_2 is the mole fraction of pure gas 2, P is the total pressure, R is the gas constant, T is the absolute temperature, and δ_{12} is defined by

$$B_{12} = \frac{1}{2}(B_{11} + B_{22}) + \delta_{12} \ ,$$

where B_{11} is the virial coefficient for interaction between pure gas 1 molecules, B_{22} is the virial coefficient for interaction between pure gas 2 molecules, and B_{12} is the virial coefficient for interaction between molecules of gas 1 and 2. For calculating fCO_2, gas 1 is here considered as the analyte gas (CO_2) and gas 2 as dry air. The mole fraction x_2 of dry air in this mixture is approximately equal to 1 for the analyte concentrations considered here. To calculate the fCO_2 for moist air conditions at the equilibrator temperature (fCO_2 of seawater) or the air–sea interface (fCO_2 of air), the mole fraction of CO_2 in dry air x_1 must be corrected to the mole fraction of CO_2 in moist air x_1'. If the

gas–water interface can be regarded as being saturated with water vapor at the water temperature, the following equation holds:

$$x_1' = x_1 \cdot \left(1 - \frac{p_{sw}}{p_{atm}}\right).$$

In this equation p_{sw} is the saturated water vapor pressure of seawater at the given temperature and p_{atm} is the total barometric pressure. Because of the thermal skin effect, the temperature at the interface is usually not the same as the mixed-layer bulk temperature (Schluessel et al. 1990). This effect, which typically accounts for an interface temperature of a few tenths of a degree below the bulk temperature, has significant implications for the effective fCO_2 difference at the air–sea interface (Robertson and Watson 1992). As the exact skin temperature is rarely known, the bulk temperature is used instead. The fCO_2 for moist air conditions can therefore be calculated according to

$$f = x_1 \cdot (p_{atm} - p_{sw}) \cdot \exp\left[\frac{p_{atm} \cdot (B + 2\delta)}{R \cdot T}\right].$$

The virial coefficient B (in cm^3/mol) of CO_2 can be calculated for the temperature range 265 to 320 K using a power series given by Weiss (1974):

$$B = -1636.75 + 12.0408 \cdot T - 3.27957 \cdot 10^{-2} \cdot T^2 + 3.16528 \cdot 10^{-5} \cdot T^3 .$$

Weiss (1974) gives the following equation for the cross virial coefficient δ of CO_2 in air as a function of temperature ($273 < T < 313$ K):

$$\delta = 57.7 - 0.118 \cdot T .$$

A.3 CORRECTION OF fCO_2 TO IN SITU TEMPERATURE

To account for the slight warming of the seawater between the seawater intake and the equilibrator, the measured fCO_2 values have to be corrected back to in situ temperature. Different equations (for pCO_2 and fCO_2) have been published in the literature (e.g., Gordon and Jones 1973; Weiss et al. 1982; Copin-Montegut 1988, 1989; Goyet et al. 1993; Takahashi et al. 1993). As the temperature changes are of the order of a few tenths of a degree only, the choice among these equations is not critical. We have used the following equation given by Weiss et al. (1982), which describes the temperature dependence of the solubility of CO_2 and the carbonic acid equilibria:

$$\frac{\partial \ln fCO_2}{\partial t} = 0.03107 - 2.785 \cdot 10^{-4} \cdot t - 1.839 \cdot 10^{-3} \cdot \ln fCO_2 ,$$

where t is the seawater temperature (in °C). The equation gives the change in the logarithm of the fugacity of CO_2 in moist air for an incremental increase of the temperature between in situ and measurement temperature.

APPENDIX B

REPRINTS OF PERTINENT LITERATURE

APPENDIX B CONTENTS AND COPYRIGHT PERMISSIONS

Marine Chemistry, 45 (1994) 257–266
0304-4203/94/$07.00

Comparison of the August–September 1991 and 1979 surface partial pressure of CO_2 distribution in the Equatorial Pacific Ocean near 150°W

Catherine Goyet, Edward T. Peltzer
Woods Hole Oceanographic Institution, Department of Marine Chemistry and Geochemistry, Woods Hole, MA 02543, USA

(Received April 16, 1993; revision accepted October 4, 1993)

Abstract

The partial pressure of CO_2 (pCO_2) in the surface seawater and marine air from 17°S to 22°N near 151°W (WOCE leg P-16c) during the period from August 31 to September 29, 1991, were measured continually. The surface seawater pCO_2 showed large latitudinal variation with a maximum of 425 μatm near the equator. These results are compared with pCO_2 measurements in 1979, in the same area and same months. The short-scale (temporal and spatial) variations in surface seawater pCO_2 (±6.1 μatm) do not allow us to unequivocally quantify the variation in ΔpCO_2 ($pCO_2^{sea} - pCO_2^{air}$) between the years 1979 and 1991 due to oceanic uptake of fossil fuel CO_2. However, the data suggest that this ocean area might be a stronger source of CO_2 for the atmosphere than may be expected from results of ocean models.

1. Introduction

The global ocean regulates the Earth's climate by continuously exchanging heat and greenhouse gases with the atmosphere. These exchange processes are poorly known. In the surface ocean, pCO_2 is controlled by the complex interactions of biological activities, the ocean chemical CO_2 buffer capacity, and the ocean circulation dynamics. The relative importance of these processes is only broadly known over the world ocean and varies with time and space. Currently, two of the principal ocean observing programs (the Joint Global Ocean Flux Study [JGOFS], and the World Ocean Circulation Experiment [WOCE]), are cooperating to address these questions and to study the oceanic carbon cycle and its interactions with the atmosphere at the world ocean scale. It is in this context that we participated in WOCE cruise P-16c in the Equatorial Pacific Ocean aboard R/V *Thomas Washington*, to carry out a JGOFS CO_2 program to create a global oceanic CO_2 data set.

The surface seawaters of the Central Equatorial Pacific Ocean are composed of the return flow of the North-Equatorial counter current and of the South-Equatorial current. They are the site of high seawater pCO_2 and high "new" production driven by upwelled nutrients (Chavez and Barber, 1987). Thus, this ocean area is potentially a major region of carbon cycling between the subsurface and deep waters and with the atmosphere.

The numerous different estimates of the amount of CO_2 gas transferred between the ocean and atmosphere (Keeling, 1968; Miyake et al., 1974; Keeling and Revelle, 1985; Broecker et al., 1986; Feely et al., 1987; Fushimi, 1987; Inoue and Sugimura, 1988, 1992; Bacastow and Maier-Reimer, 1990; Murphy et al., 1991; Lefevre and Dandonneau, 1992; Wong et al.,

SSDI 0304-4203(93)E0064-6

1993), emphasize both the high variability of the flux of CO_2 gas across the air–sea interface and the need to acquire a better understanding of pCO_2 dynamics in this area of research. Thus, one of the great scientific challenges today is to better quantify the seasonal and interannual variations of the CO_2 gas exchange across the air–sea interface.

Quantification of the net CO_2 flux across the ocean–atmosphere interface can, in principle, be accessed by direct measurements in the atmosphere (Jones and Smith, 1977; Jones, 1980). In practice however, this is extremely difficult (Broecker et al., 1986) because of the slow exchange rate. Calculation of the net flux from air–sea CO_2 partial pressure differences is the universally preferred scheme (Keeling, 1968; Broecker et al., 1978; Liss, 1983a,b). Yet, the uncertainty associated with such calculations often exceeds 50% (Goyet and Brewer, 1993) due to uncertainties in the transfer coefficient (Watson et al., 1991), and in the temperature of the skin layer (Robertson and Watson, 1992).

The validity of the results of such a calculation is further limited to a short time period since both the ΔpCO_2 [difference between surface seawater pCO_2 (pCO_2^{sea}) and atmospheric pCO_2 (pCO_2^{air})] and the wind speed used to estimate the transfer velocity are those measured instantaneously at a definite time of year and are usually not representative of an annual mean. Another uncertainty in the estimation of seasonal and interannual CO_2 flux is due to the uncertainty in the poorly documented spatial and temporal variations of pCO_2^{sea}. This is especially true in the Equatorial Pacific Ocean where El Nino-Southern Oscillation (ENSO) events (an anomalous quasi-oscillatory warming of the tropical Pacific Ocean) occur relatively frequently.

These ENSO events, which appear to be chaotic-like in nature (Gleick, 1987), change the "normal" state of the Equatorial Pacific Ocean over very large areas (Meyers, 1982; Enfield, 1989). Consequently, in addition to the earlier investigations that describe pCO_2^{sea} variations in this area (Keeling, 1968; Miyake et al., 1974; Keeling and Revelle, 1985; Broecker et al., 1986; Feely et al., 1987; Fushimi, 1987; Inoue and Sugimura, 1988, 1992; Bacastow and Maier-Reimer, 1990; Murphy et al., 1991; Lefevre and Dandonneau, 1992; Wong et al., 1993), repeated seasonal and interannual measurements of pCO_2 in the Pacific Equatorial region are needed to better quantify the net long-term CO_2 flux across the ocean–atmosphere interface.

In this paper, we present the results of underway pCO_2 measurements made in 1991 in the Central Equatorial Pacific Ocean and quantify the temporal and spatial variations of pCO_2 in this area. Our data are then compared with the 1979 data of Weiss et al. (1992).

2. Sampling and analysis

The R/V *Thomas Washington* on WOCE P16c departed from Papeete, Tahiti on August 31, 1991, and arrived in Honolulu, Hawaii on October 1, 1991, with cruise track in Fig. 1. The mole fraction of CO_2 (xCO_2) in the seawater equilibrated air and in the atmosphere were continuously measured along this cruise track using an automated underway CO_2 monitoring system with an infra-red detector.

The automated underway CO_2 monitoring system consists of a "shower-head" type equilibrator (Broecker and Takahashi, 1966; Keeling, 1968; Takahashi et al., 1970) and a non-dispersive infra-red (NDIR) CO_2 and H_2O analyzer (Li-COR 6262) with solid state detector. A system of automated valves (Fig. 2) controls the frequent and regular switching of gas flows to the NDIR analyzer between seawater equilibrated air (SEA), seasurface air sampled at the ship bow (AIR), and two gas standards (high and low CO_2 concentration, 513.5 and 320.0 μmol/mol, respectively). The small size (approximately 40 cm high) equilibrator (modified from a design used by Weiss) consists of two concentric cylindrical stages constructed of plexiglass, with a drain in the center. The seawater "showers" through the top of

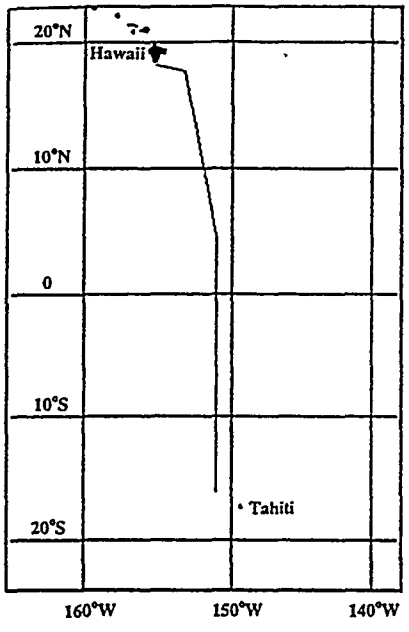

Fig. 1. Cruise track for WOCE P-16c (R/V *Thomas Washington*), between Tahiti and Hawaii, 31 August 1991–1 October 1991.

the equilibrator at a rate of about 4 l/min, and the first stage of the equilibrator is vented to the clean marine atmosphere to maintain ambient pressure. The gas phase is continuously re-circulated, at a rate of 200 ml/min, by an air pump, through a closed loop passing through the infra-red analyzer where the measurement is made. The seawater temperature in the equilibrator, as well as both atmospheric pressure and the gas pressure in the closed loop are monitored. The pressure tranducers (SETRA model 270, range 600–1100 mbar) used for the pressure measurements were calibrated and certified per the National Institute of Standards and Technology (NIST) traceable primary standard with an accuracy of ±0.05% of full scale. The temperature sensor used to measure the seawater temperature in the equilibrator was calibrated (against a platinum resistance thermometer) in our laboratory before the cruise.

The CO_2/H_2O differential, NDIR analyzer is of small size, precise, and insensitive to vibrations and lateral accelerations. The sample cells are gold-plated to enhance infra-red (IR) reflectivity and resist tarnishing over time. One set of cells is used for both H_2O and CO_2 measurements by using a dichroic beam splitter to provide radiation to two separate detectors. A 150 nm bandpass optical filter is used to select the 4.26 μm absorption band for CO_2 detection, and the H_2O detector is filtered for the 2.59 μm absorption band. Both filters provide excellent rejection of IR radiation outside the desired band, allowing the analyzer to reject the response of other IR absorbing gases. The filters are mounted directly on the detectors for thermal stability. The lead selenide solid state detectors are cooled and regulated at −12°C by thermoelectric coolers, and electronic circuits continuously monitor and maintain a constant detector sensitivity. The detector housing is maintained free of water vapor and CO_2 by internally mounted dessicant and absorbants. In order to maximize the signal sensitivity, the infra-red radiation from the source is focused through the gas cell and onto the detector by lenses at each end of the optical bench. The typical CO_2 noise level is 0.2 μmol/mol peak-to-peak (at 350 μmol/mol) when using one second signal averaging. The Li-Cor CO_2/H_2O analyzer uses an internal algorithm to correct the measurements to a dry gas scale and to a pressure of one atmosphere. Thus, this automated system allows us to directly monitor xCO_2 (mole fraction of CO_2 gas corrected to dry air and to the pressure of 1 atm) in the gas phase without having to pretreat it (no drying nor gas separation are required). This not only simplifies the measurement procedure, but also minimizes the potential errors in the measurements.

This system is regularly calibrated every 2 h, using CO_2 standard gases (320.0 and 513.5 μmol/mol) that we calibrated using a primary standard gas (352.2 μmol/mol) purchased from the National Institute of Standards and Technology (NIST). The 2 h calibration measurement indicated that the infra-red analyzer was remarkably stable to ±0.2 μmol/mol; a 6 h calibration interval would have been sufficient.

The computer recorded one xCO_2 datum per

f_R = filter; gelman 1.0 μ; reference
f_S = filter; gelman 1.0 μ; sample
V_1, V_3, V_5, V_7 = 3-way electrical valves
PT_1 = Pressure Transducer (line pressure)
PT_2 = Pressure Transducer (ambient)
RM_R = rotometer; reference
RM_S = rotometer; sample
T_R = trap; ref. (soda lime & Mg $(ClO_4)_2$)
T_S = trap; sample (soda lime & Mg $(ClO_4)_2$)
P_A = pump, Air
P_R = pump; reference
P_S = pump; sample
$^3V_A, ^3V_B$ = 3-way valves
X_1, X_2, X_3, X_4 = regulating valves
D.P.G. = Dew Point Generator
7M = 7μ filter

Tubing legend
3/8" Dekoran type 1300
1/8" copper
1/4" copper
1/8" Bev-a-line

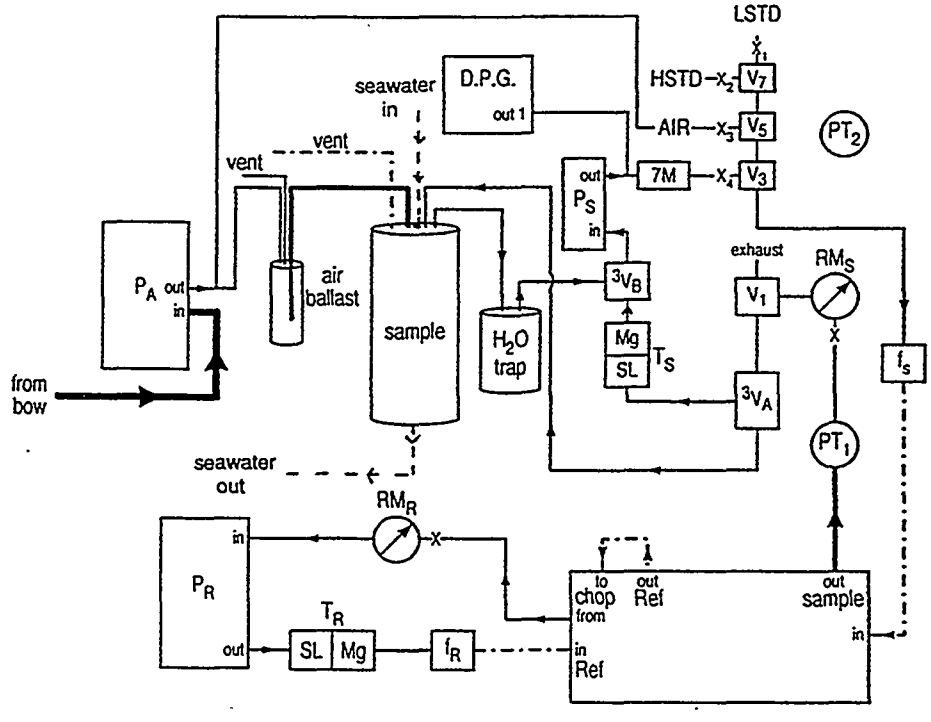

Fig. 2. Schematic diagram of infra-red analyzer based system for the determination of pCO_2 in seawater.

minute consisting of an average of 10 readings taken every 6 s. A typical duty cycle consisted of a 5-min cell flush, followed by five 1-min averages. Next, this cycle is repeated for the measurement of air (the air intake was located at the bow of the ship). The air intake system consisted of an inverted polyethylene funnel mounted on the jack-staff at the bow of the ship and 3/8" i.d. Dekoron (R, type 1300, Furon Co Inc., Aurora, OH) line. Sea surface air was pumped from the bow of the ship with an Air-Cadet® (Cole-Parmer, Chicago, IL) pump at several liters per minute. After the pump line was split, part of the air supply went to our instrument. A portion of the air we received (> 500 ml/min) was used to flush a "ballast" chamber which was

vented to the ambient atmosphere. This ballast chamber was then used to maintain ambient pressure in the equilibrator head-space. When analyzing sea air, a flowrate of 200 ml/min was maintained through the NDIR. Every 2 h the alternation of the two sample gases is interrupted with the measurement of the two reference gases according to the same 10 min cycle. The variations of pCO_2 on the time scale of 1 min or less are of little interest. We report here data averaged over the final 4 min of the duty-cycle.

We computed pCO_2 from the measured xCO_2 using the relationships (UNESCO, 1987):

$$pCO_2 = xCO_2 \times \text{pressure} \times [1 - (\text{vapour}/\text{pressure})]$$

with

$$\text{vapour} = 0.981 \times \exp(27.029 - 0.098T - 6163/T)$$

where "pressure" represents the ambient atmospheric pressure, "vapour" represents the saturation water vapour pressure at the air–sea interface, and T is the surface temperature in the equilibrator.

Since the observed temperature of the water in the equilibrator was generally 0.2 ± 0.1°C warmer than the in-situ temperature at the water intake, we made a small temperature correction using the relationships given by Copin-Montegut (1988). The accuracy associated with the present pCO_2 data set is estimated to be close to 2 μatm.

3. Results

Fig. 3 shows the in-situ pCO_2 distributions (pCO_2^{air} and pCO_2^{sea}, corrected to 100% humidity, in-situ temperature and barometric pressure) along the N–S transects at 150°W in

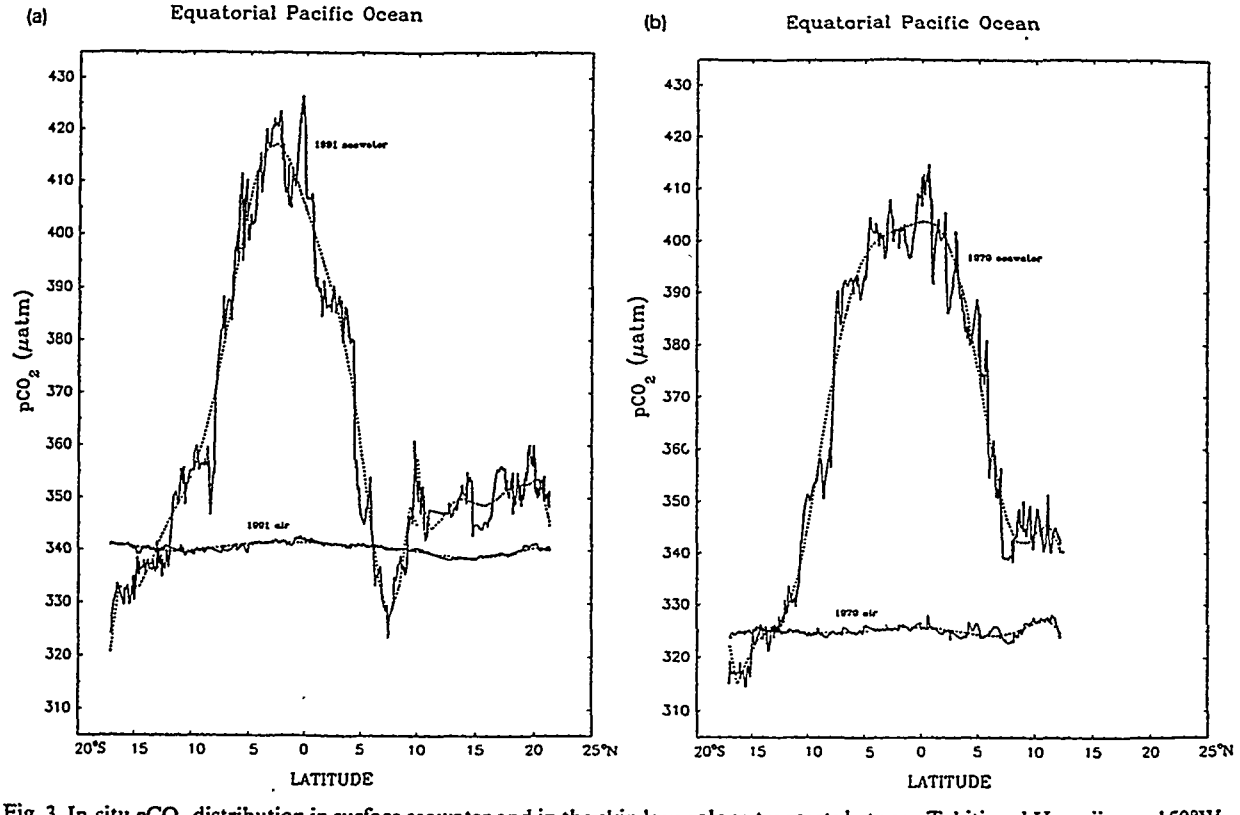

Fig. 3. In-situ pCO_2 distribution in surface seawater and in the skin layer along transects between Tahiti and Hawaii near 150°W in the Equatorial Pacific Ocean. (a) 1991 data. (b) 1979 data from Weiss et al. (1992). The dashed lines are smooth fits to the data.

the Central Pacific Ocean. Along 151°W, between 2°N and 7°S, the surface seawater pCO_2 was above 390 μatm with a maximum close to 425 μatm near the Equator.

The high spatial resolution of these pCO_2 measurements, as illustrated in Fig. 3, reveals details of the large natural variability of pCO_2 in surface seawater. One can obtain an estimate of this variability by examining the difference between the actual data and a smooth fit (see below). Very sharp gradients of pCO_2^{sea} (larger than 30 μatm), are observed at the front between different water masses associated with the equatorial upwelling band (within less than 1/2 degree latitude). Within a water mass pCO_2^{sea} variations ranging from 5 to 10 μatm are frequently observed on a very short temporal (<day) and geographical (<1/2 degree latitude) scales. However, the nature of the cruise (survey with a short station every 30′ latitude) does not allow us to separate the temporal (day/night) variations from the geographical variations. Both are intertwined. The major direct implication of these short-scale pCO_2 variations is that over large ocean areas where ΔpCO_2 is smaller than 20 μatm, the natural CO_2 flux between a single water mass and the atmosphere can vary by more than 25% due to the natural variations in pCO_2^{sea} alone.

4. Comparison with earlier data set

Current predictions of the evolution of the CO_2 fluxes across the air–sea interface (Pearman et al., 1983; Volk and Bacastow, 1989) suggest that the difference beween pCO_2^{sea} and pCO_2^{air} should decrease everywhere—although not uniformally—over the surface ocean. This prediction is based on the fact that pCO_2^{air} is increasing much faster than pCO_2^{sea} (due to the relatively large increase of anthropogenic CO_2 in the atmosphere). One of the approaches used to achieve the quantification of the increase is, when possible, a direct comparison of ΔpCO_2 data sets measured on close transects with a time interval of several years (preferably beyond a decade to be able to detect small changes).

In the Equatorial Pacific ocean, earlier published data sets (Keeling, 1968; Miyake et al., 1974; Keeling and Revelle, 1985; Broecker et al., 1986; Feely et al., 1987; Fushimi, 1987; Inoue and Sugimura, 1988, 1992; Bacastow and Maier-Reimer, 1990; Murphy et al., 1991; Lefevre and Dandonneau, 1992; Wong et al., 1993) showed the large spatial and temporal variability of seasurface pCO_2 with higher pCO_2 values in summertime than in wintertime, and higher values in the eastern area than in the western part. Thus, in order to make a comparison with earlier data sets, we needed to look for data sets for which the pCO_2 measured along a longitude close to 151°W and during the narrow time window of August–September.

The pCO_2 data from the leg 7 of the NORPAX cruises on the R/V *Wecoma* (Weiss et al., 1992) satisfy these conditions. These 1979 pCO_2 data, were measured from Tahiti to Hawaii along 149°30′W during the same period (19 August–11 September) of the year.

In order to compare the 1979 and 1991 pCO_2^{sea} data, we computed the 1979 in-situ pCO_2^{sea} dis-

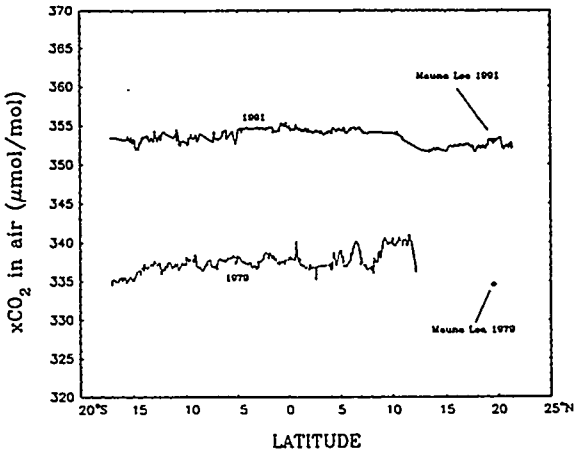

Fig. 4. Atmosperic CO_2 concentrations on a dry air basis. – – – = this work; ··· = data from leg 7 of the 1979 NORPAX cruise (Weiss et al., 1992); = September 1979 data from and September 1991 data extrapolated from the Mauna-Loa record (Keeling and Whorf, 1991).

tributions of Weiss et al. (1992), from their measured xCO_2. This data set has further been lowered by 4 μatm (Fig. 3b), to correct for the anhydrous calcium sulfate bias effect (Weiss, pers. commun., 1993). The uncertainty associated with these data is therefore in the order of 4 μatm. Fig. 4 illustrates the homogeneity and the lack of variability of CO_2 concentrations between Northern and Southern Hemisphere air masses at the time of these cruises. In September 1991, xCO_2 in the atmosphere south of 12°N was 354.5 ± 0.5 μmol/mol and xCO_2 in the atmosphere north of 12°N was 352.5 ± 0.5 μmol/mol.

A direct comparison of the variations of pCO_2^{sea} between the years 1979 and 1991 is difficult because of short-scale variability. Consequently, in order to attempt to eliminate these short-scale variations, we determined a polynomial function (order 10) which fit the data as also shown in Fig. 3. We further used the equations of these smoothing functions to determine the differences between pCO_2^{air} and pCO_2^{sea} ($\Delta pCO_2 = pCO_2^{sea} - pCO_2^{air}$) for both years 1979 and 1991 (Fig. 5), as well as the difference between these differences ($\Delta[\Delta pCO_2] = \Delta pCO_2^{1991} - \Delta pCO_2^{1979}$). It should be noted that there is an additional complication to this calculation due to error in estimating the temperature of the skin layer at the sea surface from the temperature of the bulk water beneath it (Robertson and Watson, 1992; Goyet and Brewer, 1993) and the impact of this error on the estimation of pCO_2.

Fig. 6 shows the differences between the observed in-situ pCO_2 data and the corresponding smooth fit. This figure illustrates the large variability of pCO_2^{sea} on a combination of short spatial and temporal (diurnal) scales and reflects the complexity of the processes involved in the variations of pCO_2 in the surface ocean. The standard deviation of these differences is 6.1 μatm for pCO_2^{sea} and 0.8 μatm for pCO_2^{air},

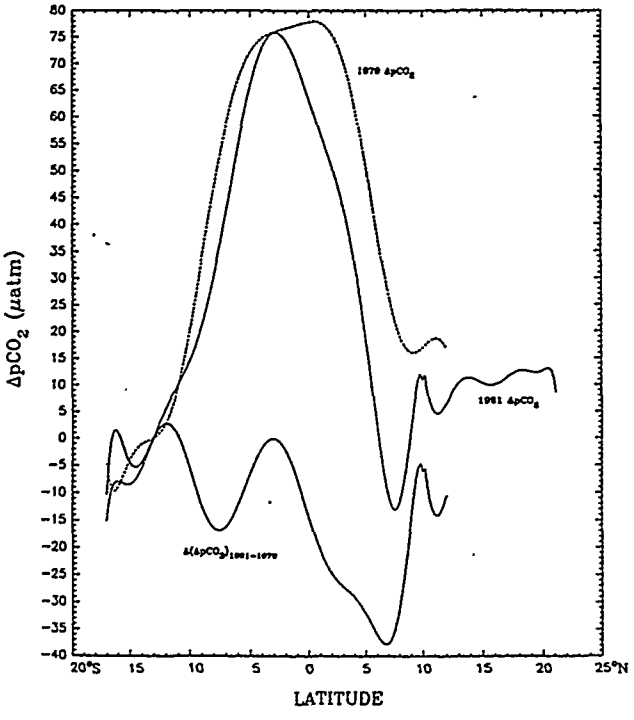

Fig. 5. Estimated ΔpCO_2 ($pCO_2^{sea} - pCO_2^{air}$) for the years 1979 and 1991 and their difference $\Delta(\Delta pCO_2)$.

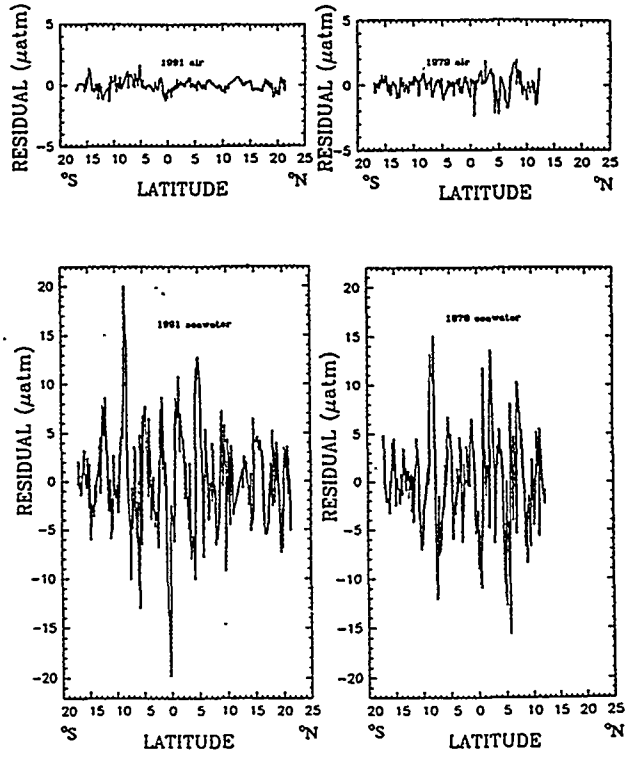

Fig. 6. Differences between the observed 1979 and 1991 in-situ pCO_2 and the smooth fit to the data.

thus suggesting that the uncertainties associated to the computed ΔpCO_2 are in the order ± 6.9 μatm with sporadic events up to ± 20 μatm. Consequently, the oscillations around zero of $\Delta[\Delta pCO_2]$ shown in Fig. 5 south of the equator and between 9 and 12°N, cannot allow us to determine whether ΔpCO_2 significantly varied or not between the years 1979 and 1991 due to anthropogenic CO_2 increase in the atmosphere. $\Delta[\Delta pCO_2]$ remained within the amplitude of variation of pCO_2^{sea}. In contrast, in the ocean area between the equator and 9°N, ΔpCO_2^{1991} is significantly lower by up to 38 ± 6 μatm than ΔpCO_2^{1979}.

In this area, air–sea CO_2 gas exchange process alone would decrease pCO_2^{sea} rather than increase in-situ pCO_2^{sea}. Consequently, between the equator and 9°N, the observed decrease in ΔpCO_2 is in good agreement with the earlier model predictions (Pearman et al., 1983; Volk and Bacastow, 1989). However, between the equator and 17°S, the present observations do not support the theoretical decrease and, within the limits of the short-scale variations, indicate that ΔpCO_2 did not significantly change between the two periods of observation.

This mismatch between model predictions and observations is not surprising. The cruise tracks and the dates of these cruises are very close to each other but are not identical. Furthermore, as we mentioned earlier, the Central Equatorial Pacific Ocean is an area where physical forcing is dominant. Not only do ENSO events occur frequently but tropical instability waves also propagate quickly (Knauss, 1957). Both of these phenomemons affect not only the surface and subsurface circulation, but also the chemical and biological properties of the surface seawaters (Feely et al., 1987, 1993; Inoue et al., 1992). Yet, the quantification of these effects on the CO_2 properties in surface seawater is not easy. As a result, the quantification of the interannual (or interdecadal) transfer of atmospheric CO_2 gas across the air–sea interface in this ocean area is extremely difficult. The small anthropogenic signal is masked by both short-scale variations and large interannual variations due to changes in circulation dynamics.

These data illustrate that along a longitude close to 151°W between the latitudes of equator and 17°S, the Pacific ocean was a stronger source of CO_2 for the atmosphere in 1991 than it could have been expected a decade ago from model calculations (Pearman et al., 1983). However, these data alone do not allow us to separate the impact of increasing CO_2 concentration in the atmosphere and of water-circulation variations on pCO_2^{sea}.

5. Effect of temperature and salinity variation on surface seawater pCO_2

One of the effects of the rapid increase of greenhouse gases in the atmosphere is a global warming of the Earth. As a result, the coastal surface ocean is becoming warmer (Roemmich, 1992). Due to this warming, the oceanic absorption of greenhouse gases might be modified. The thermodynamic process alone indicates that, as the temperature of seawater increases, the solubility of CO_2 gas in seawater decreases and consequently pCO_2^{sea} increases. Fig. 7 illustrates the observed sea surface temperature increase between August–September 1979 and August–September 1991. South of the equator the observed mean temperature increase is about 0.25°C while about 0.65°C north of the equator. These increases of temperature may be responsible for pCO_2^{sea} increases of approximately 3 and 8 μatm southward and northward of the equator, respectively. These variations are within the order of magnitude of the short-term variations of pCO_2 and therefore are difficult to extract from the observations. In addition, a temperature change of surface seawater is likely to induce a change in biological activity, thus indirectly affecting pCO_2^{sea}. Salinity variations would also influence pCO_2^{sea} (Weiss et al., 1982).

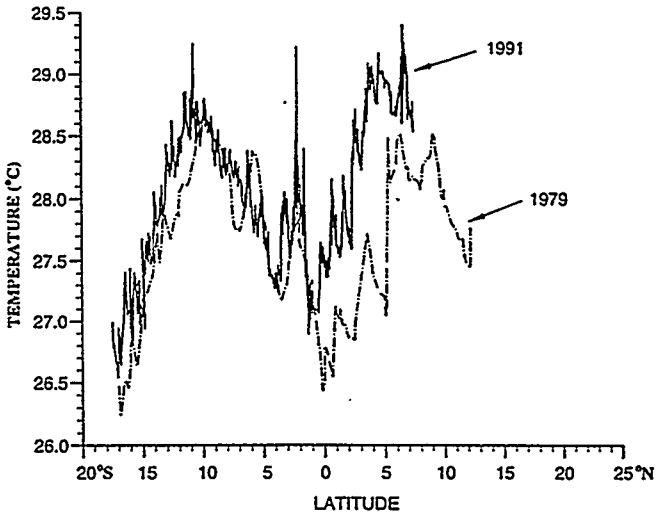

Fig. 7. Observed sea surface temperature along 149°30″W in 1979 (- -) and along 151°W in 1991 (—).

6. Conclusion

The observations in this paper suggest that in the Central Equatorial Pacific Ocean some oceanic CO_2 source areas may have remained approximately constant (not weaker) with time, while other areas are becoming much weaker CO_2 sources for the atmosphere. Over the latitudinal band between 5°N and 5°S, ΔpCO_2^{1991} decreased by approximately 22% compared to ΔpCO_2^{1979}. However, due to the large short-scale and interannual variations of pCO_2^{sea}, it is extremely difficult to detect the anthropogenic signal from such sporadic observations. Extrapolation of these data over large spatial and temporal (month, season, year) scales is virtually impossible. Only continual monitoring of the seasurface water properties can provide the necessary data to quantify and ultimately predict the overall penetration of greenhouse gases in this ocean area.

Acknowledgements

We thank the captain and the crew of the R/V *Thomas Washington* for their cooperation during the sampling cruise; the National Science Fundation and in particular N. Andersen for their support; F.J. Millero and P.G. Brewer for their helpful comments on an earlier version of the manuscript; R. Weiss for his 1979 data set and for many stimulating discussions; and C.S. Wong and R. Feely for their constructive reviews. This work was supported by the Department of Energy under grant DE-FGO2-ER60980 and the National Aeronautic and Space Administration grant NAGW-2431.

This is contribution No. 8198 of the Woods Hole Oceanographic Institution.

References

Bacastow, R. and Maier-Reimer, E., 1990. Circulation model of the oceanic carbon cycle. Climate Dyn., 4: 95–125.

Broecker, W.S. and Takahashi, T., 1966. Calcium carbonate precipitation on the Bahamas Banks. J. Geophys. Res., 71(6): 1575.

Broecker, H.C., Petermann, J. and Siems, W., 1978. The influence of wind on CO_2 exchange in a wind-wave tunnel, including the effect of monolayers. J. Mar. Res., 36: 595–610.

Broecker, W.S., Ledwell, J.R., Takahashi, T., Weiss, R., Merlivat, L., Memery, L., Peng, T.H., Jahne, B. and Munnich, K.O., 1986. Isotopic versus micrometeorologic ocean CO_2 fluxes: a serious conflict. J. Geophys. Res., 91: 1051–10527.

Chavez, F.P. and Barber, R.T., 1987. An estimate of new production during El Nino. Int. Conf. TOGA Sci. Prog., World Climate Res. Publ. Ser., 4. World Meteorol. Organ., Geneva, pp. 23–32.

Copin-Montegut, C., 1988. A new formula for the effect of temperature on the partial pressure of CO_2 in seawater. Mar. Chem., 25: 29–37.

Enfield, D.B., 1989. El Nino, Past and Present. Rev. Geophys., 27: 159–187.

Feely, R.A., Gammon, R.H., Taft, B.A., Pullen, P.E., Waterman, L.S., Conway, T.J., Gendron, J.F. and Wisegarver, D.P., 1987. Distribution of chemical tracers in the eastern equatorial Pacific during and after the 1982–1983 El Nino/Southern Oscillation event. J.Geophys. Res., 92: 6545–6558.

Feely, R.A., Wanninkhof, R., Cosca, C.E., McPhaden, M.J., Byrne, R.H., Millero, F.J., Chavez, F.P., Clayton, T., Campbell, D.M. and Murphy, P.P., 1993. The effect of tropical instability waves on CO_2 species distributions along the Equator in the Eastern Equatorial Pacific diring the 1992 ENSO event. Geophys. Res. Lett., in press.

Fushimi, K., 1987. Variation of carbon dioxide partial pressure in the western Pacific surface water during the 1982/1983 El Nino event. Tellus, 39B: 214–227.

Gleick, J., 1987. Chaos: Making a New Science. Viking Penguin, New York, NY, 352 pp.

Goyet C. and Brewer, P.G., 1993. Biochemical properties of the oceanic carbon cycle. In: J. Willebrand and D.L.T. Anderson (Editors), Modeling Oceanic Climate Interactions. Springer, Belin, pp. 271–298.

Inoue, H. and Sugimura, Y., 1988. Distribution of the pCO_2 in surface seawater of the western and central equatorial Pacific during the 1986/1987 El Nino/southern oscillation event. Geophys. Res. Lett., 15: 1499–1502.

Inoue, H. and Sugimura, Y., 1992. Variations and distributions of CO_2 in and over the equatorial Pacific during the period from the 1986/88 El Nino to the 1988/89 La Nina event. Tellus, 44B: 1–22.

Jones, E.P., 1980. Gas exchange. Air–sea interaction instruments and methods. Plenum, New York, NY, pp. 433–445.

Jones, E.P. and Smith, S.D., 1977. Eddy correlation measurement of sea–air CO_2 flux. J. Geophys. Res., 82: 5990–5992.

Keeling, C.D., 1968. Carbon dioxide in surface ocean waters, 4. Global distribution. J. Geophys. Res., 73: 4543–4554.

Keeling, C.D. and Revelle, 1985. R. Effects of El Nino/Southern Oscillation on the atmospheric content of carbon dioxide. Meteoritics, 20: 437–450.

Keeling, C.D. and Whorf, T.P., 1991. Atmospheric CO_2— Modern record Mauna Loa. In: T.A. Boden, R.J. Sepanski and F.W. Stoss (Editors), Trends '91, A Compendium of Data on Global Change. Carbon Dioxide Inf. Anal. Cent., Environ. Sci. Div., Oak Ridge Nat. Lab., Oak Ridge, TN 37831-6335, Publ. No. ORNL/CDIAC-46, ESD Publ. No. 3746, pp. 100–103.

Knauss J.A., 1957. An observation of an oceanic front. Tellus, 9: 234–237.

Lefevre, N. and Dandonneau, Y., 1992. Air–sea CO_2 fluxes in the equatorial Pacific in January–March 1991. Geophys. Res. Lett., 19(22): 2223–2226.

Liss, P.S., 1983a. The exchange of biogeochemically important gases across the air–sea interface. In: B. Bolin and R.B. Cook (Editors), The Major Biogeochemical Cycles and Their Interactions. Wiley, New York, NY, pp. 411–426.

Liss, P.S., 1983b. Gas transfer: Experiments and geochemical implications. In: P.S. Liss and W.G.N Slinn (Editors), Air–Sea Exchange of Gas Particles. Reidel, Dordrecht, pp. 241–298.

Meyers, G., 1982. Interannual variation in sea level near Truk Island—A bimodal seasonal cycle. J. Phys. Oceanogr., 12: 1161–1168.

Miyake, Y., Sugimura, Y. and Saruhashi, K., 1974. The carbon dioxide content in the surface waters in the Pacific ocean. Rec. Oceanogr. Works Jpn., 12(2): 45–52.

Murphy, P.P., Feely, R.A., Gammon, R.H., Harrison, D.E., Kelly, K.C. and Waterman, L.S., 1991. Assessment of the air–sea exchange of CO_2 in the south Pacific during austral autumn. J. Geophys. Res., 96(20): 455–467.

Pearman, G.I., Hyson, P. and Fraser, P.J., 1983. The global distribution of atmospheric carbon dioxide: 1. Aspects of observations and modeling. J. Geophys. Res., 88(C6): 3581–3590.

Robertson, J.E. and Watson, A.J., 1992. Thermal skin effect of the surface ocean and its implications for CO_2 uptake. Nature, 358: 738–740.

Roemmich, D., 1992. Ocean warming and sea level rise along the southwest U.S. coast. Science, 257: 373–374.

Takahashi, T., Weiss, R.F., Culberson, C.H., Edmond, J.M., Hammond, D.E., Wong, C.S., Li, Y.-H. and Bainbridge, A.E., 1970. A carbonate chemistry profile at the 1969 Geosecs intercalibration station in the Eastern Pacific Ocean. J. Geophys. Res., 75(36): 7649–7666.

Unesco, 1987. Thermodynamics of the Carbon Dioxide System in Seawater. Unesco Techn. Pap. Mar. Sci., 51, 31 pp.

Volk, T. and Bacastow, R., 1989. The changing paterns of ΔpCO_2 between ocean and atmosphere. Global Biogeochem. Cycles, 3(2): 179–189.

Watson, A.J., Upstill-Goddard, R.C. and Liss, P.S., 1991. Air–sea gas exchange in rough and stormy seas measured by a dual-tracer technique. Nature, 349: 145–147.

Weiss, R.F., Jahnke, R.A. and Keeling, C.D., 1982. Seasonal effects of temperature and salinity on the partial pressure of CO_2 in seawater. Nature, 300: 511–513.

Weiss, R.F., Van Woy, F.A. and Salameh, P.K., 1992. Surface water and atmospheric carbon dioxide and nitrous oxide observations by shipboard automated gas chromatography: Results from expeditions between 1977 and 1990. Scripps Inst. Oceanogr. Ref., 92-11. ORNL/CDIAC-59, NDP-044. Carbon Dioxide Inf. Anal. Cent., Oak Ridge Nat. Lab., Oak Ridge, TN, 144 pp.

Wong, C.S., Chan, Y.-H., Page, J.S., Smith, G.E. and Bellegay, R.D., 1993. Changes in equatorial CO_2 flux and new production estimated from CO_2 and nutrient levels in Pacific surface waters before and during the 1986/87 El Nino. Tellus, 45B: 64–79.

Dynamics and Characterization of Marine Organic Matter, Eds. N. Handa *et al.*, pp. 00–00.

CO_2 Exchange between the Atmosphere and the Ocean: Carbon Cycle Studies of the Meteorological Research Institute Since 1968

Hisayuki YOSHIKAWA INOUE

Geochemical Research Department, Meteorological Research Institute, Nagamine 1-1, Tsukuba, Ibaraki 305 Japan

Abstract—Since 1968, measurements of carbon dioxide in the atmosphere and in surface seawater have been made to clarify the role of the ocean in the global carbon cycle. Temporal and spatial variations in the oceanic carbonate system are summarized here, along with the techniques for atmospheric and oceanic CO_2 measurements developed by the Meteorological Research Institute, Japan Meteorological Agency.

INTRODUCTION

Atmospheric CO_2 is the most important greenhouse gas that has been increasing due to anthropogenic activities. Precise and direct measurements of atmospheric CO_2 using a non-dispersive infra-red gas analyzer (NDIR analyzer) were first made in 1957/58 by the Scripps Institution of Oceanography, USA at the South Pole and Mauna Loa in Hawaii (Keeling *et al.*, 1989). Since then, atmospheric CO_2 has been monitored at stations established in remote areas (see, for example, Trends '93, 1993; WMO WDCGG Data Report, 1995). The growth rate of atmospheric CO_2 during the1980s has been reported to be 1.5 ppm/yr (IPCC, 1994), which corresponds to about 58% of the total emissions from fossil-fuel burning and cement production. To predict future climate changes due to the increases of greenhouse gases on the basis of given CO_2 emission scenarios, it is essential to understand the current global carbon cycle that controls the atmospheric CO_2 level: the exchange fluxes between the atmosphere and surface oceans and between the atmosphere and the terrestrial biota. According to the carbon isotope measurements ($^{13}C/^{12}C$) of atmospheric CO_2, net fluxes among carbon reservoirs vary interannually (Francey *et al.*, 1995, Keeling *et al.*, 1995).

The net flux of CO_2 between the sea and the atmosphere (Fx) is given by the product of the difference in partial pressure of CO_2 (ΔpCO_2) between the sea (pCO_2^s) and the air (pCO_2^a) and the gas transfer coefficient (E).

$$Fx = E(pCO_2^s - pCO_2^a) = E\Delta pCO_2. \quad (1)$$

The gas transfer coefficient E is expressed as a function of wind speed (Liss and Merlivat, 1986; Tans *et al.*, 1990; Wannikhof, 1993). Changes in ΔpCO_2 are

mainly caused by pCO_2^s showing much larger spatial and temporal variability than pCO_2^a.

If there occurs a net exchange of CO_2 between the ocean and the atmosphere, the mole fraction of each of the dissolved inorganic carbon species in seawater varies from its original value because CO_2 acts as a weak acid. In seawater most of the dissolved inorganic carbon exists as bicarbonate ion (HCO_3^-) and carbonate ion (CO_3^{2-}), and only 1% of the total is the aqueous CO_2 that exchanges with the atmosphere. The relationship in changes between pCO_2^s and dissolved inorganic carbon concentration (TCO_2) is conventionally expressed by the homogeneous buffer factor (Revelle and Suess, 1957):

$$\beta = [(dpCO_2^s/pCO_2^s)/(dTCO_2/TCO_2)] \quad (2)$$

where $dpCO_2^s$ and $dTCO_2$ are small changes in pCO_2^s and TCO_2, respectively. Equation (2) gives the CO_2 uptake capacity of ocean water and reported values (Sundquist 1979; Wagner 1979) indicate that the relative change in pCO_2^s is about one order of magnitude larger than that of TCO_2.

Since the mid-1960s, the Meteorological Research Institute (MRI), in the Japan Meteorological Agency (JMA), began to measure the CO_2 mixing ratio in the atmosphere (xCO_2^a) and that in the air, which establishes equilibrium with a stream of flowing seawater (xCO_2^s). Miyake *et al.* (1974) developed a CO_2 measuring system consisting of a shower-head type equilibrator, chemical desiccants [$Mg(ClO_4)_2$], and a NDIR analyzer. From 1968 to 1972, they measured xCO_2^s in the Pacific on board the R/V *Hakuho-maru* (Ocean Research Institute, University of Tokyo) to find out whether the ocean acts as a sink or a source for atmospheric CO_2 (Miyake *et al.*, 1974).

After the cessation of the research program measuring xCO_2^s and xCO_2^a during the period from 1973 to 1980, the MRI restarted in January 1981 a new program to investigate temporal and spatial variations in the carbonate system of surface waters in the open ocean (Inoue *et al.*, 1987, 1995). Some of the results were reported earlier (Inoue and Sugimura, 1986, 1988a, 1988b, 1992; Inoue *et al.*, 1987, 1995, 1996; Fushimi, 1987, Ishii and Inoue 1995). In this report, we will summarize the results of research conducted by MRI researchers since the mid-1960s along with the techniques for measureing of xCO_2^a and xCO_2^s.

EXPERIMENT

Measurements of oceanic and atmospheric CO_2 prior to 1973

Measurements of xCO_2^s and xCO_2^a using a NDIR analyzer started in 1966 (Miyake and Sugimura, 1969). This system was designed for the measurements of xCO_2^s in discrete samples of seawater. Then, to investigate the role of the ocean for the global carbon cycle, Miyake *et al.* (1974) developed a CO_2 measuring system that could measure xCO_2^s and xCO_2^a quasi-continuously on board the ship (Fig. 1). Figure 1 represents a schematic diagram of the system that consisted of a NDIR analyzer (Beckman 315A), two columns of $Mg(ClO_4)_2$, two diaphragm pumps, a flow meter, a series of electromagnetic valves and a showerhead-type

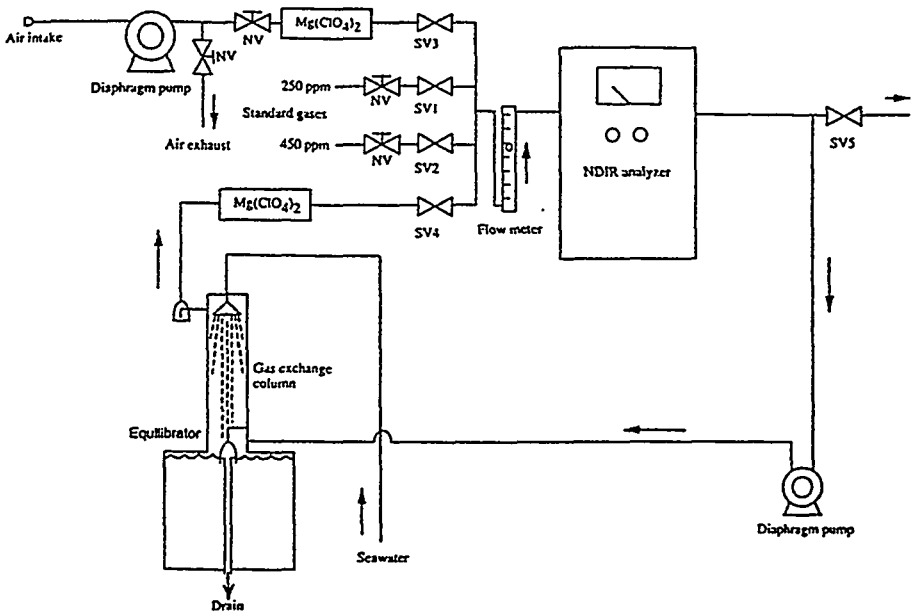

Fig. 1. A schematic diagram of the atmospheric and oceanic CO_2 measuring system used prior to 1973 (Miyake *et al.*, 1974). Arrows show the direction of air flow either for the measurement of xCO_2^a or xCO_2^s. The output voltages of the NDIR analyzer was recorded on a strip chart recorder, from which the CO_2 mixing ratio of sample airs was computed manually. SV meants the solenoid valve, and NV the flow control valve.

equilibrator. The system was operated by an electromechanical timing device that repeated the same switching with an hourly cycle. For calibration, CO_2 standard gases (250 ppm and 450 ppm, CO_2 in N_2) were introduced into the sample cell of the NDIR analyzer at 0.5 l/min alternately for 5 minutes each. Following calibration, 25 minutes were allocated for each of the measurements of xCO_2^s and for xCO_2^a. Air was pumped at 10 l/min from an inlet installed at the bow of the ship to avoid contamination. Air were introduced (0.5 l/min) into the sample cell of the NDIR analyzer after drying. Sea water was pumped up continuously from 4 meters below the surface and introduced into the equilibrator. The fixed volume of air (*ca.* 2 l) was circulated at 0.5 l/min in a closed circuit consisting of the NDIR analyzer, the diaphragm pump, the equilibrator (countercurrentwise flow), and the column of $Mg(ClO_4)_2$. The output voltage of the NDIR analyzer was recorded on a strip chart.

As reported earlier (Inoue and Sugimura, 1988), however, there were a few problems in comparing data sets collected during this period and later. We have to take into account the pressure broadening effect of the NDIR analyzer due to the use of CO_2-in-N_2 standards, changes in curvature between the output voltage of the NDIR analyzer and the CO_2 mixing ratio, temperature increase between the seawater in equilibrator and at the sea surface, and the pressure difference in the

sample cell of the NDIR analyzer during oceanic CO_2 measurements from those of standard gases and background air.

Pressure broadening effect of the NDIR analyzer

The CO_2-in-N_2 standards were used for the 1968/72 R/V *Hakuho-maru* cruises. Therefore, we have to determine the pressure broadening effect on the NDIR analyzer (Beckman 315A). Inoue and Sugimura (1988) estimated the pressure broadening effect using the standard gases (CO_2-in-N_2) prepared by Takachiho Kagaku Co., Ltd. The mole fraction of CO_2 in N_2 was determined by the manufacturer using the NDIR analyzer and CO_2-in-N_2 standards produced by the gravimetric method. A round number (3 digits) was reported as the CO_2 mixing ratio of standards. This means that the reproducibility CO_2 measurement by the NDIR analyzer could have been as large as 1 ppm prior to 1973. We compared the values determined by CO_2-in-N_2 standards with those determined by CO_2-in-air standards (Inoue and Sugimura, 1988). The least-squares fit to the data yields:

$$xCO_2 = -18.54 + 1.14xCO_2(N_2) - 2.198 \times 10^{-4}xCO_2(N_2)^2, \qquad (3)$$

where xCO_2 is the CO_2 mixing ratio determined by the CO_2-in-air standards and $xCO_2(N_2)$ is the apparent CO_2 mixing ratio determined by the CO_2-in-N_2 standards. The difference between xCO_2 and $xCO_2(N_2)$ is 2.7 ppm at 250 ppm, 3.7 ppm at 300 ppm, 3.5 ppm at 350 ppm, 2.3 ppm at 400 ppm and –0.1 ppm at 450 ppm.

The relationship between the output voltage of the NDIR analyzer and the CO_2 mixing ratio

Miyake *et al.* (1974) assumed the linearity between the output voltage of the NDIR analyzer and the CO_2 mixing ratio, in calculating the xCO_2 using only two working standard gases. However, the relationship between the output voltage and CO_2 mixing ratio varies with time. To estimate changes in this relationship, Inoue and Sugimura (1988) used the latitudinal distribution of atmospheric CO_2 reported by Bolin and Keeling (1963). Detrended seasonal variation in the atmospheric CO_2 over the ocean was assumed to be equal to that of Bolin and Keeling (1963). xCO_2^s was calculated from the reading of an analog reorder chart using Eq. (3) and the atmospheric CO_2 data.

Temperature increase between the temperature of seawater in the equilibrator and the sea surface temperature (SST)

Miyake *et al.* (1974) did not correct the temperature effect for xCO_2^s measurements. Assuming that total barometric pressure is 1 atm and salinity is 35 psu, we calculate the pCO_2^s in surface seawaters using the average temperature change (+0.3°C) during the 1983/84 BIOMASS cruise of R/V *Hakuho-maru*.

Pressure effect on xCO_2^s

Gas circulation by the diaphragm pump produced pressure changes in the closed loop. Changes in pressure in the sample cell were dependent on the flow rate and the order of connections among the parts in this loop. As discussed in Inoue *et al.* (1995), a correction was needed for pressure change during the air

circulation. However, there were no data to estimate the pressure effect on xCO_2^s. According to the archive in our laboratory, this problem was realized in earlier cruises but not checked out completely. A solution to this problem was not clear. In this study, we estimated the pressure effect by circulating the air in the closed circuit of the CO_2 measuring system used for the period from 1987 to 1993. The size of equilibrator was almost the same as that used prior to 1973, and the diameter of tubing (1/4 inch), and the orifice of the electromagnetic valves (3 mm) were the same as those used prior to 1973, although the system used in 1987/93 (Fig. 2) is more complicated. Because the diaphragm pump was installed upstream of the equilibrator (Fig. 1), the pressure in the sample cell of the NDIR analyzer decreased slightly during circulation of the equilibrating air, but increased during the measurements of standards and atmospheric CO_2. The pressure effect on xCO_2^s was examined on board the R/V *Natsushima* (Japan Marine Science and Technology Center) and M/S *Hokuto-maru* (Institute for Sea Training), during the cruises in the North Pacific where the xCO_2^s ranged from 300 to 400 ppm. The apparent decrease of the CO_2 mixing ratio during the circulation at 0.6 l/min against the open-ended configuration is -2.2 ± 0.3 ppm, and that after introducing the standard gases and background air is +1.1 ppm. The pressure change in the sample cell of the NDIR analyzer between xCO_2^s measurements and standards, therefore, required a correction in the range from -3.3 to -1.1 ppm.

For the showerhead-type equilibrator developed by the MRI, we hardly observed changes in water level in the equilibrator (typically less than 3 cm change), which supported an assessment of the relatively small change in pressure for the pre-1973 CO_2 measuring system.

Measurements of oceanic and atmospheric CO_2, 1981–1986

xCO_2^a and xCO_2^s were measured basically using the same analytical system described above except for the introduction of an electric dehumidifier (Fushimi 1987; Inoue *et al.*, 1987), and the placing of the diaphragm pump between the electric dehumidifier and the equilibrator (Fig. 3 in Inoue *et al.* (1987)). For this reason, the pressure effect on the xCO_2^s has been corrected as reported (Inoue *et al.*, 1995).

The effect of the seawater temperature change between the equilibrator and surface seawater was corrected using the equation given by Gordon and Jones (1973):

$$\frac{\delta pCO_2}{\delta t} = 4.4 \times 10^{-2}(pCO_2) - 4.6 \times 10^{-6}(pCO_2)^2. \quad (4)$$

Equation (4) was integrated and water vapor pressure in the equilibrator and sea surface was calculated, taking into account the effect of salinity (assumed to be 35 psu). The temperature increase was estimated from measurements of water temperature at the equilibrator and sea surface twice a day using a Hg-thermometer which was calibrated at the JMA.

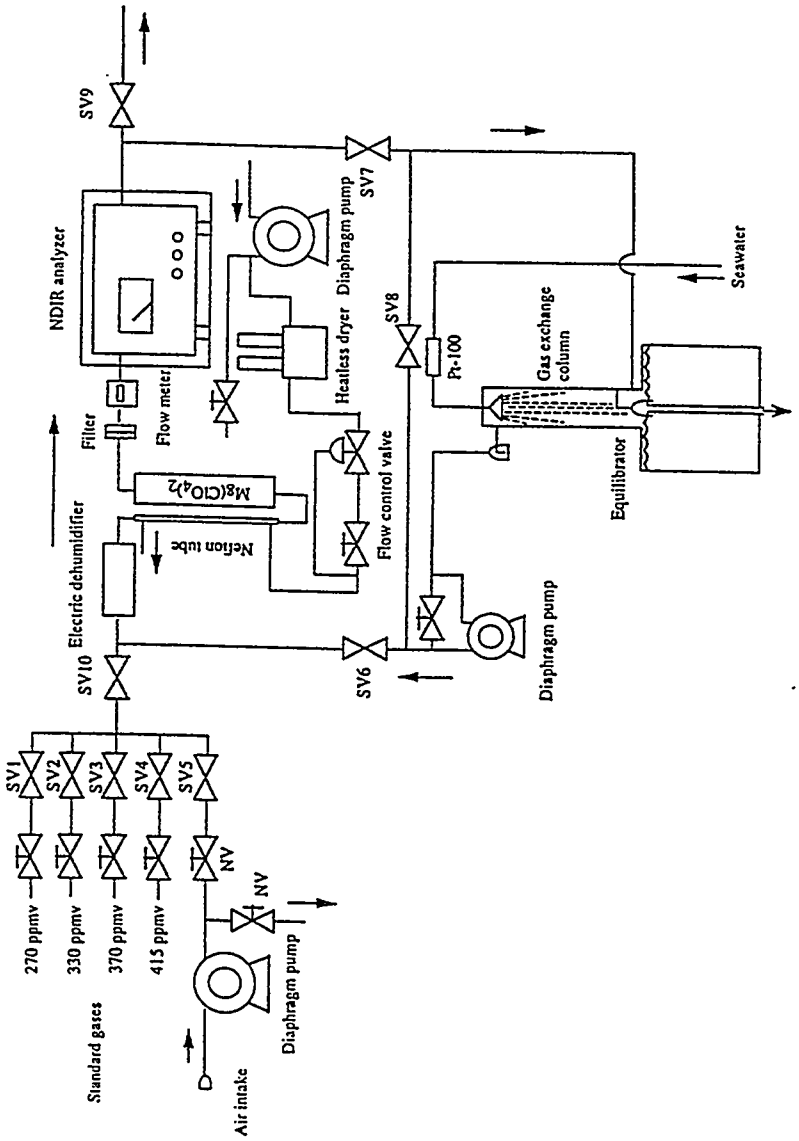

Fig. 2. A schematic diagram of the atmospheric and oceanic CO_2 measuring system used during the period from 1987 to 1993. Arrows shows the direction of air flow for either the measurement of xCO_2^a or xCO_2^s. The output voltage of the NDIR analyzer and water temperature were digitized and stored in floppy disks. SV means the solenoid valve, and NVthe flow control valve.

Other than two standard gases (250 ppm and 450 ppm CO_2 in N_2), the working standard gas (350 ppm) was usually used once a day to estimate the non-linearity between the CO_2 mixing ratio and the output voltage of NDIR analyzer.

At the end of February 1985, we improved our analytical system by using four standard gases to measure xCO_2^a and xCO_2^s instead of three (Fig. 3 in Inoue *et al.*, 1987). The four standard gases were introduced into the NDIR analyzer's cell in succession every hour. Each standard gas was introduced into the NDIR analyzer cell for 5 minutes, and the next 20 minutes was allocated for xCO_2^a. The remaining 20 minutes was used for measurements of xCO_2^s. We used this system for the period from May 1985 to July 1986.

Measurements of oceanic and atmospheric CO_2, 1987–1993

In April 1987, we changed our measurement methodology by introducing a system (Fig. 2) that was operated by a personal computer (HP 85) and a data acquisition unit (Inoue and Sugimura, 1988a, 1992). The output voltage of the NDIR analyzer and the seawater temperature at the inlet of the equilibrator were digitized and stored on floppy disks.

Changes in both the pressure and temperature in the NDIR analyzer's cell (Beckman model 864, model 865, and model 880) and water vapor in the sampled air were factors affecting the determination of xCO_2^a and xCO_2^s. The NDIR analyzer was installed in a plastic box in an air-conditioned room to keep the effects of room temperature change to within ±0.1°C. 20 seconds before the signal integration (A/D conversion), the flow of the respective sample gases was stopped and the outlet solenoid valve (No. 9) opened (open-end configuration) to equilibrate the temperature and pressure in the NDIR analyzer's cell and those of the standard gases.

The apparent time which was required to establish equilibrium between the equilibrator air in the closed circuit and seawater depends on the magnitude of disequilibrium, air flow rate, and water flow rate. We circulated air at 0.6 l/min for 10 minutes, which was enough to establish equilibrium for open ocean water. Immediately after stopping the air flow in the closed circuit, the solenoid valve No. 9 was also opened for the measurement of xCO_2^s. Because the pressure in the sample cell of the NDIR analyzer during circulation was slightly higher than the ambient air pressure, temperature and pressure equilibrium was readily attained without contamination. The length of tubing (>2.5 m, od. 0.635 mm) attached to solenoid valve No. 9 was long enough to prevent the ambient air from diffusing back into the NDIR analyzer sample cell.

To remove the water vapor from the sample gases, we used a Nefion tube (Perma Pure Ltd.) between the electric dehumidifier and the chemical desiccant column [$Mg(ClO_4)_2$]. Dry air was supplied to the Nefion tube via a diaphragm pump, a heatless-dryer (CKD) in which molecular sieves (13X) were used to remove water vapor, and a mass flow controller. The water vapor in the sample gas was removed by molecular diffusion through a film of ion exchange resin. The dew point of sample air flowing at 0.6 l/min was lower than 2°C at the outlet of the electric dehumidifier and –20°C of the Nefion tube.

Fluctuations of electric power frequency and voltage on the ship affected the determination xCO_2^a and xCO_2^s. The electric frequency and voltage supplied to, the chopper motor, detector, low-pass filter, etc., of the NDIR analyzer should be stable. But, we found that switching the heater in the NDIR analyzer disturbed them. For this reason, we isolated the electric lines that supplies the power to the chopper motor,low-pass filter, detector, etc., from that of the heating and the electric fan, etc. A voltage and frequency stabilizer (Takasago AF330) was used for the chpper motor, etc.

The precision to replicate analyses with this system in our laboratory on land is better than 0.05 ppm for Beckman models 865 and 880, and better than 0.1 ppm for Beckman model 864 (Inoue and Sugimura, 1992), and slightly worse during the shipboard analysis. It was affected mostly by the weather conditions and vibrations of the ship's engine. Taking into account the fluctuations of temperature increase of seawater in the tubing (<0.1°C) and pressure broadening effect due to the super/undersaturation of oxygen in seawater, the precision of pCO_2^s is estimated to be ±2 μatm. Seawater temperatures at the inlet of the equilibrator and that in the surface water were measured at least twice a day by an Hg-thermometer to calibrate the temperature sensor at the inlet of the equilibrator and sea surface during respective cruises.

Measurements of oceanic and atmospheric CO_2, 1993–1996

The MRI system developed in 1986/87 was replaced by a new system in September 1993, because some of the spare parts could not be obtained. A satellite navigation unit (GPS) was also introduced into the system. To measure xCO_2^a and xCO_2^s, we also adopted the "open-ended configuration" by opening solenoid valve No. 9 when A/D integration commenced. Figure 3 shows the schematic diagram currently used for quasi-continuous measurements on board. The NDIR analyzer (BINOS 4.1 Rosemount) acted as an comparator of the CO_2 mixing ratio in ambient air and the air equilibrated with seawater relative to known CO_2 mixing ratio in standard gas cylinders. As described above the NDIR analyzer was also placed in a plastic box, and the electric power for the chopper motor, the low pass-filter, the detector, etc., was supplied via a voltage and frequency power stabilizer (PCR-500L, Kikusui; AA150F or AA330F, Takasago).

Duplicate analyses of the same sample air revealed that the standard deviation (1-sigma) was less than 0.04 ppm for BINOS 4.1 in the laboratory on land (Fig. 4).

The gas exchange column of the equilibrator was thermostated by the sampled seawater, and the temperature of the seawater was monitored at the inlet and water bath of the equilibrator (Pt-100 ohm). Before entering the gas exchange column of the equilibrator, air was passed through a jacket to bring its temperature close to that of the seawater. The temperature of the air at the outlet was also monitored (Pt-100 ohm). For the safe operation of the system, a water level sensor was attached to the gas exchange column of the equilibrator.

We set up the switching sequence of the standard and sample gases within a given time interval. Figure 5 shows the standard and sample gas sequencing

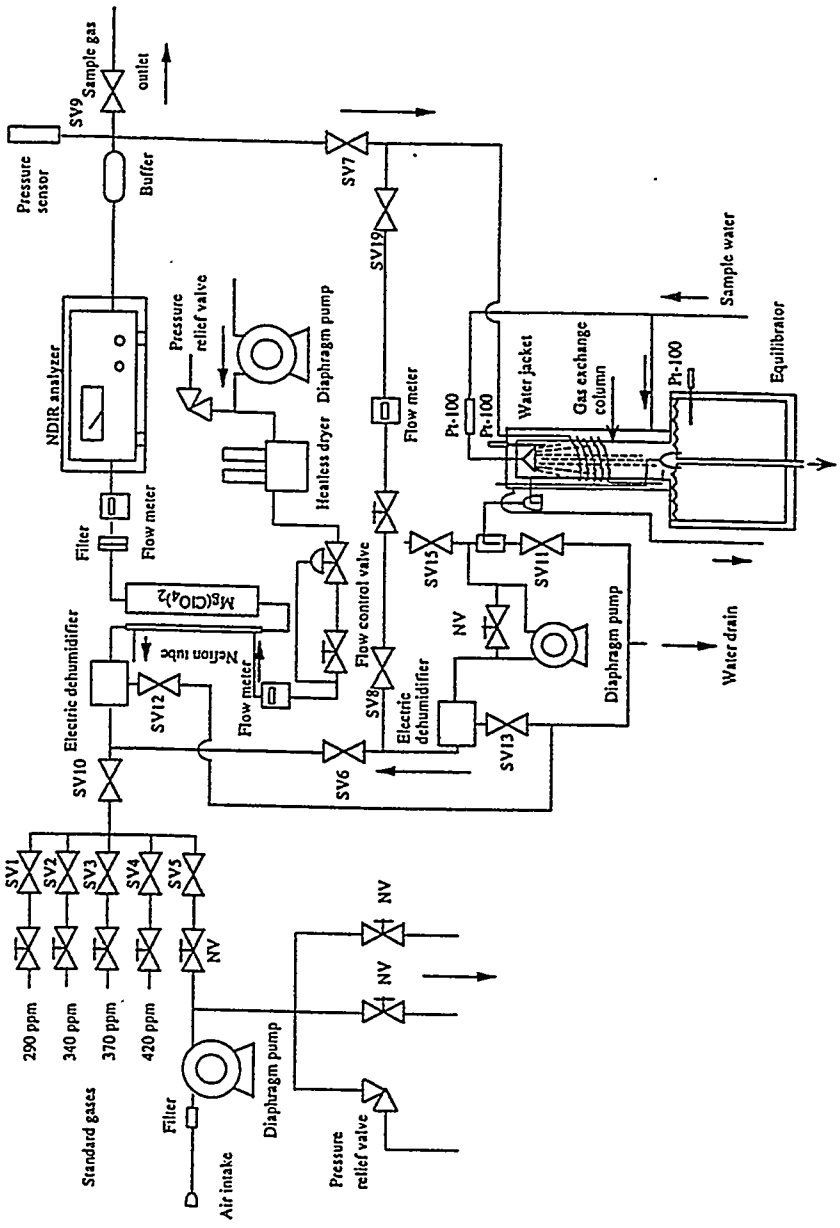

Fig. 3. A schematic diagram of the atmospheric and oceanic CO_2 measuring system that has been in use since 1993. Arrows shows the direction of air flow either for the measurement of xCO_2^a or xCO_2^s. The standard and sample gas sequence within a given time interval could be changed easily and the data was stored on memory cards. SV means the solenoid valve, and NV the flow control valve.

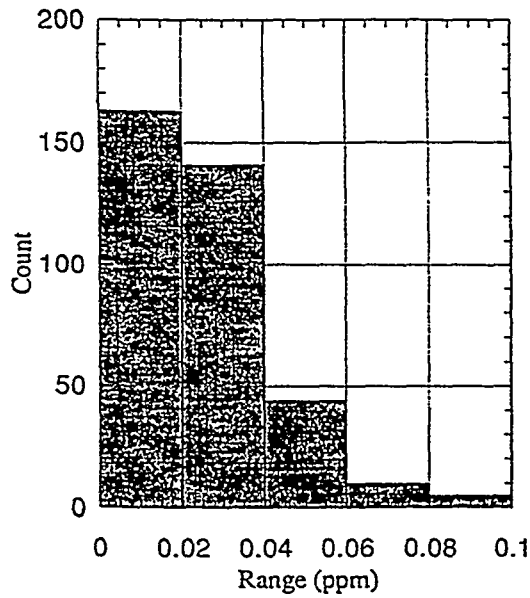

Fig. 4. Distribution of the standard deviation (1-s) of the CO_2 concentration for mean values as determined by the method of least-square fitting. Measurements were made by the NDIR analyzer (BINOS 4.1 and Beckman model 865) during the period from February 1996 to June 1996.

schemes employed for the international intercomparison of the underway pCO_2 system held on board the FS *Meteor* in the North Atlantic in June 1996. Some 22 minutes were allowed for the calibration by 4 working standard gases (250 ppm, 300 ppm, 350 ppm, 400 ppm), 16.5 minutes for measuring CO_2 in the ambient air (measured 3 times), and 50 minutes for measuring CO_2 in the air equilibrated with seawater (measured 4 times). The 1.5-hour cycle was repeated continuously. It was possible to change the 1.5-hour time intervals (max. 2-hour intervals), and order and number of measurements (max. 16). If we focused on the short-term or small-scale variations in oceanic (atmospheric) CO_2, we could measure only (xCO_2^a) xCO_2^s quasi-continuously. Raw data of output voltages of the NDIR analyzer, temperature sensors, pressure sensor, and geographical positions during each measurement were stored digitally (ASCII files) on memory cards (1 Mbytes) and transferred to a personal computer (PC 98 NEC) via an RS 232C interface.

CO_2 MIXING RATIO OF AIR SAMPLE

The output voltage for each working standard at the time of air sample measurements (V_i in Fig. 5) was obtained by linear interpolation derived from the output voltages between two successive measurements of the working standard

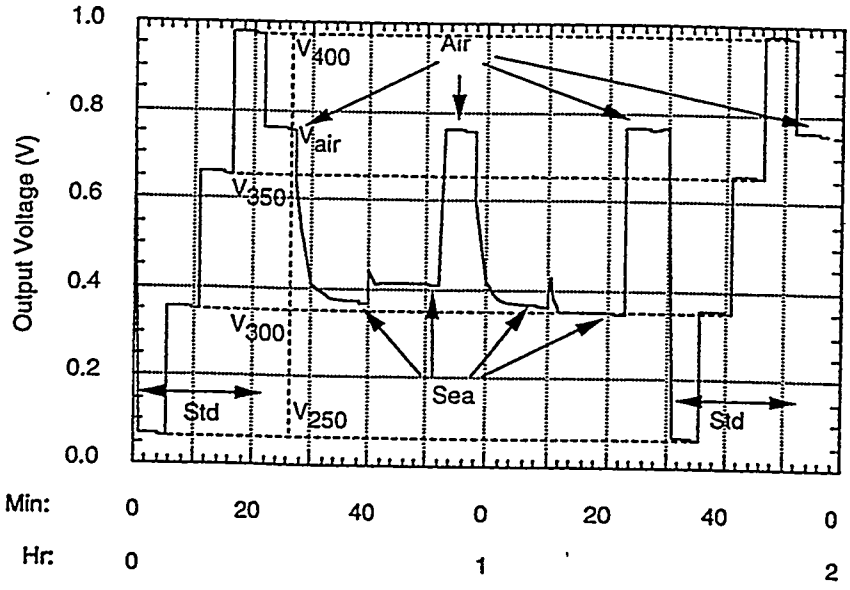

Fig. 5. Standard and sample gas sequencing schemes employed for international intercomparison of underway pCO_2 measurements on board the FS *Meteor* in the North Atlantic in June 1996. The output voltages of standard gases V_i at the time of sample gas measurements were obtained by linear interpolation between successive calibrations (see text). The subscript i meants the CO_2 mixing ratio of standard gas used on board FS *Meteor*.

gas. The coefficients of the second-degree polynomial (a, b, c) were determined by the method of least-squares fitting, and the mole fraction in the dry air was calculated using these coefficients and the output voltage of the NDIR analyzer:

$$xCO_2 = a + bV + cV^2. \tag{5}$$

The root mean squares of the residuals from the four-point fit were usually within 0.1 ppm.

The relationship between the partial pressure of CO^2 was expressed by:

$$pCO_2 = xCO_2\,(P_{atm} - p_{wat}), \tag{6}$$

where P_{atm} is the atmospheric pressure at the sea surface, and p_{wat} the saturated vapor pressure of seawater. As can be readily seen in Eq. (6), the "partial pressure of CO_2" assumed an ideal gas system with no inter-molecule interaction. When we treat the "real" gas system based on thermodynamic theory, we should take into account the inter-molecule interaction which causes deviations from those of ideal gas behaviour. When we use the fugacity for the oceanic carbonate system, we need to calculate the fugacity of CO_2 in the moist air (DOE, 1994). However, this calculation could be the subject for future change, because it does not contain

the inter-molecule interaction between CO_2 and H_2O. For this reason, we will use the partial pressure of CO_2 in wet air as reported historically.

DATA SELECTION OF xCO_2^a AND xCO_2^s

The objective of selecting atmospheric CO_2 data was to identify xCO_2^a values not affected by local sources and sinks. Since air CO_2 variabilities on a time-scale from a few minutes to an hour were clearly due to local contamination, we first rejected data showing the instability of the CO_2 mixing ratio, seen in an analog recording of the NDIR analyzer output on a strip chart recorder. If changes in the CO_2 mixing ratio measured within a few hours or a few tens of kilometers were large, we could reject the CO_2 values based on the assumption that variabilities of CO_2 mixing ratio in representative air should only vary by a small amount. The amount of CO_2 change is, however, dependent on time and geographical position. The CO_2 mixing ratio lying outside the 1-sigma (or 1.5-sigma) of an average at each latitude (or longitude) was flagged. Visual inspection of the remaining data sometimes showed that variabilities over hours at an oceanographic station were still large in comparison with those of adjacent latitudes measured by a ship under steam, probably due to local contamination from the stationary ship and station. It was dependent on the wind direction and speed. We rejected a high CO_2 mixing ratio until the standard deviation of the CO_2 mixing ratio decreased to the level of the adjacent latitudes. The standard deviation at each latitude was typically within the range of between 0.1 and 0.4 ppm for the period from 1987 to 1993.

We rejected xCO_2^s data that were contaminated by ambient air or were not obviously equilibrated due to a malfunction of the system. The xCO_2^s values falling the outside of 2-sigma of latitudinal (or longitudinal) mean were flagged.

Standard gases

During the period from January 1981 to April 1986, CO_2-in-N_2 mixtures were used as working standard gases. These gases were calibrated against the secondary standard gases (CO_2-in-air). CO_2 in N_2 gas mixtures were used because their CO_2 mixing ratio was stable with time. The secondary standard gases were calibrated at least twice a year against primary standards prepared gravimetrically by the Takachiho Co., Ltd. Both primary and secondary standard gases are composed of CO_2 in synthetic air without argon. The NDIR analyzer used for shipboard measurements (Beckman 315A) was employed to calibrate the working standard gases. Therefore, the observed value was based on a CO_2 mole fraction in synthetic air.

Since April 1987, standard gases (CO_2 in natural air) made by Nippon Sanso have been used as primary, secondary, and working standard gases. The primary standard gases were made gravimetrically following the same procedures reported by Tanaka *et al.* (1987). Within the range between 280 and 410 ppm, the relationship between the scale on the basis of primary standards made by Nippon Sanso (MRI87) and the Takachiho scale was given by

$$xCO_2O_2^{NS} = 0.247 + 1.028(xCO_2^{TK}) - 7.650 \times 10^{-5}(xCO_2^{TK})^2, \quad (7)$$

where xCO_2^{NS} is the mixing ratio in dry air based on the MRI87 scale and xCO_2^{TK} is that based on the Takachiho scale (Inoue and Sugimura, 1992). We calculated the CO_2 mixing ratios of the primary standards by a least-square fitting assuming a quadratic relationship between the output voltage of the NDIR analyzer and the mixing ratio (Table 1). This was adopted to minimize the uncertainties in calibrated values (Tanaka *et al.*, 1987) and to check the possible drift in CO_2 mixing ratio with time.

Table 1. Primary standard gases prepared by the gravimetric method in 1987. An example of least-square fitting assuming a quadratic relation between the output voltage of the NDIR analyzer (Beckman model 865) and the given CO_2 mixing ratio

Cylinder	xCO_2^{grv} (ppm)	xCO_2^{lsf} (ppm)	1-s (ppm)	No
DF4772	249.55	249.63	0.00	5
DF4764	275.45	275.38	0.01	5
DF4763	299.63	299.67	0.03	5
DF4762	325.31	325.37	0.01	5
DC9359	334.76	334.72	0.03	5
DC9357*	345.10	344.72	0.02	5
DF4776	349.90	349.90	0.03	5
DC9358	356.28	356.29	0.03	5
DF4775	375.79	375.69	0.02	5
DF4774	400.74	400.79	0.03	5
DF4773	425.07	425.10	0.03	5

xCO_2^{grv} means the CO_2 mole fraction determined by the gravimetrical method and xCO_2^{lsf} by the least-square fitting.

*CO_2 mixing ratio decreased with time. This standard gas was not used as the primary standard.

Table 2. Mean CO_2 mixing ratio determined by the MRI on the basis of MRI87 scale and those of USA-NOAA (Peterson 1993, private communication). A set of three aluminum cylinders (#11413, #13763, #11051) was circulated among laboratories inthe USA, Canada, Japan, New Zealand, and Australia during the period from April 1991 to March 1993. The other set of standards (#11429, #6272, #11062) was circulated among Germany, France, Spain, Italy, and Hungary.

Laboratory	Date	#11413	#13763	#11051
MRI	July 1992	341.60	347.48	375.15
NOAA/CMDL	April 1991	341.62	347.55	375.29
NOAA/CMDL	Dec. 1992	341.49	347.45	375.18

We participated in the CO_2 round robin intercomparison conducted in 1991 and 1992. The results of our analysis system show good agreement with the 1985 WMO mole fraction scale (determined by NOAA/CMDL) within the range from 330 to 370 ppm (Table 2) to within 0.12 ppm.

The JMA has been using four CO_2 working reference gases ranging from 290 ppm to 400 ppm to conduct operational observations from the R/V *Ryofu-maru*. These working standard gases were calibrated before and after each cruise against secondary standard gases, which were calibrated twice annually against the 1985 WMO standard gases. We sent our cylinders to the JMA annually to compare our MRI87 scale with the 1985 WMO scale. The relationship between the MRI87 scale and the 1985 WMO scale was given by

$$xCO_2^{WMO} = 5.410 + 0.975(xCO_2^{NS}) + 2.530 \times 10^{-5}(xCO_2^{NS})^2, \quad (8)$$

where xCO_2^{WMO} is the mole fraction based on the 1985 WMO scale. However, this relationship is only tentative and may change considerably in the future. The

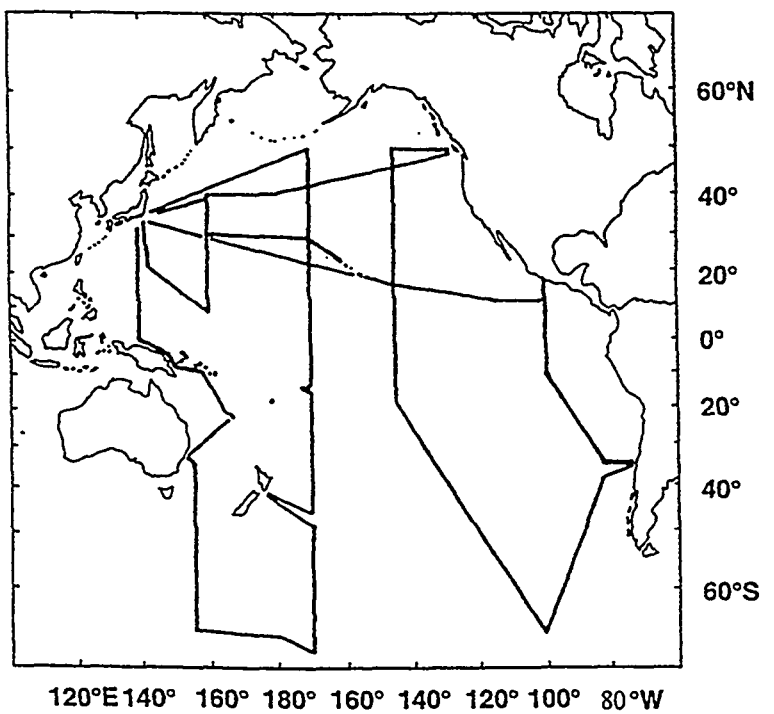

Fig. 6. The cruise tracks of R/V *Hakuho-maru* during which time measurements of pCO_2 were made throughout the period from 1968 to 1972. Fig. 1 in Miyake *et al.* (1974) was redrawn.

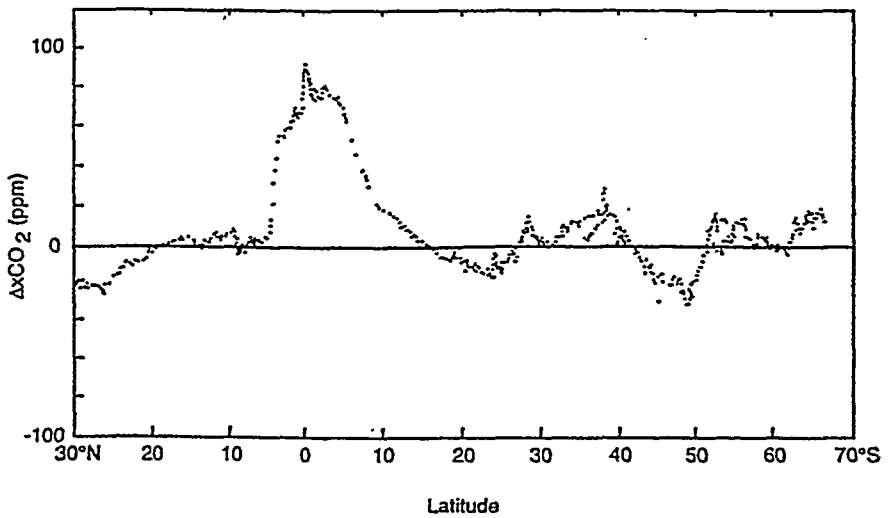

Fig. 7. Latitudinal distribution of xCO_2^a and xCO_2^s measured during the period from November 1968 to January 1969. Data south of 30°N were read from Fig. 4 in Miyake *et al.* (1974). The unit of vertical axis was changed from pCO_2 (ppm) to xCO_2 (ppm), and data north of 30°N were omitted because they were measured during a different period from April to June in 1970.

CO_2 mixing ratio sent to the JMA ranged from 290 to 400 ppm. In this paper we reported CO_2 mixing ratios based on the 1985 WMO scale as calculated by Eq. (8).

SUMMARY OF pCO_2 MEASUREMENTS

Results of pCO_2 measurements prior to 1973

Figure 6 shows the cruise tracks of R/V *Hakuho-maru* during which time quasi-continuous pCO_2 measurements were made using the CO_2 measuring system described in above. Figure 7 shows the latitudinal distribution of ΔxCO_2 along 170°W observed during the period from November 1968 to January 1969 redrawn from Fig. 4 of Miyake *et al.* (1974). The unit on vertical axis in Fig. 4 of Miyake *et al.* (1974) was expressed as ΔpCO_2 (ppm), but this should be ΔxCO_2 (ppm) after reviewing the archives in our laboratory. Because the ΔxCO_2 data north of 30°N in Fig. 4 of Miyake *et al.* (1974) were taken from another cruise conducted during the period from April to June in 1970, we did not plot the ΔxCO_2 data north of 30°N. Figure 7 shows similar features of ΔxCO_2 distribution as the current observations (Feely *et al.*, 1995; Ishii and Inoue, 1995), though corrections were needed to made both data sets compatible. In the area of equatorial upwelling, xCO_2^s was highly supersaturated with respect to xCO_2^a, and the xCO_2^s changed abruptly at the boundary (4°N) between the North Equatorial Countercurrent (NECC) and the South Equatorial Current (SEC). In contrast to the rapid

change between the NECC and the SEC, xCO_2^s decreased gradually from the equator southward.

By compiling data from 1968 to 1972, Miyake *et al.* (1974) produced a ΔpCO_2 map of the Pacific Ocean (Fig. 5 in Miyake *et al.* (1974)), and concluded that the Pacific Ocean was a source for atmospheric CO_2. In their treatment, however, seasonal variations in pCO_2^s were not considered. Even if their conclusion was not correct, we are reluctant to criticize their pioneer ΔpCO_2 map and conclusions. The method that they adopted was so excellent that their xCO_2^s data were still valid. We believe that it is invaluable to retrieve xCO_2^s data measured prior to 1973 to infer the long-term changes in the oceanic carbonate system of the Pacific. Inoue and Sugimura (1988) used this approach to deduce the increase of pCO_2^s in the Pacific between 1984 and 1969.

Seasonal variation and long-term trend of pCO_2^s in the western North Pacific

Since 1981, measurements of atmospheric and oceanic pCO_2 have been made periodically along the same cruise tracks (Inoue *et al.*, 1995) aboard the JMA ship R/V *Ryofu-maru*. Every year the R/V *Ryofu-maru* leaves Tokyo in the middle of January and arrives at the equator (or 3°N) at the end of month, while conducting oceanographic and meteorological observations along 137°E. Prior to 1989, MRI observed pCO_2^s and pCO_2^a and in 1990 JMA took over the program of operational observations aboard the R/V *Ryofu-maru* using basically the same analytical system as that of MRI (Hirota *et al.*, 1993).

Inoue *et al.* (1995) reported a long-term increase of pCO_2^s (Fig. 8). Figure

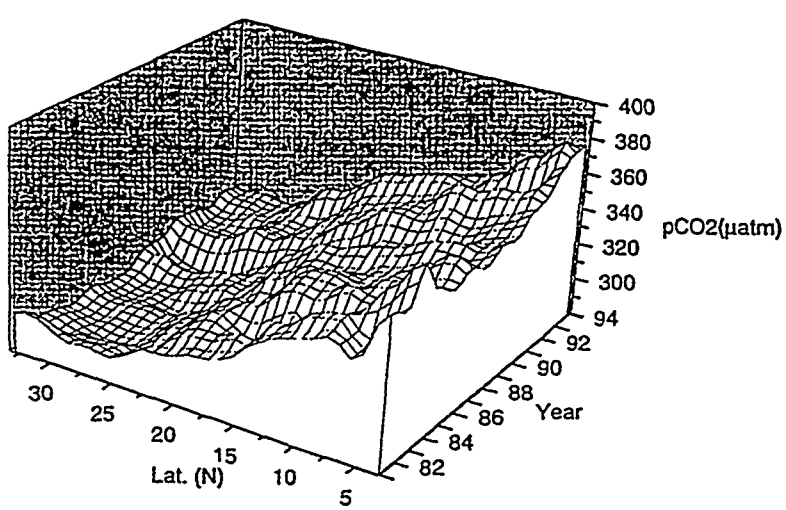

Fig. 8. Distribution of pCO_2^s in the western North Pacific (along 137°E) measured during every boreal winter since 1981. Due to the enhancement of vertical mixing, the pCO_2^s in the western equatorial Pacific increased during the El Niño event except in January and February 1987.

8 shows the latitudinal distribution of pCO_2^s along 137°E observed during every boreal winter since 1981. Every year, the pCO_2^s distribution in the subtropical area showed a similar pattern: off the coast of Japan the pCO_2^s was undersaturated with respect to pCO_2^a, and increased gradually toward the south. Near the equator, pCO_2^s was slightly larger than pCO_2^a. As reported earlier (Fushimi 1987; Inoue *et al.*, 1987), the pCO_2^s distribution near the equator is affected by the El Niño events.

Figure 8 clearly shows an increase of pCO_2^s in the whole area over periods from 1981 to 1996. By fitting a linear function to the averages at each latitude over periods from 1984 to 1993, Inoue *et al.* (1995) reported that the pCO_2^s in the subtropics has been increasing at a rate of 1.8 μatm/yr, equal to the atmospheric increase, while the rate of 0.5 μatm/yr in the western equatorial Pacific was less than that of the atmosphere. During the El Niño event, pCO_2^s data in the western equatorial Pacific were not used for this calculation. The difference in growth rate suggests temporal changes in ΔpCO_2 distribution (Volk and Bacastow, 1989). Inoue *et al.* (1995) examined thermodynamic factors controlling the oceanic carbonate system in the western North Pacific and concluded that the increase was caused by the oceanic CO_2 uptake. The oceanic TCO_2 increase was estimated to be 1 μmol/kg by using the homogeneous buffer factor.

Weiss *et al.* (1982) reported that the seasonal variations of fCO_2^s (fugacity) in the subtropics of the Pacific were mainly controlled by the thermodynamic temperature effect. In the western North Pacific, seasonal variations in pCO_2^s were found to correlate well with the sea surface temperature (Inoue *et al.*, 1995). The apparent relationship between pCO_2^s and SST is slightly different from that of the thermodynamics. Details of the difference from the thermodynamic effects was discussed in Inoue *et al.* (1995). Seasonal variations in CO_2 flux between the sea and the air calculated from Eq. (1) showed an active CO_2 uptake during the winter season in the area of the Subtropical Mode Water formation, south of the Kuroshio and east of Japan (Inoue *et al.*, 1995).

Long-term variations in pCO_2^s have been confirmed by direct and precise measurements. However, there is a lack in data to show changes in the oceanic carbonate system. At least temporal variations in one of the other variables describing the oceanic carbonate system (TCO_2, pH and alkalinity) are needed. If the condition of the homogeneous buffer factor maintains, the seasonal variation in Fx and the long-term trend of pCO_2^s require rapid transfers of anthropogenic CO_2 to middle and deep waters (Inoue *et al.*, 1995). Phytoplankton in surface waters uses CO_2 and/or bicarbonate ion to conduct photosynthesis. If phytoplankton uses bicarbonate ion and releases the OH-ion during the photosynthesis, as reported in fresh waters (Lucas, 1983), this may change the pCO_2-TCO_2 relationship. At the moment, we do not know the long-term trend of pH in seawaters. If the pH of surface seawater remains at the same level due to the biological activities, more TCO_2 can be stored in surface mixing layers with small changes in pCO_2 as compared with the pCO_2-TCO_2 relation defined by the homogeneous buffer factor. Accurate and continuous measurements of at least

two variables of the carbonate system are needed to provide useful information about the fate of anthropogenic CO_2.

Interannual changes in CO_2 flux in the tropical ocean

In this section, we describe both the spatial and temporal variations in pCO_2^s in the central and western equatorial Pacific based on measurements between 1987 and 1994. The Equatorial Pacific is known as a strong natural oceanic source of CO_2 to the atmosphere. The CO_2 outflux from the equatorial Pacific were estimated to be 1–2 Gt-C/yr (Tans *et al.*, 1990) corresponding to 15–30% of the current CO_2 emission due to fossil-fuel combustion (Marland *et al.*, 1994). Compared with that of the subtropical regions in the western North Pacific (Inoue *et al.*, 1995) and in the Indian Ocean (Poisson *et al.*, 1993), the distribution of pCO_2^s values in the equatorial Pacific exhibit more variability (Feely *et al.*, 1987, 1995; Inoue and Sugimura, 1992; Wong *et al.*, 1993). During the 1982/83 El Niño event, Feely *et al.* (1987) reported that the pCO_2^s in the central and equatorial

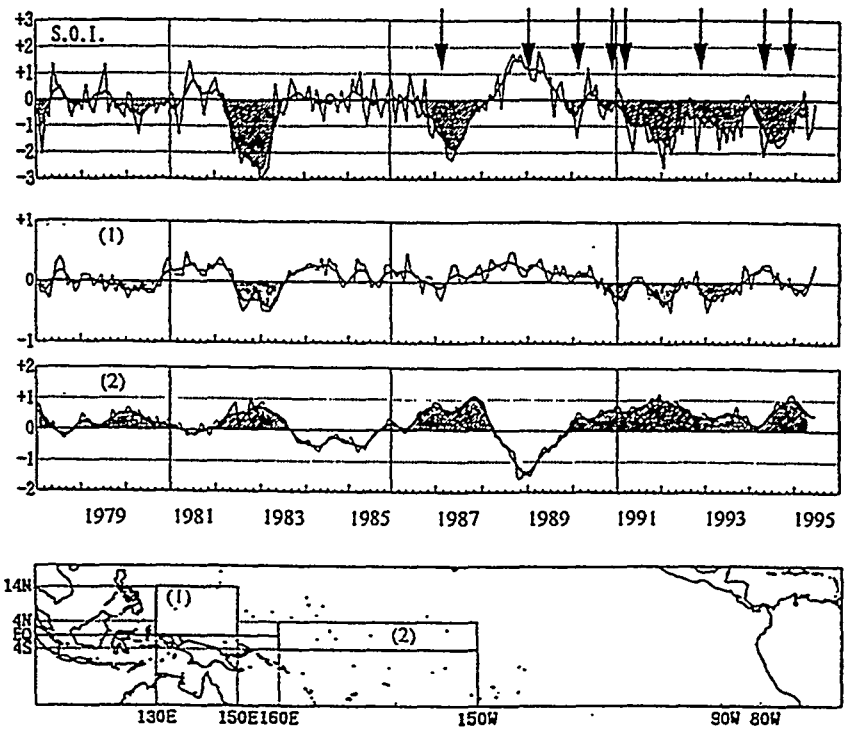

Fig. 9. Time series of SOI (solid line: running mean for 5 months) and SST anomalies (°C) in the central (160°E-150°W, 4°N-4°S) and western (130°E–150°E, 0°N–14°N) equatorial Pacific (Monthly Ocean Report, 1996). Positive anomalies in the central equatorial Pacific and negative anomalies in the western equatorial Pacific are shaded. Arrows in the top panel indicate the time for which pCO_2^s measurements were made.

Pacific decreased to a level almost equal to that of the pCO_2^a. While, during the 1988/89 La Niña event the pCO_2^s in the central and western equatorial Pacific increased considerably (Inoue and Sugimura, 1992). Figure 9 shows the anomalies of SST in the central and western equatorial Pacific (JMA, 1996). During the 1982/83 El Niño event, the pCO_2^s in the western equatorial Pacific increased with a SST decrease (Inoue *et al.*, 1987; Fushimi, 1987). In the equatorial Pacific, upwelling/vertical mixing play a major role in determining the pCO_2^s distributions.

In Fig. 10, the equatorial distributions of pCO_2^a and pCO_2^s for the period of January and February 1990 are shown. Inoue *et al.*, 1996 showed a "boundary" at which the pCO_2^s changes steeply. In the present study, the longitude where the steep change in pCO_2^s occurred is defined as P. The steep change in pCO_2^s

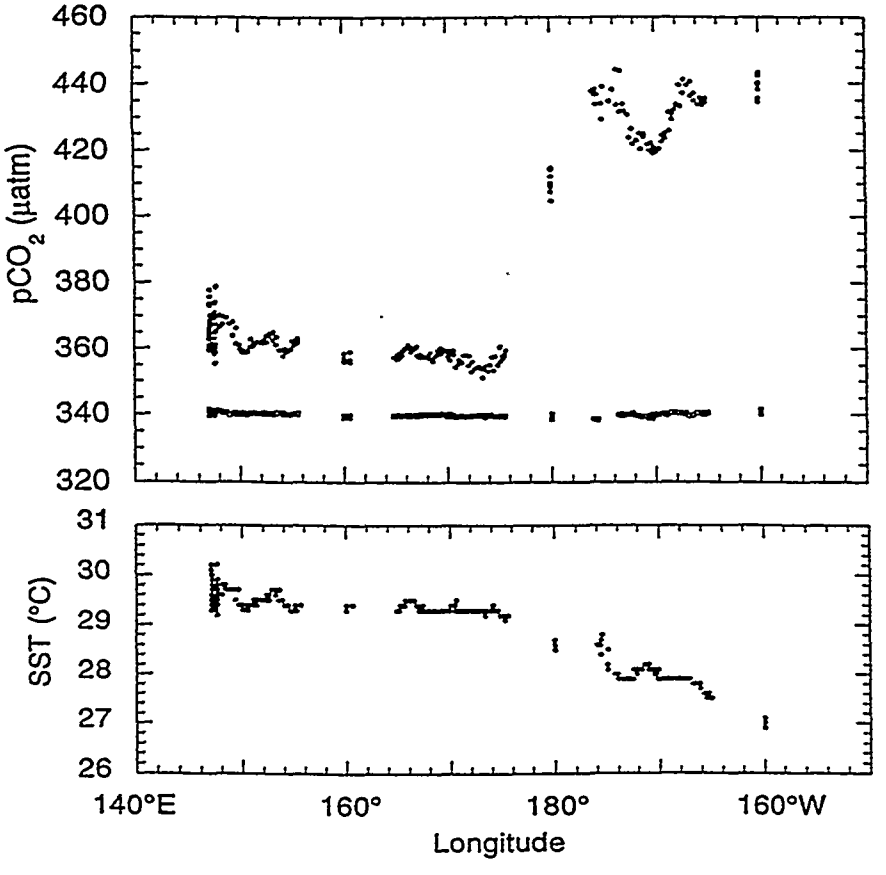

Fig. 10. The equatorial distribution of pCO_2^s and pCO_2^a (upper panel), and sea surface temperature (lower panel) for the period between January and February in 1990. A solid circle meants pCO_2^s and an open square pCO_2^a.

occurred at 180°, where the SST changed gradually. Over longitudes 176°W and 160°W, the seawater surface pCO_2^s (420–450 μatm) was highly supersaturated with atmospheric pCO_2 (340 μatm). West of 176°E the pCO_2 (350–380 μatm), was slightly supersaturated with respect to the pCO_2^a, and increased gradually toward the west. West of 176°E, the concentrations of $NO_3^- + NO_2^-$ were close to 0 μmol/kg, the sea surface salinity (SSS) was lower than 34.5 psu, and the SST around 29–30°C.

For the period November–December 1994, relatively low and rather constant pCO_2^s values were present west of 166°W (Fig. 3 in Inoue *et al.* (1996)). The pCO_2^s values began to change near 165°W as did the values of SSS. West of 166°W, the hydrographic property and nutrient concentrations exhibited patterns similar to those west of 176°E for January–February 1990.

Lower pCO_2 values always occurred in regions of high temperature (>29°C), low salinity (<34.5 psu), and low concentrations of nutrients observed west of 166°W in 1994. Conditions with low salinity and nutrient concentration and high temperature suggested a "warm water pool" in the western equatorial Pacific, closely connected with the El Niño/Southern Oscillation phenomenon. The correlation between the longitude where sharp change in pCO_2 occurs (P) and the El Niño/Southern Oscillation phenomenon was examined (Inoue *et al.*, 1996) by using the SOI (Monthly Ocean Report, 1996). A quadratic least-squares fit to the

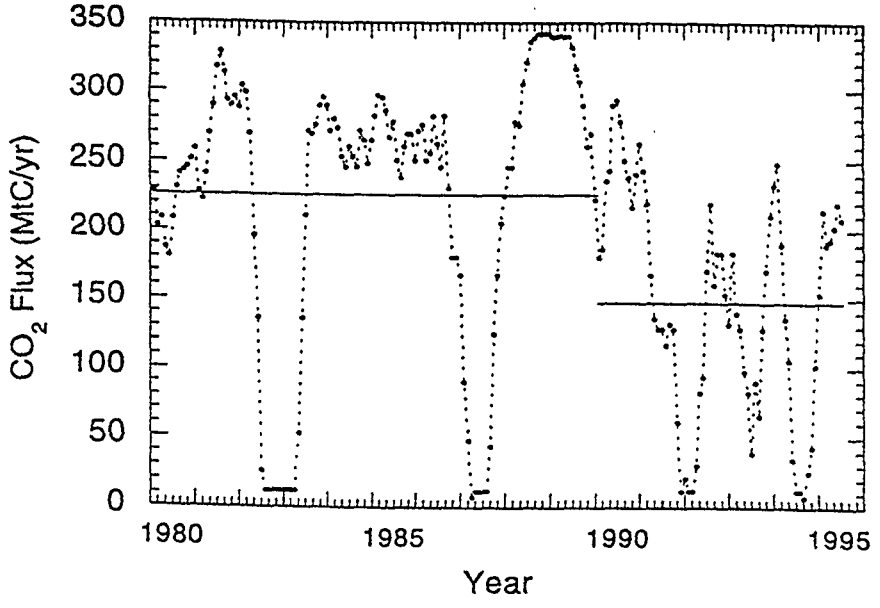

Fig. 11. Temporal changes in CO_2 outflux from the central and western equatorial Pacific (5.5°S-5.5°N, 130°E-160°W). The unit of vertical axis was Mt-C/yr (10^{12} g-C/yr). Horizontal bars indicate the average annual CO_2 outflux over 1980s and early 1990s. In this treatment, changes in ΔpCO_2 and wind field are not taken into account.

data yields $P = 163.85 - 20.33 \times (SOI) + 7.32 \times (SOI)^2$ ($N = 7$, $r = 0.97$). Clearly, the P moves eastward with a decrease in SOI, indicating that with strong CO_2 source region of the equatorial Pacific decreases with a decrease of the SOI.

In order to estimate the CO_2 outflux from the central and western equatorial Pacific, it is important to know the temporal changes in the areas of higher pCO_2^s. To know temporal changes in CO_2 outflux quickly and simply, we divided the central and western equatorial area (5.5°S-5.5°N, 130°E-160°W) into a higher pCO_2 region and a lower pCO_2 region. Then we estimated the CO_2 outflux for these areas. On the basis of CO_2 flux data by Ishii and Inoue (1995), the CO_2 outflux was estimated to be 9.6 mmol $m^{-2}day^{-1}$ for the higher pCO_2 region and 0.34 mmol $m^{-2}day^{-1}$ for lower pCO_2^s region. The average outflux for each region was simply taken from Ishii and Inoue (1995), where the relationship between gas exchange and wind speed was estimated by an equation given by Tans *et al.* (1990). The CO_2 outflux from the central and western equatorial Pacific decreases during the El Niño event, but increases during the La Niña event. This suggests significant intra- and interannual fluctuations of CO_2 outflux from the central and western equatorial Pacific (Fig. 11). This is not inconsistent with Francey *et al.* (1995) and Keeling *et al.* (1995), who suggested significant changes in ocean/plant uptake on time scales of a year to years. Over the 1980s, the average annual CO_2 outflux west of 160°W was estimated to be 230 MtC yr^{-1}, while during the period from January 1990 to June 1995 150 MtC yr^{-1} (Fig. 11). This preliminary result showed that the annual average CO_2 outflux from the central and western equatorial Pacific (5.5°S-5.5°N, 130°E-160°W) during the early 1990s decreased by one-third of the value in the 1980s.

REFERENCES

Boden, T. A., D. P. Kaiser, R. J. Sepanski and F. W. Stoss (ed.) (1994): *Trends '93: A Compendium of Data on Global Change*. ORNL/CDIAC-65, Carbon Dioxide Information Analysis Center, Oak Ridge National Laboratory, Oak Ridge, Tenn, U.S.A.

Bolin, B. and C. D. Keeling (1963): Large-scale atmospheric mixing as deduced from the seasonal and meridional variations of carbon dioxide. *J. Geophys. Res.*, 68, 3899–3920.

Conway, T. J., P. P. Tans and L. S. Waterman (1994): Atmospheric CO_2 records from sites in the NOAA/CMDL air sampling network. pp. 41–119. In *Trends '93: A Compendium of Data on Global Change*, ed. by T. A. Boden, D. P. Kaiser, R. J. Sepanski and F. W. Stoss, ORNL/CDIAC-65, Carbon Dioxide Information Analysis Center, Oak Ridge National Laboratory, Oak Ridge, Tenn, U.S.A.

DOE (1994): *Handbook of Methods for the Analysis of the Various Parameters of the Carbon Dioxide in Sea Water*; version 2, ed. by A. G. Dickson and C. Goyet, ORNL/CDIAC-74, Carbon Dioxide Information Analysis Center, Oak Ridge National Laboratory, Oak Ridge, Tenn, U.S.A.

Feely, R. A., R. H. Gammon, B. A. Taft, P. E. Pullen, L. S. Waterman, T. J. Conway, J. F. Gendron and D. P. Wisegarver (1987): Distribution of chemical tracers in the eastern equatorial Pacific during and after the 1982–83 El Niño/Southern Oscillation Event, *J. Geophys. Res.*, 92, 6545–6558.

Feely, R. A., R. Wanninkhof, C. A. Cosca, P. P. Murphy, M. F. Lamb and M. D. Steckley (1995): CO_2 distributions in the equatorial Pacific during the 1991–1992 ENSO event. *Deep-Sea Res.*, 42, 365–386.

Francey, R. J., P. P. Tans, C. E. Allison, I. G. Enting, J. W. C. White and M. Troller (1995): Changes in oceanic and terrestrial carbon uptake since 1982. *Nature*, 373, 326–330.

Fushimi, K. (1987): Variation of carbon dioxide partial pressure in the western North Pacific surface water during the 1982/83 El Niño Event. *Tellus*, **39B**, 214–227.

Gordon, L. I. and L. B. Jones (1973): The effect of temperature on carbon dioxide partial pressure in seawater. *Mar. Chem.*, 1, 317–322.

Hirota, M., K. Nemoto, A. Murata and K. Fushimi (1991): Observation of carbon dioxide in air and surface seawater in the western North Pacific Ocean. *Ocenographical Mag.*, 41, 19–28.

Inoue H. and Y. Sugimura (1986): Distribution of pCO_2 and-$\delta^{13}C$ in the air and surface sea water in the Southern Ocean, south of Australia. *Mem. Natl. Inst. Polar Res.. Spec. Issue*, **40**, 454–461.

Inoue, H. and Y. Sugimura (1988a): Distribution and variations of oceanic carbon dioxide in the western North Pacific, eastern Indian, and Southern Ocean south of Australia. *Tellus*, **40B**, 308–320.

Inoue, H. and Y. Sugimura (1988b): Distribution of the pCO_2 in surface seawater of the western and central equatorial Pacific during the 1986/87 El Niño/Southern Oscillation Event. *Geophys. Res. Lett.*, 15, 1499–1502.

Inoue, H. and Y. Sugimura (1992): Variations and distributions of CO_2 in and over the equatorial Pacific during the period from the 1986/88 El Niño Event to the 1988/89 La Niña Event. *Tellus*, **44B**, 1–22.

Inoue, H., Y. Sugimura and K. Fushimi (1987): pCO_2 and $\delta^{13}C$ in the air and surface sea water in the western North Pacific. *Tellus*, **39B**, 228–242.

Inoue, H., H. Matsueda, M. Ishii, K. Fushimi, M. Hirota, I. Asanuma and Y. Takasugi (1995): Long-term trend of the partial pressure of carbon dioxide (pCO_2) in surface waters of the western North Pacific, 1984–1993. *Tellus*, **47B**, 391–413.

Inoue, H., M. Ishii, H. Matsueda, M. Aoyama and I. Asanuma (1996): Changes in longitudinal distribution of the partial pressure of CO_2 (pCO_2) in the central and western equatorial Pacific, west of 160°W. *Geophys. Res. Lett.*, 23, 1781–1784.

Ishii, M. and H. Inoue (1995): Air-sea exchange of CO_2 in the central and western equatorial Pacific in 1990. *Tellus.*, **47B**, 447–460.

Inter-Governmental Panel on Climate Change (1990): Greenhouse gases and aerosols. pp. 5–40. In *Climate Change. The IPCC Scientific Assessment*, ed. by J. T. Houghton, G. J. Jenkins and J. J. Ephraums, Cambridge University Press, Cambridge.

Japan Meteorological Agency (1989): Marine climatological tables of the North Pacific Ocean for 1971–1980. Marine Department, JMA. Tokyo.

Keeling, C. D., R. B. Bacastow, A. F. Carter, S. C. Piper, T. P. Whorf, T. P. Heimann, W. G. Mook and H. Roeloffozen (1989): A three-dimensional model of atmospheric CO_2 transport based on observed winds: I Analysis of observational data. pp. 165–236. In *Aspect of Climate Variability in the Pacific and Western America*, ed. by D. M. Peterson, AGU Geophysical Monograph, Washington, D.C.

Keeling, C. D., T. P. Whorf, M. Wahlen and J. van der Plicht (1995): Interannual extremes in the rate of rise of atmospheric carbon dioxide since 1980. *Nature*, **375**, 666–670.

Liss, P. S. and L. Merlivat (1986): Air-sea gas exchange rates: introduction and synthesis. pp. 113–127. In *The Role of Air-Sea Exchange in Geochemical Cycling*, ed. by P. Buat-Menard, D. Reidel, Dordrecht, The Netherlands.

Lucas, W. J. (1983): Photosynthetic assimilation of exogenous HCO_3^- by aquatic plants. *Ann. Rev. Plant Physiol.*, 34, 71–104.

Marland, G., R. J. Andres and T. A. Boden (1994): Global, regional, and national CO_2 emissions. pp. 508–584. In *Trends '93: A Compendium of Data on Global Change, 1994, ORNL/CDIAC-65*, ed. by T. A. Boden, D. P. Kaiser, R. J. Sepanski and F. W. Stoss, Carbon Dioxide Information Analysis Center, Oak Ridge National Laboratory, Oak Ridge, Tenn., U.S.A.

Miyake, Y. and Y. Sugimura (1969): Carbon dioxide in the surface water and the atmosphere in the Pacific, the Indian and the Antarctic Ocean areas. *Rec. Oceanogr. Wks. Japan.*, **10**, 23–28.

Miyake, Y., Y. Sugimura and K. Saruhashi (1974): The carbon dioxide content in the surface water in the Pacific ocean. *Rec. Oceanogr. Wks. Japan.*, 12, 45–52.

Monthly Ocean Report (1996): El Niño Monitoring Center, Climate and Marine Department. Japan

Meteorological Agency, Tokyo.

Poisson, A., N. Metzl, C. Brunet, B. Schauer, B. Bres, D. Ruiz-Pino and F. Louanchi (1993): Variability of sources and sinks of CO_2 in the western Indian and southern oceans during the year 1991. *J. Geophys. Res.*, 98, 22,759–22,778.

Revelle, R. and H. E. Suess (1957): Carbon dioxide exchange between atmosphere and ocean, and the question of an increase of atmospheric CO_2 during the past decades. *Tellus*, 9, 18–27.

Sundquist, E. T., L. N. Olummer and T. M. L. Wigley (1979): Carbon dioxide in the ocean surface: the homogeneous buffer factor. *Science* 204, 1203–1205.

Tanaka, M., T. Nakazawa, and S. Aoki (1987): Time and space variations of tropospheric carbon dioxide over Japan. *Tellus*, 39B, 3–12.

Tans, P. P., I. Fung and T. Takahashi (1990): Observational constrains on the global atmospheric CO_2 budget. *Science*, 247, 1431–1438.

Volk, T. and R. Bacastow (1989): The changing patterns of ΔpCO_2 between ocean and atmosphere. *Global Biogeochem. Cycles*, 3(2), 179–189.

Wagner, K. (1979): The carbonate system of the ocean. pp. 251–258. In *The Global Carbon Cycle*, ed. by B. Bolin, E. T. Degens, S. Kempe and P. Ketner, John Wiley & Sons, Chichester.

Wanninkhof, R. (1992): Relationship between wind speed and gas exchange over the ocean. *J. Geophys. Res.*, 97, 7373–7382.

Weiss, R. F., R. A. Jahnke and C. D. Keeling (1982): Seasonal effects of temperature and salinity on the partial pressure of CO_2 in sea water. *Nature* 300, 511–513.

WMO WDCGG Data Report (1995): *WDCGG No. 7. GAW DATA. Volume IV—Greenhouse Gases and Other Atmospheric Gases*. Japan Meteorological Agency, Tokyo.

Wong, C. S., Y.-H. Chan, J. S. Page, G. E. Smith and R. D. Bellegay (1993): Changes in equatorial CO_2 flux and new production estimated from CO_2 and nutrient levels in Pacific surface waters during the 1986/87 El Niño. *Tellus*, 45B, 64–79.

ELSEVIER

Marine Chemistry 52 (1996) 133–145

MARINE CHEMISTRY

At-sea intercomparison of two newly designed underway pCO_2 systems — encouraging results

Arne Körtzinger [a,*], Helmuth Thomas [b], Bernd Schneider [b], Nicole Gronau [b], Ludger Mintrop [a], Jan C. Duinker [a]

[a] *Institute for Marine Sciences at Kiel University, Department of Marine Chemistry, Düsternbrooker Weg 20, D-24105 Kiel, Germany*
[b] *Baltic Research Institute at Rostock University (IOW), Chemistry Section, Seestraße 15, D-18119 Warnemünde, Germany*

Received 23 May 1995; accepted 1 November 1995

Abstract

Two newly designed underway systems for the measurement of CO_2 partial pressure (pCO_2) in seawater and the atmosphere are described. Results of an intercomparison experiment carried out in the North Sea are presented. A remarkable agreement between the two simultaneously measured pCO_2 data sets was observed even though the spatial variability in surface pCO_2 was high. The average difference of all 1-min averages of the seawater pCO_2 was as low as 0.15 μatm with a standard deviation of 1.2 μatm indicating that no systematic difference is present. A closer examination of the profiles shows that differences tend to be highest during maxima of the pCO_2 gradient (up to 14 μatm/min). The time constants of both systems were estimated from laboratory experiments to 45 s, respectively, 75 s thus quantitatively underlining their capability of a fast response to pCO_2 changes.

1. Introduction

Due to the burning of fossil fuel and the human impact on land biota the atmospheric concentration of CO_2 is steadily increasing (e.g. Keeling et al., 1995). As the major greenhouse gas except water vapor CO_2 interacts strongly with the radiative balance of the earth and its increasing concentration potentially influences the global climate. However, only about 45% of the total anthropogenic emissions of CO_2 remains airborne (Houghton et al., 1990). The ocean has long since been recognized as an important sink for a significant portion of the missing anthropogenic CO_2. Being the largest rapidly exchanging reservoir of carbon it will in a future steady state absorb in the order of 85% of all man-made CO_2. However, with a mean ventilation time of the world ocean of 500–1000 years as the main kinetic barrier the ocean cannot keep pace with the atmospheric perturbation. Therefore the understanding of the oceans' role in the global carbon cycle has become — as we feel — one of the most thrilling challenges in marine sciences.

The concepts in tracing and quantifying the anthropogenic carbon dioxide in the ocean are manifold and most of them are based on assumptions and parametrizations that are still not unequivocally accepted. One concept that receives particular attention among research groups not only since the intriguing

* Corresponding author. Tel.: +49-431-5974023; fax: +49-431-565876; e-mail: akoertzinger@ifm.uni-kiel.d400.de.

SSDI 0304-4203(95)00083-6

findings of Tans et al. (1990) is the ΔpCO_2 concept: the net flux of CO_2 across the air–sea interface is proportional to the difference of the partial pressures of CO_2 (ΔpCO_2) in the atmosphere and the surface water. If we were able to cover the world ocean with a grid of representative mean ΔpCO_2 values and further could assign appropriate exchange coefficients to them the global net flux of CO_2 across the air–sea interface could be calculated (Watson et al., 1995). However, if in the light of the considerable spatiotemporal variability of ΔpCO_2 this concept shall be successful a broad data base has to be generated. Only if a combined effort of research groups around the world leads to ΔpCO_2 profiles across all parts of the world ocean and at different seasons the estimate of the anthropogenic CO_2 flux into the ocean can possibly be pinned down more precisely.

In this context the question of comparability of pCO_2 data from different laboratories and different analytical systems plays a vital role for the success of the ΔpCO_2 concept. The mean global air–sea ΔpCO_2 necessary to accommodate a global oceanic sink of 2.0 Gt C yr^{-1} is in the order of 7 μatm (Wallace, 1995). This is a rather small signal compared to an analytical precision in the order of 1 μatm and an accuracy of probably not better than a few μatm. To assess the current state an international intercomparison exercise, marvellously organized by A. Dickson and co-workers (Scripps Institution of Oceanography, Marine Physical Laboratory, La Jolla/California, USA, June 6–10, 1994), was carried out as a first step. In this paper we report data from a 21-h intercomparison experiment which was carried out at sea with two newly designed underway pCO_2 systems. The results clearly show that at least with systems of similar design highly comparable measurements are possible.

2. Theoretical background

The partial pressure of an ideally behaving component i is defined as the product of its mole fraction x_i and the total pressure of the gas phase. As the partial pressure is defined for the gas phase only the term "seawater partial pressure" of a volatile component means the partial pressure of this component in a gas phase which is in equilibrium with seawater with respect to this component. To take into account the non-ideal character of a gas like CO_2 the fugacity should be used rather than the partial pressure (DOE, 1994). It can be calculated from an equation given by Weiss (1974). Since the difference is rather small most data presented in the literature are still given as pCO_2 values instead of fCO_2 values.

The net flux F of CO_2 across the air–sea interface can be calculated from the partial pressure difference between seawater and atmosphere:

$$F = k \cdot K^0(\Delta pCO_2)$$

where k is the transfer velocity, K^0 is the solubility coefficient of CO_2 in seawater and ΔpCO_2 is the difference of pCO_2 in the corresponding bulk layers (i.e., surface mixed layer and air). The partial pressure difference ΔpCO_2 is the thermodynamic driving force of the net gas flux. The transfer velocity k mainly depends on wind speed and seawater temperature (Liss, 1983; Liss and Merlivat, 1986; Wanninkhof, 1992) while K^0 depends on temperature and salinity (Weiss, 1974).

3. Materials and methods

3.1. The systems

The principle of pCO_2 measurement is based on the equilibration of a carrier gas phase with a seawater sample and subsequent determination of the CO_2 volume mixing ratio in the carrier gas. As the pCO_2 in seawater strongly varies with temperature a correction is necessary to compensate for the difference between equilibration temperature and the in-situ seawater temperature. Different equations have been proposed for the temperature dependence of CO_2 partial pressure/fugacity in seawater (Gordon and Jones, 1973; Weiss et al., 1982; Copin-Montegut, 1988, 1989; Goyet et al., 1993; Takahashi et al., 1993).

A great variety of pCO_2 systems and equilibrators has been described in the literature. Essentially three different design principles can be distinguished, i.e., (1) the "shower type" equilibrator (e.g., Keeling et al., 1965; Kelley, 1970; Weiss, 1981; Inoue et

al., 1987; Robertson et al., 1993; Goyet and Peltzer, 1994), (2) the "bubble type" equilibrator (e.g., Takahashi, 1961; Goyet et al., 1991; Schneider et al., 1992; Kimoto and Harashima, 1993; Ohtaki et al., 1993), and (3) the "laminary flow type" equilibrator (Poisson et al., 1993). A design described by Copin-Montegut (1985) combines aspects of the shower and bubble type.

Two underway pCO_2 systems, developed independently at the Institute for Marine Sciences, Kiel

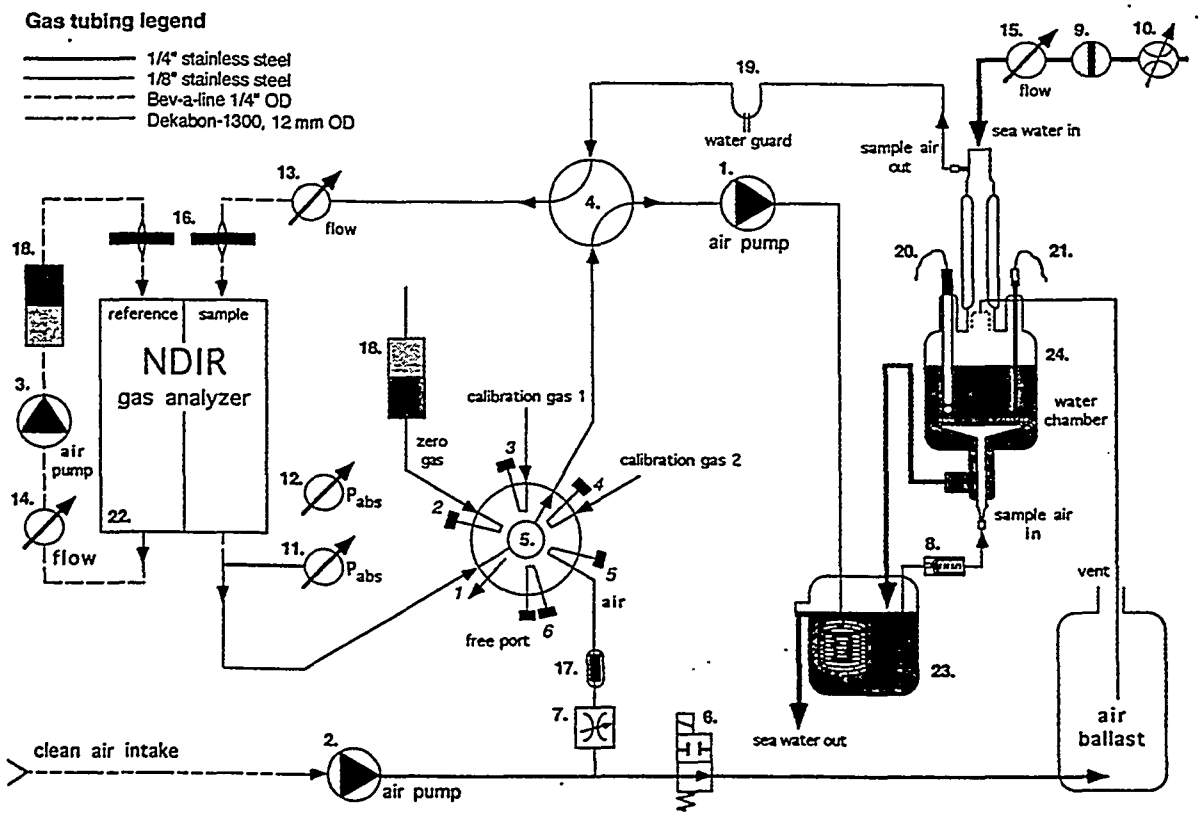

Fig. 1. Schematic diagram of the Kiel underway system (IFM) for the determination of pCO_2 in seawater and air. 1. Air pump, max. flow = 9.0 l/min, Δp max. = 780 mbar, Erich Fürgut Miniaturgaspumpen, Aitrach, Germany. 2. Air Cadet® pump, max. flow = 22 l/min, Δp max. = 600 mbar, Cole-Parmer International, Niles, IL, USA. 3. Air pump, max. flow = 1.6 l/min, Δp max. = 100 mbar, Erich Fürgut Miniaturgaspumpen, Aitrach, Germany. 4. 2-position valve, electric actuator, Valco Instruments Co. Inc., Houston, TX, USA. 5. Multiposition valve (6 positions, 13 ports, flow-through flowpath), electric actuator, Valco Instruments Co. Inc., Houston, TX, USA. 6. 2-way PTFE solenoid valve, normally open, Neptune Research Inc., Maplewood, NJ, USA. 7. Needle valve with calibrated micrometer head, NUPRO Company, Willoughby, OH, USA. 8. Check valve, opening pressure 20 mbar, NUPRO Company, Willoughby, OH, USA. 9. Ball valve, manually actuated. 10. Flow controller (0.2–2.0 l/min), Cole-Parmer International, Niles, IL, USA. 11, 12. Pressure transducer (600–1100 mbar, accuracy 0.05% full scale), Setra Systems Inc., Acton, MA, USA. 13. Gas flowmeter with needle valve (10–100 l/h), Kobold Meßring GmbH, Hofheim, Germany. 14. Gas flowmeter with needle valve (33–430 ml/min), Kobold Meßring GmbH, Hofheim, Germany. 15. Liquid flowmeter (0.25–2.5 l/min), Kobold Meßring GmbH, Hofheim, Germany. 16. PTFE membrane filter (1 μm), Gelman Sciences, Ann Arbor, MI, USA. 17. Particle filter (2 μm), NUPRO Company, Willoughby, OH, USA. 18. Gas purification tube with CO_2 scrubber (Ascarite II®, Aldrich-Chemie GmbH, Steinheim, Germany) and chemical desiccant ($Mg(ClO_4)_2$, dto). 19. Water guard (platinum electrodes in U-shaped glass tube). 20. pH glass electrode (ROSS series, ORION Research Inc., Boston, MA, USA) with pH/mV meter 530, Wissenschaftlich-Technische Werkstätten GmbH, Weilheim, Germany. 21. Pt-100 temperature probe (4-wire technique) with temperature monitor, Burster Präzisionsmeßtechnik GmbH and Co. KG, Gernsbach, Germany. 22. NDIR CO_2/H_2O gas analyzer, model LI-6262, LI-COR Inc., Lincoln, NE, USA. 23. Reservoir. 24. Equilibrator (made of DURAN® glass, consisting of water chamber and column with evacuated jacket).

(IFM) and at the Baltic Sea Research Institute, Warnemünde (IOW) were used in the present intercomparison experiment. Both systems are of the "bubble type" and similar in principle though different in detail. Therefore common aspects will be discussed first. This is followed by two chapters with a more detailed description of the individual design of both systems.

A continuous flow of seawater passes through an open system equilibration cell, which is vented to the atmosphere. This allows the equilibrium process to take place at ambient pressure at any time. A fixed volume of air is re-circulated continuously through the system so as to be in almost continuous equilibrium with the constantly renewed seawater phase. In a "bubble type" equilibrator this airflow is bubbled through the water phase. After passage through the equilibration cell the air stream is pumped to a non-dispersive infrared gas analyzer, where the mole fraction of CO_2 is measured relative to a dry and CO_2-free reference gas (absolute mode). Both systems feature a LI-COR® LI-6262 CO_2/H_2O gas analyzer, which is a dual-channel instrument that simultaneously measures the CO_2 and H_2O mole fractions. The gas stream needs no drying prior to infrared gas detection as the biasing effect of water vapor on the measurement of CO_2 is eliminated based on the H_2O measurement. The appropriate internal algorithms not only correct for dilution of the sample gas by the "additional" (compared to calibration gases) component water but also for gas phase interactions of CO_2 with water vapor which cause a broadening of the absorption band of CO_2 (McDermitt et al., 1993). The various advantages of this particular NDIR system and its perfect seagoing performance have been described in more detail by Goyet and Peltzer (1994). Both gas circuits (components and fittings) were checked for leakages with elevated CO_2 levels in the surrounding air.

3.1.1. The Kiel underway pCO_2 system (IFM)

The schematic drawing in Fig. 1 depicts the general design of the Kiel underway pCO_2 system (hereafter IFM system). All numbers in the description below refer to numbers appearing in Fig. 1.

The equilibrator (24) combines two equilibration concepts which are realized in two subsequent stages. One stage operates as a "bubble type" equilibrator in which a water chamber is filled with appr. 1000 ml of constantly renewed water. The air enters from below through a coarse glass frit and is bubbled through the water. The second stage acts as a "laminary flow" equilibrator. A 45-cm glass column is centered on top of the water chamber. The seawater enters from the top and forms a laminary flow on the inner walls of the column, while the air coming from the water chamber below passes through the column before it leaves the equilibrator at the head of the column. The counter-current flow direction of seawater and air as well as the large surface area facilitate the establishment of equilibrium. An evacuated jacket minimizes temperature changes of the water flow during passage through the column. Typically the temperatures differ by a few tens of a degree and differences rarely exceed 1°C. The flow rate of seawater is set to 1.5–2.0 l/min. A PC-interfaced flow controller (10) adjusts the flow rate to the pre-set value and compensates for pressure changes which frequently occur when the ship's own seawater pumping systems are used.

The air circuit (total volume approx. 400 ml) is maintained with air pump 1 at a flow rate of 1.0–1.2 l/min. After leaving the equilibrator the air is pumped through water guard 19, valve 4, a flowmeter/needle valve combination (13) and a 1-μm PTFE membrane filter (16) to the NDIR gas analyzer (22). Its CO_2 and H_2O mole fractions are monitored continuously, and the air stream is re-circulated via multiposition valve 5, valve 4 and the air pump (1) to a reservoir (23) which is flushed with waste water from the equilibrator. The gas tubing is coiled within the reservoir to adjust the air stream to the seawater temperature before re-entering the equilibrator. A check valve (8) avoids invasion of water through the frit into the gas lines in case of pump failure.

The reference gas circuit is a closed loop system which consists of a flowmeter/needle valve (14), a miniature air pump (3), a gas purification tube (18) and a 1-μm PTFE membrane filter (16). This feature provides a constant supply of dry and CO_2-free air as a zero reference gas and thus strongly reduces gas requirements to just one set of calibration gases.

For the measurement of ambient atmospheric pCO_2 an Air Cadet® diaphragm pump (2) continuously draws uncontaminated air from the compass platform of the research vessel through a Dekabon®-

type flexible tubing (Furon Dekoron Division, Aurora, OH, USA, 12 mm OD) to the pCO_2 system. When atmospheric pCO_2 is not being measured this air is used to flush the air ballast bottle which provides a clean air buffer to the equilibrator vent. If any volume change occurs in the re-circulated air only clean outside air can invade the system through the vent line. For air measurements valve 6 is closed and the air enters the system via needle valve 7 and a 2-μm pre-filter (17).

Three different types of measurements (calibration, measurement of atmospheric or seawater equilibrated air) are controlled with valves 4 and 5. Fig. 2 is a schematic drawing of the valve concept with the two different general states described below. Valve 4 separates the equilibrator circuit from the measuring circuit. Thus during air measurement or calibration of the system pump 1 keeps the short-circuited equilibration circuit in progress (Fig. 2, right), while the separated measuring circuit is flushed with ambient air respectively calibration gases. Valve 5 selects the gas to be measured.

For measurements of pH and seawater temperature the equilibrator is equipped with a pH glass electrode (20) and a platinum resistance thermometer (21). Two high-accuracy pressure transducers (11, 12) are used to monitor barometric pressure as well as pressure in the NDIR cell.

For automation of the system a special software has been developed. It carries out two different functions: (1) all data generated by the system (raw mV readings, xCO_2, xH_2O, T_{NDIR}, p_{NDIR}, p_{atm}, T_{eq}, pH_{eq}) or provided by the data distribution system of the vessel (GPS latitude and longitude, $T_{in\text{-}situ}$, salinity) are interrogated, averaged and logged at user-chooseable intervals. A typical routine comprises an interrogation interval of 6 s and an averaging interval of 1 min; (2) the fully accessible duty cycle is carried out by remote control of the three valves. The duration and interval of measurement states (calibration, measurement of seawater equilibrated or atmospheric air) can be chosen from a set-up menu. A typical routine consists of initial calibration, then 57 min measurement of pCO_2 (seawater) and 3 min measurement of pCO_2 (air) alternating, with re-calibration after 4–6 cycles (i.e., approx. 4–6 h). A delay interval can be defined to avoid logging of data during a time interval after

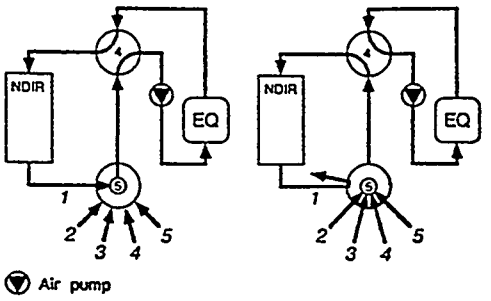

Fig. 2. Valve concept for gas control in the IFM underway pCO_2 system. The interaction of valves 4 and 5 is shown schematically for the measurement of seawater equilibrated air (left) and ambient air resp. calibration gases (right).

valve switching. An interval of 60 s has been shown to be sufficient to allow the reading to re-stabilize after a change of the measured gas.

For calibration of the NDIR instrument a set of three calibration gases is used (CO_2-free air, low and high CO_2 standard gas). All air mixtures are based on the "natural" air concept and contain nitrogen, oxygen and argon in the natural proportions (i.e., 780 pptv N_2, 210 pptv O_2, 9.3 pptv Ar). The CO_2-free air is purified with a CO_2 scrubber (Ascarite II®) and a desiccant (magnesium perchlorate). The LI-COR® instrument comes with an individual calibration polynomial. User calibration consists of setting the "zero" and "span" of the system (low standard gas). Rather than being done manually the "zero" and "span" set is performed automatically by the software during each calibration procedure. The high standard gas is run regularly as a calibration check.

The whole system (except the PC) is contained in a plexiglass/polyethylene chassis that fits almost fully assembled into an aluminium case for easy shipping.

3.1.2. *The Warnemünde underway pCO_2 system (IOW)*

Fig. 3 shows a schematic drawing of the general design of the Warnemünde underway pCO_2 system (hereafter IOW system). All numbers in the description below refer to numbers appearing in Fig. 3.

3.1.2.1. Water supply. The continuous flow of seawater through the equilibrator is generated by a

submerged pump (2), which is mounted in the moon poole of the vessel. Hence, the seawater is pumped all the way to the equilibrator at overpressure hereby avoiding any outgassing. From the total water flow of 60–100 l/min the sample flow is teed off just in front of the equilibrator and finally adjusted to a flow rate of approx. 1 l/min by means of valve 14. The high flow rate in the main by-pass and additional heat insulation of the tubing keeps the water in the equilibrator close to in situ temperature.

The seawater volume in the equilibrator is given by the height of the water outlet and corresponds to a volume of about 200 ml. In order to increase the efficiency of the water exchange, a pipe connects the water outlet with the water close to the bottom of the equilibrator. At a flow rate of 1 l/min a time constant of 12 s results for the water renewal in the equilibrator. The water from the equilibrator flows through a heat insulated bath which serves as a temperature buffer between the equilibrator and ambient air. The water temperature in the equilibrator is recorded continuously with a precision of 0.05°C. Additionally, pH is measured and used to examine qualitatively consistency with the pCO_2 measurements.

3.1.2.2. Equilibration. A membrane pump (15a) is used to circulate a volume of about 100 ml of air at a flow rate of 200 ml/min through the water column in the equilibrator and the NDIR detection system. Like in the IFM system air is pre-tempered to the seawater temperature before entering the equilibrator. The air is led through a heat exchange coil submerged in the temperature buffer bath. Bubbles in

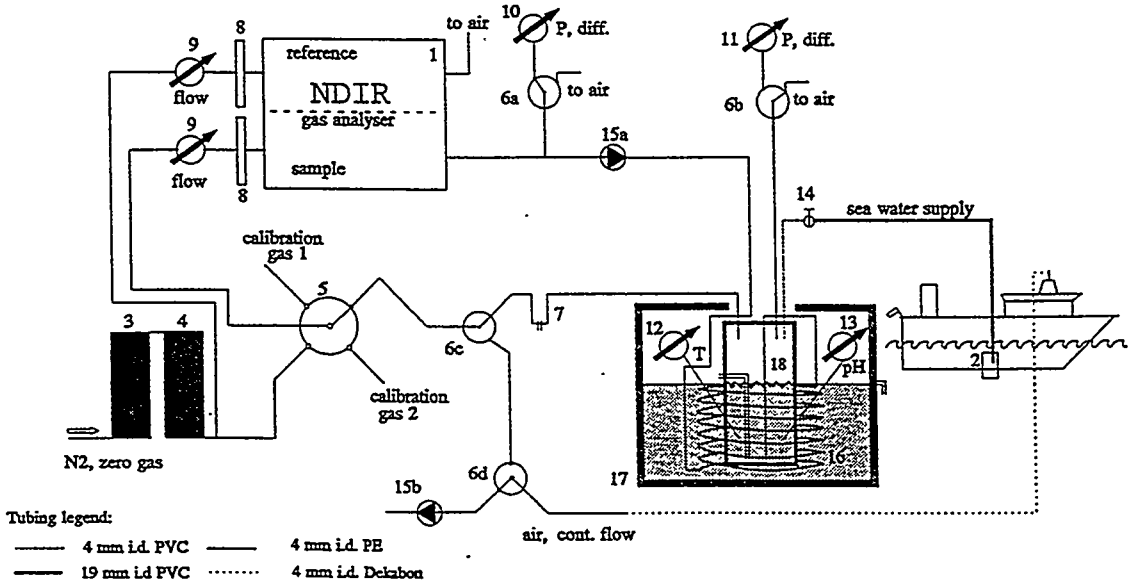

Fig. 3. Schematic diagram of the Warnemünde underway system (IOW) for the determination of pCO_2 in seawater and air. 1. NDIR CO_2/H_2O gas analyzer, model LI-6262, LI-COR Inc., Lincoln, NE, USA. 2. Immersion pump, max. flow = 100 l/min, Flygt GmbH.3. Gas purification tube with CO_2 scrubber (soda lime pellets, Merck, Darmstadt, Germany). 4. Gas purification tube with chemical desiccant (Anhydrone®, J.T. Baker Inc, Phillipsburg, NJ, USA). 5. 5-way ball valve, manually actuated, Whitey Co., Highland Heights, OH, USA. 6a–d. 2-way ball valve, manually actuated, Whitey Co., Highland Heights, OH, USA. 7. Water guard (platinum electrodes in U-shaped glass tube). 8. PTFE membrane filter (1 μm), Gelman Sciences, Ann Arbor, MI, USA. 9. Gas flowmeter with needle valve (0–1 l/min), Dwyer Instruments Inc., Michigan City, USA. 10. Differential pressure transducer (0–50 mbar), model P592-1D-A1A, accuracy 1% full scale, Kavlico Corp., USA. 11. Differential pressure manometer (0–5 mbar), Dwyer Instruments Inc., Michigan City, USA. 12. Pt-100 temperature probe (4-wire technique) with temperature monitor, Burster Präzisionsmeßtechnik GmbH and Co. KG, Gernsbach, Germany. 13. pH glass electrode (model E 56, Wissenschaftlich-Technische Werkstätten GmbH, Weilheim, Germany) with pH/mV meter (model 647, Knick Elektronische Meßgeräte GmbH and Co., Berlin, Germany). 14. Valve, manually actuated. 16. Stainless steel heat exchange coil. 17. Heat insulated bath (Plexiglass®, Styropor®). 18. Equilibrator, glass.

the equilibrator are generated by pressing the air through the capillary tip of a PTFE tube. The air leaving the equilibrator passes a conductivity cell (7) by which the pump is switched off in case of a seawater breakthrough. Via valves 6c and 5, a flow meter (9), and a 1 μm PTFE membrane filter (8) the air enters the IR detector cell. The pressure difference between the exit of the IR cell and ambient air is measured (10) and used together with the barometric pressure from the ship's sensor. The air is re-circulated via pump 15a. Like in the IFM system the equilibrator is open to atmospheric pressure to avoid any over- or underpressure in the headspace. To check this, the pressure difference between the head space and the atmosphere is sporadically measured (11).

For the measurement of atmospheric pCO_2 valves 6c and 6d are switched. Pump 15b continuously pumps clean air from the compass platform out to the system. Calibration is carried like described for the IFM system with a gas flow rate of about 200 ml/min.

3.2. The experiment

The intercomparison experiment was carried out on board R/V *Valdivia* during cruise no. 148-2 in September, 1994. The 21-h intercomparison experiment was performed on transect A–B in the eastern North Sea (Fig. 4). The R/V *Valdivia* departed from Kiel on September 11, 1994, and arrived back to Kiel on September 14, 1994, after sailing around Denmark. When designing the experiment care was taken to operate the systems under conditions as comparable as possible. First of all both system were run simultaneously on the water supply system as described in Section 3.1.2.1 for the IOW system. The systems were operated side by side and the water flows required by each of them were teed off right at the systems. In-situ temperature and salinity of the seawater were monitored continuously with a temperature/salinity (conductivity) probe mounted close to the seawater intake. Corrections for temperature changes were performed based on these in-situ temperature readings and the equilibrator temperatures measured and logged by each of the systems. Barometric pressure was taken from the ship's meteorological pressure sensor. Ambient air was drawn from

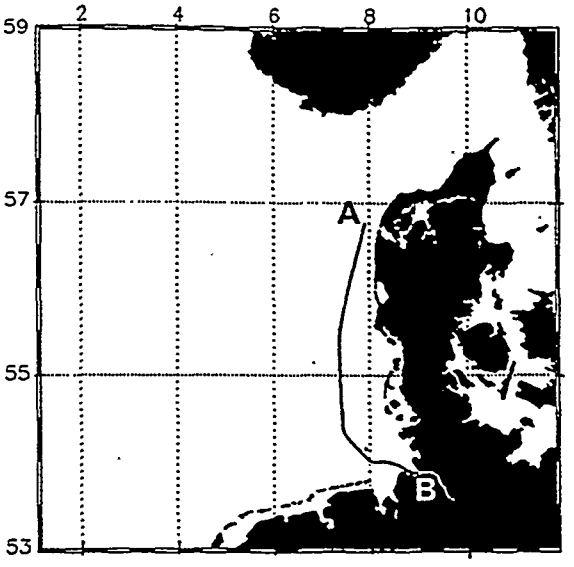

Fig. 4. Location of transect A–B during R/V *Valdivia* cruise no. 148-2 in September 11–14, 1994.

the compass platform of R/V *Valdivia* and the airflow split for the two systems.

A consistent set of calibration gases with known amounts of CO_2 ($\pm$0.3 ppmv) in "natural" air was used although different pressure requirements of the systems prohibited the use of the same cylinders. Nitrogen was used as a zero reference gas. The IFM system was calibrated on an hourly basis, the IOW system once during the experiment. During the 1-h calibration intervals (IFM) the NDIR analyzer remained remarkably stable with a drift in the order of +0.1 μmol/mol. The 24-h interval was correspondingly accompanied by a drift of the CO_2 analyzer of approx. +2.5 μmol/mol. The drift was not accompanied by an apparent drift of the IR cell temperature. This drift was removed linearly from the IOW data set. It was concluded that a calibration interval of 4–6 h would be a reasonable compromise.

The conversion of detector mV readings into CO_2 mole fractions based on internal algorithms (1) to (5) of the LI-COR analyzer and the calculation of partial pressure of CO_2 according to Eqs. (6) and (7) was performed identically for the to data sets comprising the following steps:

1. user calibration of the IR analyzer by setting the "zero point" as an offset z (calculated from measurement of a CO_2-free calibration gas) and

"span" as a factor s (calculated from measurement of a calibration gas with known CO_2 mixing ratio), applied internally to the raw detector readings mV:

$$mV^* = s \cdot mV + z$$

2. the mV^* readings are linearly corrected from the cell pressure p (kPa) during the measurement to a pressure of 1 atmosphere ($p_0 = 101.325$ kPa):

$$mV' = mV^* \cdot \frac{p_0}{p}$$

3. the CO_2 mole fraction xCO_2^{ws} (μmol/mol) from wet sample measurement with water vapor mole fraction xH_2O (mmol/mol) is calculated on the basis of the individual factory calibration polynomial and the pressure broadening effect of water vapor (for details see: McDermitt et al., 1993):

$$xCO_2^{ws} = \chi(xH_2O) \cdot (a_1 \cdot y + a_2 \cdot y^2 + a_3 \cdot y^3 + a_4 \cdot y^4 + a_5 \cdot y^5)$$

with

$$\chi(xH_2O) = 1 + (a_w - 1) \cdot \frac{xH_2O}{1000}$$

and

$a_w = 1.57$

and

$$y = \frac{mV'}{\chi(xH_2O)}$$

The "foreign gas broadening coefficient" a_w reflects the pressure broadening effectiveness of water vapor on the CO_2 measurement relative to nitrogen ($a_{N_2} = 1$). Its value has been determined experimentally (McDermitt et al., 1993). The mole fraction of water vapor xH_2O is provided by the simultaneous measurements in the H_2O channel;

4. the CO_2 mole fraction xCO_2^{ws} is linearly corrected for the deviation of cell temperature T (K) during measurement from factory calibration temperature T_0 (K):

$$xCO_2^{*,ws} = xCO_2^{ws} \cdot \frac{T}{T_0}$$

5. CO_2 mole fraction $xCO_2^{*,ws}$ is corrected (to dry air) for dilution of the gas phase by measured water vapor mole fraction xH_2O (mmol/mol).

$$xCO_2^{*,dry} = xCO_2^{*,ws} \cdot \left(\frac{1}{1 - \frac{xH_2O}{1000}} \right)$$

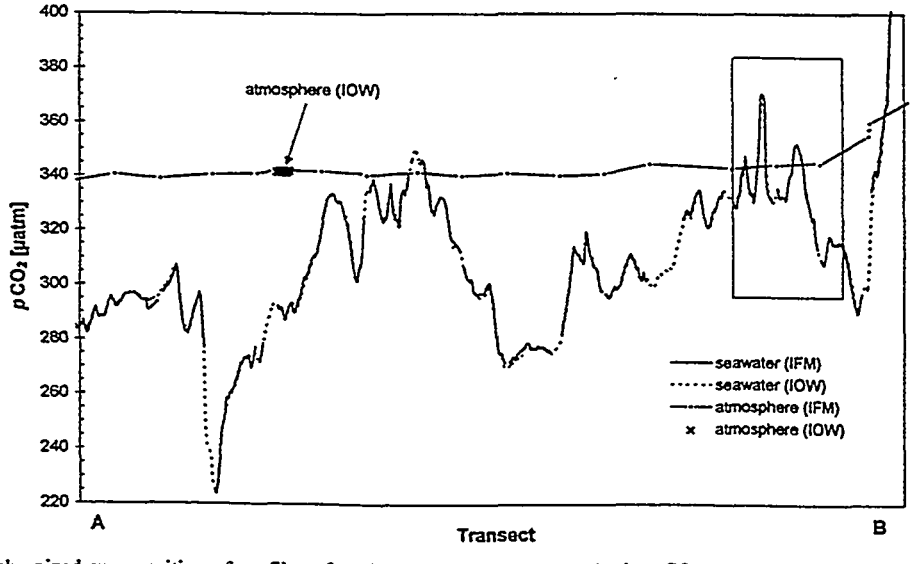

Fig. 5. Time-synchronized superposition of profiles of surface seawater and atmospheric pCO_2 on transect A–B as measured simultaneously by the IFM and IOW underway pCO_2 systems. The box indicates the location of the enlargement area in Fig. 7.

6. the pCO_2^* (μatm) at 100% humidity is calculated based on the ambient (= equilibrator) pressure p (atm) and saturation water vapor pressure w (atm).

$$pCO_2^* = xCO_2^{*,dry} \cdot (p - w)$$

The saturation water vapor pressure w (mbar) is calculated from the following equation:

$$w = 0.981 \cdot \exp\left(27.029 - 0.0098 \cdot T_{abs} - \frac{6163}{T_{abs}}\right)$$

where T_{abs} is the absolute temperature of the seawater. The seawater pCO_2 is calculated from the seawater temperature in the equilibrator while for the atmospheric pCO_2 the mixed layer temperature has to be used. If the temperature of the skin layer is known and differs from the mixed layer temperature the former should be used (Robertson and Watson, 1992). The present calculations are based on mixed layer temperatures;

7. the pCO_2^* is corrected for the temperature shift between in-situ temperature T_{is} and equilibrator temperature T_{eq} using an empirical equation (DOE, 1994) which was originally proposed by Takahashi et al. (1993):

$$pCO_2 = pCO_2^* \cdot \exp\left(0.0423(T_{is} - T_{eq})\right)$$

4. Results and discussion

The pCO_2 profiles generated by each of two systems during the 21-h experiment were compared based on the UTC time of the 1-min intervals. A time synchronized superposition of the profiles along transect A–B (for location refer to Fig. 4) is shown in Fig. 5. The solid line (IFM) is interrupted during the hourly calibration and measurement of atmospheric pCO_2 routine while the dashed line (IOW) gives a more or less continuous record. The pCO_2 values along transect A–B are plotted against time rather than geographical position in order to display the 1-min averages equidistantly. Otherwise they would have been stretched or distorted according to the changing speed of the vessel. In any other application plotting against a distance axis instead of a

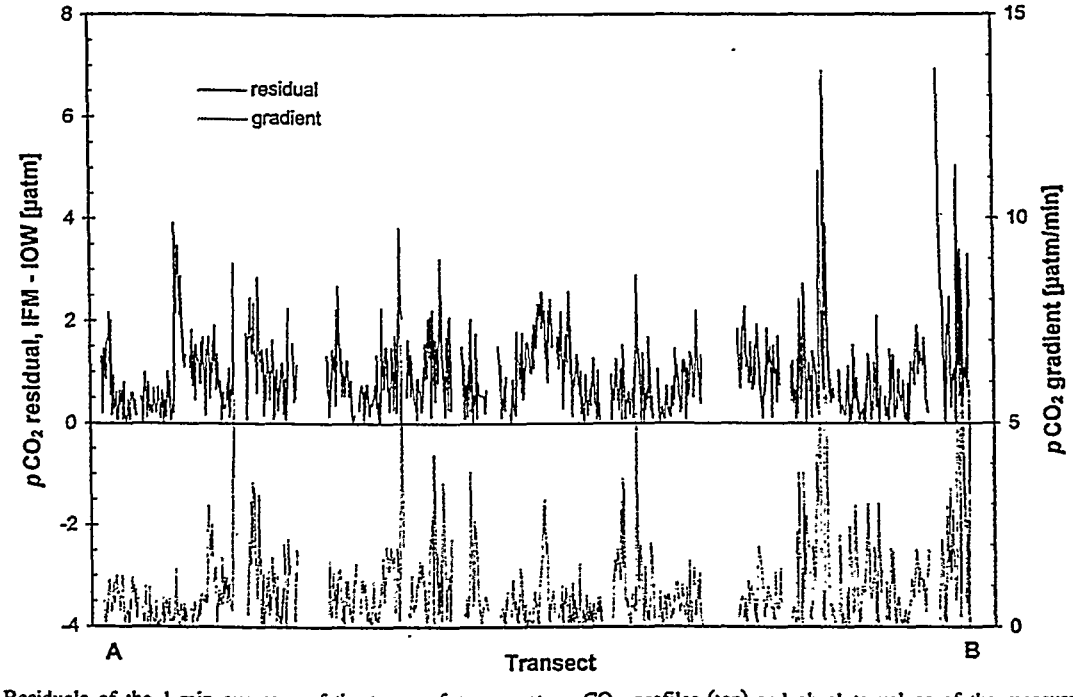

Fig. 6. Residuals of the 1-min averages of the two surface seawater pCO_2 profiles (top) and absolute values of the measured pCO_2 gradient as calculated from the IFM profile (bottom).

time axis would have been more useful but in this discussion we focus on a time synchronized comparison of the data points.

The striking feature of Fig. 5 is a marked qualitative and quantitative conformity of the profiles. Even though the North Sea offered a kind of worst case situation with a highly variable spatial pCO_2 distribution there is no significant difference in the profiles at this level. The 1-min averages of the whole experiment show a mean difference (IFM – IOW) of +0.15 μatm (IFM: 310.32 ± 29.59 μatm; IOW: 310.16 ± 29.79 μatm) which indicates that there is no systematic difference between the systems. The standard deviation of 1.2 μatm of the differences between the 1-min averages can in part be attributed to the differences occurring during high pCO_2 gradients. In most cases peaks in the differences coincide with peaks in the gradient (Fig. 6). The pCO_2 gradient as calculated from the IFM profile reached peak values as high as 10–14 μatm/min, which were followed by both systems. At a mean ship speed of appr. 8 knots a 1-min average corresponds to a distance of 250 m in which changes in the pCO_2 of up to 14 μatm were measured.

The atmospheric pCO_2 shows a steady level of approx. 342 μatm. Towards the inner German Bight the atmospheric pCO_2 level is raised by some 30 μatm which can be attributed to the influence of air masses contaminated by industrial areas of northern Germany. The single atmospheric measurement cycle carried out by the IOW system during the experiment is in full agreement with the atmospheric pCO_2 profile of the IFM system during that period (IFM: 342.24 ± 0.11 μatm; IOW: 341.84 ± 0.35 μatm).

Encouraged by the general agreement of these measurements we took a closer look at the "fine structure" of the profiles. For this purpose a 165-min interval was enlarged to reveal any further features (Fig. 7). The mean difference (IFM – IOW) of the 1-min averages in this enlargement interval is +0.5 μatm. Still the conformity of the profiles at this level is remarkable. The IFM system shows slightly higher maxima and lower minima than the IOW system with the slopes of the pCO_2 peaks being little steeper in the IFM profile (i.e., more positive in the uprise and more negative in the fall). This feature of the profiles can also be seen if the pCO_2 gradient as calculated from the IOW profile is plotted versus the pCO_2 gradient as derived from the IFM profile (Fig. 8). In a correlation analysis after Bartlett (1949) a straight line was fitted to these two variables which are subject to the same order of error. The estimated slope of 0.86 indicates that the IOW gradient is on the average by 14% lower than the IFM profile.

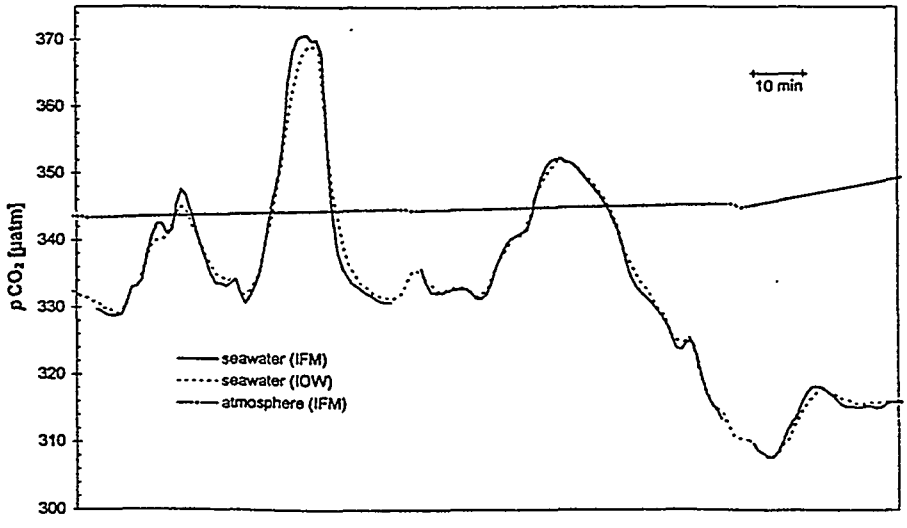

Fig. 7. Enlargement of a 165-min interval of the superimposed pCO_2 profiles. For location of the enlarged profile in the 21-h section refer to Fig. 5.

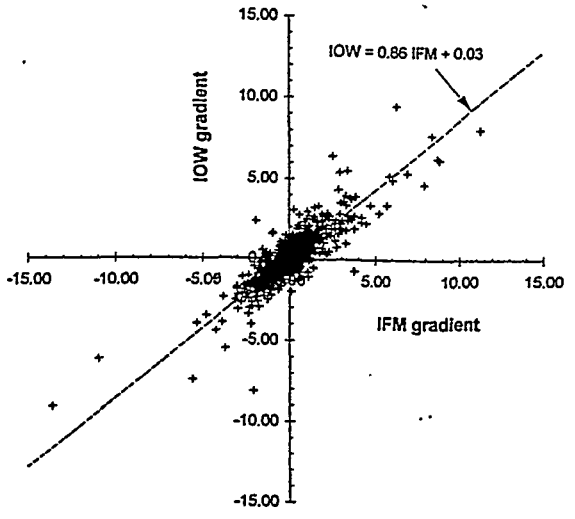

Fig. 8. Plot of the pCO_2 gradient as calculated from the IOW profile versus the pCO_2 gradient derived from the IFM profile. The straight line was fitted to the data after a correlation analysis after Bartlett (1949).

From these findings and the qualitative examination of the profiles in Fig. 7 a slightly different time constant can be inferred.

In order to estimate the time constants a step experiment was carried out with both pCO_2 systems. For this purpose two batches of water characterized by different pCO_2 and T were provided in plastic bags which allowed the water to be kept out of contact with a headspace throughout the whole experiment. Both batches were run subsequently through the systems. After a steady reading of the first batch was achieved the water supply was switched steplike to the second batch and the change of measured pCO_2 and T were followed in short time intervals (Fig. 9). Under the assumption that the re-equilibration can be described as a first-order process the following equation holds:

$$\frac{dp_a}{dt} = k(p_w - p_a)$$

in which p_a stands for the measured pCO_2 in the carrier gas stream, p_w for the pCO_2 of the water phase and k represents the rate constant of the process. Integration yields an exponential equation:

$$p_a = p_w + (p_a^0 - p_w) \cdot e^{-kt}$$

with p_a^0 and p_w being the pCO_2 values of the first and second batch, respectively, and p_a the measured pCO_2 at time t. A plot of $-\ln(p_a - p_w/p_a^0 - p_w)$ vs. t shows an almost perfect linear correlation thus justifying the a priori assumption of a first-order rate

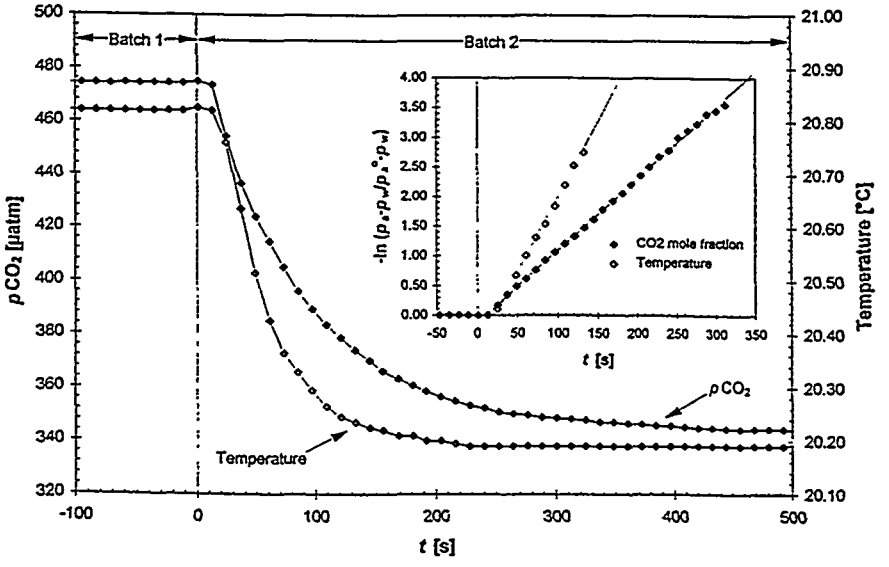

Fig. 9. Results from a step experiment with 12-s averages for pCO_2 and water temperature (IFM system). The step from batch 1 to batch 2 occurs at $t = 0$. The insert shows a plot of $-\ln(p_a - p_w/p_a^0 - p_w)$ vs. time axis of the experiment (analogous for temperature). From the slope of the regression lines the time constants were calculated.

law (Fig. 9). The time constant $(1/k)$ can be calculated from the slope. Assuming that the heat exchange between the water and the gas phase or the equilibrator walls is small, temperature changes in the equilibrator after the change between the batches give information about the water exchange rate in the equilibrator. From experimental runs with different step directions, step magnitudes and water flow rates the following time constants for pCO_2 were evaluated: IFM system, 75 ± 6 s (42 s); IOW system, 46 ± 1 s (22 s). The numbers in parentheses give the corresponding time constants for temperature. While the time constants for pCO_2 can be regarded as overall time constants the time constants for temperature represent the physical mixing in the equilibration cell.

The results underline the observation that both systems are characterized by a fast response to pCO_2 changes. However, the slight differences between the profiles discussed above cannot be explained by the experimental time constants. One reason for this discrepancy could be the fact that seawater flow rates of the IOW system were not monitored at sea. As changing flow rates affect the time constants these may have been different at sea from the experimentally measured time constants. It should also be mentioned that as the experiment was not designed for such detailed examination the interpretability of such miniature differences is clearly limited. For example the 1-min averages were not taken fully synchronized throughout the experiment, so that they are out of phase at between 0 and 30 s. We would like to emphasize that the observed differences in the "fine structure" of the profiles are negligible with respect to the scales of the ΔpCO_2 concept.

5. Conclusions

The findings reported in this paper clearly demonstrate that an excellent at-sea agreement of data from different pCO_2 systems can be achieved. Both new systems have shown their capability of a fast response to pCO_2 changes. However, the sharing of facilities like the water supply system, in-situ temperature and pressure data and calibration gases and the identical mathematical treatment of the data have excluded possible sources of errors. As temperature and pressure measurements can be done with the necessary accuracy rather conveniently and as calibration gases can be prepared carefully enough the possible errors contributed by this can be minimized. The conclusions of this experiment are certainly somewhat restricted by the fact that two system of rather similar design were compared. The results may therefore be regarded as a first check at-sea under ideal circumstances. Encouraged by the reported excellent agreement a next step should be a more general at sea intercomparison of underway pCO_2 systems which includes systems of very different design.

Acknowledgements

We thank the captain and crew of R/V *Valdivia* and the chief scientist of cruise no. 148-2, C. Osterroht from IFM, for the flexibility they showed when this experiment was incorporated in the cruise plan as a late proposal. We also would like to express our special thanks to Catherine Goyet who with good ideas and valuable discussions contributed to the development of the Kiel system. This work was supported by the German Ministry of Research and Technology under research grants BMFT 03F0092A and BMFT 03F0108F.

References

Bartlett, M.S., 1949. Fitting a straight line when both variables are subject to error. Biometrics, 5: 207–212.

Copin-Montegut, C., 1985. A method for the continuous determination of the partial pressure of carbon dioxide in the upper ocean. Mar. Chem. 17: 13–21.

Copin-Montegut, C., 1988. A new formula for the effect of temperature on the partial pressure of CO_2 in seawater. Mar. Chem., 25: 29–37.

Copin-Montegut, C., 1989. A new formula for the effect of temperature on the partial pressure of CO_2 in seawater (corrigendum). Mar. Chem., 27: 143–144.

DOE, 1994. A.G. Dickson and C. Goyet (Editors), Handbook of Methods for the Analysis of the Various Parameters of the Carbon Dioxide System in Sea Water, Version 2. ORNL/CDIAC-74.

Gordon, L.I. and Jones, L.B., 1973. The effect of temperature on carbon dioxide partial pressure in seawater. Mar. Chem., 1: 317–322.

Goyet, C. and Peltzer, E., 1994. Comparison of the August–Sep-

tember 1991 and 1979 surface partial pressure of CO_2 distribution in the Equatorial Pacific Ocean near 150°W. Mar. Chem., 45: 257–266.

Goyet, C., Beauverger, C., Brunet, C. and Poisson, A., 1991. Distribution of carbon dioxide partial pressure in surface waters of the Southwest Indian Ocean. Tellus, 43B: 1–11.

Goyet, C., Millero, F.J., Poisson, A. and Shafer, D.K., 1993. Temperature dependence of CO_2 fugacity in seawater. Mar. Chem., 44: 205–219.

Houghton, J.T., Jenkins, G.T. and Ephraums, J.J., 1990. Climate Change — The IPCC Scientific Assessment. Cambridge Univ. Press, Cambridge.

Inoue, H., Sugimura, Y. and Fushimi, K., 1987. pCO_2 and $\delta^{13}C$ in the air and surface sea water in the western North Pacific. Tellus, 39B: 228–242.

Keeling, C.D., Rakestraw, N.W. and Waterman., L.S., 1965. Carbon dioxide in surface waters of the Pacific ocean. 1. Measurements of the distribution. J. Geophys. Res., 70: 6087–6097.

Keeling, C.D., Whorf, T.P., Wahlen, M. and van der Plicht, J., 1995. Interannual extremes in the rate of rise of atmospheric carbon dioxide since 1980. Nature, 375: 666–670.

Kelley Jr., J.J., 1970. Carbon dioxide in the surface waters of the North Atlantic Ocean and the Barents and Kara Seas. Limnol. Oceanogr., 15: 80–97.

Kimoto, T. and Harashima, A., 1993. High resolution time/space monitoring of the surface seawater CO_2 partial pressure by ship-of-opportunity. Paper presented at the 4th Int. CO_2 Conf., Carqueiranne, September 14–19.

Liss, P.S., 1983. Gas transfer: experiments and geochemical implications. In: P.S. Liss and W.G.N. Slinn (Editors), Air–Sea Exchange of Gases and Particles. Reidel, Dordrecht, pp. 241–298.

Liss, P.S. and Merlivat, L., 1986. Air–sea exchange rates: introduction and synthesis. In: P. Buat-M-nard (Editor), The Role of Air–Sea Exchange in Geochemical Cycling. Reidel, Dordrecht, pp. 113–127.

McDermitt, D.K., Welles, J.M. and Eckles, R.D., 1993. Effects of temperature, pressure and water vapor on gas phase infrared absorption by CO_2. Poster and manuscript presented at the AGU Fall Meeting, San Francisco, December 6–10.

Ohtaki, E., Yamashita, E. and Fujiwara, F., 1993. Carbon dioxide in surface sea waters of the Seto Inland Sea. Jpn. J. Oceanogr., 49: 295–303.

Poisson, A., Metzl, N., Brunet, C., Schauer, B., Bres, B., Ruiz-Pino, D. and Louanchi, F., 1993. Variability of sources and sinks of CO_2 in the Western Indian and Southern Oceans during the year 1991. J. Geophys. Res., 98(C12): 22,759–22,722, 22,778.

Robertson, J.E. and Watson, A.J., 1992. Thermal skin effect of the surface ocean and its implications for CO_2 uptake. Nature, 358: 738–740.

Robertson, J.E., Watson, A.J., Langdon, C., Ling, R.D. and Wood, J.W., 1993. Diurnal variations in surface pCO_2 and O_2 at 60°N, 20°W in the North Atlantic. Deep-Sea Res., 40: 409–422.

Schneider, B., Kremling, K. and Duinker, J.C., 1992. CO_2 partial pressure in Northeast Atlantic and adjacent shelf waters: Processes and seasonal variability. J. Mar. Syst., 3: 453–463.

Takahashi, T., 1961. Carbon dioxide in the atmosphere and in Atlantic Ocean water. J. Geophys. Res., 66: 477–494.

Takahashi, T., Olafsson, J., Goddard, J.G., Chipman, D.W. and Sutherland, S.C., 1993. Seasonal variation of CO_2 and nutrient salts in the high latitude oceans: a comparative study. Global Biogeochem. Cycles, 7: 843–848.

Tans, P.P., Fung, I.Y. and Takahashi, T., 1990. Observational constraints on the global atmospheric CO_2 budget. Science, 247: 1431–1438.

Wallace, D.W.R., 1995. Monitoring global ocean carbon inventories. Ocean Observing System Development Panal, Texas A&M Univ., College Station, TX, 54 pp.

Wanninkhof, R., 1992. Relationship between wind speed and gas exchange over the ocean. J. Geophys. Res., 97: 7373–7382.

Watson, A.J., Nightingale, P.D. and Cooper, D.J., 1995. Modelling atmosphere–ocean CO_2 transfer. Philos. Trans. R. Soc. London B, 348: 125–132.

Weiss, R.F., 1974. Carbon dioxide in water and seawater: the solubility of a non-ideal gas. Mar. Chem., 2: 203–215.

Weiss, R.F., 1981. Determinations of CO_2 and methane by dual catalyst flame ionization chromatography and nitrous oxide by electron capture chromatography. J. Chromatogr. Sci., 19: 611–616.

Weiss, R.F., Jahnke, R.A. and Keeling, C.D., 1982. Seasonal effects of temperature and salinity on the partial pressure of CO_2 in seawater. Nature, 300: 511–513.

Journal of Oceanography
Vol. 49, pp. 295 to 303. 1993

Carbon Dioxide in Surface Seawaters of the Seto Inland Sea, Japan

EIJI OHTAKI[1], EIJI YAMASHITA[2] and FUKUICHI FUJIWARA[3]

[1]*College of Liberal Arts and Sciences, Okayama University, Okayama 700, Japan*
[2]*Environmental Resources Research Center, Okayama University of Science, Okayama 700, Japan*
[3]*Department of Public Health, City of Okayama, Okayama 700, Japan*

(Received 6 May 1992; in revised form 31 October 1992; accepted 5 November 1992)

Observations were made of time variations of carbon dioxide in seawater, pCO_2, and in the atmosphere, PCO_2, in the Seto Inland Sea of Japan. The pCO_2 data showed well defined diurnal variation; high values at nighttime and low values during daylight hours. The pCO_2 correlated negatively with dissolved oxygen. These results denote that the diurnal variation of pCO_2 is associated with effects of photoplankton's activity in seawater. The pCO_2 measured in the Seto Inland Sea showed higher values than the PCO_2 during June to November, denoting transport of carbon dioxide from the sea surface to the atmosphere, and lower values during December to May, denoting transport of carbon dioxide from the atmosphere to the sea surface. The exchange rates of carbon dioxide were calculated using working formula given by Andrié *et al.* (1986). The results showed that the Seto Inland Sea gained carbon dioxide of 1.0 m-mol m^{-2} d^{-1} from the atmosphere in March and lost 1.7 m-mol m^{-2} d^{-1} to the atmosphere in August.

1. Introduction

The exchange of carbon dioxide between the atmosphere and the sea is of major importance to our understanding of the climatic consequences of anthropogenic carbon dioxide. The exchange rate of carbon dioxide depends upon the concentration difference of carbon dioxide between seawater and atmosphere, gas transfer velocity and the solubility of carbon dioxide in seawater. A key factor on the carbon dioxide exchange, however, is the accurate determination of carbon dioxide concentration dissolved in seawater.

The equilibrator technique has been used to measure the pCO_2 by many researchers employing a non-dispersive infrared gas analyzer, NDIR (e.g., Fushimi, 1987; Gordon *et al.*, 1971; Oudot and Andrié, 1989; Takahashi, 1961; Weiss *et al.*, 1982; Wong and Chan, 1991). We measured the pCO_2 in the Seto Inland Sea of Japan by the equilibrator technique using the NDIR (Shimazu Co., URA-106). A minor modification was done in the present instrument. The carrier gas line for the NDIR was opened to the atmosphere to maintain the gas line as barometric pressure. This technique makes free from the correction for addition or extraction of the carbon dioxide from sample seawater due to circulating air.

The experiments were carried out using facility of Observatory for Environmental Research of Okayama University (34.27°N, 133.54°E). Seawater was sampled at 0.5 m below the surface. Seawater temperature, Ts, salinity, S, and pH value were measured every sample seawater. The carbon dioxide concentration in the atmosphere, PCO_2, has been measured at the Observatory together with wind speed, temperature and humidity at 10 m height above the sea surface.

The present paper describes the characteristics of diurnal and seasonal variations of pCO_2 and PCO_2 measured. Exchange rates of carbon dioxide between seawater and atmosphere are estimated.

2. Measuring Procedure of pCO_2

Figure 1 shows a block diagram of measuring instrument which consists of a plastic chamber, NDIR, a water bath and a recorder. The plastic chamber had a cross section of 3 cm^2 and 15 cm tall. The plastic chamber was immersed into a water bath whose temperature was controlled by a regulator within an accuracy of 0.1°C to that of sample seawater. The sample bottle of seawater was also immersed into the water bath to keep its temperature under field conditions.

The NDIR was used in a differential mode: A known concentration of carbon dioxide standard gas was continuously passed through a reference cell of the NDIR at a rate of 5 ml per min. Other carbon dioxide standard gases were used as the carrier gas. The flow rate of the carrier gas was regulated by a mass flow meter to be 100 ml per min. The carrier gas line was opened to the atmosphere to maintain the gas line as barometric pressure. The carrier gas was, at first, passed through the gas line with diffuser (illustrated by 1 in the figure). Then, the gas flow was changed by a three way valve to another gas line (illustrated by 2 in the figure) in order to purge the carrier gas into dead spaces in the equilibrating chamber. Water sample of 18 ml was pumped up into the chamber.

The output signal of the NDIR appears to be constant when the carrier gas is purged into the equilibrating chamber. This stage is specified as "purging" in Fig. 2. Again, the carrier gas line was changed to the diffuser circuit. Small bubbles of carrier gas interact with water during drifting about 6 cm in sample seawater. This stage is specified as "bubbling" in Fig. 2. The carrier gas was then passed through a drying column with $Mg(ClO_4)_2$ and led to a measuring cell of

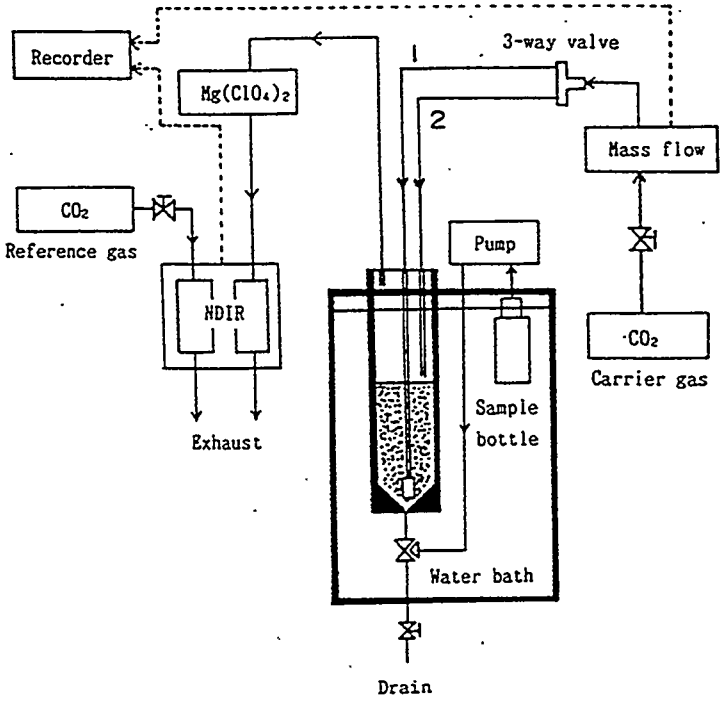

Fig. 1. Block diagram of measuring instrument for carbon dioxide concentration in seawater.

the NDIR.

If the carbon dioxide concentration of carrier gas equals to that in seawater, dissolved carbon dioxide and various carbonate species do not change their equilibrium condition during bubbling procedure. The output signal of the NDIR shows constant corresponding to the carrier gas level under such equilibrium conditions. In general, we can use standard gases with discrete concentration. Thus, the output signal of the NDIR becomes to have a positive or a negative peak. The peak height (cf. CPH in Fig. 2) is associated with the concentration difference between carrier gas and seawater. The positive peak means that the carbon dioxide is extracted from seawater, and the negative peak means that the carbon dioxide in carrier gas is added to seawater when small bubbles of carrier gas are passing through sample seawater. In order to find out the carbon dioxide concentration of carrier gas, which the peak height of the NDIR is zero, we repeated the purging and bubbling procedures five times using different concentrations of carrier gas, and measured values of CPH. The sample seawater of 18 ml in equilibrating chamber was changed every trial. Figure 3 shows the relationship between CPH and carbon dioxide concentration of carrier gas. The carbon dioxide concentration of seawater was determined to be 333 ppm from the concentration of carrier gas which the CPH was zero. To check the precision of present technique, eight trials of concentration measurements of carbon dioxide were carried out using seawater sampled. Their mean value was 578 ppm with standard deviation of 1.6 ppm.

Ten compressed gas tanks, five containing CO_2/N_2 mixtures from 300 to 700 ppm and five CO_2/air mixtures from 300 to 700 ppm, were used to check the precision of the carrier gas error of the instrument. The NDIR analyzer indicated carbon dioxide concentration in the CO_2/N_2 mixtures 0.5 ppm below the value in the CO_2/air mixtures. The pCO_2 values in seawater were compared for seven seawater samples using carrier gases containing CO_2/N_2 mixtures and CO_2/air mixtures. It is noted that the pCO_2 determined by CO_2/N_2 mixtures was larger by 1.1 ppm than that determined by CO_2/air mixtures. Here, we can conclude that the significant error of greater than 1 ppm in pCO_2 is not considered from the pressure broadening effects due to different gas mixtures of CO_2/N_2 and CO_2/air.

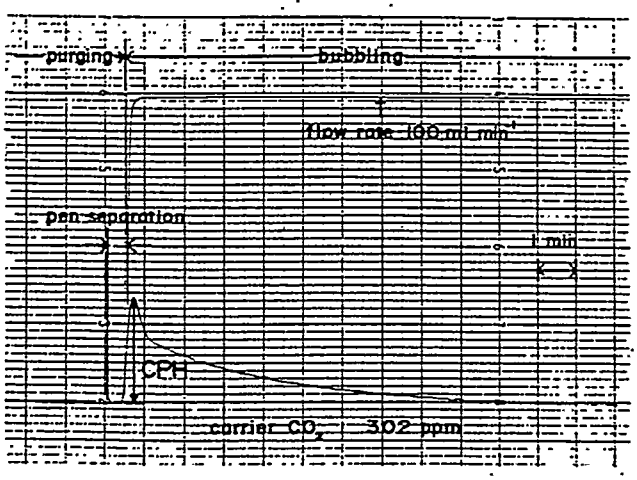

Fig. 2. Output signal of non-dispersive gas analyzer (NDIR). Positive peak denotes that the carbon dioxide is extracted from sample seawater.

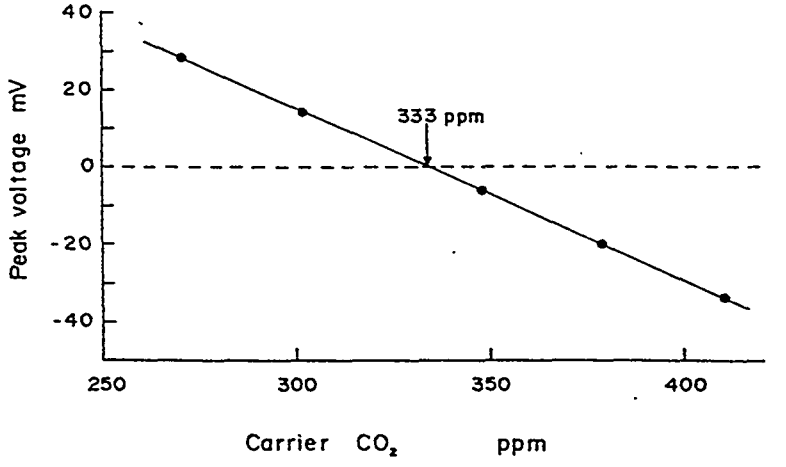

Fig. 3. Relationship between peak voltage (CPH in Fig. 2) of NDIR and carbon dioxide concentration of carrier gas. Carbon dioxide concentration in seawater is assumed to the carrier gas concentration where CPH is zero.

3. Results

3.1 Diurnal variation of pCO_2

Figure 4 shows a time variation of pCO_2 measured on August 27 to 28, 1991. The carbon dioxide concentration in the atmosphere, PCO_2, seawater temperature, *Ts*, and dissolved oxygen, *DO*, are together plotted in the figure. The mean value of pCO_2 measured was 671 ppm. It is apparent that the pCO_2 shows well defined diurnal variation characterized by the low values during daylight hours, and high values in the nighttime. The amplitude was about 85 ppm. To eliminate the temperature effect on pCO_2, we apply the temperature coefficient of 4%(°C) $^{-1}$ to the pCO_2 measured (e.g., Oudot and Andrié, 1989). The pCO_2 data corrected show that the biological factors outweigh physicochemical effects associated with temperature adjustment in determining the diurnal cycle. It is also noted that the pCO_2 data correlate negatively with the *DO* data. These results mean that the diurnal variation of pCO_2 is associated with the photosynthetic activity by photoplanktons in seawater. Figure 5 shows diurnal variations of pCO_2 measured in early spring of March 2 to 3, 1991. The amplitude of diurnal change in pCO_2 was reduced to 8.5 ppm under periods of low seawater temperature. The seawater temperature was 8 to 10°C.

Figure 6 shows the relationship between amplitude of diurnal variation of pCO_2 and seawater temperature, *Ts*. The regression curve plotted in the figure shows that the amplitude of pCO_2 varies as Ts^2. This denotes that the photosynthetic effect on pCO_2 can be represented by the square law of seawater temperature.

The examples of diurnal change of pCO_2 in surface seawater reported in the literature have been scarce. Recently, Oudot and Andrié (1989) showed that a decrease in PCO_2 was occurred most of the time between morning and evening in eastern tropical Atlantic Ocean. They discussed three factors that alter pCO_2 in surface seawater; temperature, gas exchange across the air-sea interface and biological consumption of carbon dioxide through photosynthesis. They concluded that the decrease in pCO_2 during daylight hours can be resulted from the photosynthetic fixation

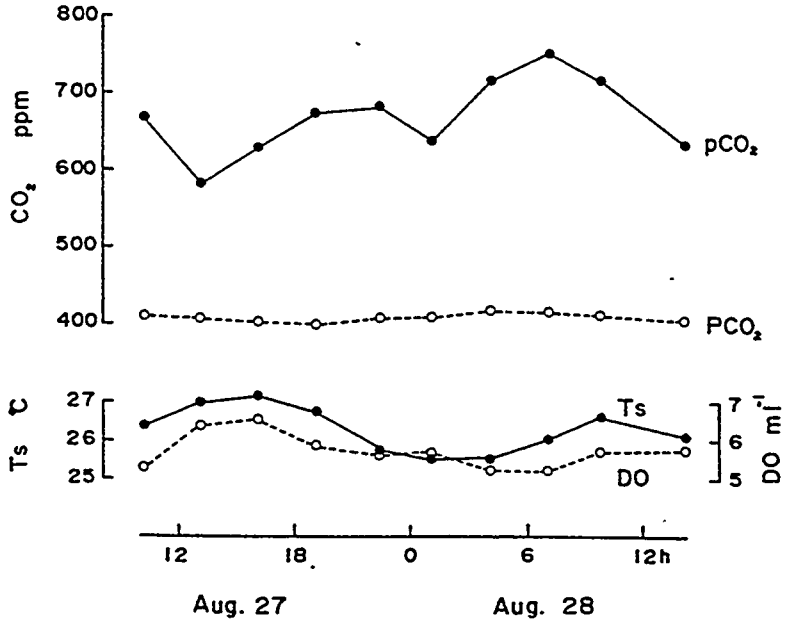

Fig. 4. Example of diurnal variation of pCO_2 measured on August 27/28, 1991. pCO_2 in atmosphere, seawater temperature, *Ts*, and dissolved oxygen, *DO*, are plotted for reference.

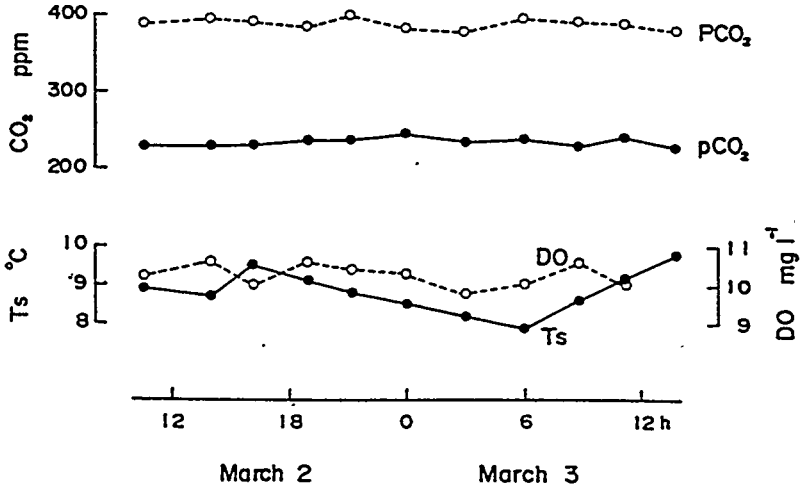

Fig. 5. Example of diurnal variation of pCO_2 measured on March 2/3, 1991. PCO_2 in atmosphere, seawater temperature, *Ts*, and dissolved oxygen, *DO*, are plotted for reference.

of carbon dioxide. Takahashi (1961) also demonstrated in the pioneering work that the pCO_2 of 330 ppm can be reduced to 210 ppm by the biological activities at the most productive areas of phytoplanktons. These results support that the diurnal change in pCO_2 measured in the present study are associated with the photosynthetic activity by photoplanktons in seawater.

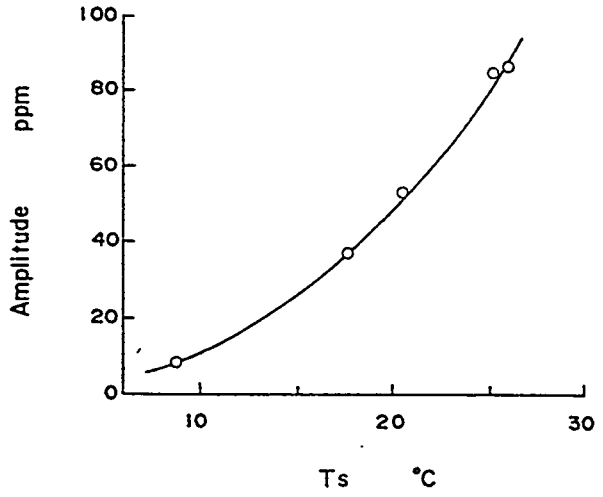

Fig. 6. Amplitude of diurnal variation of pCO_2 as a function of seawater temperature, *Ts*.

3.2 Seasonal variation of pCO_2

The seasonal variation of pCO_2 and PCO_2 are plotted in Fig. 7. The seasonal cycle of pCO_2 had an amplitude of 218 ppm with high values in summer and low values in winter. Data for checking the seasonal changes of pCO_2 are not available around the measuring site in the Seto Inland Sea of Japan. For data of open oceans, Weiss *et al.* (1982) showed well defined seasonal variations of surface water fugacity of carbon dioxide. Their data were measured in the tropical areas of the north and south Pacific Oceans. The amplitude of seasonal variations was about 10 μatm, with both hemispheres showing summer maxima. Wong and Chan (1991) also showed that the average amplitude of the oceanic pCO_2 cycle was about 28 μatm using data obtained from Ocean Station P. It is noted that the amplitude of seasonal variation of our pCO_2 data showed ten times larger than those for open oceans. This result means that the pCO_2 obtained in the Seto Inland Sea is inebitably local in character.

Comparing with the PCO_2, the pCO_2 in seawater is larger than that of the atmosphere during periods from June to November, transporting carbon dioxide from the sea surface to the atmosphere and smaller during periods from December to May through January, transporting carbon dioxide from the atmosphere to the seawater. It is noted that the PCO_2 showed high values in summer season compared with those in winter season. This seasonal variation differs from that of monitoring stations sited in northern phemisphere (e.g. Komhyr *et al.*, 1985). The result can be interpreted as follows: The measuring site is located near the coast of the Seto Inland Sea. The atmospheric surface layer is characterized by stable stratification even in daytime hours during April to October. Thus, the vertical mixing of the air mass is suppressed. The carbon dioxide released from nearby factories and dwellings accumulates in the atmospheric surface layer and results in high concentrations in summer months (Ohtaki *et al.*, 1984).

3.3 Carbon dioxide exchange across air-sea interface

The net carbon dioxide flux, F, across the air-sea interface can be estimated from the gas exchange equation reported by Andrié *et al.* (1986):

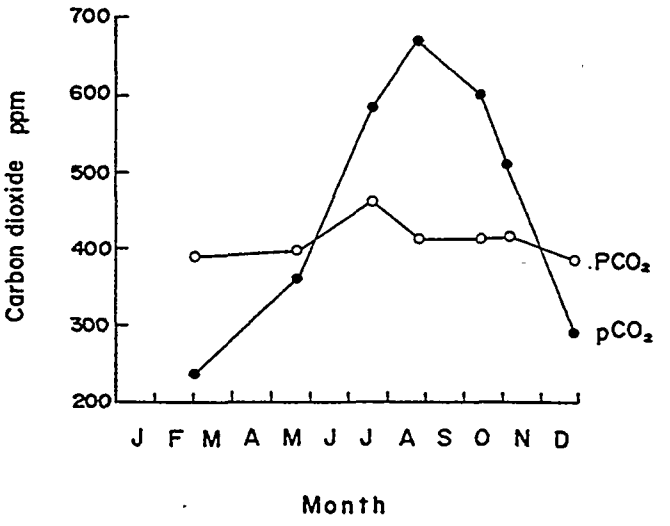

Fig. 7. Seasonal variation of carbon dioxide concentration in seawater, pCO_2, and in atmosphere, PCO_2.

$$F = 0.24\, K\alpha\Delta pCO_2$$

where K is the carbon dioxide transfer velocity and α is the carbon dioxide solubility in seawater. Using K expressed in cm h^{-1}, α expressed in mol $kg^{-1}atm^{-1}$, and $\Delta pCO_2 = pCO_2 - PCO_2$ expressed in μatm, the F is given in m-mol m^{-2} d^{-1}. The α presented by Weiss (1974) was used. The K was calculated using relationships proposed by Oudot and Andrié (1989). Though their K values are defined for temperature ranges from 20 to 30°C, we assume that the relationships can be extrapolated to the temperature ranges encountered in the present study. The calculated exchange rates in March therefore became rough estimates, because the average values of Ts were about 8°C in March.

The carbon dioxide exchange rates measured on August 27 to 28, 1991 are shown in Fig. 8. For reference, the wind speed, U, measured at 10 m height, partial pressure difference, ΔpCO_2, and transfer velocity, K, are plotted in the figure. It is noted that U had an appreciable effect on the values of K and thus F. For $U > 3.6$ m s^{-1}, the F increased to 8 m-mol m^{-2} d ^{1}, but for $U < 3.6$ m s^{-1}, the F reduced rapidly less than 1 m-mol m^{-2} d^{-1}. The daily average of carbon dioxide exchange rate was about 1.7 m-mol m^{-2} d^{-1} in the present case representing upward transport of carbon dioxide from the sea surface to the atmosphere. This is very close to those in Guinea Dome measured by Oudot and Andrié (1989), and in the tropical Atlantic Ocean during FOCAL cruises (Andrié *et al.*, 1986). These two examples of carbon dioxide exchange rates were taken from an important source zones of carbon dioxide for the atmosphere.

The example of carbon dioxide exchange rates measured on March 2 to 3, 1991 is plotted in Fig. 9. It is noted that F is negative, representing downward transport of carbon dioxide from the atmosphere to the sea surface. The daily average of carbon dioxide exchange rate was about −1.0 m-mol m^{-2} d^{-1}.

It is interested to see the annual cycle of carbon dioxide exchange rates at the Seto Inland Sea. Taking into account of the seasonal variation of pCO_2 and PCO_2 illustrated in Fig. 7, the carbon dioxide may be transported from the sea surface to the atmosphere during June to

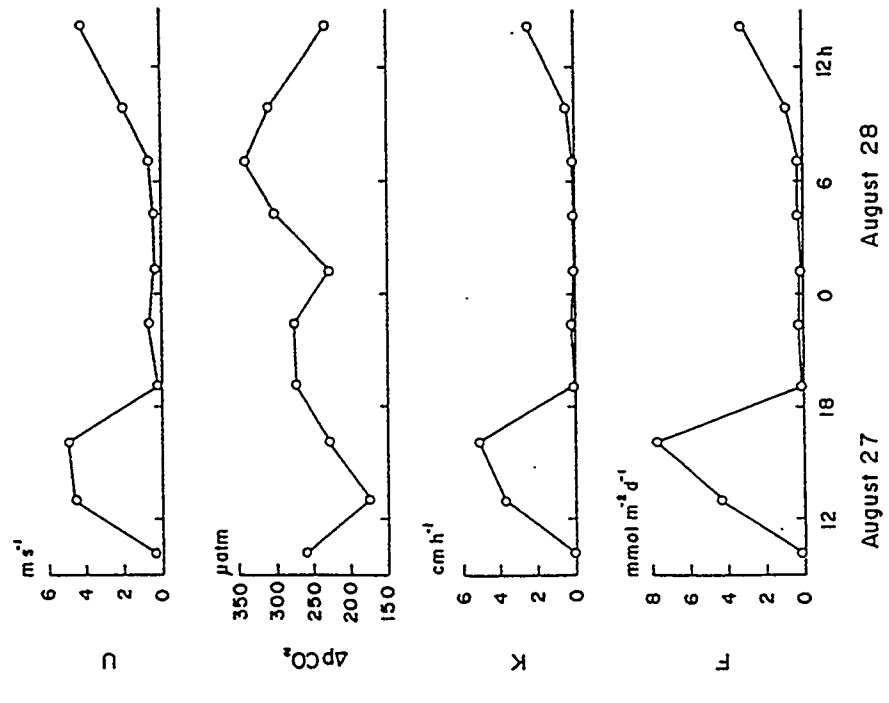

Fig. 8. Example of diurnal variation of carbon dioxide flux measured on August 27/28, 1991. Positive values represent upward transport of CO_2 from seawater to atmosphere. *F*: carbon dioxide flux, *U*: wind speed at 10 m height above sea surface, ΔpCO_2: $pCO_2 - PCO_2$, *K*: transfer velocity.

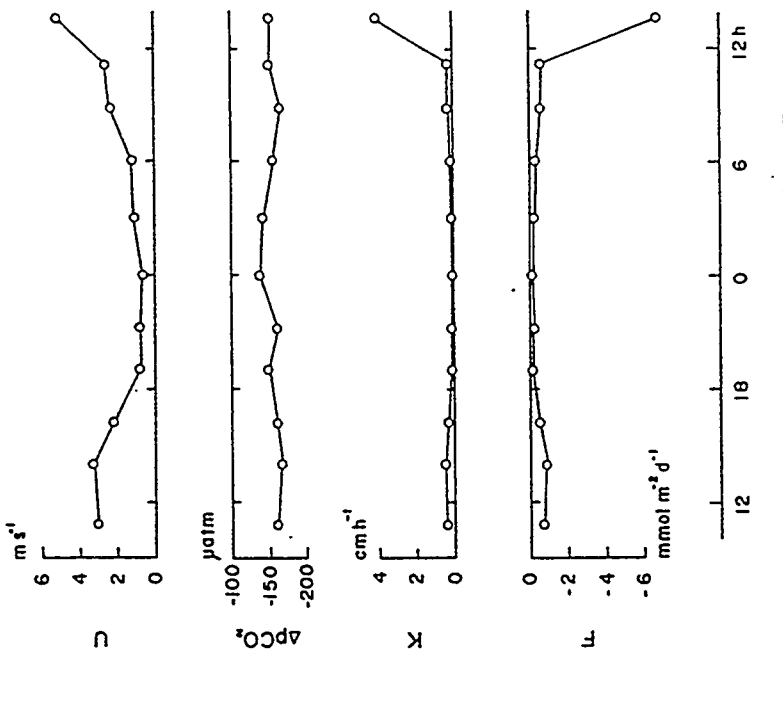

Fig. 9. Example of diurnal variation of carbon dioxide flux measured on March 2/3, 1991. Negative values represent downward transport of CO_2 from atmosphere to seawater. Symbols used are specified in Fig. 8.

November, and transported from the atmosphere to the sea surface during December to May. Here, we would like to emphasize that more attention should be noted to the transfer velocity of carbon dioxide between atmosphere and seawater. The accuracy of F estimated depends on the transfer velocity, K. In order to examine whether the parameter K proposed by Oudot and Andrié (1989) can be applied to our data obtained in the Seto Inland Sea or not, similar experiments have to be duplicated with the eddy correlation technique (e.g., Ohtaki *et al.*, 1989).

4. Conclusions

The pCO_2 in seawater was measured in the Seto Inland Sea of Japan. The results obtained are inevitaly local in character. However, the pCO_2 data demonstrate characteristic diurnal and seasonal variations. The high value of 670 ppm occurred in August, and the low value of 235 ppm occurred in March.

The concentration difference of carbon dioxide between seawater and atmosphere showed positive from June to November, and negative from December to May through January. Sample calculation showed that the carbon dioxide flux of 1.7 m-mol m^{-2} d^{-1} was transported from the sea surface to the atmosphere in August, and 1.0 m-mol m^{-2} d^{-1} was transported from the atmosphere to the sea surface in March.

Acknowledgements

This work was partly supported by the Scientific Research on Priority Areas (No. 03248211) of The Ministry of Education, Science and Culture.

References

Andrié, C., C. Oudot, C. Genthon and L. Merlivat (1986): CO_2 fluxes in the tropical Atlantic during FOCAL cruise. *J. Geophys. Res.*, **91**, 11741–11755.

Fushimi, K. (1987): Variation of carbon dioxide partial pressure in the western North Pacific surface water during the 1982/83 El Niño event. *Tellus*, **39B**, 214–227.

Gordon, L. I., P. K. Park, S. W. Hager and T. R. Parsons (1971): Carbon dioxide partial pressures in north Pacific surface waters—Time variations. *J. Oceanogr. Soc. Japan*, **27**, 81–90.

Komhyr, W. D., R. H. Gammon, T. B. Harris, L. S. Waterman, T. J. Conway, W. R. Taylor and K. W. Thoning (1985): Global atmospheric CO_2 distribution and variations from 1968–1982 NOAA/GMCC CO_2 flask sample data. *J. Geophys. Res.*, **90**, 5567–5596.

Ohtaki, E., T. Maitani and T. Seo (1984): Atmospheric carbon dioxide variations at coastal site, Shibukawa, in Seto Inland Sea, Japan. *Arch. Met. Geoph. Biocl. Ser. B*, **35**, 31–44.

Ohtaki, E., O. Tsukamoto, Y. Iwatani and Y. Mitsuta (1989): Measurements of the carbon dioxide flux over the ocean. *J. Met. Soc. Japan*, **67**, 541–554.

Oudot, C. and C. Andrié (1989): Short-term changes in the partial pressure of CO_2 in eastern tropical Atlantic surface seawater and in atmospheric CO_2 mole fraction. *Tellus*, **41B**, 537–553.

Takahashi, T. (1961): Carbon dioxide in the atmosphere and in Atlantic Ocean water. *J. Geophys. Res.*, **66**, 477–494.

Weiss, R. F. (1974): Carbon dioxide in water and seawater: The solubility of non-ideal gas. *Marine Chem.*, **2**, 203–215.

Weiss, R. F., R. A. Jahnke and C. D. Keeling (1982): Seasonal effects of temperature and salinity on the partial pressure of CO_2 in seawater. *Nature*, **300**, 511–513.

Wong, C. S. and Y. H. Chan (1991): Temporal variations in the partial pressure and flux of CO_2 at ocean station P in the subarctic Pacific Ocean. *Tellus*, **43B**, 206–223.

Limnol. Oceanogr., 42(8), 1997, 1774–1783

Accurate headspace analysis of fCO_2 in discrete water samples using batch equilibration

Craig Neill, Kenneth M. Johnson, Ernie Lewis, and Douglas W. R. Wallace[1]
Department of Applied Science, Brookhaven National Laboratory, P.O. Box 5000, Upton, New York 11973-5000

Abstract

A high-accuracy, batch-equilibration, static-headspace technique for the determination of the fugacity of CO_2 (fCO_2) in discrete water samples is described. The technique was designed for monitoring small changes of CO_2 in the ocean and has accuracy and precision (<1% for water samples) comparable to that of the best techniques available. The method uses several novel approaches to maximize accuracy, requires only a small water sample (60 ml), and is very rapid (~2 min per analysis). Precision of the calculated total alkalinity, based on the measured fCO_2 and C_T, is comparable to or better than is generally attained using potentiometric titration. Compared with C_T and total alkalinity measurements, the small sample volume and rapid analysis time makes it practical to perform analysis of multiple replicates in order to improve confidence in the result. The method is readily applicable to experimental studies such as incubations as well as to time-series measurements of in situ biological metabolism. Because the analysis employs gas chromatography, the technique can be adapted to measure simultaneously a suite of gases dissolved in seawater.

To characterize the speciation of inorganic carbon in seawater it is necessary to measure at least two of four measurable parameters: C_T (total dissolved inorganic carbon concentration), pH, fCO_2 (fugacity of CO_2), and total alkalinity. Established methods for the measurement of pH (*see* Dickson 1993 for review), total alkalinity (e.g. Millero et al. 1993), and C_T (e.g. Johnson et al. 1985, 1993; Robinson and Williams 1991) are well described in the literature. Note that fCO_2 at 1 atm total pressure is 0.3–0.4% lower than its partial pressure (pCO_2) because of nonideal behavior.

High-accuracy measurements of inorganic carbon in the ocean can potentially be used to determine directly the oceanic uptake of excess, or anthropogenic, CO_2 from the atmosphere and are powerful constraints for models of this uptake process (e.g. Gruber et al. 1996; Wallace 1995). Such evaluations of large-scale distributions and long-term changes of CO_2 concentration in the oceans must be based upon data collected by different measurement groups and cruises and is therefore usually limited by accuracy rather than analytical precision.

Currently, the most accurate measurement is that of C_T that can be measured routinely (at sea) to an accuracy of 0.1% using coulometric titration (Johnson et al. 1993) and for which certified standards (UNESCO 1991) are now well accepted. Total alkalinity is one of the more commonly measured parameters with a potential measurement accuracy of 0.2% (Millero et al. 1993); however, certified standards for this parameter are only now becoming available (A. Dickson pers. comm.). Both measurements are relatively slow at ~15–30 min per analysis. A potential advantage of measuring fCO_2 is that calibration can be tied to the analysis of gas-phase standards that can be prepared gravimetrically to high accuracy, maintained for long periods and are readily intercompared with certified standards that have been developed for atmospheric CO_2 monitoring.

fCO_2 can also be a sensitive measure of the small temporal changes of CO_2 concentration caused by biological metabolism in the oceans. Chipman et al. (1993) noted that fCO_2 was a particularly sensitive measure of the small diurnal variations associated with organic carbon production and respiration in seawater because the associated percentage change in fCO_2 is an order of magnitude greater than the corresponding percentage change in C_T.

There have been relatively few descriptions of methods for the determination of the fCO_2 of discrete water samples. Notable exceptions include the gas chromatography (GC)-based method described by Chipman et al. (1993) and an infrared detection variant of this described by Wanninkhof and Thoning (1993) and Chen et al. (1995). Whereas both methods give good precision and accuracy, they require relatively large (>0.5 liter) water samples and long (~10–20 min) analysis times. Both factors can become a problem on oceanographic research cruises where the number of samples that can be analyzed is usually a limiting factor, and where the available volume of water from a particular Niskin bottle may be restricted.

Here we present an alternative method of measuring the fCO_2 of small samples (60 ml) with an average analysis time of ~2 min per sample. The approach involves off-line equilibration of the sample and an introduced headspace within a small serum bottle, followed by analysis of the mole fraction of CO_2 in the equilibrated headspace by GC with flame-ionization detection (GC-FID). The method is derived from a method initially developed for methane analysis (Johnson

[1] Corresponding author.

Acknowledgments

The authors thank Dave Chipman, Rik Wanninkhof, and Andrew Dickson for advice and help throughout the development of this technique. Dave Chipman and co-workers kindly offered to intercalibrate our fCO_2 standards with primary standards maintained at Lamont-Doherty Earth Observatory. Much of the early experience with this technique was thanks to the efforts of Bob Ramirez and Rick Wilke. This research was supported by the U.S. Department of Energy under Contract No. DE-AC02-76CH00016. Measurements aboard the Polar Sea were supported by the National Science Foundation, Office of Polar Programs (grant OPP 91-13818).

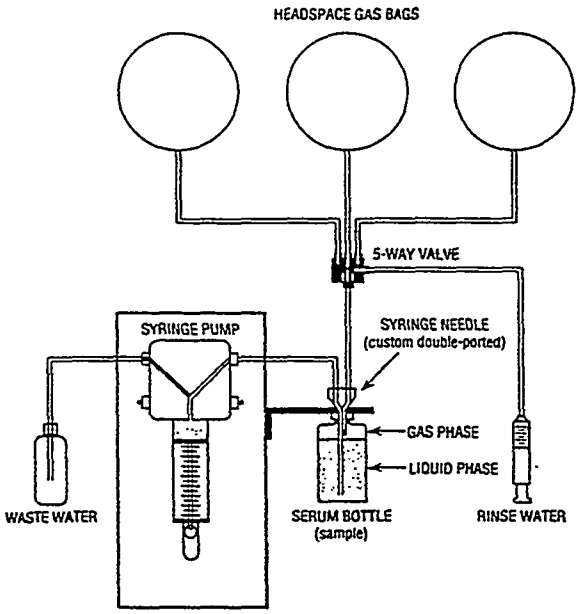

Fig. 1. Schematic representation of the headspace-introduction system. The syringe needle is concentric with two ports. The outer tube has a gas port at the top of the needle. The inner tube has a liquid port at the base of the needle (*see text*).

et al. 1990). Because the method uses small serum bottles and GC, it is particularly well suited to experimental studies of metabolism, such as microbiological incubations, and could readily be extended to measure a wide suite of gases in addition to CO_2.

Materials and methods

Sampling and headspace introduction—Subsamples are collected in 60-ml serum bottles whose volume has been calibrated gravimetrically (Johnson et al. 1990). The bottles are filled using a piece of latex or tygon tubing, being careful to avoid bubbles and overflowing at least one full volume. The sampling tube is carefully withdrawn from the serum bottle while maintaining some flow in order to leave a meniscus of water at the neck of the bottle. The serum bottle is immediately sealed with a 20-mm Teflon-faced butyl rubber septa and aluminum crimp seal (Wheaton, part no. 224168). The sample must be sealed with no air bubbles inside in order that the initial water volume in the serum bottle agrees with the calibrated value. We evaluated several types of septa and determined that this type combined the best sealing qualities together with resistance to leakage after puncturing with a needle.

A headspace is then introduced as follows (*see Fig. 1*): The septum is pierced with a custom-designed concentric needle comprised of an (inner) long, side-port style needle that is used to remove water from the sample, and an (outer) short piece of needle tubing that is used to introduce headspace gas. When the needle is fully inserted into a serum bottle (Fig. 1), the "gas port" in the outer tubing is located just beneath the septum, such that when water is withdrawn through the long needle ("liquid port"), gas enters through the gas port to form the headspace. Typically 6.0 ml (±0.0005) of water is withdrawn, using a stepper motor-driven syringe (Kloehn, model 50100).

Three headspace gases with different CO_2-in-air mole fractions (usually 350×10^{-6}, 750×10^{-6}, and $1{,}500 \times 10^{-6}$) are stored in 5-liter gas bags (Calibrated Instruments) and connected to the gas port of the needle via a five-port selector valve (Fig. 1). Gas bags are used in order to ensure that the initial headspace is introduced into the serum bottles at atmospheric pressure, which is recorded. The selector valve is used to select a headspace gas with a fCO_2 that is close to that expected for the particular water sample being processed. This matching of the water sample and headspace fCO_2 minimizes the amount of CO_2 exchanged during the subsequent equilibration (*see below*). The fourth position on the selector valve is used to flush the valve and needle with distilled water, followed by air. This is performed regularly to prevent salt from accumulating in the tubing.

Equilibration—After all samples from a hydrographic cast have been collected and the headspaces introduced, the samples are equilibrated in a constant temperature bath that is controlled to within ±0.02°C. A plastic-lined polystyrene beverage cooler is used as the bath, with the bath water circulated directly through a constant temperature circulator (this requires a circulator with both pressure and suction pumps). The bath is mounted on a reciprocating shaker table. The serum bottles are placed in the bath on their sides and shaken along their long axis at a frequency that maximizes the motion of the headspace bubble (Johnson et al. 1990). The temperature of the bath is measured by a thermistor with NIST-traceable calibration to an accuracy of 0.005°C. After putting samples in the bath, the temperature stabilizes in <1 h. Samples are equilibrated on the shaker for 3–4 h prior to headspace analysis.

Headspace analysis—Following equilibration, sample analysis consists of (1) measuring the pressure of the headspace, (2) displacing some of the headspace into a gas sample loop, and (3) analysis of the contents the sample loop by GC. The shaker is left on throughout the analyses and samples are removed one at a time, using tongs to reduce thermal perturbations of the bath. The elapsed time between when a sample is removed from the bath and the gas sample loop is loaded is about 30 s. Care is taken to avoid agitation and temperature change of the samples following their removal from the bath.

The headspace pressure of the samples is measured with a quartz crystal pressure transducer (Paroscientific, model 216B, 0–45 PSIA) that is connected to a fixed, low-dead-volume side-port needle that is pointed downward. The dead volume of the transducer-needle assembly in use with our system was determined to be 290 μl, compared with a headspace volume of ~6 ml, and all headspace pressure data have been corrected accordingly. When making a pressure measurement, the sample is held by the lower half of the

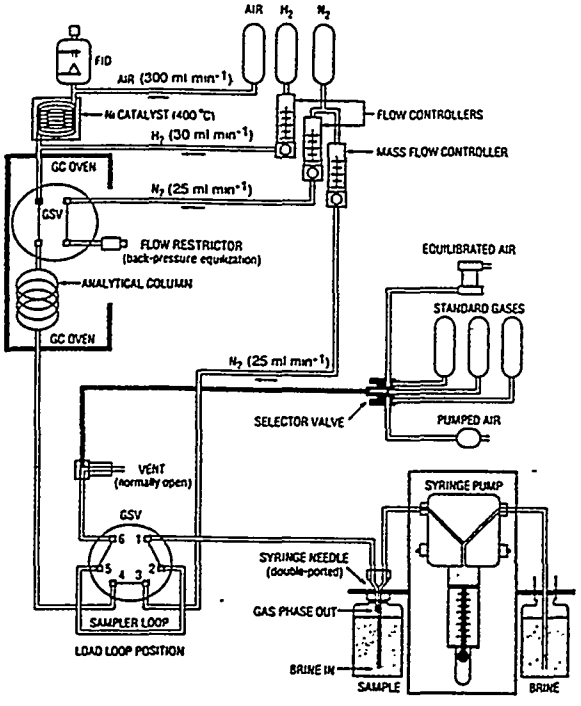

Fig. 2. Schematic representation of the gas chromatography analytical system, including the subsystem used to transport the equilibrated headspace from the serum bottle to the gas sample loop.

bottle so as not to warm the glass around the headspace. After the needle is inserted through the septum, the pressure reading stabilizes very quickly, and, with practice, a reading can be made in 1–2 s. To avoid contamination of the headspace contents during this pressure measurement, there must be a positive pressure in the headspace following equilibration, which implies that seawater samples should be equilibrated at temperatures above their potential temperatures.

Immediately after the pressure measurement, the headspace of the sample is displaced into a gas sample loop using a concentric needle and syringe (as described above) to dispense ~4.5 ml of a dense brine solution (~3× seawater salinity) into the bottom of the sample bottle. This forces the gas in the headspace through the short needle and into the gas sample loop (Fig. 2). The volume of connecting tubing between the needle and the gas sample valve is kept to a minimum (10–20 μl). Brine is used so that the introduced liquid remains in the bottom third of the sample bottle, out of contact with the headspace. The brine is prepared from water that has been partially degassed by boiling in order to prevent bubbles from forming in the syringe and the connecting tubing. Addition of a little food coloring to the brine makes it easy to determine whether any mixing takes place during sample introduction.

The equilibrated headspace contains air that is water saturated at the temperature of equilibration. To avoid water vapor condensation within the gas sample loop and connecting tubing, it is important that these components be maintained at a higher temperature than the equilibration temperature.

The plumbing arrangement for the chromatographic analysis of headspace and other gas samples is shown in Fig. 2. CO_2 is chromatographically separated, followed by catalytic reduction of CO_2 to methane and detection with a FID. Gases, including calibration standards and air, are injected using the same gas sample loop (~0.45 ml) as is used for the headspace content. When analyzing standards or air samples, the gas source is selected using a 10-position selector valve (Valco), and flow is routed through the gas sample valve by switching the solenoid valve (*see Fig. 2*). Gas is flushed through the loop and vented through the gas port of the concentric needle for 30 s before the solenoid valve is switched back to its "normally open" position. There is then a 6-s delay for pressure equilibration, during which time the loop temperature and atmospheric pressure are measured, before the gas sample valve injects the loop contents onto the GC column.

Separation of CO_2 from other gases in the sample loop is achieved using a 10 ft × $\frac{1}{16}$-in. (outer diam) Hayesep N column, operated at 60°C with a carrier flow rate of high-purity N_2 at ~20 ml min^{-1}. Oxygen scrubbers are used on the N_2 supplies. Column flow is regulated using a mass flow controller (Tylan, model FC-180). Normally, the column effluent is directed to vent, with the catalyst and detector supplied by an auxiliary carrier gas supply. The CO_2 peak (retention time of ~1.2 min) is "heartcut" by switching a four-port valve (Valco) so that it is eluted through the catalyst and detector. This procedure prevents oxygen and other gases from passing over (and potentially degrading) the catalyst and is carefully timed to ensure that the entire CO_2 peak passes through the catalyst and detector. The reduction of CO_2 to methane is accomplished by mixing the column flow with 30 ml min^{-1} hydrogen gas and passing the mixture over a nickel catalyst at 360°C. The catalyst is purchased prepacked in $\frac{1}{8}$-in. tubing (Varian). The heartcut switching, data acquisition, and peak integration are all performed using a PC-based chromatography software package (Baseline, Waters Assoc.).

Calibration and analysis sequence—Instrument response is calibrated with gaseous standards with an accurately known mole-fraction of CO_2 that cover the range encountered in the equilibrated water samples. Normally a four- or five-point calibration curve, fitted to a quadratic function, is used to evaluate the detector response. Atmospheric pressure and sample loop temperature are recorded for each injection. Calibration curves are run at the beginning and end of a series of analyses with instrument response being interpolated between these curves based on pairs of midrange check standards run regularly throughout the series. Interpolation uses either a linear or quadratic function, based on a subjective judgment of the fit. Typical variation in detector response during a series of analyses is ~0.3% over 2–3 h. Normally a complete series of analyses would correspond to a hydrographic cast of 24–36 samples with accompanying standards.

Calculation of fCO_2—The process of equilibrating the water samples with an introduced headspace involves the repartitioning of CO_2 between the liquid and gas phases. This in turn alters the C_T of the water sample and its fCO_2. This effect can be corrected for by using a mass balance for inorganic carbon, together with knowledge of the solubility and apparent dissociation constants of CO_2 in seawater, and by using the constraint that the total alkalinity of the water sample remains unchanged during the equilibration. The motivation for the use of variable headspace gases (*see above*) was to minimize the magnitude of these corrections by closely matching the fCO_2 of the introduced headspace to that of the sample. The corrections require knowledge of the salinity and C_T of the original water sample from measurements made on separate aliquots of the same water sample.

The total number of moles of inorganic carbon within the serum bottle (N_T) immediately after headspace introduction and prior to equilibration (i.e. at $t = 0$) is calculated from the mass of water in the serum bottle (m_{sw}), its C_T concentration prior to equilibration ($C_{t=0}$), the mole fraction of CO_2 in the introduced headspace ($X_{t=0}$), the atmospheric pressure ($P_{t=0}$), the headspace volume ($V_{h,t=0}$), and the temperature ($T_{t=0}$) immediately after the headspace was introduced. $T_{t=0}$ is generally assumed to be same as the temperature of the water sample. Assuming for this calculation an ideal gas (the effect of nonideality is not significant):

$$N_T = (C_{t=0}m_{sw}) + \frac{X_{t=0}P_{t=0}V_{h,t=0}}{(RT_{t=0})}. \quad (1)$$

After equilibration, the fCO_2 ($fCO_{2(eq)}$) can be calculated from measurement of the mole fraction (X_{eq}) of CO_2 in the headspace together with the headspace pressure measured after equilibration (P_{eq}):

$$fCO_{2(eq)} = X_{eq}P_{eq}\exp\left[\frac{(B_{11} + 2\delta_{12})P_{eq}}{RT_{eq}}\right], \quad (2)$$

where the subscript "eq" refers to time after equilibration is complete, and the exponential term is a correction for the nonideality of the CO_2 in air mixture, which is on the order of 0.996–0.997 for our analyses (B_{11} is the second virial coefficient of pure CO_2 and δ_{12} is the cross-virial coefficient for an air–CO_2 mixture [Weiss 1974]). Note that the GC measurement of the CO_2 mole fraction in the headspace is made on water-saturated air, and that P_{eq} can depart significantly from 1 atm because equilibration takes place in a closed system.

The C_T of the water after equilibration (C_{eq}) can be calculated from a mass balance for inorganic carbon:

$$C_{eq} = \frac{\left[N_T - \frac{(X_{eq}P_{eq}V_{h,eq})}{RT_{eq}}\right]}{m_{sw}}, \quad (3)$$

where the volume of the headspace after equilibration ($V_{h,eq}$) is calculated from the initial temperature, seawater and headspace volumes, the thermal expansion coefficients for glass, and the equation of state for seawater.

The total alkalinity of the water (A_T) is then calculated from $fCO_{2(eq)}$ and C_{eq} using standard equations such as described in DOE (1994). Note that in regions with very high nutrient concentrations, it may be necessary to incorporate explicitly the contributions of inorganic phosphorus and silicon species to the total alkalinity. The constants used for the calculations in this paper were the CO_2 solubility (K_0) according to Weiss (1974), the first and second apparent dissociation constants for carbonic acid (K_1 and K_2) of Roy et al. (1993), and the apparent dissociation constant for boric acid (K_B) of Dickson (1990). The alkalinity contributions of phosphate and silicate, together with K_w, were taken from Millero (1995) as reported in DOE (1994). The boron concentration of seawater was taken from Uppstrom (1974). All the equilibrium constants were evaluated on the total hydrogen ion scale, with concentrations in mol (kg seawater)$^{-1}$. Unit and pH-scale conversions were made as required. These constants are used for all calculations in this paper.

Because the total alkalinity of the water sample is conserved during the equilibration, the fCO_2 of the water sample prior to equilibration, at any temperature, can be calculated with the same standard equations (e.g. DOE 1994) based upon the C_T measured prior to the equilibration, and the calculated total alkalinity. The final result is generally reported as the fCO_2 (μatm) at the temperature of equilibration, as well as at some standard temperature (e.g. 20°C used throughout this paper).

Results

Equilibration—Key issues are (1) the extent to which equilibrium is attained between the gas and liquid phases within the serum bottles, and (2) the extent to which the exchange of CO_2 during the equilibration is adequately described by the calculation procedures. To examine these issues, a time course of equilibration was monitored for samples with introduced headspaces with fCO_2 both much higher and much lower than the fCO_2 of a water sample.

A glass carboy was filled with several liters of $HgCl_2$-poisoned seawater that was driven to a fCO_2 of ~1,000 μatm by bubbling a CO_2-in-air mixture through the water for several hours with stirring. The gas supply was then rerouted so that rather than bubbling through the water, the gas was continuously flushing the headspace. Samples for fCO_2 analysis were drawn by siphoning water from the carboy into serum bottles. Samples were drawn in sets of three, and headspaces with CO_2 in air mole fractions of 26, 972, and $1{,}954 \times 10^{-6}$ were introduced as described above. Each set of three samples was shaken in the water bath for a different length of time (from 5 s to 1.5 h) prior to being analyzed as described above. Duplicate samples of the water from the carboy were analyzed for C_T by coulometric titration.

Table 1 and Fig. 3 show that the introduced headspace approached equilibrium with the water in two stages, with most of the equilibration taking place very rapidly (time constant ~30 s) but with a slower process (time constant several minutes) making the overall time required for complete equilibration 1–1.5 h. The slower equilibration step may reflect the time required to restore a stable waterbath and serum bottle temperature after an initial disturbance associated

Table 1. Results of fCO_2 equilibration experiment. Equilib. time refers to the period that samples were physically shaken (equilibrated) following headspace introduction. Apparent fCO_2 at 20°C refers to the estimate of fCO_2 of water samples based on an analysis of the headspace contents after the specified period of equilibration. $X_{h,t=0}$ refers to the mole fraction of CO_2 within the introduced headspace.

Equilib. time (min)	Apparent fCO_2 at 20°C		
	$X_{h,t=0}$: $1{,}954\times10^{-6}$	$X_{h,t=0}$: 972×10^{-6}	$X_{h,t=0}$: 26×10^{-6}
0.08	1,605.9	1,009.0	381.8
0.17	1,519.0	989.8	366.8
0.33	1,437.0	1,037.4	512.3
0.5	1,348.6	1,060.6	744.4
1.0	1,269.6	1,062.0	935.1
2.0	1,147.6	1,072.8	1,024.4
16.0	1,080.6	1,075.3	1,072.6
37.0	1,076.1	1,068.8	1,069.0
82.0	1,071.9	1,073.3	1,072.8
129.0	1,072.2	1,073.9	1,071.6

with adding a batch of samples to the bath. The data also show that the same initial fCO_2 is calculated, after corrections for the CO_2 exchanged during the equilibration step, whether the initial headspace fCO_2 is higher or lower than that of the water. The finding that samples with initial headspaces of much higher ($1{,}954 \times 10^{-6}$), closely matched (972×10^{-6}), and much lower (26×10^{-6}) fCO_2 levels relative to the water all equilibrated to the same final value within ±1 μatm or ±0.1% strongly indicates that equilibrium was achieved and that the algorithm used to correct for the CO_2 exchanges during equilibration is appropriate. Fig. 3 shows that the time courses do not extrapolate back to the exact values of the introduced headspace gases at $t = 0$. This is because during the early stages of headspace introduction the gas port of the concentric needle is located slightly beneath the water within the serum bottle. The headspace gas is therefore bubbled through a thin layer of water for a short period, which allows some equilibration to take place before headspace introduction is complete.

Precision and accuracy—An extensive fCO_2 dataset was collected during the cruise of the USCGC *Polar Sea* to the northeast coast of Greenland in the summer of 1993 (Wallace et al. 1995). Data from this cruise, acquired over the course of a month, were used to evaluate precision and other aspects of the analysis.

Precision for gas samples was assessed by repeated measurements of a single standard, with appropriate corrections for temperature and pressure variations. Based on 178 separate sets of duplicate measurements of a calibration standard with a CO_2 mole fraction of $\sim 350 \times 10^{-6}$, the relative standard deviation of gas sample analyses, as calculated from the differences between duplicate analyses (DOE 1994), was 0.54%. This reflects the short-term repeatability of the gas chromatograph.

Precision for water samples was evaluated on the basis of triplicate analyses. Based on the analyses of 57 sets of triplicate samples collected during the *Polar Sea* cruise, each set having been collected from an individual Niskin bottle, the pooled relative standard deviation was ~0.83%. Similarly, on a recent cruise to the South Atlantic Ocean (WOCE A8; Meteor cruise number 28; Johnson and Wallace unpubl. data), 22 duplicate sets were analyzed. The relative standard deviation calculated from the differences between these duplicate analyses (DOE 1994) was 0.96%.

Overall accuracy of the technique was assessed through

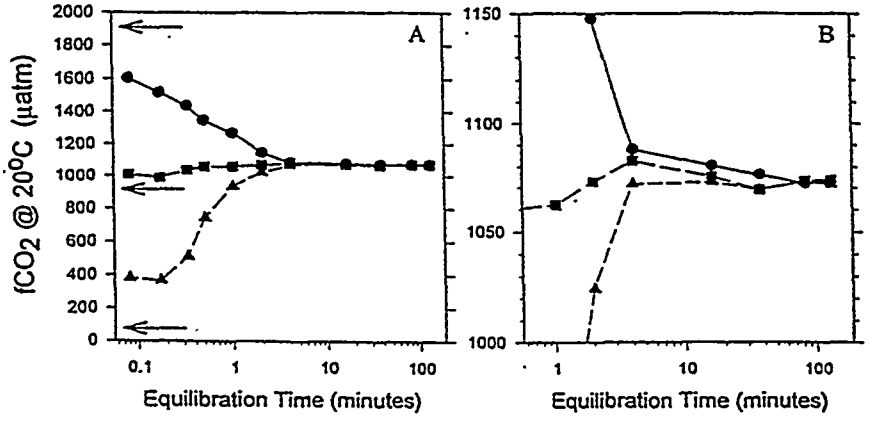

Fig. 3. Time-series plots of the approach to equilibrium between an introduced headspace and a water sample contained within a 60-ml serum bottle. The results of each analysis have been expressed as the apparent fCO_2 of the water sample at 20°C (i.e. by assuming the headspace had come to equilibrium with the water). In this way, the time course of approach to equilibrium within the serum bottle can be observed by the convergence of the three treatments on a stable and consistent value. (A) All data from the experiment. Arrows denote the fCO_2 of the three initially introduced headspace gases. (B) Data from the later stages of the experiment, on a greatly expanded vertical scale.

Table 2. Results of discrete fCO_2 analyses on poisoned seawater samples used in an interlaboratory alkalinity intercomparison study during 1993. $X_{CO_2,wet}$ refers to the mole fraction of CO_2 in the introduced headspace. Multiple aliquots were withdrawn and analyzed from each sample bottle. Total alkalinity was calculated from C_T and fCO_2 (at the temperature of equilibration) using Weiss (1974) and Roy et al. (1993*b*) CO_2 constants and Dickson (1990) borate constants. The sample salinity was 33.704.

CRM sample no.	$X_{CO_2,wet}$ (ppmv)	Equil. temp. (°C)	Calc. total alk (μmol kg^{-1})	fCO_2 at 20°C (μatm)
1	750	19.90	2,262.5	401.6
1	750	19.90	2,262.6	401.4
1	750	19.90	2,263.9	399.3
2	352	19.90	2,262.3	401.9
2	352	19.90	2,261.2	403.9
2	352	19.90	2,262.1	402.3
3	352	25.00	2,262.5	401.7
3	352	25.00	2,262.8	401.1
3	352	25.00	2,262.2	402.1
4	352	25.00	2,264.2	398.8
4	352	25.00	2,264.7	397.8
5	352	25.00	2,262.0	402.5
5	352	25.00	2,263.1	400.6
5	352	25.00	2,262.4	401.8
6	352	25.00	2,263.2	400.4
6	352	25.00	2,246.4	398.3
6	352	25.00	2,263.8	399.4
7	352	25.00	2,260.8	404.5
7	352	25.00	2,261.2	403.8
7	352	25.00	2,261.9	402.7
8	352	25.00	2,261.4	403.6
8	352	25.00	2,261.4	403.6
8	352	25.00	2,261.9	402.7
9	352	25.00	2,261.8	402.8
9	352	25.00	2,261.5	403.3
9	352	25.00	2,261.4	403.6
10	352	25.00	2,260.9	404.4
10	352	25.00	2,262.1	402.3
10	352	25.00	2,261.4	403.5

an intercomparison with other investigators. In 1993, Andrew Dickson of the Scripps Institution of Oceanography conducted an intercomparison experiment that involved distribution of poisoned-seawater samples (~500 ml), similar to those used as certified reference materials (CRMs) for C_T analyses (UNESCO 1991), to various groups. Our group and two other groups measured fCO_2 on these samples. In our laboratory, subsamples were carefully siphoned from each sample into three serum bottles and processed as described above. In order to ensure overpressure in the serum bottle headspace, most of the samples were analyzed at 25°C. Results from these analyses have been corrected to 20°C in order to facilitate comparisons with measurements made by the other two groups who equilibrated their samples at very close to 20°C. A few of our samples were also equilibrated near 20°C and gave identical results to the temperature-corrected values (Table 2). The overall mean and standard deviation of these analyses was 401.9 ± 1.8 μatm (n = 29; relative SD of 0.45%).

In processing the samples, the total alkalinity was calculated based on the independently measured C_T value of 2,004.04 μmol kg^{-1} and a salinity of 33.704. The mean and standard deviation of the total alkalinity was 2,262.3 (±1.06) μmol kg^{-1}. Note that this precision for the calculated total alkalinity is significantly better than the precision of direct total alkalinity determinations using potentiometric titration, which is 2–4 μmol kg^{-1} (Millero et al. 1993).

Table 3. Comparison of reported discrete fCO_2 data from three groups that analyzed aliquots of the same batch of poisoned seawater during an interlaboratory comparison of total alkalinity measurement during 1993. Values in parentheses are standard deviations. The C_T values are based on analyses by coulometric titration prior to equilibration. Group B did not analyze the samples for C_T and a value of 2,004.04 μmol kg^{-1} was used for calculation of the total alkalinity in this case.

Group	fCO_2 at 20°C (μatm)	n	Calc. total alk* (μmol kg^{-1})	C_T (μmol kg^{-1})
BNL	401.9(1.8)	29	2,262.3(1.1)	2,004.04
A	402.8(2.0)	4	2,262.0(1.2)	2,004.2
B	395.3(1.6)	48	2,266.2(1.0)	ND†

* Calculated from C_T and fCO_2 (at temperature of equilibration) using Weiss (1974) and Roy et al. (1993) CO_2 constants and Dickson (1990) borate constants. Sample salinity = 33.704.
† No data.

The accuracy of the technique can, at present, only be assessed through comparison with fCO_2 values determined using the significantly different techniques described by Wanninkhof and Thoning (1993) and Chipman et al. (1993). These results are presented in Table 3 (R. Wanninkhof et al. pers. comm.). The mean and standard deviation of the three separate fCO_2 determinations (corrected to 20°C) was 400.0 (±4.7). Hence, it seems that three independent techniques can achieve consistency in fCO_2 determinations to an order of ~1%, which we take to be a measure of accuracy. When the fCO_2 and TCO_2 pair is used to calculate the alkalinity for these samples, the calculated total alkalinity ranges from 2,262.0 to 2,266.2. This corresponds to consistency in the calculated total alkalinity, based on three separate techniques of determining the fCO_2, to an order of 0.1%.

Discussion

Factors affecting the precision and accuracy of fCO_2— The gas sample precision of 0.54% presented above is random and could likely be reduced through the use of improved chromatographic technique. An equilibration temperature uncertainty of ±0.02°C (given above) creates an uncertainty of ±0.08% in fCO_2 because the latter varies by ~4% per degree temperature change.

Uncertainty for water sample analyses is directly proportional to the precision and accuracy of the headspace pressure measurement (Eq. 2). Because equilibration takes place in a closed system, headspace pressures after equilibration can deviate significantly from atmospheric pressure (*see below*). Precision of headspace pressure measurements, assessed from differences between measurements made on multiple sets of duplicate samples (DOE 1994), is ~0.5% and can account for ~50% of the overall imprecision of water analyses. To check that the headspace pressure mea-

surements are accurate and that the septa do not consistently leak, we routinely compare the predicted pressure of equilibration (based on a mass balance for the major gases found in air and water) with that which is measured using the needle probe and pressure sensor.

A mass balance is obtained based on knowledge of the volume, pressure, and composition of the introduced headspace (usually air at atmospheric pressure), together with the water volume and its oxygen, nitrogen, and argon concentrations. Water vapor pressure changes are taken into account and additional corrections are made to account for volume changes of the gas and liquid phases associated with the thermal expansion of water (significant) and glass (almost insignificant) during the equilibration.

The predicted headspace pressure after equilibration (P_{eq}) is given by

$$P_{eq} = P_{N_2} + P_{O_2} + P_{Ar} + P_{H_2O}, \quad (4)$$

with the equilibrium partial pressures of N_2, O_2, and Ar being calculated from

$$P_G = \frac{N_G R T_{eq}}{\left(1 + \frac{V_{w,eq} L_G}{V_{h,eq}}\right) V_{h,eq}}, \quad (5)$$

where P_G is the partial pressure of an individual gas (e.g. N_2) after the equilibration, $V_{w,eq}$ and $V_{h,eq}$ are, respectively, the volumes of seawater and headspace after equilibration, R is the gas constant, T_{eq} is the temperature of equilibration (°K), and L_G is the Ostwald solubility coefficient. The latter is equivalent to $\beta_G(T_{eq}/273.15)$, where β_G is the Bunsen solubility coefficient of the gas at the sample salinity and the temperature of equilibration (Weiss 1970). P_{H_2O} at the sample salinity and the temperature of equilibration is calculated using the formula given by Weiss and Price (1980). N_G is the total number of moles of an individual gas contained within the serum bottle and is calculated using a mass balance similar to Eq. 1. The initial oxygen concentration of the water is measured (e.g. by Winkler titration) whereas the concentrations of nitrogen and argon in the water, which are not normally measured, are assumed equivalent to 100% saturation with air at the potential temperature and salinity of the water sample.

During the *Polar Sea* cruise, fCO_2 samples were equilibrated at temperatures of 17–18°C whereas the original temperatures of the water samples were close to the freezing point of seawater (Fig. 5A). The major gases in seawater (Eq. 4) are generally present at concentrations that are close to equilibrium with air at the potential temperature and salinity of the sample. Warming of up to 20°C during equilibration in the serum bottles causes outgassing, which, coupled with thermal expansion of the water sample, can create final headspace pressures as high as 1.18 atm (Fig. 5B). Fig. 5A presents a depth profile of the difference between the predicted headspace pressure, based on Eq. 4 and 5, and that directly measured with the barometer. Also shown is a composite vertical temperature profile. Septa leakage during equilibration would result in positive values for the pressure difference. Based on analysis of 973 separate analyses, 7 outliers were identified as being >3 SDs removed from the overall mean. All of the outliers were positive and are likely a result of septum leakage. Fig. 5b presents the pressure difference plotted against the predicted headspace pressure. Predicted and observed headspace pressures agreed very closely, with the mean difference (predicted − observed), after outlier removal being +0.0045 atm (±0.0079, n = 966). If this difference is the result of error in the headspace pressure measurement, which is not necessarily the case, it would imply a systematic bias on the order of 0.4% in the results of the fCO_2 analysis. Note that this finding is based on experimental conditions that led to unusually high overpressures within the serum bottles because of the unusually large sample warming and may therefore represent a worst-case scenario. Negative values of the pressure difference are harder to explain: the four very negative values in Fig. 5

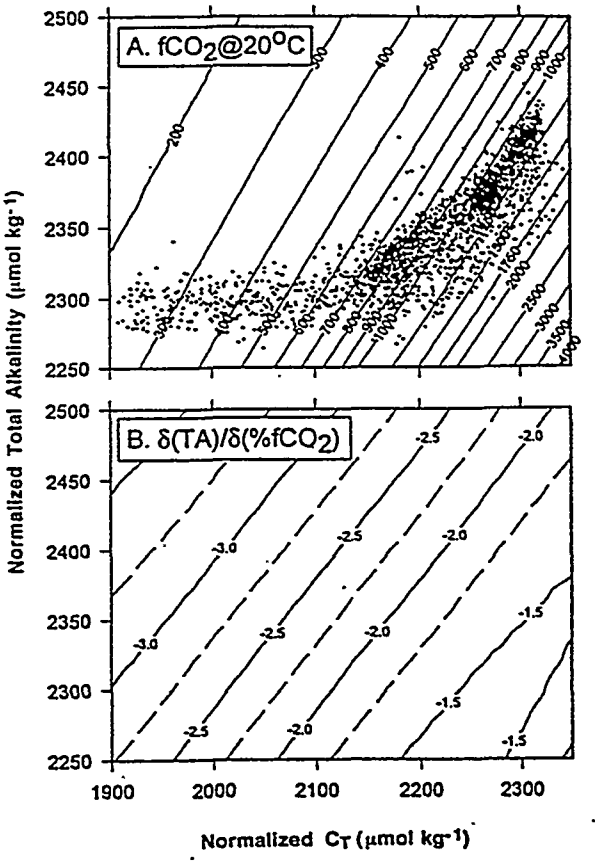

Fig. 4. (A) Calculated fCO_2 at 20°C as a function of C_T and total alkalinity. Superimposed on this plot are the C_T and total alkalinity data measured globally during the GEOSECS survey of the Atlantic, Indian, and Pacific Oceans. The C_T and total alkalinity data have been normalized to a constant salinity of 35. Note that the contour intervals are not constant. Calculations were performed as described in the text. (B) Contours of the sensitivity of the calculated total alkalinity (in μmol kg⁻¹) to a 1% uncertainty in fCO_2 at 20°C. C_T and total alkalinity space are the same as in A.

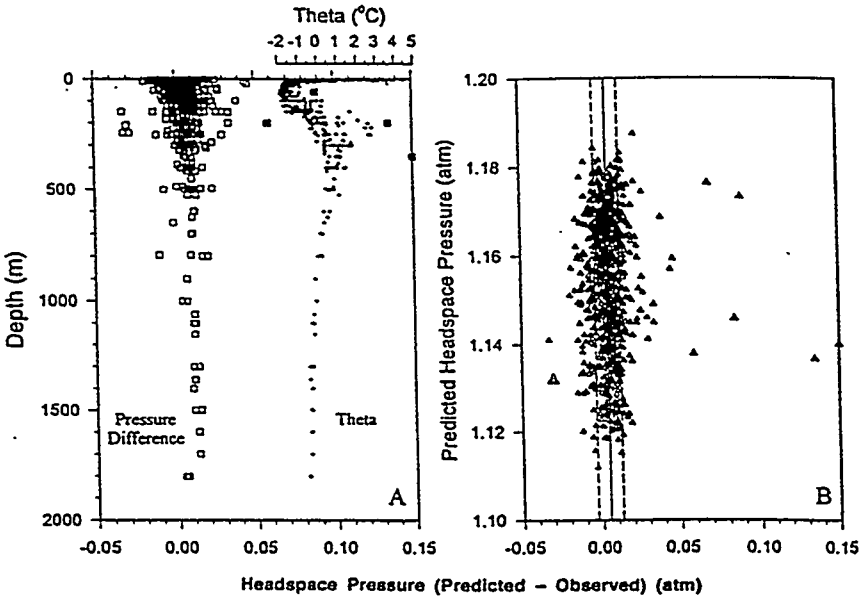

Fig. 5. (A) Vertical profiles of the difference between the "predicted" equilibrium headspace pressure within a serum bottle based upon a mass balance (*see text*) and that which was observed, or measured, using a barometer. Outliers (*see text*) are plotted as filled symbols. These data were collected during the *Polar Sea* cruise to the East Greenland shelf, which sampled in ice-covered waters. Also presented are profiles of the potential temperatures at which these samples originated; most samples were equilibrated at 17–18°C. (B) Based on the same data as shown in A, the predicted pressure after equilibration is plotted against the difference between measured and predicted values. Outliers are plotted as filled triangles. Control lines are plotted for the mean and standard deviation.

were all collected from the same hydrocast, and it is possible that the temperature of equilibration was incorrectly recorded for these samples.

There was a tendency for near-surface samples to have lower values of the pressure difference. This depth range also exhibited very strong vertical temperature and salinity gradients, to which two factors likely contributed. First, seasonal warming of the upper layers, compounded by strong salinity stratification, may have created in situ nitrogen supersaturation. Our predictions, on the other hand, assumed that both nitrogen and argon were at 100% saturation. Nitrogen supersaturation would tend to create negative values for the pressure difference, with the change in predicted pressure being −0.0012 atm for each percent change in initial nitrogen saturation. Second, an offset between the water temperature, which was recorded by a conductivity–temperature–depth package, and that which was appropriate for the water that was actually trapped within the Niskin bottle when it closed may have been a factor. The extremely steep gradients in these near-surface waters made such offsets likely.

The pressure differences for samples collected from below 200 m were consistently positive and averaged +0.0075. These samples were collected from Arctic intermediate water, which is ultimately derived from North Atlantic surface water that has been strongly cooled. Whereas most oceanic water masses are within a percent or two of equilibrium with atmospheric N_2 (e.g. Kester 1975), undersaturation of nitrogen can be created when the rate of cooling is rapid relative to the rate of air–sea gas exchange, particularly if ice cover restricts gas exchange. Under this scenario, nitrogen undersaturation could be a cause of some (but probably not all) of the observed positive pressure difference. We are not aware of any measurements from this region that can be used to check this hypothesis. In summary, the close overall agreement between predicted and measured headspace pressures shows that the septa do not leak significantly during the equilibrations and also suggest that the headspace pressure measurement is accurate to <0.7%.

As noted above, the fCO_2 measured after equilibration ($fCO_{2(eq)}$) must be corrected back to a value that the water sample would have had at the temperature of equilibration if no CO_2 had been exchanged with the headspace (i.e. a nonperturbed value, $fCO_{2(i)}$). In practice, the correction is applied exactly using the calculation procedures described above; however, its magnitude, expressed as a percentage of $fCO_{2(i)}$, can be approximated by

$$100\frac{fCO_{2(eq)} - fCO_{2(i)}}{fCO_{2(i)}} \simeq 100\frac{Rv\dfrac{V_h}{V_w}(fCO_{2(h,t=0)} - fCO_{2(i)})}{\rho C_T R T_{eq}}. \quad (6)$$

where Rv is the Revelle (or homogeneous buffer) factor (e.g. Sundquist et al. 1979) and ρ is the density of seawater. Rv depends upon temperature, salinity, and the total alkalinity and C_T of seawater. When evaluated for an equilibration temperature of 20°C, a salinity of 35, and over the range of total alkalinity and C_T found in the ocean (see Fig. 4A), Rv varies from 8 to 17. Eq. 6 shows that the magnitude of the correction, expressed as a percentage of $fCO_{2(i)}$, is proportional to Rv, the headspace-to-water phase ratio in the serum bottle, and the mismatch between the fCO_2 of the introduced headspace and that of the initial water sample, evaluated at T_{eq}. Hence at 20°C, for typical C_T (2,100 μmol kg^{-1}), phase ratio (0.1), and for an extreme initial fCO_2 mismatch of 1,000 μatm, Eq. 6 implies a percentage correction equivalent to (0.2 × Rv), or 1.6–3.4%. Note that this represents the magnitude of the correction to $fCO_{2(eq)}$; the uncertainty of the correction must be very much smaller and, in practice, even the magnitude is minimized through the preselection of headspace gases. Uncertainty in the correction is dominated by uncertainty in the phase ratio. Eq. 6 shows that even a gross error in (V_h/V_w) of 10% would cause a maximum error of 0.34% in the correction and hence in $fCO_{2(i)}$.

Factors affecting the calculation of total alkalinity—It is worth examining the accuracy and precision required of oceanic discrete fCO_2 measurements to make them of comparable sensitivity to the best available measurements of total alkalinity. Fig. 4A presents the parameter space of C_T and total alkalinity in the World Ocean, as measured during the GEOSECS program in the Pacific, Indian, and Atlantic Oceans. Concentrations have been normalized to a constant salinity of 35. On this same figure we superimposed contours of the calculated values of fCO_2 at 20°C corresponding to this parameter space. Oceanic values of this quantity fall into the range 200–2,000 μatm. In Fig. 4B we have contoured the uncertainty in the calculation of total alkalinity that would result from a 1% uncertainty in the measured value of fCO_2 at 20°C. This figure shows that a 1% relative uncertainty in fCO_2 translates into a relative uncertainty of between 1.5 and 3 μmol kg^{-1} in the calculated total alkalinity. Uncertainties are smallest at high values of C_T and become larger with decreasing C_T and increasing total alkalinity. Note that uncertainties in the constants used for the calculations contribute additional systematic uncertainties to the calculation of the total alkalinity.

Summary, future improvements, and extensions—Based on intercomparison studies and analysis of likely sources of systematic bias, the discrete fCO_2 method seems to be accurate to better than 1%. Measurement of the pressure of equilibration is a key determinant of accuracy with systematic bias in this measurement apparently being ≤0.7%. Such bias could likely be reduced by equilibration of samples at temperatures chosen to minimize overpressure in the equilibrated headspace. Imprecision of water sample analyses (currently ~0.9%) originates largely with the repeatability of the GC analysis (0.54%) and with the headspace pressure measurement (~0.5%). Note that the short analysis time for the fCO_2 analysis (~2 min) allows multiple replicates to be analyzed efficiently in order to improve overall confidence in a sample analysis. We suspect that one remaining significant source of imprecision, and possibly bias, results from small temperature changes and consequent repartitioning of gases that may occur between the time of removal of the serum bottle from the water bath and headspace injection.

Because separation and detection of CO_2 is achieved by GC, the potential exists to extend this technique to the simultaneous detection of many other trace gases found in seawater. Use of a related technique for methane analysis has been previously described (Johnson et al. 1990). Additional detectors could be used for the simultaneous analysis of other important gases such as N_2O, N_2, O_2, and Ar. Miyajima et al. (1995) recently described a GC with isotope-ratio mass spectrometry method for the measurement of carbon isotopes in lake water. The more accurate and controlled equilibration procedures described here could be readily applied to their detection methodology, allowing measurements of fCO_2 and $\delta^{13}C$ to be made with a single analytical system.

References

CHEN, H., R. WANNINKHOF, R. A. FEELY, AND D. GREELEY. 1995. Measurement of fugacity of carbon dioxide in seawater: An evaluation of a method based on infrared analysis. NOAA Tech. Mem. ERL AOML-85. 49 p.

CHIPMAN, D. W., J. MARRA, AND T. TAKAHASHI. 1993. Primary production at 47°N and 20°W in the North Atlantic Ocean: A comparison between the ^{14}C incubation method and mixed layer carbon budget observations. Deep-Sea Res. II 40: 151–169.

DICKSON, A. G. 1990. Thermodynamics of the dissociation of boric acid in synthetic seawater from 273.15 to 318.15 K. Deep-Sea Res. 37: 755–766.

———. 1993. The measurement of sea water pH. Mar. Chem. 44: 131–142.

DOE. 1994. Handbook of methods for the analysis of the various parameters of the carbon dioxide system in sea water. Version 2. A. G. Dickson and C. Goyet [eds.]. ORNL/CDIAC—74.

GRUBER, N., J. L. SARMIENTO, AND T. F. STOCKER. 1996. An improved method for detecting anthropogenic CO_2 in the oceans. Global Biogeochem. Cycles 10: 809–837.

JOHNSON, K. M., J. E. HUGHES, P. L. DONAGHAY, AND J. MCN. SIEBURTH. 1990. Bottle calibration static-headspace method for the determination of methane in seawater. Anal. Chem. 62: 2408–2412.

———, A. E. KING, AND J. M. SIEBURTH. 1985. Coulometric TCO_2 analysis for marine studies: An introduction. Mar. Chem. 16: 61–82.

———, K. D. WILLS, D. B. BUTLER, W. K. JOHNSON, AND C. S. WONG. 1993. Coulometric TCO_2 analysis for marine studies: Maximizing the performance of an automated continuous gas extractor system and coulometric detector. Mar. Chem. 44: 167–187.

KESTER, D. R. 1975. Dissolved gases other than CO_2, p. 498–556. *In* J. P. Riley and G. Skirrow [eds.], Chemical oceanography. V. 1, 2nd ed. Academic.

MILLERO, F. J. 1995. The carbon dioxide system in the oceans. Geochim. Cosmochim. Acta 59: 661–667.

———, J.-Z. ZHANG, K. LEE, AND D. M. CAMPBELL. 1993. Titration alkalinity of seawater. Mar. Chem. 44: 153–165.

MIYAJIMA, T., Y. YAMADA, Y. T. HANBA, K. YOSHII, T. KOIABASHI, AND E. WADA. 1995. Determining the stable isotope ratio of total dissolved carbon in lake water by GC/C/IRMS. Limnol. Oceanogr. 40: 994–1000.

ROBINSON, C., AND P. J. LEB. WILLIAMS. 1991. Development and

assessment of an analytical system for the accurate and continual measurement of total dissolved inorganic carbon, Mar. Chem. 34: 157–175.

ROY, R. N., AND OTHERS. 1993. The dissociation constants of carbonic acid in seawater at salinities 5 to 45 and temperatures 0 to 45°C. Mar. Chem. 44: 249–267.

SUNDQUIST, E. T., L. N. PLUMMER, AND T. M. L. WIGLEY. 1979. Carbon dioxide in the ocean surface: The homogeneous buffer factor. Science 204: 1203–1205.

UNESCO. 1991. Reference materials for oceanic carbon dioxide measurements. UNESCO Technical Papers in Marine Science, No. 60.

UPPSTROM, L. R. 1974. Boron/chlorinity ratio of deep-sea water from the Pacific Ocean. Deep-Sea Res. 21: 161–162.

WALLACE, D. W. R. 1995. Monitoring global ocean carbon inventories. OOSDP Background Report 5, Ocean Observing System Development Panel, Texas A&M Univ.

———, AND OTHERS. 1995. Collaborative research on the Northeast Water Polynya: NEWP93. Hydrographic data report. USCGC Polar Sea cruise, 18 July–20 August 1993. Brookhaven National Laboratory Informal Report, BNL-61922.

WANNINKHOF, R., AND K. THONING. 1993. Measurement of fugacity of CO_2 in surface water using continuous and discrete sampling methods. Mar. Chem. 44: 189–204.

WEISS, R. F. 1970. The solubility of nitrogen, oxygen and argon in water and seawater. Deep-Sea Res. 17: 721–735.

———. 1974. Carbon dioxide in water and seawater: The solubility of a non-ideal gas. Mar. Chem. 2: 203–215.

———, AND B. A. PRICE. 1980. Nitrous oxide solubility in water and seawater. Mar. Chem. 8: 347–359.

Received: 26 July 1996
Accepted: 15 April 1997

JOURNAL OF GEOPHYSICAL RESEARCH, VOL. 98, NO. C12, PAGES 22,759–22,778, DECEMBER 15, 1993

Variability of Sources and Sinks of CO_2 in the Western Indian and Southern Oceans During the Year 1991

ALAIN POISSON, NICOLAS METZL, CHRISTIAN BRUNET, BERNARD SCHAUER, BERNARD BRES, DIANA RUIZ-PINO, AND FERIAL LOUANCHI

Laboratoire de Physique et Chimie Marines, Université Pierre et Marie Curie, Paris

For the period from January to September 1991 we describe spatial and temporal variations of sea surface carbon dioxide fugacity (fCO_2) in the Antarctic, Subantarctic, subtropical, and tropical regions of the Indian Ocean (including the Red Sea). The measurements were made continuously with an infrared technique during seven cruises. We study the temporal variations of fCO_2 at daily, monthly and seasonal scales in selected areas. High-frequency variabilities of 20 µatm/d have been observed near polar frontal zone. Both spatial and temporal fCO_2 variations are large near the subtropical and Subantartic fronts. In the subtropical domain, fCO_2 decreases regularly from austral summer to winter. In January this region is a small CO_2 sink with values near equilibrium with the atmosphere. In July, low fCO_2 (300 µatm) leads to a CO_2 flux of -4.5 mmol/m^2/d into the ocean for the zonal band 23°S-35°S. A quantitative study of monthly and seasonal fCO_2 budgets is presented for the subtropical area. Considering first the observations at seasonal scale, it is shown that changes in fCO_2 can be explained by temperature variations and air-sea exchanges; the sum of biological and mixing processes, considered as the balance of the seasonal fCO_2 budget, is close to zero. The monthly fCO_2 budgets are then calculated. In that case, other processes must be taken into account to close the budget: the observations indicate that the effect of productivity exceeds the one of mixing in austral summer and the opposite in winter. We then describe the seasonal air-sea fCO_2 differences (ΔfCO_2) for the whole western Indian Ocean and corresponding Antarctic sector (18,000 observations). In the equatorial and tropical regions the ocean is a CO_2 source as was previously observed in the 1960s. In the subtropical area the CO_2 sink dominates but varies strongly on a monthly scale. In the circumpolar front zones there is a large potential CO_2 sink in summer. In the Antarctic waters, fCO_2 spatial variability is very high at mesoscale, especially in the area of the Kerguelen plateau. Finally, it is shown that in some oceanic areas, well-defined relations exist between fCO_2 distribution and temperature and salinity. If we want to use them to constrain mappings of continuous fCO_2 fields from sparse observations, such relations must be considered at regional and at least seasonal scales.

INTRODUCTION

A knowledge of the fugacity of carbon dioxide, fCO_2 (or the partial pressure, pCO_2), in oceanic surface water is needed to estimate the air-sea flux of CO_2. (The fugacity takes into account the non-ideal nature of the gas. Numerically, fCO2 is closely equivalent to pCO_2.) The spatiotemporal variations of fCO_2 have to be measured in order to quantify the variability of the air-sea exchanges as well as to understand the processes which govern it. Then it will be possible to estimate, at a large scale, realistic integrated fluxes and the associated uncertainties that one needs for global modeling purposes and to improve predictive parameterizations of biogeochemical processes.

In the sixties it had been observed that spatial variations of sea surface pCO_2 can be large at basin and regional scales [*Takahashi*, 1961; *Keeling*, 1968; *Miyake and Sugimura*, 1969]. The data obtained in the 1970s and early 1980s (GEOSECS, TTO, and other expeditions) also showed large variations on these scales; part of these data have been reassembled by *Broecker et al.* [1986] in constructing a world map of zonal air-sea CO_2 gradients (or ΔpCO_2) which has been used to quantify air-sea CO_2 fluxes at a global scale [*Etcheto and Merlivat*, 1988; *Merlivat et al.*, 1991]. Errors and variabilities in the air-sea CO_2 fluxes have also been estimated, these being generally associated with the gas transfer coefficient determination alone [*Thomas et al.*, 1988; *Boutin*, 1990; *Murphy et al.*, 1991b]. Few studies consider the CO_2 flux variabilities associated with spatial and temporal sea surface pCO_2 variability [*Thomas et al.*, 1988]; this can be explained by the poor coverage of pCO_2 data. Although additional data were published in the 1980s [*Smethie et al.*, 1985; *Brewer*, 1986; *Andrié et al.*, 1986; *Takahashi et al.*,1986 ; *Goyet et al.*, 1991; *Metzl et al.*, 1991; *Murphy et al.*, 1991a; *Inoue and Sugimura*, 1992], some of which were used to draw a new world map of ΔpCO_2 [*Takahashi*, 1989; *Tans et al.*, 1990], fCO_2 observations are still distributed sparsely in space and time. To improve the determination of regional or global air-sea CO_2 flux (and the associated uncertainties), it is clear that more fCO_2 observations are needed; there are big gaps, for instance, in the Pacific and Indian sectors of the southern ocean [*Tans et al.*, 1990]. Furthermore, very few cruises have been made during the winter, especially in the southern ocean (south of 50°S) for which

Paper number 93JC02501.
0148-0227/93/93JC-02501$05.00

the potential of CO_2 sink/source (ΔpCO_2 or at least the sign of the flux) remains unknown. This ocean has been labeled as an active sink [*Broecker et al.*, 1986] although pCO_2 measurements show that sources and near-equilibrium value exist in the Atlantic sector [*Keeling*, 1968], the Pacific sector [*Keeling et al.*, 1965; *Miyake et al.*, 1974; *Inoue and Sugimura*, 1988; *Murphy et al.*, 1991*a*, *b*], and the Indian sector [*Miyake and Sugimura*, 1969; *Metzl et al.*, 1991]. Modeling studies also show that CO_2 sources south of 50°S could balance the global CO_2 budget, including atmospheric, oceanic, terrestrial, and anthropic subsystems [*Tans et al.*, 1990]. The southern ocean is not the only zone subject to controversy and in many regions the potential for air-sea CO_2 exchange remains uncertain. For example, recent observations in the North Atlantic show large pCO_2 variations associated with phytoplankton blooms [*Watson et al.*, 1991] and hence averaging seasonal pCO_2 data can cause significant uncertainties in the air-sea CO_2 flux estimates in this region [*Taylor et al.*, 1991]. Seasonal data are highly recommended for a realistic estimate of planetary CO_2 fluxes. Unfortunately, observations of seasonal pCO_2 variations are generally localized [*Weiss et al.*, 1982; *Peng et al.*, 1987; *Wong and Chan*, 1991; *Keeling* 1992].

Beyond the knowledge of the contemporary distribution of fCO_2 and the corresponding air-sea CO_2 fluxes, the processes which govern fCO_2 variations have to be understood. On the one hand, fCO_2 distributions and/or variations can be explained with in situ data analysis through relationships such as fCO_2/temperature, fCO_2/oxygen or fCO_2/chlorophyll A [*Kelley et al.*, 1971; *Weiss et al.*, 1982; *Copin-Montegut*, 1989b; *Metzl et al.*,1991; *Murphy et al.*, 1991*a*; *Watson et al.*,1991]. On the other hand, models can be used to quantify the respective influence of these processes on the variation of fCO_2 on various time scales [*Goyet*, 1987; *Peng et al.*, 1987; *Garçon et al.*, 1989; *Taylor et al.*, 1991; *Garçon et al.*, 1992; *Keeling*, 1992]. It is now admitted that variations of sea surface CO_2 concentrations are mainly controlled by dynamic processes (mixing in the surface layer), thermodynamic processes (variation of temperature and salinity), exchanges of CO_2 between the atmosphere and the ocean and biological processes (primary production). Many of these processes have a high-frequency component, thus understanding them requires instrumentation which allows us to observe the oceanic carbon system at these frequencies.

Section 2 of this paper presents the method of continuous measurement of fCO_2 used during the 1991 MINERVE (Mesure à l'INterface Eau-aiR des Variations des Echanges de CO_2) cruises, which enables to observe high-frequency spatial and temporal variations of surface fCO_2. To study a wide oceanic area, this apparatus was set up onboard the R/V *Marion Dufresne* (Terres Australes et Antarctiques Françaises, TAAF) and operated from January to September 1991 in the western Indian Ocean, the Indian sector of the southern ocean and the Red Sea (figure 1). We first describe (section 3) the high-frequency CO_2 variability (several hours, several kilometers) on short repeated tracks in the southern ocean. Monthly and seasonal fCO_2 variations are then described in detail for the subtropical and subantarctic zones (section 4). A quantitative and comparative study of monthly and seasonal fCO_2 budgets is also presented for the subtropical region. Finally we use the whole 1991 MINERVE data set (18,000 observations) to describe the seasonal distribution of CO_2 sources and sinks in the western Indian Ocean and corresponding Antarctic sector (section 5) and we discuss regional and seasonal relations between fCO_2 and temperature or salinity (section 6).

METHOD

Fugacity of carbon dioxide (fCO_2) in air and in surface seawater was measured with an infrared technique based on those described by *Takahashi* [1961] and *Copin-Montégut* [1985]. The system consists mainly of an equilibrator and an IR analyzer (SIEMENS, type Ultramat 5F); a series of valves, heater, pumps, cold traps, ..., comprises the rest of the intrumentation (Figure 2) and a PC-AT microcomputer is used to automate the whole system. The measuring system is connected to the thermosalinograph and satellite navigation system of the R/V *Marion Dufresne*. Seawater, pumped from 5 m deep, circulates in the equilibrator at a rate of 2 L/min; a closed loop of about 100 ml of air circulates as a countercurrent in the equilibrator and then goes through an automatic cold trap system and the IR analyzer. The equilibrator is designed in such a way that there are no bubbles at the air-seawater interface.The characteristic time of equilibration of the cell depends mainly on the magnitude of the disequilibrium itself, on the value of the fugacity and on the fluxes of seawater and air into the cell. For example, it needs less than 10 min to reequilibrate a seawater with a fugacity of 350 µatm In equilibrium with air,when the fugacity in air increases abruptly from 350 to 400 µatm or decreases from 350 to 300 µatm in 5 s. During the routine measurements the rate of change is, in all cases including high gradients in frontal zones, smaller than 1 µatm/ 5 s and the two phases, air and seawater, are always in equilibrium.

The CO_2 standards, the atmospheric air, and the air equilibrated with the sea samples are not measured exactly at atmospheric pressure; this is because the gas circulation using a pump implies small pressure desiquilibrium in the various parts of the circuit. To take into account these pressure effects [see, for example, *Copin-Montégut*, 1985], we use three pressure sensors: one measures the atmospheric pressure (Patm); the other two measure the difference between Patm and the pressure in the IR cell and between Patm and the pressure in the equilibrator cell. To make the temperature correction as small as possible, the cell is thermostated with the same surface seawater as that used for the fCO_2 measurement. The temperature measured in the equilibrator with a platinum thermometer (PT100) is always higher than the in situ temperature (sea surface temperature, SST), but by less than 1°C in the range $-1.8°C < SST < 31°C$ encountered during the cruises. The cold trap (-35°C) system has two traps in parallel to ensure the continuity of the measurement: when trap A is connected to the closed loop of air, trap B is heated by a warm airflow to melt the trapped ice and to dry it. The two traps are alternated every hour. All the instrumental functions of the system are automatic. Atmospheric air is pumped at the bow or at the stern of the ship, depending on the direction of the wind; the atmospheric CO_2 is measured every 7 hours and followed by standardization (except at the beginning of the cruise when the standards are first measured). Standards [Air Liquide company] with 260, 350, and 479 ppm CO_2 in dry air were used to calibrate the IR analyzer. During the seawater sampling cycle (7 hours), fCO_2 in surface seawater, atmospheric pressure, temperature and pressure in the equilibrator, pressure in the IR spectrometer cell, salinity and SST, and the navigation parameters are stored every 12 s and the arithmetic means of these data are automatically calculated and recorded every 10 min. Each of the results presented in this paper is the average of 50 measurements recorded during 10 min, whatever the speed of the ship.

The IR measurements are first corrected to pressure effects mentionned above; then we correct fCO_2 for water vapor pressure [*Weiss and Price*, 1980] and IR spectrometer drift (calculated for each 7-hour cycle). As mentioned above, a small correction is always needed for the difference between equilibrator temperature and SST; we have used the polynomials established by *Copin-Montégut* [1988, 1989*a*] which are based on dissociation constants for carbonic acid in seawater recommended by the CO_2 Subpanel of the Joint Panel of Oceanographic Tables and Standards [*UNESCO*, 1987] which are valid for the temperature range $0°C \leq SST \leq 30°C$. Copin-Montégut proposed

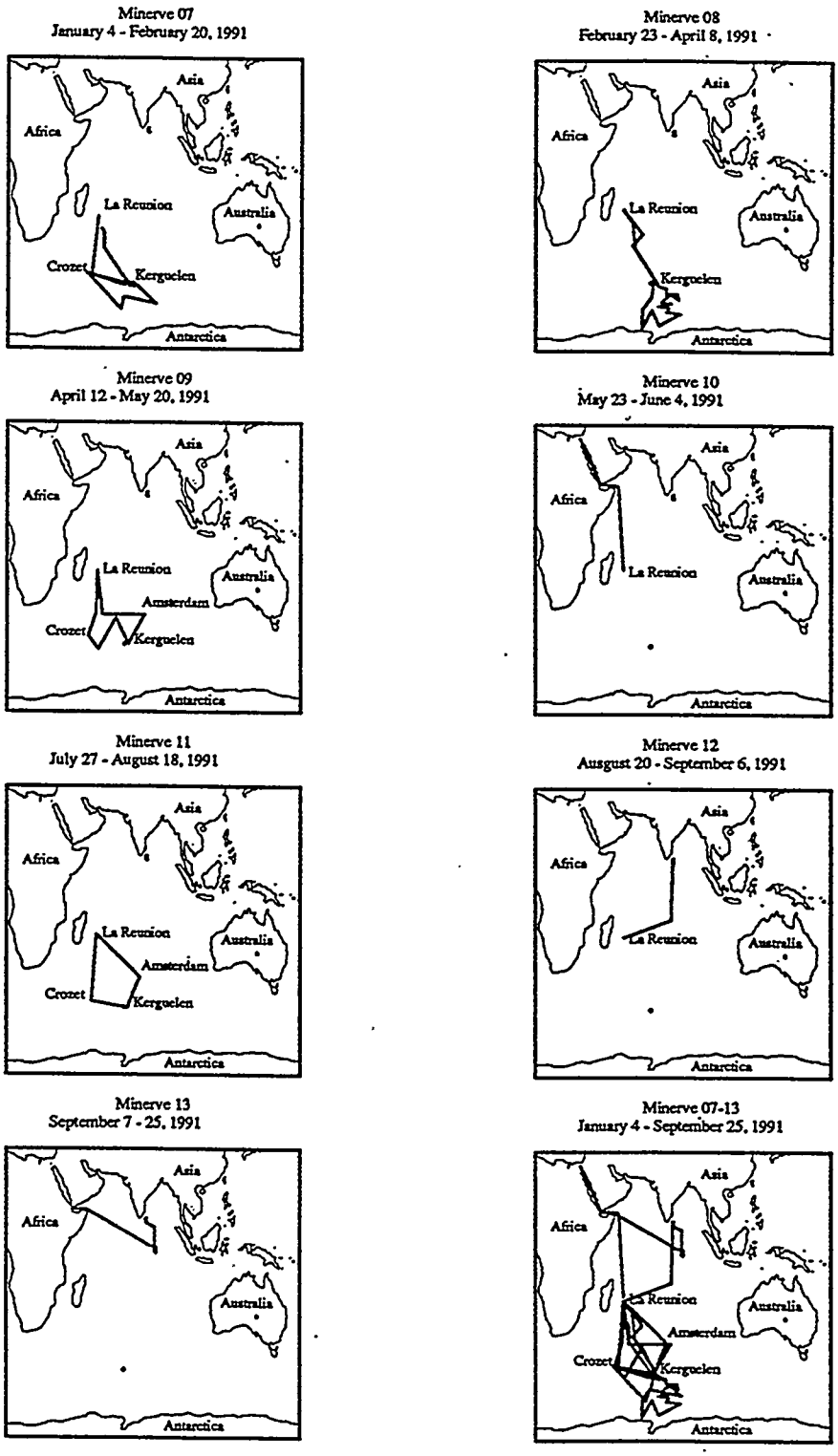

Fig. 1. Locations and periods of the measurements of CO_2 during MINERVE cruises from January to August 1991.

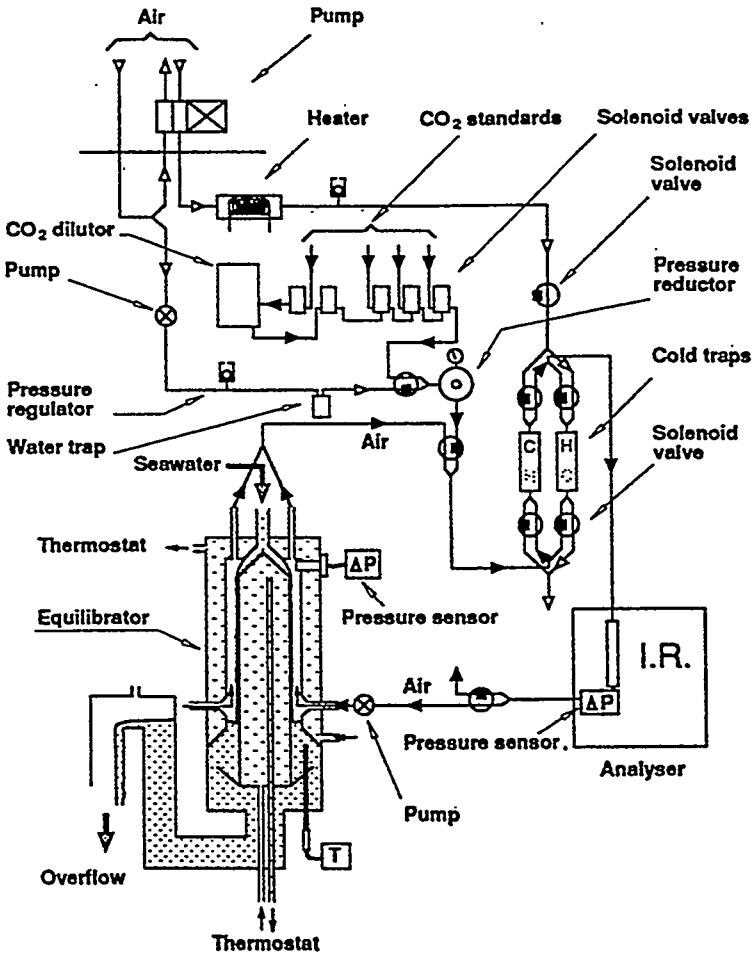

Fig. 2. Schematic diagram of the system used for IR measurement of carbon dioxide in seawater and of the equilibration cell for fCO_2 measurement in surface seawater. P is a pressure gauge and T is a platinum thermometer. The cell is thermostated with surface seawater.

two sets of constants depending on the DIC/TA ratio ($0.83 \le DIC/TA \le 0.93$ and $0.93 \le DIC/TA \le 0.948$). In the western Indian Ocean, DIC/TA ratios deduced from the INDIGO data [*Poisson et al.*, 1988, 1989, 1990] lie between 0.84 and 0.96 (this extreme value is encountered south of 60°S); therefore we have chosen to use the polynomial corresponding to $0.83 \le DIC/TA \le 0.93$. Note that if one uses the second constants proposed by Copin-Montégut, differences of corrected fCO_2 are lower than 1 µatm/°C for the whole temperature range $0°C \le SST \le 30°C$ and for fCO_2 from 200 to 500 µatm. The surface water Salinity was calibrated by collecting samples, the salinity of which was measured with a Guildine salinometer (Autosal type). The meteorological parameters were stored every hour. The fCO_2 data presented in the figures are normalized to a standard pressure of one atmosphere, but ΔfCO_2 is referred to local pressure in order to calculate instantaneous air-sea fluxes (ΔfCO_2 is the difference between oceanic and atmospheric fCO_2).

The precision of the IR analyzer is estimated by the manufacturer to be better than 0.5 ppm. During some cruises, measurements were made during the time of occupation of hydrographic stations to test the precision of the data (i.e. over several hours). Figure 3 shows the standard deviations for some of these measurements; these include both the in situ variability and the variability of the measuring system. Except when the stations were located near or in a front zone where the hydrological and geochemical variabilities are high, the standard deviation of fCO_2, corrected to the in situ condition, is lower than 0.3% (about 1 µatm).

DAILY VARIATIONS

During the MINERVE 7 cruise (January-February 1991) small tracks were repeated over periods of about 3 days (tracks are shown in Figure 4*a*). Two tracks (T1 and T2) are situated near the polar front southeast of the Kerguelen archipelago; the others (T3 to T7) are at the same latitude, around 57°-58°S. To show the regional differences in fCO_2 variations, the fCO_2 scale is the same in Figures 4*b*-4*h* (100 µatm).

In the open ocean zone around 57°S-58°S, temporal variations (over several hours) are not significant (Figures 4*c*-4*g*). Spatial variations are also weak except along the easternmost track T3 which is on the eastern edge of the Kerguelen plateau (85°E; see Figure 4*a*). There we observed a large fCO_2 horizontal gradient (40 µatm/10 km) linked to a well- marked hydrological front (1°C/10 km). We will return to the effect of the Kerguelen plateau topography on fCO_2 distribution in sections 4 and 5. Near the

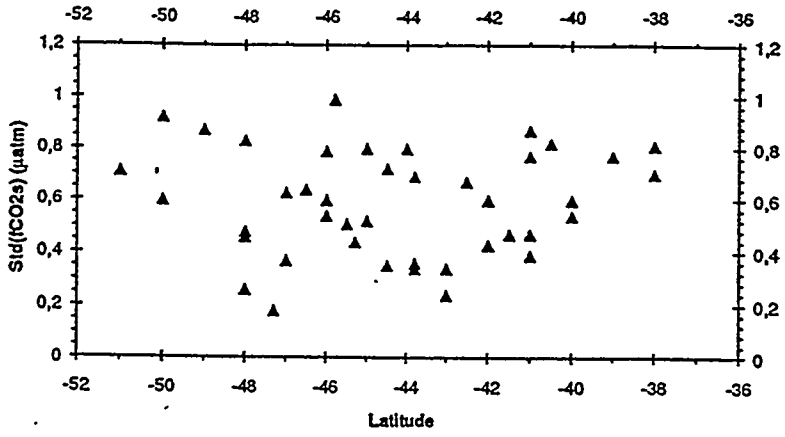

Fig. 3. Standard deviations of fCO_2 measured during the time of occupation of hydrographic stations made during the MINERVE 9 cruise in the southwestern Indian Ocean in May 1991.

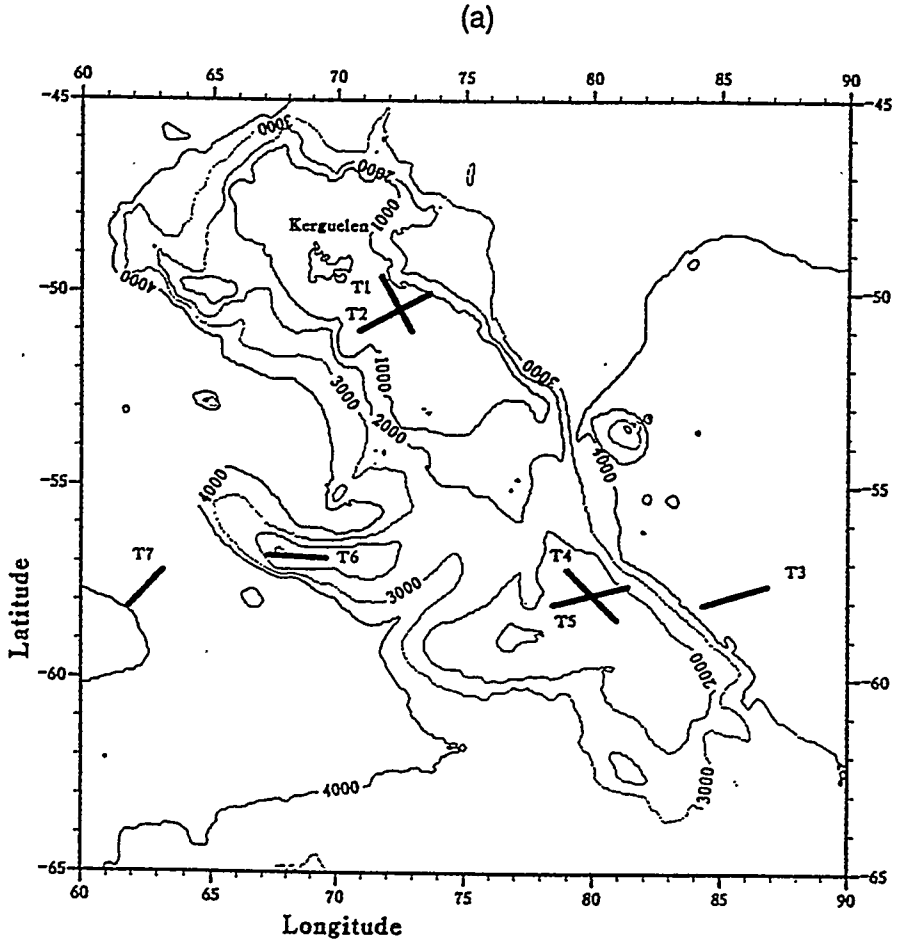

Fig. 4. (*a*) Position of the tracks T1 to T7 repeated for 3 days during the MINERVE 7 cruise in January-February 1991. (*b-h*): fCO_2 measured along daily repeated tracks shown in figure 4*a* during the MINERVE 7 cruise in January-February 1991. The dashed line represents the atmospheric fCO_2.

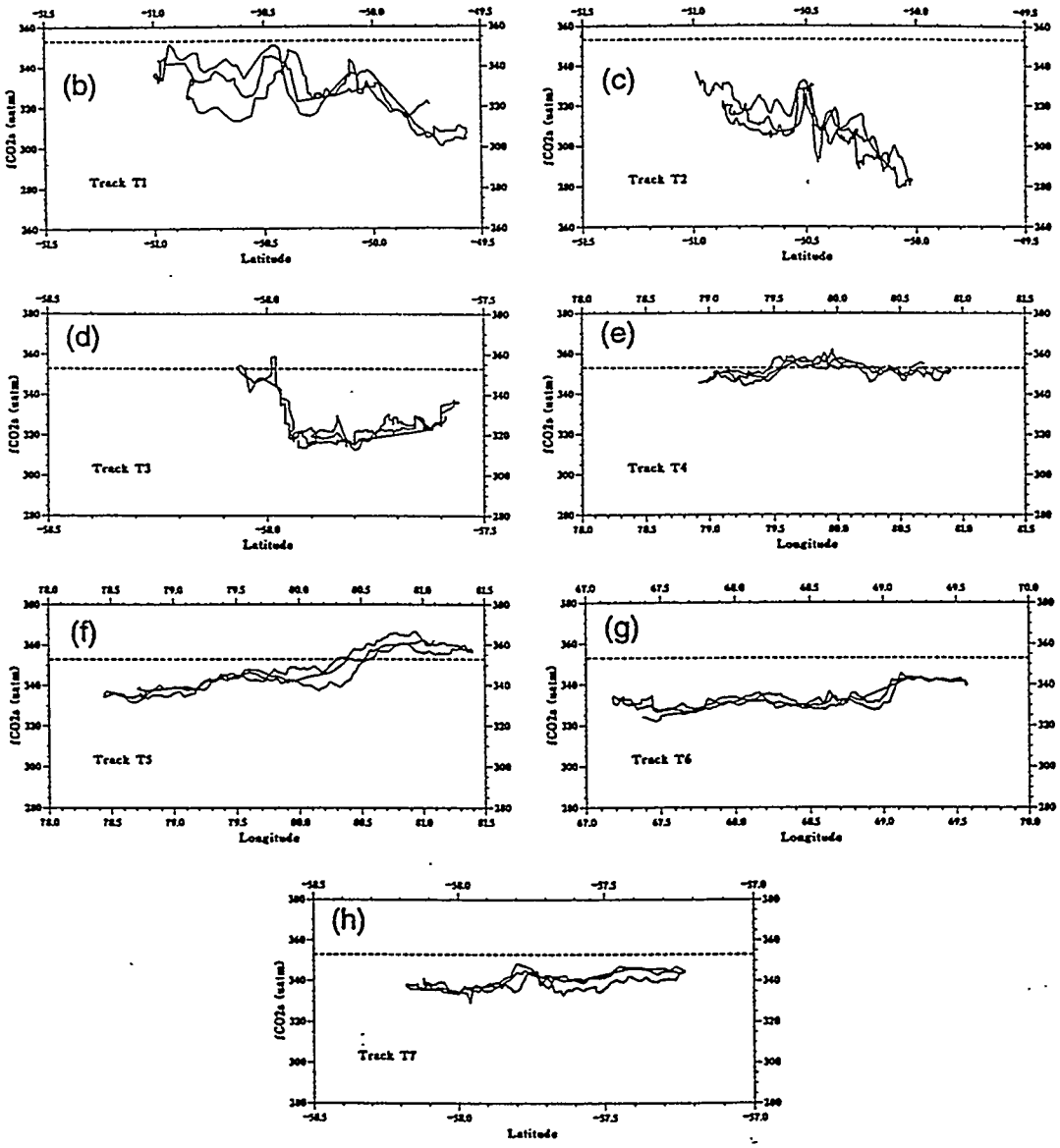

Fig. 4. (continued)

polar front (tracks T1 and T2) we also encountered large horizontal gradients reaching 2 µatm/km near 50°30'S; this was observed at each crossing (Figures 4*b* and 4*c*). Along these tracks, daily variations in fCO_2 are significant. Around 50°40'S (Figure 4*b*), fCO_2 decreased 10 µatm in 10 hours (1µatm/h) between the first and the second leg and the SST was 0.25°C colder. Between the second and the third leg, fCO_2 continued to decrease by 16 µatm in 17 hours (again about 1µatm/h) but the SST was 0.25°C warmer this time. At this timescale, several hours, one can assume that the water masses sampled are the same for the repeated track T1. This is supported by the steady position of the hydrological front we observed during the three passages. In addition, surface currents estimated in this area are generally weak [*Gambéroni et al.*, 1982; *Park et al.*, 1991]. Therefore biological activity is likely to be responsible for such rapid and continuous decrease in fCO_2 (26 µatm in 27 hours).

MONTHLY AND SEASONAL VARIATIONS

In all the MINERVE cruises, three tracks were repeated between January and August 1991: La Réunion-Crozet, Crozet-Kerguelen, and Kerguelen-Amsterdam (see Figure 1). This allows the study of monthly and seasonal fCO_2 variations at a large scale (Plates 1, 2, and 3). The track between La Réunion and Kerguelen archipelago (Plates 1*a* and 1*b*) was visited 5 times in 1991: January and February (MINERVE 7), April and May (MINERVE 9) and July (MINERVE 11). This track, from 23°S to 46°S, crosses the subtropical and Subantarctic zones. Because fCO_2 seasonal variations are regionally different, they will be described in two areas: the subtropical gyre and the frontal zone to the south of 35°S. We first describe the subtropical zone for which it is possible to compare the fCO_2 variation and budget on both monthly and seasonal scales.

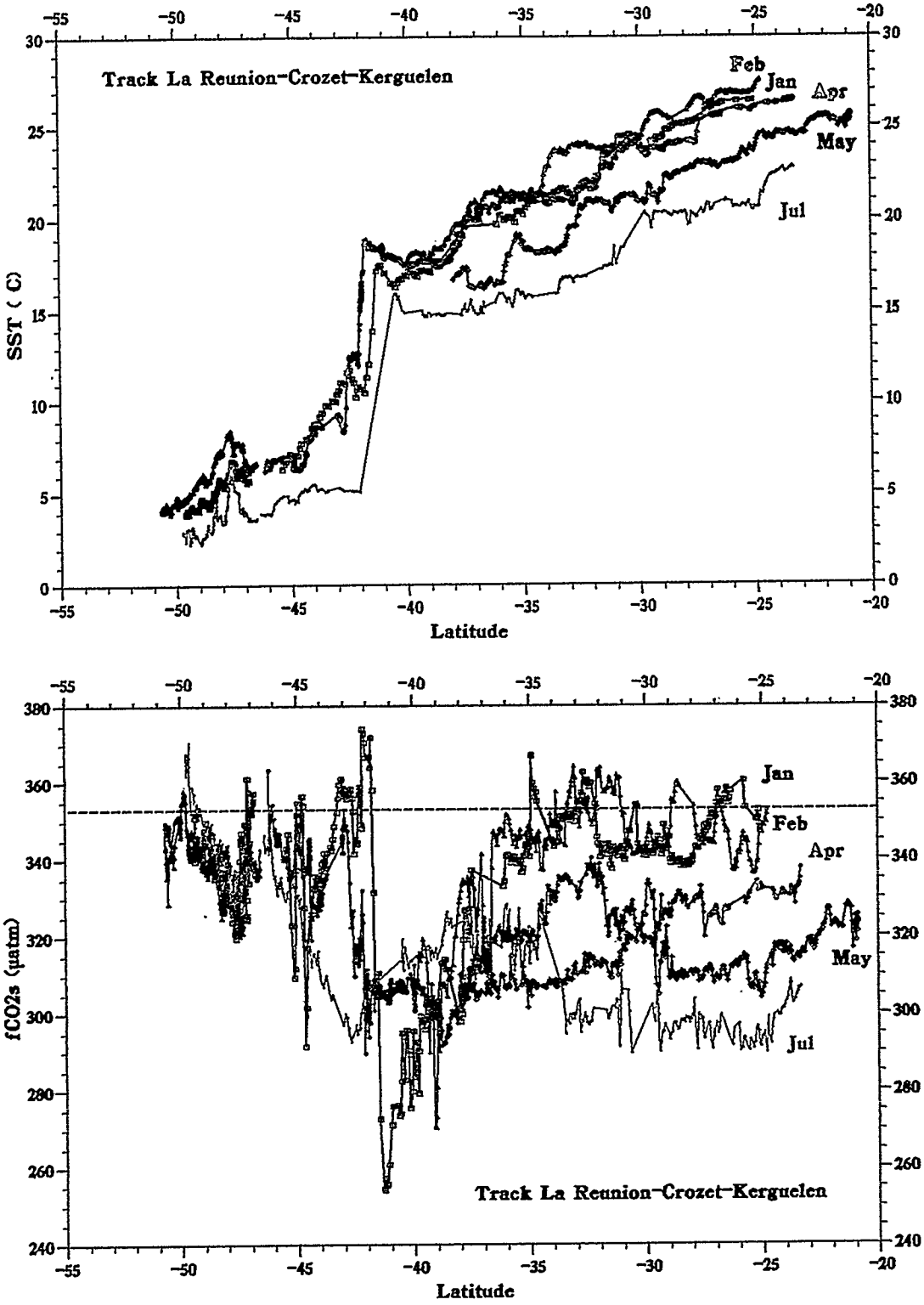

Plate 1. (*a*) Temperature and (*b*) fCO_2 along the track La Réunion-Crozet-Kerguelen during five periods from January to July 1991. The dashed line in Plate 1(*b*) represents the atmospheric fCO_2.

Subtropical Gyre

Spatial distribution. In the subtropical zone, North of 35°S, the fCO_2 spatial distribution is characterized by a series of maxima and minima which are associated with meridional SST gradients (Plate 1). One can follow these structures from month to month: for example, fCO_2 extrema observed at 33°S, 30°S, and 27°S in April have been measured again at 31°S, 29°S, and 25°S, respectively, in May. Such structures have also been encountered along the track La Réunion-Crozet during the cruise MINERVE 2 in June 1990 [*Poisson et al.*, 1991]. Measurements made in 1962 also show pCO_2 minima and maxima around 30°S to the East of

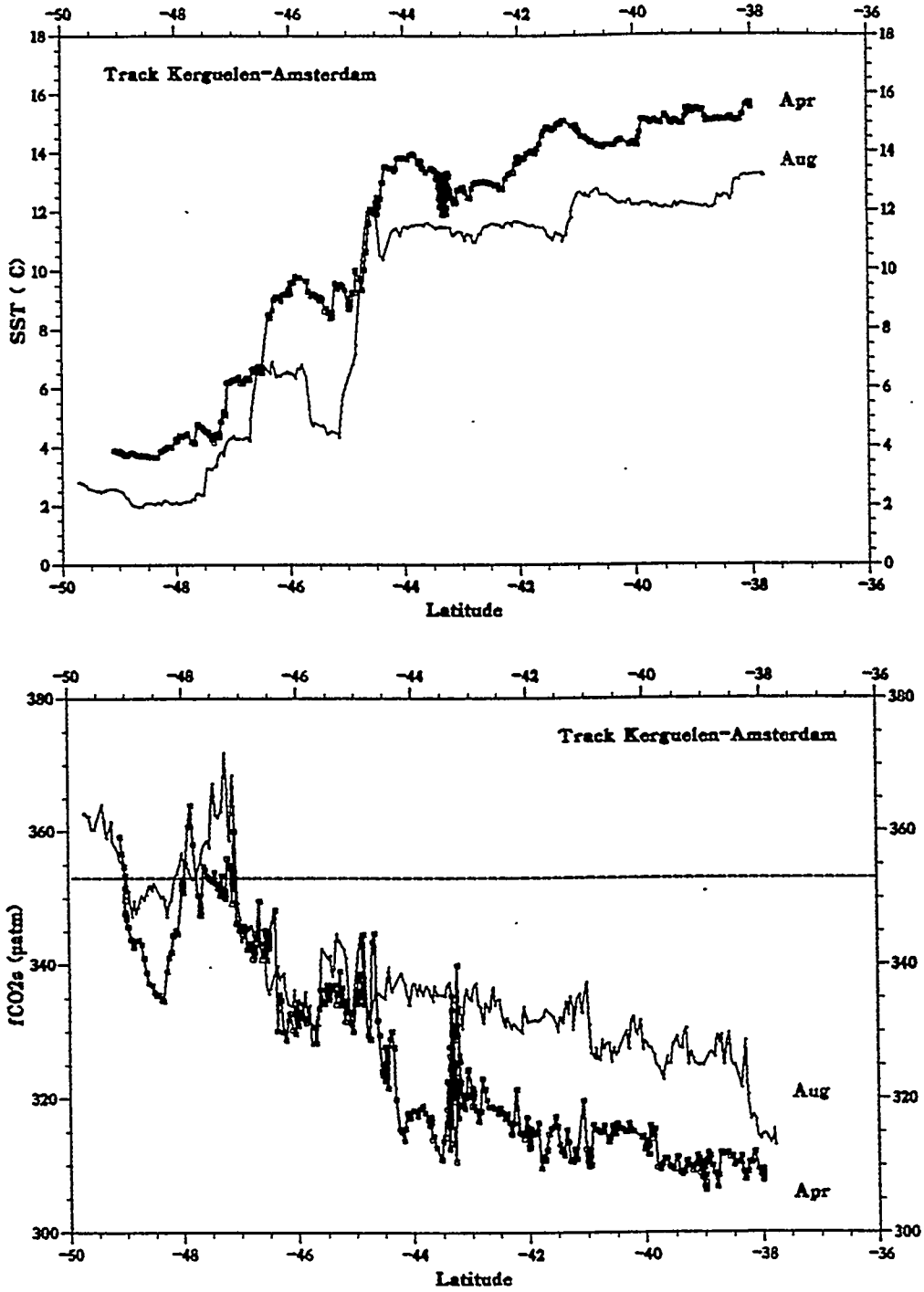

Plate 2. (*a*) Temperature and (*b*) fCO_2 along the track Kerguelen-Amsterdam in April and August 1991. The dashed line in Plate 2(*b*) represents the atmospheric fCO_2.

Madagascar [*Keeling and Waterman*, 1968]. These comparisons indicate that at monthly, yearly, or even decadal scales the sea surface fCO_2 spatial distribution (but not the fCO_2 value) maintains some specific structures which are certainly governed by large-scale and permanent processes. However, it must be noted here that the fCO_2 distribution tends to be less variable from austral summer to winter.

Temporal variations. To quantify the temporal changes in the subtropical area, we have computed the mean of the observed parameters between 23°S and 35°S (the southern boundary of the

subtropical gyre). Averages of the measured parameters are presented in Table 1 along with their standard deviations and the calculated parameters used for air-sea CO_2 flux estimates. The air-sea exchange has been computed at each fCO_2 observation using the air-sea gradient relation:

$$F = k.s.\Delta fCO_2 \quad (1)$$

where k, the piston velocity, depends on wind following the trilinear formulation proposed by *Liss and Merlivat* [1986] and depends on temperature [*Jähne*, 1980]. The CO_2 solubility (s) of a nonideal gas depends on temperature and salinity [*Weiss*, 1974].

The wind was measured each hour. To couple k with oceanic parameters in equation (1), we combine the wind data with the continuous measurements (fCO_2, SST and salinity) recorded in the following hour. For mean CO_2 flux calculations in the band 20°S-35°S this is sufficient since the hourly wind variability is weak. Moreover, wind speed is mainly in the range 3.6 to 13 m/s. Consequently, among the three regimes proposed by *Liss and Merlivat* [1986], one linear equation has been largely selected to compute the piston velocity k. High wind speeds in February lead to a high transfer coefficient (k.s=5.8 10^{-2} mol/m^2/atm/yr; see Table 1). Interestingly, it is also for February that k.s computed from meteorological winds is the largest (k.s=5.1 10^{-2} mol/m^2/atm/yr) for the area we investigate here [*Thomas et al.*, 1988]. The order of magnitude is comparable because in this region SST is close to 20°C which is the temperature normalization used by Thomas et al. We also note that mean calculations of climatological winds in the region 20°S-35°S/53°E-57°E is also a maximum in February and March [*Hellerman and Rosenstein*, 1983] when cyclone frequency is at a maximum [*Ramage*, 1983]. We thus believe that mean CO_2 fluxes computed by using wind observations on board for 2 days, the period for sailing from La Réunion to 35°S, are reasonably representative of the monthly scale.

Over the subtropical zone, averages of oceanic parameters (fCO_2, SST, salinity) are at a maximum in February and decrease regularly until July. Salinity varies weakly; its effect on CO_2 temporal variation [*Weiss et al*, 1982] will not be studied here. At a seasonal scale, from January-February to July, fCO_2 temporal variations in the subtropical zone are clear: fCO_2 is near atmospheric equilibrium in January and February; in July the potential for a CO_2 sink is large (ΔfCO_2=-60 µatm). Calculated air-sea CO_2 fluxes indicate that the subtropical CO_2 sink increases from January to July. This is governed by a progressive decrease in ΔfCO_2.

In the subtropical gyre the spatial variabilities of oceanic parameters are quite constant from month to month in contrast to the atmospheric parameters (pressure, wind); this is described by the standard deviations in Table 1. Wind variability is large in February, May, and July leading to large variability in k, k.s, and CO_2 fluxes for these months. In February the standard deviation of ΔfCO_2 is large relative to the mean, and the sign of the averaged CO_2 fluxes becomes uncertain (-0.5 ± 1 mmol/m^2/d). The mean air-sea CO_2 exchanges over the selected zone and for each period have been computed in two ways (columns 11 and 12 in Table 1). Firstly, equation (1) has been applied to each observation and the mean air-sea CO_2 fluxes correspond to the average of the indivudual CO_2 fluxes. Secondly, CO_2 fluxes has been calculated by using the average of wind, SST, and salinity (to calculate a mean transfer coefficient) and the average of ΔfCO_2. The differences of these mean CO_2 fluxes are small (maximum difference of 10% in February). This is because equation (1) is almost linear for the subtropical domain; as mentioned above, the gas transfer coefficient k has been computed by using mostly a single linear function depending on

TABLE 1. Mean and Standard Deviation of Parameters Measured and Calculated in the Domain 23°S-35°S (see plate 2)

		Measured Parameters						Calculated Parameters			
Period	Number of Data	fCO_2 µatm	ΔfCO_2 µatm	Temperature °C	Salinity	Patm mb	Wind (10 m) m/s	k cm/h	k.s (x100) mol/m^2/yr/µatm	CO_2 flux mmol/m^2/d	CO_2 flux(mean)* mmol/m^2/d
						Mean					
January	173	347.2	-9.59	23.76	35.42	1023.9	5.8	7.6	1.9	-0.47	-0.51
February	200	348.2	-3.88	24.90	35.51	1010.5	10.6	23.5	5.8	-0.53	-0.62
April	214	328.8	-28.25	23.72	35.46	1024.8	6.4	9.5	2.4	-1.84	-1.89
May	303	314.1	-41.98	22.40	35.41	1021.7	7.0	11.8	3.1	-3.45	-3.39
						Standard Deviation					
January	173	6.7	6.78	1.82	0.10	0.9	1.2	4.0	1.0	0.39	
February	200	6.8	6.62	1.73	0.12	3.7	1.9	6.3	1.5	1.07	
April	214	4.7	4.98	1.82.	0.17	5.0	1.2	3.8	1.0	0.77	
May	303	5.5	6.26	2.26	0.23	3.4	2.8	7.9	2.0	2.28	
July	198	6.2	5.75	2.10	0.15	2.6	2.5	6.3	1.8	2.99	

The wind dependent gas exchange k is calculated by using the relation of *Liss and Merlivat* [1986] and a temperature dependent schmidt number [*Jähne*,1980].
For k.s we used a temperature and salinity dependent CO_2 solubility coefficient proposed by *Weiss* [1974].
* See the text for explanations of the two ways to calculate the mean CO_2 flux

wind speed. The weak and constant variabilities and the small differences in CO_2 flux computations justify the choice of meridional extension (20°S-35°S) to estimate the fCO_2 budgets presented below.

To describe the processes (thermodynamic, air-sea exchanges, biological activity, and mixing) which govern these variations, we separate the fCO_2 temporal changes according to the equation

$$\Delta f/\Delta t = [\delta f/\delta t]_T + [\delta f/\delta t]_F + [\delta f/\delta t]_B + [\delta f/\delta t]_K \qquad (2)$$

where f stands for fCO_2, $\Delta f/\Delta t$ is the temporal fCO_2 variatons during the period Δt, $[\delta f/\delta t]_T$ represents the fCO_2 variations due to changes in SST, $[\delta f/\delta t]_F$ represents the fCO_2 variations due to air-sea exchanges, $[\delta f/\delta t]_B$ represents the fCO_2 variations due to biological activity and $[\delta f/\delta t]_K$ represents the fCO_2 variations due to water mixing.

The measurements made on board allow us to quantify the first three terms in equation (2). The other terms $[\delta f/\delta t]_B$ and $[\delta f/\delta t]_K$ will be considered as the difference, $\Delta f/\Delta t - [\delta f/\delta t]_T - [\delta f/\delta t]_F$.

Seasonal budget. From January to July we observed a total variation of -48 µatm over 204 days and $[\delta f/\delta t]_T$=-56 µatm/204d using fCO_2 temperature dependent relations established by *Copin-Montegut* [1988, 1989*a*, *b*) together with the observed $\Delta T/\Delta t$ = -4.2°C/204d. The net residual $Df/Dt-[\delta f/\delta t]_T$ or $[\delta f/\delta t]_F+[\delta f/\delta t]_K+[\delta f/\delta t]_B$ is 8 µatm/204 days (or 0.04 µatm/d). To balance the budget of $\Delta f/\Delta t$ in equation (2) the sum of the other processes (air-sea exchange, biological activity, mixing) should be close to zero at seasonal scale (Table 2) and one can conclude that the SST variations explain the seasonal fCO_2 variations observed in the subtropical zone. This was also the conclusion of *Goyet et al.* [1991] in the same region and of *Weiss et al.* [1982] in the South Pacific subtropical gyre.

Monthly budgets. We now look at the terms of the fCO_2 budget (equation (2)) on a monthly scale (Table 2). We include here the quantification of the term $[\delta f/\delta t]_F$. It is integrated daily by assuming a linear temporal evolution of the air-sea CO_2 fluxes between each period of measurements and of the depth of the mixed layer, Zm, taken from the Indian Ocean atlas of *Wyrtki* [1971, plate 328-331]. Total dissolved inorganic carbon (DIC) and buffer factor $ß=\partial \ln[fCO_2]/\partial \ln[DIC]$ are taken from the literature. Measurements made during the INDIGO cruise in February-March 1985 on the transect La Réunion-Crozet show that surface DIC increases southward from 1957 µmol/kg at 23°S to 2027 µmol/kg at 35°S [*Poisson et al.*, 1988]. When averaging over five INDIGO stations between 23°S and 35°S, one obtains 1996.8 µmol/kg. A comparison between March 1985 and July 1985 showed that maximum seasonal DIC variations do not exceed 50 µmol/kg in this region [*Goyet et al.*, 1991]. Note that a variation of 2.5% in DIC or 5% in ß only affects $[\delta f/\delta t]_F$ weakly. For our purpose we have chosen a fixed value of DIC (DIC=2000 µmol/kg) and of ß (ß=8.5, used by *Weiss et al.* [1982] for the subtropical zone in the South Pacific).

From January to February the observed variation in fCO_2 is small ($\Delta f/\Delta t$= 1 µatm/46d; see Table 2 and Plate 1). During this period the temperature increases by 1°C; the thermodynamic effect leads to an increase of 16.5 µatm for fCO_2 (Table 2). We have seen that the observed fCO_2 is near atmospheric equilibrium for both January and February. The net accumulation of CO_2 by air-sea exchange would be smaller than 1 µatm. The residual of budget (equation (2)) $\Delta f/\Delta t-[\delta f/\delta t]_T-[\delta f/\delta t]_F$ or $[\delta f/\delta t]_K+[\delta f/\delta t]_B$ tells us that biological activity and mixing should decrease fCO_2 by 16 µatm during this period, which is the same amount as the SST effect. From February to April, decreasing SST explains the

TABLE 2. Observed Variations of fCO_2 ($\Delta f/\Delta t$) and Temperature ($\Delta T/\Delta t$) Between Period of Measurements and Calculated fCO_2 Change Due to Temperature Variation $(\delta f/\delta)_T$ or Due to Air-Sea Exchange $(\delta f/\delta)_F$.

Period	Observed Variations			Thermodynamical Effect			Estimated Air-Sea Exchange Effect			Residual Budget
	Δt,	$\Delta f/\Delta t$,	$\Delta T/\Delta t$,	$(\delta f/\delta)_T$,		$\Delta f/\Delta t-(\delta f/\delta)_T$,	CO_2 flux,	Zm,	$(\delta f/\delta)_F$,	$\Delta f/\Delta t-(\delta f/\delta)_T-(\delta f/\delta)_F$
	day	µatm/Δt	°C/Δt	µatm/Δt	µatm/day	µatm/Δt µatm/day	mmol/m2/d	m	µatm/Δt µatm/day	µatm/Δt µatm/day
From Jan. to July	204	-48	-4.20	-56.0	-0.27	8.0 0.04	0.47 to 4.66	40 to 100	10.45 0.05	-2.45 -0.01
From Jan. to Feb.	46	1	1.14	16.5	0.36	-15.5 -0.34	0.47 to 0.53	40	0.83 0.02	-16.33 -0.36
From Feb. to April	52	-19	-1.18	-16.0	-0.31	-3.0 -0.06	0.53 to 1.84	40 to 60	1.75 0.03	-4.75 -0.09
From April to May	35	-15	-1.30	-17.3	-0.49	2.3 0.07	1.84 to 3.45	60 to 80	1.77 0.05	0.53 0.02
From May to July	71	-15	-2.85	-35.6	-0.50	20.6 0.29	3.45 to 4.66	80 to 100	4.23 0.06	16.37 0.23

The difference $\Delta f/\Delta t-(\delta f/\delta)_T$ must be balanced by air-sea exchange, biological activity and mixing (see text, equation (2)).
The difference $\Delta f/\Delta t-(\delta f/\delta)_T-(\delta f/\delta)_F$ must be balanced by biological activity and mixing.
Zm is the mean depth of the mixed layer [*Wyrtki*, 1971].

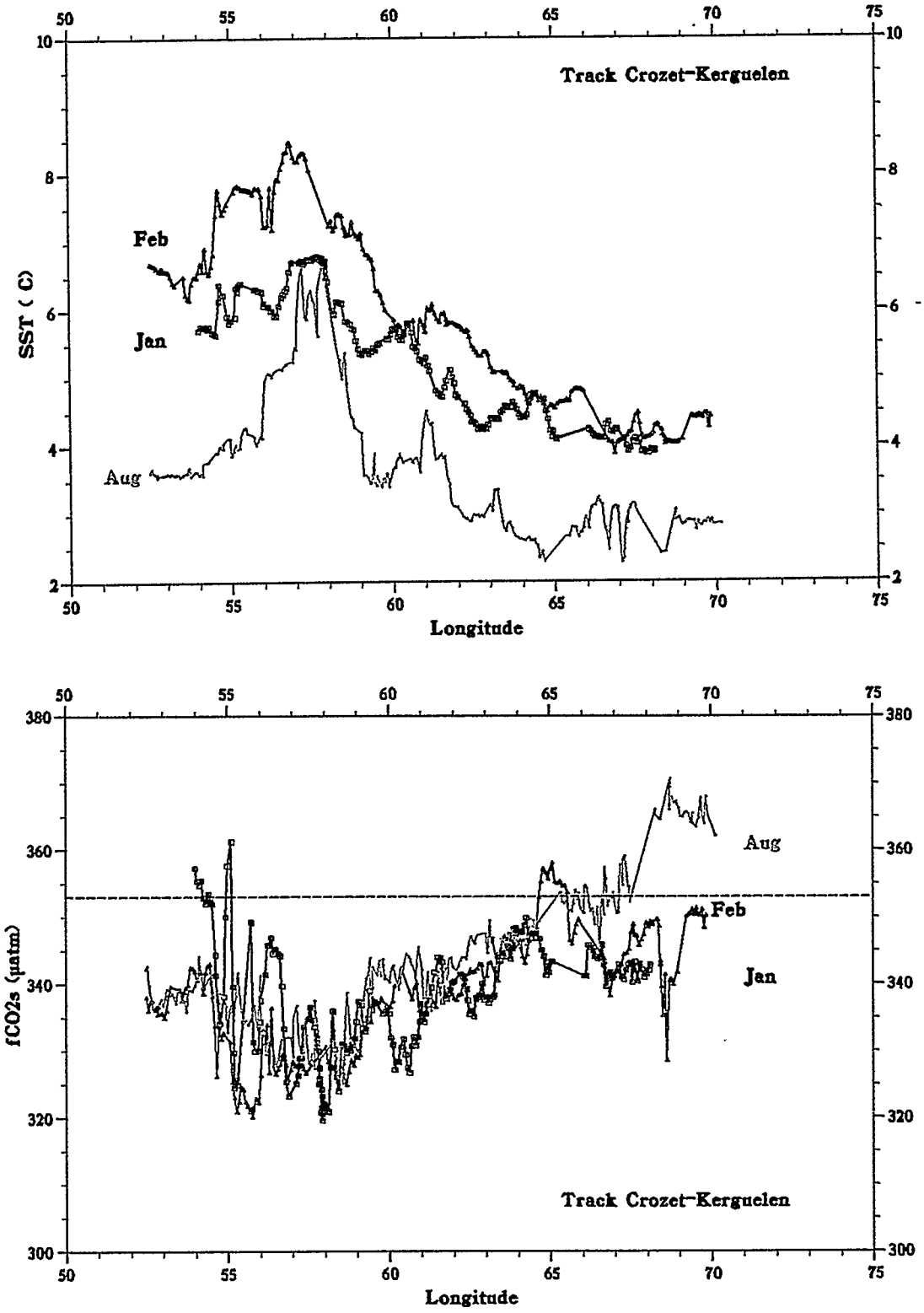

Plate 3. (*a*) Temperature and (*b*) fCO_2 along the track Crozet-Kerguelen in January, February and August 1991. The dashed line in Plate 3(*b*) represents the atmospheric fCO_2.

observed fCO_2 variations; the difference $\Delta f/\Delta t$-$[\delta f/\delta t]_T$ is low (-0.06 µatm/d). This is also the case from April to May (0.07 µatm/d). The subtropical CO_2 sink is well formed in April and air-sea exchange tends to increase fCO_2 by 2 µatm. The daily residual $\Delta f/\Delta t$-$[\delta f/\delta t]_T$-$[\delta f/\delta t]_F$ is negative and low for the period February to April; it is positive and low from April to May (this is 6 to 10 times lower than summer period residuals).

From May to July the fCO_2 decrease due to SST variations is large (-36 µatm/71d). To balance the observed fCO_2 change (-15 µatm/71d) one has to take other processes into account. The

subtropical CO_2 sink is potentially important (-42 µatm in May, -60 µatm in July) but is not sufficient to balance the large fCO_2 decrease due to thermal effects. In winter the mixed layer is deeper: it tends to minimize the net gain of CO_2 by air-sea exchanges and to increase the mixing with subsurface water. The positive residual results from a significant supply of CO_2 by mixing and a rather ineffectual CO_2 pumping by photosynthesis. If one cannot separate the roles of biology and of mixing here, the temporal evolution of the residuals qualitatively indicates the relative role of the processes governing fCO_2 in the subtropical zone. In summer, biological activity dominates over mixing (the residual is negative). From February to May both processes are in balance (residuals are small). From May to July the mixing overrides the CO_2 pumping by photosynthesis (the residual is positive).

This was not revealed by the seasonal information alone. Computing budget (equation (2)) with only the January and July data (row 1 in Table 2) would overestimate the thermodynamic effect by 7% and the air-sea exchange effect by 20%. Compared to the sum of the budgets computed for each period, the seasonal residual differs by 41%. This is related to the nonlinearity of the temporal variations of various terms in equation (2). As already mentioned by *Taylor et al.* [1991], the knowledge only of seasonal fCO_2 leads to uncertainties in CO_2 flux estimate. We also see that conclusions on processes governing the fCO_2 budget can change when subseasonal data are available.

Frontal Zone

South of 35°S, four hydrological fronts have been crossed: the front associated with the Agulhas return current (AGR), the subtropical convergence (STC), the subantarctic front (SAF), and the polar front (PF). In the southwestern area of the Indian Ocean the subtropical gyre, the southeastern Madagascar current, the Agulhas current, the Agulhas return current, and the circumpolar current form a zone of well-known high dynamical variability at a mesoscale, as shown by in situ observations [*Lutjeharms*, 1981], altimeter data [*Cheney et al.*, 1983; *Gordon et al.*, 1983], drifting buoys [*Daniault and Ménard*, 1985] and models [*Semtner and Chervin*, 1988, 1992; *Webb et al.*, 1991]. These turbulence scales are reflected in the fCO_2 distributions for which spatial and temporal variations are less clear compared to the subtropical zone.

To the north of the STC. Between 35°S and the northern boundary of the STC (around 40°S),. the meridional fCO_2 gradients are large in January and February (Plate 1) and should be governed by biological enhancement associated with the AGR frontal zone as has been observed in the Agulhas current system in summer [*Lutjeharms et al.*, 1985]. In April and May there is a decrease of fCO_2 in the band 35°S-38°S (as in the subtropical zone), but in July, although SST is lower, fCO_2 comes back to the level observed in April. We also observed a winter fCO_2 increase to the north of the subtropical convergence (38°S-44°S) along the transect between Kerguelen and Amsterdam (Plate 2). The winter fCO_2 increase in this latitudinal band may originate from the wind which is stronger during this season [*Taljaard and Van Loon*, 1983]. Firstly, low winds in summer would increase the stratification, which is an important factor for primary productivity. On the other hand, higher winds would increase the gas transfer coefficient and thus the air-sea CO_2 flux but they also increase the mixed layer depth increasing the mixing with CO_2-enriched subsurface waters. The latter process would reduce the net gain of CO_2 due to air-sea exchanges in this sink zone. The processes governing winter fCO_2 increase in this region can be found in such explanations. For a quantitative estimate as in equation (2) we need more data in a region where fCO_2 variations are significant but lower and much less clear than in the subtropical gyre.

STC and SAF zone. In summer the STC and SAF are marked by large fCO_2 spatial variations to the west and to the east (Plates 1*b* and 2*b*). In summer these large gradients near the fronts can be related to localized biological activity [*Jacques and Minas*, 1981; *Lutjeharms et al.*, 1985; *Metzl et al.*, 1991]. In winter the fCO_2 distribution is more homogeneous with a regular increase southward from 42°S to 46°S (Plates 1*b* and 2*b*). The reasons for winter homogeneity have been indicated previously as due to higher winds. In addition, for the STC and SAF zone we know that primary productivity is lower in winter [*Krey and Babenerd*, 1976]. Along the track La Réunion-Crozet the center of the STC (around 42°S) marks a typical boundary with regard to temporal variations: to the south (42°S-46°S), fCO_2 decreases from January to July; to the north (37°S-41°S), fCO_2 increases from January to July. The latter increase was also observed along the eastern track, north of 44°S (Plate 2*b*). Note that around 43°S the ship sailed in a circle for 1 day explaining relatively large SST and fCO_2 variations at this latitude (Plate 2) and indicating that high fCO_2 variations, up to 25 µatm, can exist at small scale in the region. To the south (45°S-50°S) the signals of spatial and temporal variations are quite confused. This has to be related to the complex dynamics in the area where one observes a confluence of the STC and the SAF and where the polar front is shifted to the north because of bottom topography near the Kerguelen plateau [*Gambéroni et al.*, 1982; *Park et al.*, 1991].

Polar front zone. In the polar front zone, between Crozet and Kerguelen, the seasonal fCO_2 distribution varies weakly (Plate 2). Along the three tracks made in January, February, and August, a SST maximum and a fCO_2 minimum have been found at around 57°E. From there the SST decreases and fCO_2 increases southeastward. High and low fCO_2 levels around 68°E correspond to measurements made when approaching the Kerguelen islands. Contrary to observations made in the the subtropical regions, fCO_2 seasonal variations are weak although there are significative SST variations. To balance a fCO_2 decrease of about 30 µatm from January to August (this corresponds to observed SST decrease), one must take into account physical processes (stronger mixing in winter) and air-sea exchanges which tend to increase fCO_2.

LARGE-SCALE SEASONAL ΔfCO_2 DISTRIBUTIONS

The monthly and seasonal variations observed in the subtropical and Subantarctic regions are such that we have chosen to describe the large-scale ΔfCO_2 distribution in two periods: January to April (Plate 4*a*) and May to September (Plate 4*b*). Note that cruises in the northern Indian Ocean occurred from June to September only. Data for ΔfCO_2 presented in Plate 4 have been calculated for each fCO_2 observation (about 18000 observations) and relative to the mean atmospheric CO_2 measured on board from January to September. Temporal varations of the CO_2 concentration in air have not been taken into account here beause they are very weak compared to oceanic variations. However, quite a large atmospheric fCO_2 interhemispheric gradient was observed around 12°N. Therefore for the whole Indian basin south of 12°N, ΔfCO_2 was calculated with a mean atmospheric fCO_2 of 353.2 µatm; north of 12°N the atmospheric mean is 358.2 µatm (in the Gulf of Aden and the Red Sea).

Equatorial and tropical zones. In the Indian Ocean this area is a CO_2 source as has been previously observed [*Keeling and Waterman*, 1968; *Miyake and Sugimura*, 1969; *Poisson et al.*, 1991] similar to the corresponding sectors in the Atlantic [*Keeling*, 1968; *Smethie et al.*, 1985; *Andrié et al.*, 1986] and Pacific [*Keeling et al.*, 1965; *Miyake et al.*, 1974; *Feely et al.*, 1987; *Murphy et al.*, 1991*a*, *b*; *Inoue and Sugimura*, 1988, 1992; *Lefevre and Dandonneau*, 1992; *Wong et al.*, 1993]. However, in September 1991 there was a significant sink zone around 80°-

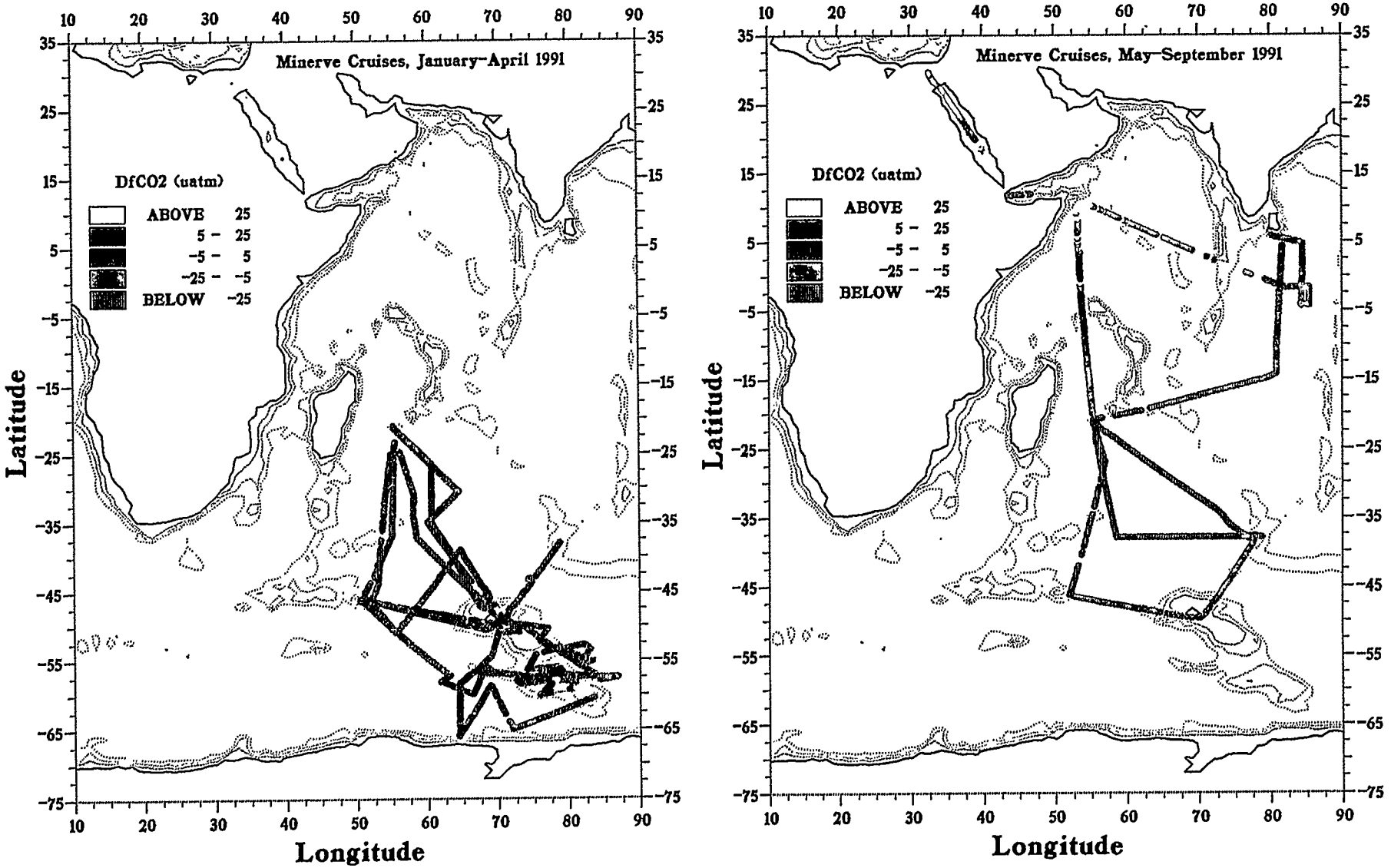

Plate 4. ΔfCO_2 maps obtained during MINERVE cruises in 1991: (*a*) for the period January-April and (*b*) for the period May-September. The color scale corresponds to CO_2 sources zones (yellow and red), near equilibrium (brown) and CO_2 sink zones (green and blue).

85°E south of the equator; in July-September 1962 this region was a source [*Keeling and Waterman*, 1968]. Compared to 1962 data, 1991 sea surface fCO_2 is higher of about 10 µatm in that region; during this 30-year period the increasing of atmospheric fCO_2 is about 40 µatm. This source to sink transition is due to the atmospheric CO_2 increase. In June 1991, large gradients and high fCO_2 (> 400 µatm) have been encoutered around 10°N in the upwelling areas formed during the summer monsoon offshore from the Somali coast. High fCO_2 have also been measured in the Gulf of Aden and in the Red Sea where CO_2 fluxes are generally larger in the south than in the north of the basin [*Metzl et al.*, 1989]. Along the Red Sea (13°N-27°N), fCO_2 decreases regularly northward (this is strongly correlated to SST distribution; see Figure 5) and at 23°N it is below the equilibrium level (a CO_2 sink).

Subtropical zone. The subtropical gyre (15°S-35°S) is a CO_2 sink from January to September. This was also observed by *Keeling and Waterman* [1968] in the zonal band 15°S-45°S in November-December 1962 (in 1991 we have no data for this period) and by *Goyet et al.* [1991] in the zonal band 30°S-40°S in July 1984. On a large scale the subtropical gyre in the Indian Ocean appears to act as a CO_2 sink along the year (this is clearly revealed on a north-south section; Figure 5*b*). We note however that significant variations exist at smaller scales. In January and February, near-equilibrium or CO_2 source zones have been observed (red and brown dots in Plate 4*a*). From May to September the subtropical CO_2 sink is much more homogeneous (blue dots in Plate 4b).

Frontal zone. The lowest ΔfCO_2 observations (<-60 µatm) are located around 40°S in the so-called "circumpolar sink zone" [*Takahashi and Chipman*, 1985]. The sink is permanent with extreme negative values in January and February (Plate 1). To the south, between the SAF and the PF, ΔfCO_2 increases rapidly (Figure 5*b*). In the shallow oceanic domain near the Crozet and Kerguelen archipelagos, spatial and temporal variability in ΔfCO_2 is large.

Antarctic zone. The southern ocean (south of the polar front) was visited from January to March (Plate 4*a*). The observations show a mosaic of CO_2 sink, source, and near-equilibrium zones. On a mesoscale and smallscale (100 km-10 km), fCO_2 variabilities can be large especially around 60°S-80°E. In this area the origin of localized minima and maxima in fCO_2 as well as in other biogeochemical parameters such as chlorophyll [*Krey and Babenerd*, 1976, map n°23; *Goffart and Hecq*, 1989] is probably associated with the high dynamical variability on a mesoscale that is observed in the region of the Kerguelen plateau [*Cheney et al.*, 1983]. Near the packice, low fCO_2 was found in February 1991 at 65°E as in January 1987 at the same location where high chlorophyll values were observed [*Metzl et al.*, 1991]. The large fCO_2 variability leads to a high variability in the air-sea CO_2 fluxes. For example, the average of instantaneous air-sea CO_2 fluxes calculated using equation (1) along the track of the MINERVE 8 cruise south of 50°S is 1.5 [±4.6] mmol/m²/d or 0.5 [±1.7] mol/m²/yr (see the corresponding track in Figure 1). The average is comparable to CO_2 fluxes estimated in some region of the Pacific sector of the southern ocean [*Murphy et al.*, 1991*b*]. In

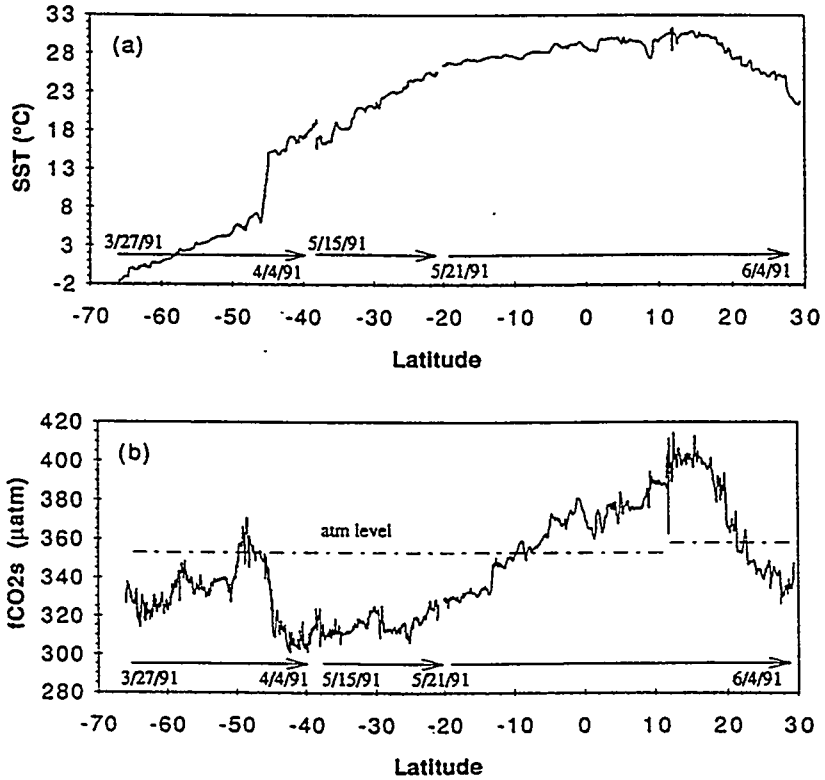

Figure 5. (*a*) A complete north-south profile of temperature and (*b*) fCO_2 along the western Indian Ocean. The profile was constructed by using observations from MINERVE 8 (from 67°S to 38°S), MINERVE 9 (38°S-22°S) and MINERVE 10 (22°S-30°N). The dashed line in Figure 5*b* represents the atmospheric fCO_2 (353.2 µatm south of 12°N and 358.2 µatm north of 12°N).

our computation the large CO_2 flux standard deviation is related to observed ΔfCO_2 spatial variability [6.6 ±20 µatm]. We conclude that during February 1991 the 60°E-90°E zone of the southern ocean was a CO_2 source region, on average, but with a large spatial variability.

RELATIONS BETWEEN fCO_2 AND SEA SURFACE HYDROLOGICAL PROPERTIES

The potential CO_2 sink/source zones are now relatively well identified in the western Indian Ocean. However, spatial and temporal variations are such that it is still unrealistic to interpolate fCO_2 observations to construct fCO_2 continuous fields in order to validate global ocean carbon models or to estimate the air-sea CO_2 fluxes (and associated errors) on the overall domain. A possible direct way to improve the planetary air-sea CO_2 fluxes would consist in coupling nearly continuous information on hydrological or biogeochemical properties with sporadic in situ fCO_2 observations. In this way, *Tans et al.* [1990] extrapolate ΔpCO_2 in areas where observations were not available, by coupling regional and nonseasonal pCO_2/SST relationships with a climatological SST data set. In the near future this could be achieved by coupling remote sensing data (SST, color of the sea) with in situ fCO_2. As a first step toward such an approach we describe the relations between fCO_2 and in situ hydrological parameters obtained on the whole domain between 10°N and 67°S in the western Indian Ocean in each of the two seasons defined in the previous section (January to April and May to September).

Considering the SST/salinity characteristics of the regions we explored during each season in 1991 (Figures 6*a* and 6*b*), the whole area can be treated as four zones.

The equatorial and tropical zone. this has been mainly sampled in June and September (austral winter season). This area extends southward to the hydrological front around 10°S which is well defined by a salinity meridional gradient. The tropical zone is characterized by high SST and high-salinity. The whole area includes the high salinity signal of the Red Sea and the low SST in the Somali gyre.

The subtropical gyre. This region was visited during both seasons. It is well defined by its maximum in salinity located at 30°S-35°S. The SST range varies from 18°C<SST<28°C in summer to 16°C<SST<24°C in winter [*Wyrtki*, 1971]. At the salinity maximum location, the SST varies from 24°C in summer to 22°C-18°C in winter depending on the longitude.

The frontal zone: this includes the STC, the SAF and the PF. The SST range varies from 8°C<SST<18°C in summer and from 6°C<SST<16°C in winter within the STC and SAF; the salinity range is about 35.5-33.5 for both seasons.

The Antarctic waters. The oceanic region south of the PF was visited mostly in austral summer. The Antarctic waters are characterized by low SST (<6°C) and low salinity which increases when approaching the Antarctic divergence.

In these four regions the fCO_2/SST and fCO_2/salinity plots (Figures 6*c*-6*f*) show very distinctive patterns. In a similar fashion to SST/salinity diagrams these plots represent mainly how fCO_2 is spatially distributed with regard to water mass variations at a large scale; they also enable us to identify anomalies from the general shapes.

In the tropics and the subtropical gyre the fCO_2/SST trend is positive: in austral summer (Figure 6*c*) the region which corresponds to the positive trend extends southward to the STC; in winter (Figure 6*d*) the positive trend is limited in the south to the center of the subtropical gyre at 30°S. Similar positive fCO_2/SST trends have been also reported in the 0°-5°S Atlantic region [*Oudot and Andrié*, 1986] and in the eastern Pacific [*Murphy et al.*, 1991*a*]

The fCO_2/salinity plots show important seasonal changes. In summer (Figure 6*e*) the in situ data are much like a coarse cloud with a positive trend for salinities higher than 35; in winter (Figure 6*f*), two groups emerge starting from a minimum in salinity around 34. The domain where the fCO_2/salinity relationship is positive corresponds to the equatorial bands. For the subtropical region the fCO_2/salinity relation is negative, opposite to the summer distribution; the winter negative fCO_2/salinity relation also includes the frontal zone.

The northern edge of the frontal zone shows an abrupt change in the shapes. The relation between fCO_2 and SST is now clearly negative between 18°C and 6°C. It is less clear in the fCO_2/salinity plots because salinities 33.5-34 are found in both the frontal zone and in the Antarctic waters. As for the subtropical zone, we also identified seasonal differences in the frontal zone. During the summer the well-defined fCO_2/SST relationship involves the north of the frontal zone (STC and SAF); in winter, the negative fCO_2/SST relation concerns the region between the center of the subtropical gyre and the STC. It should be noted that the distribution of fCO_2/SST observed in the Indian Ocean for the range 8°C<SST<13°C is quite comparable to the relation that has been observed in the North Atlantic for the same SST range [*Watson et al.*,1991].

In the southern ocean (SST<6°C, salinity<34), where the fCO_2 spatial variability at mesoscale is large compared to the variability of the hydrological properties, no trend can be identified.

In the western Indian Ocean, from 10°N to 50°S, the fCO_2 distribution is not random when compared with the distribution of the hydrological properties; clear but different relations exist within the tropical, subtropical and frontal zones, especially for fCO_2/SST plots. An important discontinuity is observed at the northern boundary of the circumpolar waters. It thus appears that regional and seasonal variations have to be taken into account if we want to quantify these property/property relationships and to use them to extrapolate fCO_2 where and when data are not available. However, it will not be possible from such a computation to represent the fCO_2 distribution in regions where mesoscale forcing dominates and for which fCO_2/SST anomalies clearly differ from the general pattern. Measurements made in the Somali gyre in June and September (Figures 6*d* and 6*f*), in the frontal zone in January and February or in the southern ocean (Figures 6*c* and 6*e*), show large anomalies in the fCO_2/SST and fCO_2/salinity patterns. They indicate spatial distributions which are not representative of the large oceanic scale. Most of these anomalies correspond to local biological activities which are not revealed by the SST distribution. Therefore relations between fCO_2 and biological properties, like chlorophyll [*Watson et al.*, 1991], are needed to extend the present descriptions.

CONCLUSIONS

The contemporary fCO_2 data obtained during the MINERVE cruises from January to September 1991 show that at large scale and in areas where a comparison can be made, the fCO_2 distribution has not changed fundamentally since the 1960s: the equatorial and tropical Indian Ocean is a CO_2 source for the atmosphere; a new feature concerns a subequatorial sink zone near 80°E. The large subtropical zone and the narrow but windy Subantarctic zone are potential CO_2 sinks. These sinks vary significantly from summer to winter. A next step would be to compare at decadal scale, not only the fCO_2 distribution but also the fCO_2 level. At mesoscale and small spatial scales the continuous measurement techniques reveal very high fCO_2 variability that was not observed previously. This is particularly important in the regions where dynamic variability is high like the

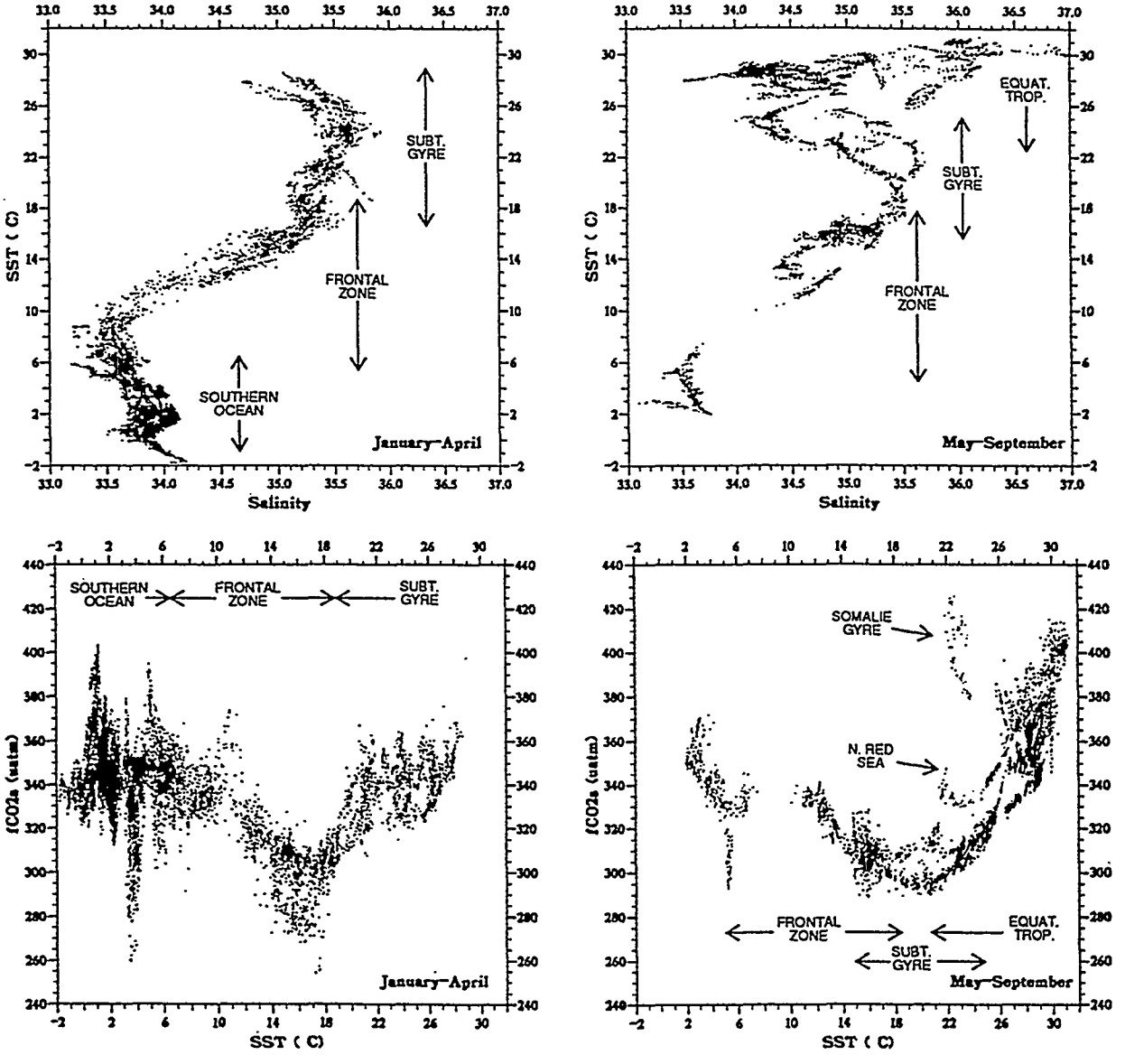

Figure 6. Temperature/salinity and fCO_2/temperature or salinity diagrams for the whole MINERVE measurements (18000 observations) in the Indian and Southern oceans in 1991. The two periods, January-April and May-September are indicated in the Figures.

northwestern Indian Ocean and near the frontal zones. In the newly explored regions of the southern ocean our observations show very high spatial variability at mesoscale (see Plate 4*a*): the ocean acts as a CO_2 source or sink depending on the area. This implies a very large variability on flux estimates: for example, mean CO_2 flux was 1.5 (±4.6) mmol/m^2/d for the zone of the southern ocean visited in February 1991 (see Figure 1, cruise MINERVE 8 south of 50°S]. If we use a climatological wind data set [*Hellerman and Rosenstein*, 1983] for the gas transfer coefficient calculation, one obtains a mean CO_2 flux of 0.8 mmol/m^2/d toward the atmosphere. Recall that this calculation does not include the uncertainty of the gas transfer coefficient determination, the latter being generally the parameter selected for sensitivity studies in air-sea CO_2 flux estimates [e.g., *Murphy et al.*, 1991*b*]. In the sea surface Antarctic waters, where SST variations are weak, localized primary productivity and mesoscale dynamic processes certainly have an important role to explain the high-frequency fCO_2 spatial variability, especially in the regions where bottom topography changes abruptly.

Repeated tracks made in 1991 provide a first picture of monthly fCO_2 distributions at large scales. These observations show that temporal fCO_2 variations are different in subtropical and frontal zones. Figure 7 is a schematic representation of the seasonal ΔfCO_2 distribution for the latitudinal band 20°S-50°S in the western Indian Ocean. In the subtropical zone the structure of the ΔfCO_2 distribution appears steady, but ΔfCO_2 levels vary enormously from summer to winter. In January, ΔfCO_2 was about -10 µatm on average. Interestingly, this is the mean $\Delta pCO2$

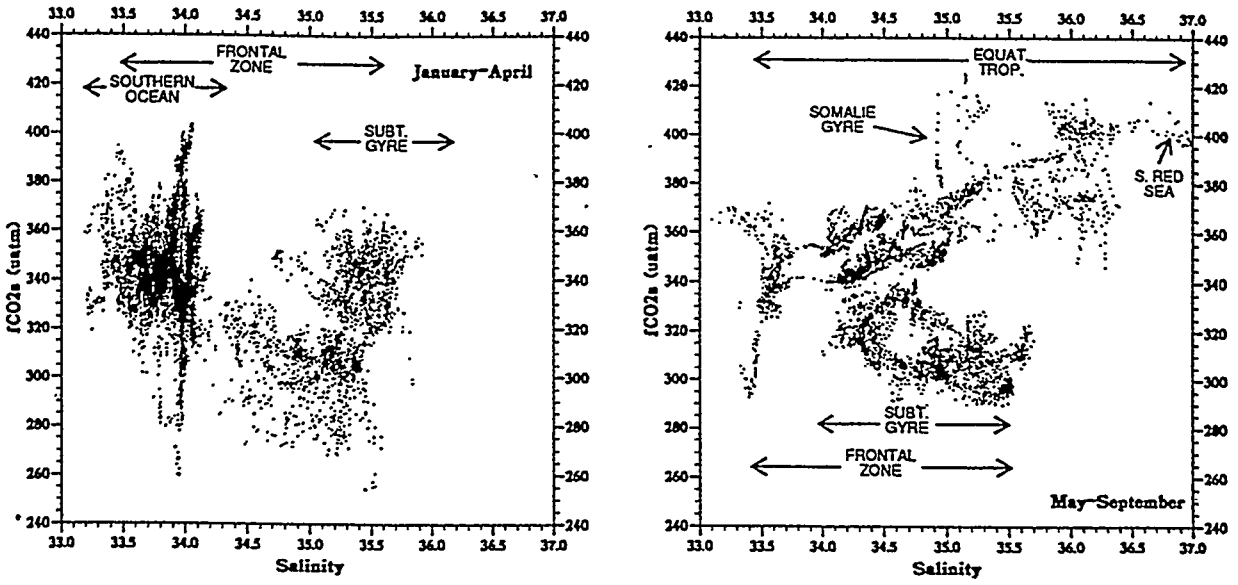

Fig. 6. (continued)

computed using observations from the 1970s [*Broecker et al.*, 1986]. However, in July the subtropical zone becomes a strong potential CO_2 sink [ΔfCO_2=-60 µatm]. We observed a different potential variation near and within the frontal zone compared to the subtropical region. The ΔfCO_2 level does not change dramatically from summer to winter, but the ΔfCO_2 distribution varies strongly (Figure 7). In summer, primary production occurring near the fronts produces large horizontal ΔfCO_2 gradients. In winter, when biological activity is weak and mixing with CO_2 enriched subsurface waters increases, the ΔfCO_2 distribution becomes much more homogeneous.

In the subtropical zone, where temporal fCO_2 variations are large, it is possible from our observations to estimate the magnitude of the processes that govern these variations. It appears that thermodynamic processes control the main part of the seasonal changes. At a monthly scale, however, other processes must be taken into account. The monthly observations reveal that in summer the biological activity must dominate over the mixing with subsurface CO_2-enriched waters; in winter, on the contrary, the mixing dominates. In the Subantarctic regions, fCO_2 does not vary regularly from summer to winter. For this region, more data are needed at a monthly scale in order to compute the mean fCO_2 budget and to explain the origin of its variability. On the other hand, for a more complete description of the fCO_2 variations and in order to distinguish the biological and physical processes in the fCO_2 budgets, other biogeochemical

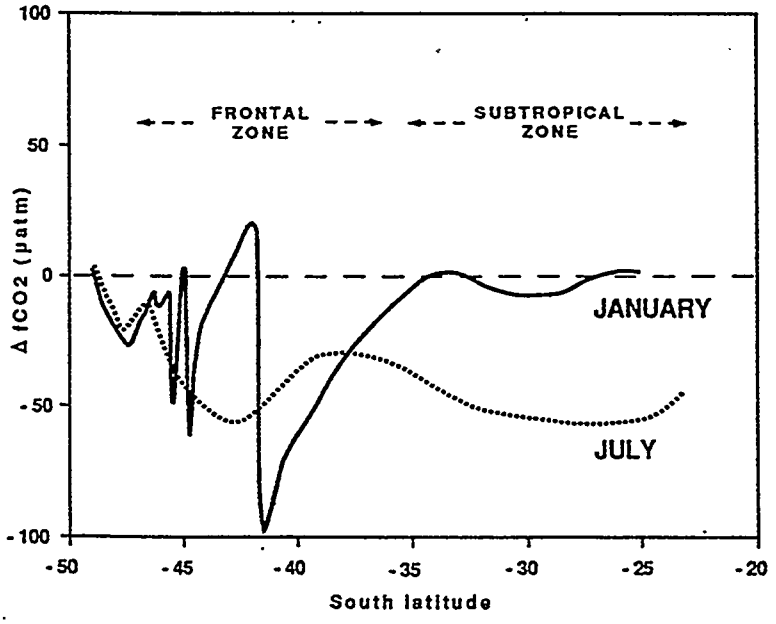

Figure 7. A sketch representing the seasonal variation of ΔfCO_2 in the southwestern Indian Ocean.

parameters like fluorescense have to be continuously measured. This has been organized on board the R/V *Marion-Dufresne* since the MINERVE cruises in 1992. With this future data set, it will also be possible to study the range of interannual variability and compare it to monthly and seasonal scales.

With such complex spatiotemporal variations, our understanding of the actual carbon budget would certainly benefit by taking into account the seasonal scale in global modeling and the subseasonal observations are certainly needed to make this reliable. On the other hand, the quantification of the air-sea CO_2 fluxes on regional and basin scales, not only along ship tracks, is not immediate. As a matter of fact, it will be not possible to measure fCO_2 everywhere and at all times. Remote sensing observations related to the oceanic carbon cycle (SST, color of the sea and winds) will certainly play an important role in constructing fCO_2 continuous fields and in estimating with more accuracy the air-sea CO_2 fluxes in the future. A simple way would consist of finding statistical relations between fCO_2 and other parameters (SST, Chlorophyll) from in situ observations [e.g., *Watson et al.*, 1991] and then using these statistical relations together with satellite data to interpolate in situ fCO_2 observations. A description of such relations, fCO_2/SST and fCO_2/salinity from the whole MINERVE 1991 data set, shows that statistical study has to be applied at regional and, at least, at seasonal scale. In particular, for the southern ocean, which is poorly sampled on large scales and for which one still does not know the CO_2 source/sink potential, it is clear that if a relation such as fCO_2/SST exists, its use to constrain fCO_2 continuous fields would be important. This method has been employed previously [*Tans et al.*, 1990]. However, fCO_2 variability is so large in some parts of the ocean and the fCO_2/SST relation is so poor (see Figure 7*a* for SST<6°C) that it is, at present, unrealistic to use it to improve the regional estimate of CO_2 air-sea exchanges. Certainly, biological processes, which are not sufficiently understood in the southern ocean, play a crucial role in the fCO_2 distribution. Ocean color from satellite may provide some hope for taking into account the high-frequency variability of fCO_2 revealed by continuous instrumentation.

Acknowledgments. The cruises of the R/V *Marion-Dufresne* were sponsored by the Terres Australes et Antarctiques Françaises (TAAF); we thank Y. Balut for his assistance in the organization of the MINERVE program and B.Ollivier and P.Sangiardi in setting up the pumping system and for their continuous help in the electronic and navigation record system.We wish to thank all the captains and crew members of the R/V *Marion-Dufresne* and the officers who recorded hourly the meteorological parameters during these cruises from January to September 1991. Françoise Dagault, Phillipe Laurent and Nathalie Poisson are gratefully acknowledged for their very active participation during some of the cruises. The correction of the manuscript by Andrew Dickson was very much appreciated. This program was also supported by the French program PNEDC/CO_2, the Europeen program EPOCH, and the mission de recherche des TAAF.

REFERENCES

Andrié, C., C. Oudot, C. Genthon, and L. Merlivat, CO_2 Fluxes in the tropical Atlantic during FOCAL cruises, *J. Geophy. Res., 91* (C10), 11,741-11,755, 1986.

Boutin J., Utilisation et validation des vents satellitaires pour l'étude à l'échelle globale de l'échange du gaz carbonique entre l'océan et l'atmosphère, 93 pp., Ph. D. dissertation, Univ. Paris, 1990.

Brewer, P.G., What controls the variability of carbon dioxide in the surface ocean? A plea for complete information, in: *Dynamic Processes in the Chemistry of the Upper Ocean, edited by* J.D. Burton, P.G. Brewer, and R. Chesselet, pp. 215-231, Plenum, New York, 1986.

Broecker, W.S., J.R. Ledwell, T. Takahashi, R. Weiss, L. Merlivat, L. Memery, T.H. Peng, B.Jähne, and K.O. Munnich, Isotopic versus micrometeorologic ocean CO_2 fluxes: A serious conflict, *J. Geophys. Res., 91*, 10,517-10,527, 1986.

Cheney, R.E., J.G. Marsh, and B.D. Beckley, Global mesoscale variability from collinear tracks of SEASAT altimeter data. *J. Geophy. Res., 88*(C7), 4343-4354, 1983.

Copin-Montégut, C., A method for the continuous determination of the partial pressure of carbon dioxide in the upper ocean, *Mar. Chem., 17*, 13-21, 1985.

Copin-Montégut, C., A new formula for the effect of temperature on the partial pressure of CO_2 in seawater. *Mar. Chem., 25*, 29-37, 1988.

Copin-Montégut, C., A new formula for the effect of temperature on the partial pressure of CO_2 in seawater, Corrigendum, *Mar. Chem., 27*, 143-144, 1989*a*.

Copin-Montégut, C., Influence de la production biologique en période hivernale sur la répartition du CO_2 et de l'oxygène dans les couches superficielles de l'upwelling Péruvien, in Colloque IFREMER, "Tour du Monde du J.Charcot", IFREMER, Paris, 1989*b*.

Daniault, N., and Y. Ménard, Eddy kinetic energy distribution in the southern ocean from altimetry and FGGE drifting buoys., *J. Geophy. Res., 90*(C6), 11,877-11,889, 1985.

Etcheto, J., and L. Merlivat, Satellite determination of the carbon dioxide exchange coefficient at the ocean-atmosphere interface: A fisrt step, *J. Geophys. Res., 93*(C12), 15,669-15,678, 1988.

Feely, R.A., R.H. Gammon, B.A. Taft, P.E. Pullen, L.S. Waterman, T.J. Conway, J.F. Gendron, and D.P. Wisegraver, Distribution of chemical tracers in the eastern equatorial Pacific during and after the 1982-1983 El Niño/Southern Oscillation event, *J. Geophys. Res., 92*(C6), 6545-6558, 1987.

Gambéroni, L., J. Géronimi, P.F. Jeanin, and J.F. Murail, Study of frontal zones in the Crozet-Kerguelen region, *Oceanol. Acta, 5*(3), 289-299, 1982.

Garçon, V., L. Martinon, C. Andrié, P. Andrich, and J.-F. Minster, Kinematics of CO_2 fluxes in the tropical Atlantic Ocean during 1983 northern summer, *J. Geophys. Res., 94*, 855-870, 1989.

Garçon, V., F. Thomas, C.S. Wong, and J.-F. Minster, Gaining insight into the seasonal variability of CO_2 at Ocean Weather Station P using an upper ocean model, *Deep Sea Res., 39*, 931-938, 1992.

Goffart, A., and J.H. Hecq, Zooplankton biochemistry and ecodynamics, Antarctica, in *Belgian Scientific Research Programme on Antarctica. Scientific Results of Phase One* (Oct 85-Jan 89), *Plankton Ecology*, edited by S.Caschetto, vol. 1, 1989.

Gordon, A.L., K.-I. Hoari, and M. Donn, Southern hemisphere western boundary current variability revealed by GEOS 3 altimeter, *J. Geophys. Res., 88* (C1), 755-762, 1983.

Goyet, C., Variations saisonnières de pCO_2 dans les eaux de surface du Sud Ouest de l'Océan Indien, Ph.D. dissertation, 144 pp., Univ. Paris, 1987.

Goyet, C., C. Beauverger, C. Brunet, and A. Poisson, Distribution of carbon dioxide partial pressure in surface waters of the southwest Indian ocean, *Tellus, 43*(B), 1-11, 1991.

Hellerman, S., and M. Rosenstein, Normal monthly wind stress over the world ocean with error estimates. *J. Phys. Oceanogr., 13*, 1093-1104, 1983.

Inoue, H., and Y.Sugimura, Distribution and variations of

oceanic carbon dioxide in the western North Pacific, eastern Indian, and Southern Ocean south of Australia. *Tellus, 40*(B), 308-320, 1988.

Inoue, H.Y., and Y.Sugimura, Variations and distributions of CO_2 in and over the equatorial Pacific during the period from 1986/88 El Nino event to the 1988/89 La Nina event, *Tellus, 44*(B), 1-22, 1992.

Jähne, B., Zur Parametrisierung des Gas antaushes mit Hilfe von Laborexperimenten. Ph. D. dissertation, 124 pp., Univ. Heidelberg, Heidelberg, Germany, 1980.

Jacques, G., and M. Minas, Production primaire dans le secteur indien de l'océan Antarctique en fin d'été, *Océanol. Acta, 4*(1), 33-41, 1981.

Keeling, C.D., Carbon dioxide in surface ocean waters, 4, Global distribution, *J. Geophys. Res., 73*(14), 4543-4553, 1968.

Keeling, C.D., Surface ocean CO_2. in The Global Carbon Cycle, NATO Advanced Study Institut, in press, 1992.

Keeling, C.D., and L.S. Waterman, Carbon dioxide in surface ocean waters. 3, Measurements on Lusiad expedition 1962-1963, *J. Geophys. Res., 73*(14), 4529-4541, 1968.

Keeling, C.D., N.W. Rakestraw, and L.S. Waterman, Carbon dioxide in surface waters of the Pacific Ocean, 1, Measurements of the distribution, *J. Geophys. Res., 70*(24), 6087-6097, 1965.

Kelley, J.J., L.L. Longerich and D.W. Hood, Effect of upwelling, mixing and high primary productivity on CO_2 concentrations in surface waters in the Bering Sea, *J. Geophys. Res, 76*(36), 8687-8693, 1971.

Krey, J., and B. Babenerd, Phytoplankton production, Atlas of the International Indian Ocean Expedition, Institut für Meereskunde and der Universität Kiel, *Int. Ocean. Comm. UNESCO*, 70 pp., 1976.

Lefevre, N. and Y. Dandonneau, Air-sea CO_2 fluxes in the equatorial Pacific in January-March 1991, *Geophys. es. Lett., 19*(22), 2223-2226, 1992.

Liss, P., and L. Merlivat, Air-sea exchange rates, introduction and synthesis, In The Role of Air-Sea Exchange in Geochemical Cycling, edited by P. Buat-Ménard, pp. 113-127, *NATO/ASI Ser.*, D.Reidel, Norwell, Mass., 1986.

Lutjeharms, J.R.E., Spatial scales and intensities of circulation in the ocean areas adjacent to South Africa, *Deep Sea Res., 28(A11)*, 1289-1302, 1981.

Lutjeharms, J.R.E., N.M. Walters, and B.R. Allanson, Oceanic frontal systems and biological enhancement, in *Antarctic Nutrient Cycles and Food Webs* , edited by W.R. Siegfried, P.R. Condy, and R.M. Laws, New York, pp. 11-21, Springer-Verlag, 1985.

Merlivat, L., J. Etcheto, and J. Boutin, CO_2 exchange at the air-sea interface: Time and space variability, *Adv. Space Res., 11*(3), 77-85, 1991.

Metzl, N., B. Moore III, A. Papaud, and A. Poisson, Transport and carbon exchanges in Red Sea, Inverse Methodology, *Global Biogeochem. Cycles, 3*(1), 1-26, 1989.

Metzl, N., C. Beauverger, C. Brunet, C. Goyet and A. Poisson, Surface water pCO_2 in the western Indian sector of the southern ocean: A highly variable CO_2 source/sink region during the austral summer, *Mar. Chem. 35*, 85-95, 1991.

Miyake, Y., and Y. Sugimura, The carbon dioxide in the surface water and the atmosphere in the Pacific, the Indian and the Antarctic Ocean areas, *Rec. Oceanogr.Works in Japan, 10*(1), 28-33, 1969.

Miyake, Y., Sugimura, Y., and K. Saruhashi, The carbon dioxide content in the surface waters in the Pacific Ocean, *Rec. Oceanogr. Works in Japan, 12*(2), 45-52, 1974.

Murphy, P.P., R.A. Feely, R.H. Gammon, K.C. Kelly, and L.S. Waterman, Autumn air-sea disequilibrium of CO_2 in the South Pacific Ocean, *Mar. Chem., 35*, 77-84, 1991*a*.

Murphy, P.P., R.A. Feely, R.H. Gammon, D.E. Harrison, K.C. Kelly, and L.S. Waterman, Assesment of the Air-Sea Exhange of CO_2 in the South Pacific during austral autumn, *J. Geophys. Res., 96*(C11), 20,455-20,465, 1991*b*.

Oudot, C., and C. Andrié, Variabilité des pressions partielles de CO_2 océanique et atmosphérique dans l'Atlantique tropical, *Oceanol.Acta, 9*(2), 169-177, 1986.

Park, Y.-H., L. Gambéroni, and E. Charriaud, Frontal structure and transport of the Antarcic Circumpolar Current in the South Indian Ocean sector, 40°-80°E, *Mar. Chem., 35*(1-4), 45-62, 1991.

Peng, T.-H., T. Takahashi, W.S. Broecker, and J. Olafsson, Seasonal variability of carbon dioxide, nutrients and oxygen in the northern North Atlantic surface water : Observations and a model, *Tellus, 39B*(5), 439-458, 1987.

Poisson, A., B. Schauer, and C. Brunet, MD43/INDIGO 1, in *Les rapports des campagnes à la mer, 85*(06)Les publications de la Mission de Recherche des Terres Australes et Antarctiques Françaises, Paris, 267 pp., 1988.

Poisson, A., B. Schauer and C. Brunet, MD43/INDIGO 2, in *Les rapports des campagnes à la mer, 85*(02)Les publications de la Mission de Recherche des Terres Australes et Antarctiques Françaises, Paris, 234 pp., 1989.

Poisson, A., B. Schauer and C. Brunet, MD43/INDIGO 3, in *Les rapports des campagnes à la mer, 87*(02)Les publications de la Mission de Recherche des Terres Australes et Antarctiques Françaises, Paris, 269 pp., 1990.

Poisson, A., N. Metzl, C. Brunet, B. Schauer, and B. Brès, ΔpCO_2 in the western and northern Indian Ocean and in the corresponding sector of the southern ocean. Paper presented at the Sun Yat-Sen Conference on Marine Science and Technology, pp. 85-100, National Sun Yat-Sen University, Kaohsiung, Taiwan, November 12-14, 1990, 1991.

Ramage, C.S., Climate of the Indian Ocean north of 35°S, in *World Survey of Climatology*, Edited by H.E. Landsberg, vol 15, pp.603-671, 1983.

Semtner, A.J. Jr., and R.M. Chervin, A simulation of the global ocean circulation with resolved eddies, *J. Geophys. Res., 93*(C12), 15,502-15,522, 1988.

Semtner, A.J. Jr., and R.M. Chervin, Ocean general circulation from a global eddy-resolving model, *J. Geophy. Res., 97*(C4), 5493-5550, 1992.

Smethie, W. M., Jr., T. Takahashi, D.W. Chipman and J.R. Ledwell, Gas exchange and CO_2 flux in the tropical Atlantic Ocean determined from 222Rn and pCO_2 measurements. *J. Geophys. Res., 90*(C4), 7005-7022, 1985.

Takahashi T., Carbon dioxide in the Atmosphere and in Atlantic Ocean water, *J. Geophys. Res., 66*(2), 477-494, 1961.

Takahashi T., The carbon dioxide puzzle, *Oceanus, 32*(2), 22-29, 1989.

Takahashi T., and D.W. Chipman, Circumpolar oceanic CO_2 sink zone (abstract), *IAMAP/IAPSO, p. 34*, Joint Assembly Program, Honolulu, Hawaii, 1985.

Takahashi, T., J. Goddard, S. Sutherland, D.W. Chipman and C.C. Breeze, Seasonal and geographic variability of carbon dioxide sink/source in the oceanic areas: Observations in the North and equatorial Pacific Ocean, 1984-1986, and global summary, final technical report, LDGO, 52 pp., Columbia Univ., Palisades, N.Y., 1986.

Taljaard, J.J., and H. Van Loon, Climate of the Indian Ocean South of 35°S. in *World Survey of Climatology*, edited by H.E. Landsberg, vol. 15, pp. 505-601, 1983.

Tans, P.P., I.Y. Fung, and T. Takahashi, Observational constraints on the global atmospheric CO_2 Budget, *Science, 247*, 1431-1438, 1990.

Taylor, A.H., A.J. Watson, M. Ainsworth, J.E. Robertson, and D.R. Tuner, A Modelling investigation of the role of phytoplankton in the balance of carbon at the surface of the

North Atlantic, *Global Biogeochem. Cycles, 5*(2), 151-171, 1991.

Thomas, F., C. Perigaud, L. Merlivat, and J.-F. Minster, World-scale monthly mapping of the CO_2 ocean-atmosphere gas-transferred coefficient, *Phil. Trans. R. Soc. London., Ser. A, 325*, 71-83, 1988.

UNESCO, Thermodynamics of the carbon dioxide system in seawater, Report by the carbon dioxide subpanel of the Joint Panel on Oceanographic Tables and Standards,*Tech. Pap. Mar. Sci. 51*, 55 pp., Paris, 1987.

Watson, A.J., C. Robinson, J.E. Robinson, P.J. le B. Williams, and M.J.R. Fasham, Spatial varibility in the sink for atmospheric carbon dioxide in the North Atlantic, *Nature, 350*, 50-53, 1991.

Webb, D.J., P.D. Killworth, A.C. Coward, and S.R. Thompson, in The FRAM Atlas of the Southern Ocean, *NERC Pub.*, 67 pp., Nat. Environ. Res. Council, Swindon, England, 1991.

Weiss, R.F., Carbon dioxide in water and seawater: The solubility of a non-ideal gas, *Mar. Chem., 2*, 203-215, 1974.

Weiss, R.F. and B.A. Price, Nitrous oxide solubility in water and seawater, *Mar. Chem., 8*, 347-359, 1980.

Weiss, R.F., R.A. Jahnke, and C.D. Keeling, Seasonal effects of temperature and salinity on the partial pressure of CO2 in seawater, *Nature, 300*, 511-513, 1982.

Wong, C.S., and Y.-H. Chan, Temporal variations in the partial pressure and flux of CO_2 at ocean station P in the subarctic Northeast Pacific Ocean, *Tellus. 43*(B), 206-223, 1991.

Wong, C.S., Y.-H. Chan, J.S. Page, G.E. Smith, and R.D. Bellegay, Changes in equatorial CO_2 flux and new production estimated from CO_2 and nutrient levels in Pacific surface waters during the 1986/87 El Niño, *Tellus, 45*(B) 64-79, 1993.

Wyrtki, K., *Oceanographic Atlas of the International Indian Ocean Expedition, 531 pp.*, National Science Foundation, Washington, D.C., 531 pp, 1971.

B. Brès, C. Brunet, F. Louanchi, N. Metzl, A. Poisson, D. Ruiz-Pino, and B. Schauer, Laboratoire de physique et Chimie Marines, Université Pierre et Marie Curie, case 134, 4 place Jussieu, 75252, Paris Cedex 05, France.

(Received December 14, 1992;
revised June 14, 1993;
accepted July 15, 1993.)

Corrigendum

In the final reprint of the paper "Variability of Sources and Sinks of CO2..." by Poisson et al., 1993, JGR, 948, C12, 22,759-22,778, one line has been ommited in **Table 1**: it corresponds to mean parameters observed in **July** (whereas standard deviations were listed for this month !)

You'll find below the complete table, as originally constructed, including average of parameters for **July**

TABLE 1. Mean and Standard Deviation of Parameters Measured and Calculated in the Domain 23°S-35°S (see plate 2)

		Measured Parameters						Calculated Parameters			
Period	Number of Data	fCO_2 µatm	ΔfCO_2 µatm	Temperature °C	Salinity	Patm mb	Wind (10 m) m/s	k cm/h	k.s (x100) mol/m^2/yr/µatm	CO_2 flux mmol/m^2/d	CO_2 flux(mean)* mmol/m^2/d
						Mean					
January	173	347.2	-9.59	23.76	35.42	1023.9	5.8	7.6	1.9	-0.47	-0.51
February	200	348.2	-3.88	24.90	35.51	1010.5	10.6	23.5	5.8	-0.53	-0.62
April	214	328.8	-28.25	23.72	35.46	1024.8	6.4	9.5	2.4	-1.84	-1.89
May	303	314.1	-41.98	22.40	35.41	1021.7	7.0	11.8	3.1	-3.45	-3.39
July	198	299.1	-60.36	19.55	35.30	1031.0	6.7	9.9	2.8	-4.66	-4.49
						Standard Deviation					
January	173	6.7	6.78	1.82	0.10	0.9	1.2	4.0	1.0	0.39	
February	200	6.8	6.62	1.73	0.12	3.7	1.9	6.3	1.5	1.07	
April	214	4.7	4.98	1.82	0.17	5.0	1.2	3.8	1.0	0.77	
May	303	5.5	6.26	2.26	0.23	3.4	2.8	7.9	2.0	2.28	
July	198	6.2	5.75	2.10	0.15	2.6	2.5	6.3	1.8	2.99	

The wind dependent gas exchange k is calculated by using the relation of *Liss and Merlivat* [1986] and a temperature dependent schmidt number [*Jähne*,1980].
For k.s we used a temperature and salinity dependent CO_2 solubility coefficient proposed by *Weiss* [1974].
* See the text for explanations of the two ways to calculate the mean CO_2 flux

INTERNAL DISTRIBUTION

1. T. A. Boden
2. M. D. Burtis
3. R. M. Cushman
4–53. S. B. Jones
54. D. P. Kaiser
55. P. Kanciruk
56. J. M. Loar
57. T. E. Myrick
58. D. E. Shepherd
59. L. D. Voorhees
60. Central Research Library
61–64. ESD Library
65–66. Laboratory Records Department
67. Laboratory Records Department ORNL- RC
68. Y-12 Technical Library

EXTERNAL DISTRIBUTION

69. J. Afghan, Marine Physical Laboratory, Scripps Institution of Oceanography, 9500 Gilman Drive, La Jolla, CA 92093-0902
70. A. G. Alexiou, UNESCO/IOC, 1 rue Miollis, 75732 Paris Cedex 15, France
71. W. E. Asher, University of Washington, Joint Institute for the Study of the Atmosphere and the Ocean, Box 354235, Seattle, WA 98195
72. J. Banasek, UIC, Inc., P.O. Box 83, 1225 Channahon Road, Joliet, IL 60434
73. N. Bates, Bermuda Biological Station for Research, Ferry Reach GE 01, Bermuda
74. R. Bidigare, University of Hawaii, Department of Oceanography, 1000 Pope Road, Honolulu, HI 96822
75. P. G. Brewer, Monterey Bay Aquarium Research Institute, P.O. Box 628, 7700 Sandholt Road, Moss Landing, CA 95039
76. M. Broido, Department of Energy, Office of Biological and Environmental Research, Environmental Sciences Division, ER-74, 19901 Germantown Road, Germantown, MD 20874
77. O. B. Brown, University of Miami, 4500 Rickenbacker Causeway, Miami, FL 33149
78. C. Brunet, Laboratoire de Physique et Chimie Marines, Université Pierre et Marie Curie, 4 place Jussieu, 75252 Paris Cedex 05, France
79. R. H. Byrne, University of South Florida, Department of Marine Science, 140 Seventh Avenue S., St. Petersburg, FL 33701
80. Challenger Oceanic Systems and Services, 6 Meadow Vale, Haslemere, Surrey GU27 1DH, United Kingdom
81. C.-T. A. Chen, Institute of Marine Geology and Chemistry, National Sun Yat-Sen University, Kaohsiung 804, Taiwan, Republic of China
82. D. W. Chipman, Columbia University, Lamont-Doherty Earth Observatory, Route 9W, P.O. Box 1000, Palisades, NY 10964
83. E. G. Cumesty, ORNL Site Manager, Department of Energy, Oak Ridge National Laboratory, P.O. Box 2008, Oak Ridge, TN 37831-6269
84. G. Cutter, Old Dominion University, Department of Oceanography, Norfolk, VA 23529
85. Y. Dandonneau, LODYC, Université Pierre et Marie Curie, 4 place Jussieu, 75252 Paris Cedex 05, France

86. G. Daneri, CEA Universidad del Mar, Dept. de Oceanografia y Biologia Pesquera, Amunaategui 1838, Vina Del Mar, Chile
87. A. G. Dickson, Scripps Institution of Oceanography, University of California, San Diego, Marine Physical Laboratory, 9500 Gilman Drive, La Jolla, CA 92093
88. S. Doney, National Center for Atmospheric Research, Oceanography Section, P.O. Box 3000, Boulder, CO 80307
89. H. W. Ducklow, College of William and Mary, Virginia Institute of Marine Sciences, P.O. Box 1346, Gloucester Point, VA 23062
90. G. Eischeid, Woods Hole Oceanographic Institution, 360 Woods Hole Road, Woods Hole, MA 02543-1541
91. J. W. Elwood, Department of Energy, Office of Biological and Environmental Research, Environmental Sciences Division, ER-74, 19901 Germantown Road, Germantown, MD 20874
92. G. Esser, Justus-Liebig-University, Institute for Plant Ecology, Heinrich-Buff-Ring 38, D-35392 Giessen, Germany
93. R. A. Feely, NOAA/PMEL, 7600 Sand Point Way NE, Seattle, WA 98115
94. W. Ferrell, Department of Energy, Office of Biological and Environmental Research, Environmental Sciences Division, ER-74, 19901 Germantown Road, Germantown, MD 20874
95. R. H. Gammon, University of Washington, Chemistry Department, Box 351700, Seattle, WA 98195
96. J.-P. Gattuso, Observatoire Océanologique Européen, Avenue Saint-Martin, MC-98000, Monaco
97. J. P. Giesy, Michigan State University, College of Natural Science, Department of Zoology, 203 Natural Science Building, East Lansing, MI 48824-1115
98. J. Goddard, Columbia University, Lamont-Doherty Earth Observatory, Climate/Environment/Ocean Division, Rt. 9W, Palisades, NY 10964
99. C. M. Goyet, Woods Hole Oceanographic Institute, Marine Chemistry and Geochemistry Department, 360 Woods Hole Road, MS #25, Woods Hole, MA 02543
100. N. Gruber, Princeton University, Atmospheric and Oceanic Sciences, 304A Sayre Hall, Princeton, NJ 08544
101. P. Guenther, Geosciences Research Division 0220, University of California, San Diego, 9500 Gilman Drive, La Jolla, CA 92093-0220
102. D. O. Hall, University of London, Division of Life Science, King's College London, Campden Hill Road, London W8 7AH, United Kingdom
103. A. Harashima, Japan Environment Agency, Global Environmental Research Division, 16-2 Onogawa, Tsukuba, Ibaraki 305, Japan
104. M. Hein, Freshwater Biological Laboratory, Helsingoersgade 51, DK-3400 Hilleroed, Denmark
105. A. Hittelman, WDC-A for Solid Earth Geophysics, NOAA Code E/GC1, 325 Broadway, Boulder, CO 80303
106. H. Hodgson, British Library, Boston Spa, DSC, Special Acquisitions, Wetherby, West Yorkshire, LS23 7BQ, United Kingdom
107. H. Hong, Xiamen University, Environmental Science Research Center, Post Code 361005, Mail Box 1085, Xiamen, Fujian, Peoples Republic China
108. C. A. Hood, GCRIO, 2250 Pierce Road, Bay City, MI 48710
109. J. C. Houghton, Department of Energy, Office of Biological and Environmental Research, Environmental Sciences Division, ER-74, 19901 Germantown Road, Germantown, MD 20874

110. H. Y. Inoue, Geochemical Research Department, Meteorological Research Institute, Nagamine 1-1, Tsukuba, Ibaraki 305-0032, Japan
111. M. Ishii, Geochemical Research Department, Meteorological Research Institute, Nagamine 1-1, Tsukuba, Ibaraki 305-0032, Japan
112. K. M. Johnson, Brookhaven National Laboratory, Oceanographic and Atmospheric Sciences Division, Department of Applied Science, Building 318, Upton, NY 11973
113. F. Joos, University of Bern, Physics Institute, KUP, Sidlerstr. 5, Bern CH-3012, Switzerland
114. D. M. Karl, University of Hawaii, Department of Oceanography, 1000 Pope Road, Honolulu, HI 96822
115. T. R. Karl, National Climatic Data Center, 151 Patton Avenue, Federal Building, Room 516E, Asheville, NC 28801
116. S. Kempe, Schnittspahnstr. 9, D-64287 Darmstadt, Germany
117. R. M. Key, Princeton University, Geology Department, Princeton, NJ 08544
118. K.-R. Kim, Seoul National University, Dept. of Oceanology, Seoul 151-7442, Korea
119. T. Kimoto, Research Institute of Oceano-Chemistry, Osaka Office, 3-1 Fumahashi-cho, Tennoji-ku, Osaka 543, Japan
120. D. Kitzis, Environmental Research Laboratories, NOAA, 325 Broadway, Boulder, CO 80308-3328
121. B. Klein, University Laval, GIROQ, Pav. Vachon, Quebec, PQ, G1K 7P4, Canada
122. J. C. Klink, Miami University, Department of Geography, 217 Shideler Hall, Oxford, OH 45056
123. J. Val Klump, University of Wisconsin, Center for Great Lakes Studies, 600 E. Greenfield Avenue, Milwaukee, WI 53204
124–163. A. Körtzinger, Institut für Meereskunde, Düsternbroker Weg 20, 24105 Kiel, Germany
164. A. Kozyr, The University of Tennessee, Pellissippi Research Facility, 10521 Research Drive, Suite 100, Knoxville, TN 37923
165. N. Lefevre, Plymouth Marine Laboratory, Prospect Place, West Hoe, Plymouth PL1 3DH, United Kingdom
166. S. Levitus, National Ocean Data Center, National Oceanic and Atmospheric Administration, E/OC5, 1315 East-West Highway, Room 4362, Silver Spring, MD 20910
167. E. Lewis, Brookhaven National Laboratory, Upton, NY 11973
168. A. A. Lucier, National Council of the Paper Industry for Air and Stream Improvement, Inc., P.O. Box 13318, Research Triangle Park, NC 27709-3318
169. P. Lunn, Department of Energy, Office of Biological and Environmental Research, Environmental Sciences Division, ER-74, 19901 Germantown Road, Germantown, MD 20874
170. T. H. Mace, U.S. Environmental Protection Agency, National Data Processing Division, 79 TW Alexander Drive, Bldg. 4201, MD-34, Durham, NC 27711
171. J. J. McCarthy, Harvard University, Museum of Comparative Zoology, 26 Oxford Street, Cambridge, MA 02138
172. M. C. McCracken, National Assessment Coordination Office, Suite 750, 400 Virginia Avenue, Washington, DC 20546
173. L. Merlivat, LODYC, Université Pierre et Marie Curie, 4 place Jussieu, 75252 Paris Cedex 05, France
174. N. Metzl, Université Pierre et Marie Curie, Laboratory de Physique et Chimie Marines, T 24-25-Case 134, 4 place Jussieu, 75252 Paris Cedex 05, France
175. F. J. Millero, University of Miami, RSMAS, 4600 Rickenbacker Causeway, Miami, FL 33149

176. L. Mintrop, Institute for Marine Research, Marine Chemistry Department, Duesternbrooker Weg 20, D-214105 Kiel, Germany
177. J. W. Morse, Texas A & M University, Department of Oceanography, College Station, TX 77843
178. R. E. Munn, University of Toronto, Institute for Environmental Studies, Haultain Building, 170 College Street, Toronto, Ontario M5S 1A4, Canada
179. S. Murayama, National Institute for Resources and Environment, Environmental Assessment Department, 16-3 Onogawa, Tsukuba, Ibaraki 305, Japan
180. P. P. Murphy, National Oceanic and Atmospheric Administration, Pacific Marine Environmental Laboratory, Building 3, 7600 Sand Point Way NE, Seattle, WA 98115
181. C. Neil, 913 NE 73rd Street, Seattle, WA 98115
182. S. Nishioka, National Institute for Environmental Studies, Global Environment Research Division, 16-2 Onogawa, Tsukuba, Ibaraki 305, Japan
183. Y. Nojiri, National Institute for Environmental Studies, Tsukuba, Ibaraki 305-0053, Japan
184. J. R. Oh, Korea Ocean Research and Development Institute, Chemical Oceanography Division, An San P.O. Box 29, Seoul 4325-600, Korea
185. E. Ohtaki, Environmental Science and Technology, Okayama University, Tsushima-Naka 2-1-1, Okayama 700, Japan
186. J. Olafsson, Marine Research Institute, P.O. Box 1390, Skulagata 4, 121 Reykjavik, Iceland
187. C. Oudot, Centre ORSTOM de Cayenne, B.P. 165-97323, Cayene Cedex, Guyana
188. A. C. Palmisano, Department of Energy, Office of Biological and Environmental Research, Environmental Sciences Division, ER-74, 19901 Germantown Road, Germantown, MD 20874
189. B. Parra, Department of Energy, Office of Biological and Environmental Research, Environmental Sciences Division, ER-74, 19901 Germantown Road, Germantown, MD 20874
190. A. Patrinos, Department of Energy, Office of Biological and Environmental Research, Environmental Sciences Division, ER-74, 19901 Germantown Road, Germantown, MD 20874
191. T.-H. Peng, NOAA/AOML, Ocean Chemistry Division, 4301 Rickenbacker Causeway, Miami, FL 33149
192. F. F. Perez, Instituto de Investigaciones Marinas, Eduardo Cabello 6, 36208 Vigo, Spain
193. J. M. Gago Pineiro, Instituto de Investigaciones Marinas, Eduardo Cabello 6, 36208 Vigo, Spain
194. A. Poisson, Laboratoire de Physique et Chimi Marines, Université Pierre et Marie Curie, 4 place Jussieu, 75252 Paris Cedex 05, France
195. B. Preselin, University of California, Department of Biological Sciences, Santa Barbara, CA 93106
196 P. D. Quay, University of Washington, School of Oceanography, Box 357940, Seattle, WA 98195
197. R. Y. Rand, USDA, Global Change Data and Information Management, 10301 Baltimore Boulevard, Beltsville, MD 20705
198. J. L. Reid, Scripps Institution of Oceanography, University of California San Diego, M/C 0230, 9500 Gilman Drive, La Jolla, CA 92093-0230
199. J. Ribbe, University of Washington, Joint Institute for the Study of the Atmosphere and Oceans, Box #35425, Seattle, WA 98195

200. M. R. Riches, Department of Energy, Office of Biological and Environmental Research, Environmental Sciences Division, ER-74, 19901 Germantown Road, Germantown, MD 20874
201. M. F. Roberts, Pacific Marine Environmental Laboratory, National Oceanic and Atmospheric Administration, 7600 Sand Point Way NE, Seattle, WA 98115
202. J. Robertson, Southampton University, Highfield, Southampton SO17 1BJ United Kingdom
203. L. Robinson, Director, Environmental Sciences Institute, Florida A&M University, Science Research Facility, 1520 S. Bronough Street, Tallahassee, FL 32307
204. S. Rubin, Lamont-Doherty Earth Observatory of Columbia University, Palisades, NY 10964
205. C. L. Sabine, Princeton University, Geology Department, Guyot Hall, Princeton, NJ 08544
206. M. M. Sarin, Physical Research Laboratory, Navrangpura, Ahmedabad 380009, India
207. J. L. Sarmiento, Princeton University, Atmospheric and Oceanic Sciences Program, P.O. Box CN710, Sayre Hall, Princeton, NJ 08544
208. B. Schauer, Laboratoire de Physique et Chimie Marines, Université Pierre et Marie Curie, 4 place Jussieu, 75252 Paris Cedex 05, France
209. B. Schneider, Baltic Sea Research Institute, Seestrase 15, Warnmunde D-18 119, Germany
210. G. Shaffer, Niels Bohr Institute for Astronomy, Physics, and Geophysics, University of Copenhagen, Juliane Maries Vej 30, 2100 Copenhagen, Denmark
211. K. Shitashima, Central Research Institute of Electric Power Industry, Marine Science Group, 1646 Abiko, Abiko-City, Chiba, 270-11, Japan
212. N. Silva, Universidad Catolica de Valparaiso, Escuela de Ciencias de Mar, Casilla 1020, Valparaiso, Chile
213. M. H. C. Stoll, Netherlands Institute for Sea Research, Dept. MCG, P.O. Box 59, 1790 Ab den Burg-Texel, The Netherlands
214. E. T. Sundquist, U.S. Geological Survey, Quissett Campus, Branch of Atlantic Marine Geology, Woods Hole, MA 02543
215. S. C. Sutherland, Columbia University, Lamont-Doherty Earth Observatory, P.O. Box 1000, Route 9W, Palisades, NY 10964
216. J. H. Swift, Scripps Institution of Oceanography, University of California, San Diego Oceanographic Data Facility, 9500 Gilman Drive, La Jolla, CA 92093-0124
217. T. Takahashi, Columbia University, Lamont-Doherty Earth Observatory, Climate/Environment/ Ocean Division, Route 9W, Palisades, NY 10964
218. L. Talley, Scripps Institution of Oceanography, University of California San Diego, M/C 0230, 9500 Gilman Drive, La Jolla, CA 92093-0230
219. P. Tans, Climate Monitoring and Diagnostics Laboratory, NOAA, 325 Broadway, Boulder, CO 80308-3328
220. J. A. Taylor, Australian National University, CRES, GPO Box 4, Canberra, ACT 0200, Australia
221. J. M. Tiedje, University Distinguished Professor and Director, Michigan State University, 540 Plant and Soil Sciences Building, East Lansing, MI 48824
222. B. Tilbrook, CSIRO Division of Marine Research, P.O. Box 1538, Hobart TAS 7001, Australia
222. R. Torres, University of Göteborg and Chalmers University of Technology, Department of Analytical and Marine Chemistry, S-412 96 Göteborg, Sweden
223. P. Towler, 35 Eric Avenue, Lower Templestowe, Victoria 3107, Australia
224. J. R. G. Townshend, University of Maryland, Dept. of Geography, 1113 Lefrak Hall, College Park, MD 20742

225. J. Tucker, Marine Biological Laboratory, Woods Hole, MA 02543
226. D. Turner, University of Göteborg, Department of Analytical and Marine Chemistry, S-41296 Göteborg, Sweden
227. D. W. R. Wallace, Abteilung Meereschemie, Institut für Meereskunde, Düsternbrooker Weg 20, 24105 Kiel, Germany
228. R. H. Wanninkhof, NOAA/AOML/OCD, 4301 Rickenbacker Causeway, Miami, FL 33149
229. A. J. Watson, School of Environmental Sciences, University of East Anglia, Norwich NR4 7TJ, United Kingdom
230. C. Watts, National Oceanic and Atmospheric Administration, Central Library, 1315 East-West Highway, 2nd Floor, SSMC 3, Silver Spring, MD 20910
231. F. Webster, University of Delaware, College of Marine Studies, Lewes, DE 19958
232. R. F. Weiss, Scripps Institution of Oceanography, University of California, Mail Code A-020, Room 2271, Ritter Hall, La Jolla, CA 92093
234. C. Winn, University of Hawaii, Department of Oceanography, 1000 Pope Road, MSB 610, Honolulu, HI 96822
235. C. S. Wong, Government of Canada, Institute of Ocean Sciences, P.O. Box 6000, 9860 West Saanich Road, Sidney, BC V8L 4B2, Canada
236. L. Xu, Xiamen University, Environmental Science Research Center, Xiamen, Fujian, Peoples Republic of China
237. E. Yakushev, Shirshov Institute of Oceanology, 23 Krasikova, Moscow 117218, Russia
238. E. Yamashita, Research Institute of Technology, Okayama University, Ridaicho 1-1, Okayama 700, Japan
239. Y. Yosuoka, National Institute for Environmental Studies, Center for Global Environment Research, 16-2 Onogawa, Tsukuba, Ibaraki 305, Japan
240. Database Section, National Institute for Environmental Studies, Center for Global Environmental Research, 16-2 Onogawa, Tsukuba, Ibaraki 305, Japan
241. Energy Library (HR-832.2/WAS), Department of Energy, Office of Administration and Management, GA-138 Forrestal Building, Washington, DC 20585
242. Energy Library (HR-832.1/GTN), Department of Energy, Office of Administration and Management, G-034, Washington, DC 20585
243–244. Office of Scientific and Technical Information, P.O. Box 62, Oak Ridge, TN 37831